The deoxypyrimidine nucleotide metabolism in plant mitochondria

Von der Naturwissenschaftlichen Fakultät der

Gottfried Wilhelm Leibniz Universität Hannover

zur Erlangung des Grades

Doktor der Naturwissenschaften (Dr. rer. nat.)

genehmigte Dissertation

von

Markus Niehaus, M. Sc.

2022

Referent: Prof. Dr. Claus-Peter Witte

Korreferent: Prof Dr. rer. nat. Hans-Peter Braun

Tag der Promotion: 05.05.2022

Contributing publications

The following publications contributed to this thesis:

1. **Niehaus, M.**, Straube, H., Künzler, P., Rugen, N., Hegermann, J., Giavalisco, P., Eubel, H., Witte, C-P., Herde, M. (2020):
   Rapid affinity purification of tagged plant mitochondria (Mito-AP) for metabolome and proteome analyses
   Plant Physiology, Vol. 182, Issue 3, Pages 1194 - 1210
   DOI: 10.1104/pp.19.00736

2. Straube, H., **Niehaus, M.**, Zwittian, S., Witte, C-P., Herde, M. (2020):
   Enhanced nucleotide analysis enables the quantification of deoxynucleotides in plants and algae revealing connections between nucleoside and deoxynucleoside metabolism
   The Plant Cell, Vol. 33, Issue 2, Pages 270 – 289
   DOI: 10.1093/plcell/koaa028

3. **Niehaus, M.**, Herde, M. (2022):
   Rapid Affinity Purification of Tagged Plant Mitochondria
   Methods in Molecular Biology, Affinity Chromatography, Pages 121 – 133
   DOI: 10.1007/978-1-0716-2176-9_9

4. **Niehaus, M.**, Straube, H., Specht, A., Baccolini, C., Witte, C-P., Herde, M. (2022)
   The nucleotide metabolome of germinating Arabidopsis thaliana seeds reveals a central role for thymidine phosphorylation in chloroplast development
   The Plant Cell
   DOI: 10.1093/plcell/koac207

Abstract

The synthesis of deoxythymidine triphosphate (dTTP), as one of the four building blocks of DNA, plays a crucial role for the plant. Each cell compartment with its own sub genome therefore has a subset of enzymes necessary for the formation of thymidylates. However, the respective compartments are not purely self-sufficient systems, but are in constant exchange and can support each other depending on the developmental stage. Furthermore, the contribution of individual steps of thymidylate metabolism to the thymidylate pools varies in importance over time.

According to current knowledge, the essential enzymes involved in the synthesis of dTTP in *Arabidopsis thaliana* are Dihydrofolate Reductase-Thymidilate Synthase (DHFR-TS), Thymidine Kinase (TK) and Deoxythymidine Monophosphate Kinase (TMPK, ZEU1). Complete loss of these enzymes is lethal for the plant, or in the case of TK, leads to a plant that can no longer reproduce. However, in the case of DHFR-TS and TK, only one of the two homologues is required for the development of a viable plant.

This work shows that at germination, *de novo* biosynthesis, which proceeds via DHFR-TS, plays a minor role compared to salvage. However, the exclusively mitochondrial DHFR-TS2 isoenzyme appears to be more important than its cytosolic counterpart DHFR-TS1. A similar picture emerges for salvage. TK1b, present in chloroplasts and mitochondria, plays a more important role than its cytosolic representative TK1a. Particularly the chloroplastic TK1b has a greater impact in supplying the cell with thymidylates, which coincides with the synthesis of cpDNA being also the greatest sink during this time. A *TK1b* mutant shows a severe arrest in cpDNA synthesis during germination. The synthesis of cpDNA is partially restored in the established seedling and thymidylate pools are then also affected in a mutant lacking cytosolic TK1a suggesting that the supply of thymidylates is then secured by both cytosolic and organellar salvage.

Among the less important enzymes, appear to be dUTP Pyrophosphatase 1 localized in chloroplasts and mitochondria ($DUT1_{org}$) and dCMP Deaminase (DCD) localized in mitochondria. Both enzymes play a minor role in providing dUMP for DHFR-TS. In neither of the two associated mutants a serious disruption of thymidylate formation is observable. This may be due to an involvement of both enzymes in the formation of dUMP, as indicated by preliminary data suggesting that a *DCD* $DUT1_{org}$ mutant is not viable.

Keywords: deoxyribonucleosides, thymidylates, germination, *Arabidopsis thaliana*

Zusammenfassung

Die Synthese von Deoxythymidintriphosphat (dTTP), einem der vier Bausteine der DNA, spielt für die Pflanze eine entscheidende Rolle. Jedes Zellkompartiment mit eigenen Subgenom verfügt daher über die Enzyme, die für die Bildung von Thymidilaten notwendig sind. Die jeweiligen Kompartimente sind jedoch keine rein autarken Systeme, sondern die einzelnen Kompartimente stehen in ständigem Austausch und können sich je nach Entwicklungsstadium gegenseitig unterstützen. Darüber hinaus ist der Beitrag einzelner Schritte zu den Thymidilatkonzentrationen von unterschiedlicher Bedeutung.

Nach heutigem Kenntnisstand sind die wesentlichen Enzyme, die an der Synthese von dTTP in *Arabidopsis thaliana* beteiligt sind, DHFR-TS, TK und TMPK (ZEU1). Der vollständige Verlust dieser Enzyme führt dazu, dass die Pflanze nicht mehr lebensfähig ist, bzw. im Fall von TK, dass sie sich nicht mehr fortpflanzen kann. Im Falle von DHFR-TS und TK ist jedoch nur eines der beiden Homologe für die Entwicklung einer lebensfähigen Pflanze erforderlich.

Diese Arbeit zeigt, dass zum Zeitpunkt der Keimung die *De-novo*-Biosynthese, die über DHFR-TS abläuft, eine geringere Rolle spielt als der *Salvage*. Allerdings scheint DHFR-TS2, welches nur im Mitochondrium vorhanden ist, wichtiger zu sein als sein zytosolisches Gegenstück DHFR-TS1. Ein ähnliches Bild ergibt sich für den *Salvage*. Auch hier spielt TK1b, welches in den Mitochondrien sowie Chloroplasten vorkommt, eine wichtigere Rolle als sein zytosolischer Vertreter TK1a. Hier hat die chloroplastidäre Variante von TK1b hat einen größeren Einfluss auf die Versorgung der Zelle mit Thymidilaten, wobei zeitgleich die Synthese von cpDNA auch der größte Verbraucher ist. Eine *TK1b* Mutante zeigt einen erheblichen Stillstand der cpDNA-Synthese während der Keimung. Die Synthese von cpDNA wird im etablierten Keimling teilweise wiederhergestellt, und die Thymidilatkonzentrationen sind in einer Mutante, der TK1a fehlt, beeinträchtigt, was darauf hindeutet, dass sich die Versorgung mit Thymidilaten von einer überwiegend organellaren Versorgung zu einer zytosolischen/organellaren Versorgung verschiebt.

Zu den weniger wichtigen Enzymen gehören offenbar DUT1, das in Chloroplasten und Mitochondrien lokalisiert ist ($DUT1_{org}$), und DCD, welches in Mitochondrien vorkommt. Beide Enzyme spielen eine untergeordnete Rolle bei der Bereitstellung von dUMP für DHFR-TS. Bei keiner der beiden assoziierten Mutanten ist eine ernsthafte Störung der Thymidilatbildung zu beobachten. Dies könnte darauf zurückzuführen sein, dass beide Enzyme an der Bildung von

dUMP beteiligt sind, wie vorläufige Daten in Bezug auf eine nicht lebensfähige *DCD DUT1*$_{org}$ Mutante vorschlagen.

Schlagworte: Deoxyribonukleotide, Thymidilate, Keimung, *Arabidopsis thaliana*

Abbreviations

A	adenine
ADP	adenosine diphosphate
ATM-1	Ataxia-Telangiectasia Mutated 1
ATR-2	Ataxia-Telangiectasia Mutated and RAD3-Related
C	cytosine
CDA	Cytidine Deaminase
CDP	cytidine diphosphate
CEN2	Centrin 2
cpDNA	chloroplastic DNA
dADP	deoxyadenosine diphosphate
dATP	deoxyadenosine triphosphate
dC	deoxycytidine
DCD	dCMP Deaminase
dCDP	deoxycytidine diphosphate
dCMP	deoxycytidine monophosphate
dCTP	deoxycytidine triphosphate
DDB1-A	Damaged DNA Binding Protein 1A
DDGC	Differential and Density Gradient Centrifugation
DDR	DNA damage repair
dGDP	deoxyguanosine diphosphate
dGTP	deoxyguanosine triphosphate
DHFR-TS	Dihydrofolate Reductase-Thymidilate Synthase
DNA	deoxyribonucleic acid
dNK	Deoxynucleoside Kinase
dNMP	deoxyribonucleotide monophosphate
dNTP	deoxyribonucleotide triphosphate
dT	deoxythymidine
dTDP	deoxythymidine diphosphate
dTMP	deoxythymidine monophosphate
dTTP	deoxythymidine triphosphate
dU	deoxyuridine
dUDP	deoxyuridine diphosphate
dUMP	deoxyuridine monophosphate
DUT1	dUTP Pyrophosphatase 1
dUTP	deoxyuridine triphosphate
EMS	ethyl methanesulfonate
ENT	Equilibrative Nucleoside Transporters
G	guanine
GDP	guanosine diphosphate
HPLC	High Performance Liquid Chromatography
LC	Liquid Chromatography

MCF	Mitochondrial Carrier Family
MS	Mass Spectrometry
ncDNA	nuclear DNA
NDPK	Nucleoside Diphosphate Kinase
NSH1	Nucleoside Hydrolase 1
PCR	Polymerase Chain Reaction
RAD1	UV Radiation 1
RNA	ribonucleic acid
RNAi	RNA interference
RNR	Ribonucleotide Reductase
SPE	Solid Phase Extraction
T	thymine
TCA	trichloroacetic acid
TDP	thymidine diphosphate
TK	Thymidine Kinase
TMPK	Deoxythymidine Monophosphate Kinase
U	uracil
UDP	uridine diphosphate

Contents

Contributing publications i

Abstract ii

Zusammenfassung iii

Abbreviations v

1 Introduction 7

1.1 Rapid Affinity Purification of Tagged Plant Mitochondria (Mito-AP) 10

1.2 Enhanced Nucleotide and Nucleoside Analysis using a Solid Phase Extraction 13

1.3 *De Novo* Synthesis of Deoxyribonucleotides 15

1.3.1 Deoxypurine Synthesis 16

1.3.2 Deoxypyrimidine Synthesis 17

1.4 Thymidylate Synthesis during Germination 21

1.4.1 *De novo* Biosynthesis 22

1.4.2 Conversion of C to T 26

1.4.3 Salvage Pathway 29

1.5 References 34

2 Publications and Manuscripts 41

2.1 Rapid affinity purification of tagged plant mitochondria (Mito-AP) for metabolome and proteome analyses 42

2.2 Enhanced nucleotide analysis enables the quantification of deoxynucleotides in plants and algae revealing connections between nucleoside and deoxynucleoside metabolism 73

2.3 Rapid Affinity Purification of Tagged Plant Mitochondria 118

2.4 The nucleotide metabolome of germinating *Arabidopsis thaliana* seeds reveals a central role for thymidine phosphorylation in chloroplast development 132

3 Appendix 175

3.1 Curriculum Vitae 176

3.2 List of publications 177

Acknowledgements 178

1 Introduction

It is known today that all known living organisms depend on deoxyribonucleic acid (DNA) as a carrier of genetic information. The first verifiable scientific mention of DNA was made in 1866 by the German zoologist Ernst Haeckel. He postulated that the factors necessary for the transmission of heritable traits are localized in the cell nucleus. Later, in 1869, the Swiss biologist and physician Friedrich Miescher was the first to isolate DNA from purified cell nuclei, which he referred to as nuclein. He also roughly described its properties. In the following years, the German physician and biochemist Albrecht Kossel succeeded in further unravelling the properties of DNA on the basis of Miescher's findings. Among other things, he identified the four nucleobases of DNA: guanine, adenine, thymine and cytosine. For this and other discoveries, he received the Nobel Prize for Physiology and Medicine in 1910. In the early 1900s, the American biochemist Phoebus Levene, was actively working to understand the structure and functions of nucleic acids. He had a major impact on the identification of the carbohydrate components ribose of RNA and 2-deoxyribose of DNA. Additionally, he postulated the structure of nucleotides having a linkage between a phosphate, a sugar and a nucleobase, and that these can be linked through the phosphate groups. It took until 1944 to prove conclusively that DNA, and not proteins, is the carrier of the hereditary information. Oswald Avery, a Canadian physician, took the experiment by Frederick Griffith (Griffith 1928), in which mice were treated with dead and living pneumococcal bacteria, as a template and repeated it with purified DNA instead and came to the same conclusion (Avery et al. 1944). This discovery was a turning point in DNA research and led to other important discoveries such as the double helix structure, Watson-Crick base pairing (Watson and Crick 1953), and finally the deciphering of the genetic code by the American biochemist Marshall Nirenberg and his group in 1966 (Dahm 2005).

Nowadays it is common knowledge that DNA is essential for every living organism, whether it is archaeal, bacterial or eukaryotic. A significant feature of Eukarya domain representatives is that they have more than one genome. In addition to the nuclear genome, all representatives also possess the mitochondrial genome, which is localized in the mitochondrion. In the case of the plant representatives, another sub genome is present, the plastid genome. The origin of these sub genomes can be explained by the endosymbiont theory. In this hypothesis, some

prokaryotes took in other prokaryotes by endocytosis without killing them, thereby acquiring endosymbionts. According to phylogenetic studies, the ancestors of mitochondria are the alphaproteobacteria (Gray et al. 1999), while the chloroplasts are probably derived from a single cyanobacterium species (McFadden and van Dooren 2004).

Another aspect of the endosymbiont theory and the formation of the sub genomes is reductive evolution. Both organelles have shifted a large part of their genome into the nucleus in the course of their evolutionary history, which is also known as endosymbiotic gene transfer (Cavalier-Smith and Lee 1985; Ku et al. 2015). Along with redundant genes, also genes encoding for metabolic pathways have been transferred, even if some of these genes were essential for organelle sustainability. This led to organelle dependence on the cytosol for both protein and metabolite import and requires communication between these compartments. Among the genes remaining in the respective sub genomes are those for the respiratory chain, photosynthesis, and genes required for gene expression (Gray et al. 1999; Dobrogojski et al. 2020).

As in the nuclear genome, the integrity of the DNA is crucial also for sub genomes. Defects can lead to a variety of diseases, some of which are serious, so-called genetic disorders. They can either occur spontaneously in the DNA of the affected organism or, if there is a mutation in the DNA of the germ cells, they can be inherited, in which case they are referred to as hereditary diseases. These diseases are not only limited to humans and animals, but can also have drastic consequences in plants. For example, a genetic alteration was discovered in 2009 in the model plant *Arabidopsis thaliana* in which a repetitive sequence, consisting of codons encoding for glutamine, within an intron of the gene At1g13430 was multiplied. As a result, the affected plants showed severe growth retardation and died eventually under certain growth conditions (Sureshkumar et al. 2009). This discovery shows strong similarities with the underlying causes of Huntington's disease, a hereditary disease that is fatal in humans and animals. However, not every mutation has to be considered negative, because mutations act as the driving force of evolution. But the severe consequences of genetic disorders highlight the importance of preserving DNA and its integrity.

The cause of mutations can be complex. They occur spontaneously, caused for example by the altered base pairing of tautomeric forms of the nucleotides. Another possibility is a spontaneous chemical change of a base, such as the deamination of cytosine to uracil. However, genetic changes can also be induced artificially, for example by the application of

chemicals such as ethyl methanesulfonate (EMS), which can lead to alkylation of the nucleobase. All these causes result in a base pairing error during replication. But mutations can also be caused by physical forces in the form of ionizing radiation, e.g. UV radiation.
Additionally, the process of replication itself is also not free of errors. The DNA polymerase responsible for the synthesis of DNA has some control and repair mechanisms itself, such as the pre-control of the deoxyribonucleotide triphosphate (dNTP) to be inserted or the 3'-5' exonuclease activity, also known as proofreading function, nevertheless, errors also occur here. This can be explained by considering that the polymerase must be able to recognize all dNTPs as substrates although these are structurally quite different. This broad substrate spectrum is consequently associated with a certain error rate. In order to keep this error rate low, it is therefore advantageous, on the one hand, to adjust the pool sizes of dNTPs according to the consumption rate of dNTPs by the DNA polymerase. On the other hand, the ratios of the individual dNTPs to each other should also be monitored and re-adjusted if necessary (Straube et al. 2021a), but if this ratio changes, this is accompanied by an increase in mutation frequency (Kunz and Kohalmi 1991; Kumar et al. 2011; Buckland et al. 2014). Additionally, if the abundance of at least one dNTP is too low, replication may also slow down, pause, or stop altogether. This may be reflected in the total DNA content or the ratio of sub genomes to each other (Le Ret et al. 2018, Niehaus et al., 2022). The most significant factors affecting the dNTP pools are their own synthetic pathways, *de novo* biosynthesis and salvage.

The aim of this work was to investigate and evaluate the contribution of these processes to the thymidylate pools in plants. Seed germination in *Arabidopsis thaliana* was chosen as suitable biological context, since it represents a critical phase for DNA synthesis and plastid DNA is particularly required here. The aim was not only to assess the biological significance of individual enzymes, but also to investigate their varying importance during different phases of germination.
For answering this question, I will refer in the following (from chapter 1.3) mainly to the publication Niehaus et al., 2022 (see chapter 2.4). In this work, I will not only describe the main aspects already shown in the publications, but I will also expand them with new considerations and discuss them.

1.1 Rapid Affinity Purification of Tagged Plant Mitochondria (Mito-AP)

In order to elucidate the influence and specific role of the mitochondrion in the context of dTTP synthesis, two important problems arise. First, the metabolic pathway under investigation is not only located in the mitochondrion, but also occurs in the cytosol and plastid. Therefore, in order to analyze the mitochondrial pools of the contributing metabolites it is necessary to enrich the mitochondria and separate them from the other compartments. Second, the time aspect plays an important role. Metabolites are subject to constant changes, they can be further metabolized, degraded or leak out of the mitochondrion. Therefore, in order to perform an evaluation of the *in vivo* metabolites concentrations, the isolation process must be performed swiftly (Roberts et al. 1997; Agius et al. 2001) and metabolic activity has to be halted (Bieleski 1964).

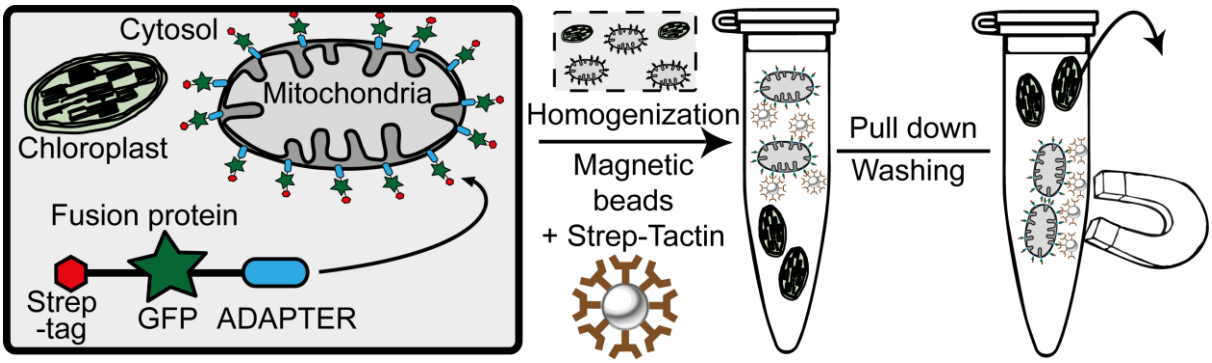

Figure 1. Workflow of Mito-AP. An ectopically expressed protein, which integrates into the outer mitochondrial membrane, fused with an N-terminal Strep-tag and a GFP-tag facing the cytosol can be used as an anchor for affinity purification of mitochondria with Strep-Tactin-coated magnetic beads. Reproduced and modified from Niehaus et al., 2020 (www.plantphysiol.org, Copyright American Society of Plant Biologists).

Mito-AP (Figure 1, Niehaus et al. 2020), an isolation method for intact mitochondria from plants, enriches mitochondria with a purity comparable to the previous state-of-the-art method, the combination of differential and density gradient centrifugation (DDGC). However, the duration of the isolation was reduced from about 6 hours using DDGC to about 30 minutes using Mito-AP. In addition, the amount of starting material needed was greatly reduced, which is advantageous when working with growth-impaired mutants or specific plant tissues. However, the amount of mitochondria isolated is smaller, but still sufficient for subsequent analyses such as metabolomics, proteomics and respiratory activity measurements.

Despite the possibility of using Mito-AP to extract and measure metabolites from plant mitochondria, it should be noted that while saving a lot of time, the results obtained do

probably not reflect *in vivo* concentrations because enzyme activities are not inhibited during the purification. Nevertheless, it is debatable whether potential differences between a mutant and a wild type in metabolite content would be still valid, provided they were isolated under the same conditions. In order to measure metabolites at *in vivo* concentrations, isolation would have to occur within fractions of a second, because this is the time scale in which chemical reactions occur. Alternatively, it is also possible to rapidly stop the continuation of metabolism within the whole cell, and subsequently perform the isolation (Dietz 2017). An example for this is non-aqueous fractionation (Behrens and Thalaker 1957; Heber 1957), which maybe can be combined with affinity purification of mitochondria. The combined approach has never been done successfully because many affinity purification procedures rely on protein interactions requiring aqueous solutions. One way to circumvent this problem could be to replace the protein-based Strep-tag label with a site-specific biotinylation (Fairhead and Howarth 2015) which might keep its structure and integrity during non-aqueous conditions.

Although ribonucleotides could be measured and quantified from mitochondria isolated with Mito-AP, deoxyribonucleotides could not be detected. One reason for this may be that in the whole cell the amount of ribonucleotides compared to their corresponding deoxyribonucleotides is about 1000-fold higher (Nygaard 1972; Straube et al. 2021a). Probably the amounts of mitochondria isolated were too small to obtain a signal for deoxyribonucleotides in downstream mass spectrometry. Secondly, it was observed that the surface of the magnetic beads used in the purification process had a strong affinity for nucleotides. Therefore, during the disruption of the mitochondria bound to the beads, the released nucleotides are likely to be directly absorbed by the beads, and subsequently lost for the analysis. This problem occurs presumably due to the fact that some of the surface coating carboxyl groups required for the binding of Strep-Tactin are not fully saturated and hence are able to interact with the phosphate residues of the nucleotides by forming a salt bridge with positively charged ions. One possibility to overcome this problem would be to chemically block the remaining free carboxyl groups after Strep-Tactin coating, e.g. by using an amine-containing reagent. However, it is also conceivable that the nucleotides can be bound by the oxidized surface of exposed iron cores, such as those found in damaged beads (Gilar et al. 2021). One way to circumvent both problems mentioned could be the elution of the mitochondria from the beads after isolation, allowing removal of the beads before lysis. One

way to elute bound mitochondria is the use of biotin, which binds to Strep-Tactin with higher affinity than the Strep tag itself and thus displaces it. However, this approach again requires more time and also results in lower yields.

Despite great progress and advantages of Mito-AP compared to previous methods, this method is not yet suitable for elucidating the specific role of the mitochondria in the context of dTTP synthesis. For this reason, specific measurements of the mitochondrial pool could not be made in this work, but were limited to measurements of whole cell extracts.

1.2 Enhanced Nucleotide and Nucleoside Analysis using a Solid Phase Extraction

A prerequisite for characterizing processes that result in the formation of thymidylates is the ability to measure and quantify the metabolites involved in the process of dTTP synthesis. Many of the enzymes involved in deoxyribonucleotide metabolism are known, but their characterization is limited to *in vitro* enzymatic assays and visible phenotypes. However, it remains unclear how their respective loss-of-function affects the associated metabolite pools *in vivo*. As a consequence, enzymes that have a smaller impact on these pools and do not cause a phenotypic alteration may have been insufficiently characterized.

While it has been possible for some time to measure and quantify ribonucleotides in plants using High Performance Liquid Chromatography (HPLC) coupled with photometric detection (Meyer and Wagner 1985; Sawert et al. 1987), measuring the corresponding deoxyribonucleotides has proven to be more difficult. The most significant contributing factor here is the substantially lower abundance of these compounds compared to the ribonucleotides. Previous measurement methods for the canonical dNTPs were based on a PCR assay (Solter and Handschumacher 1969; Roy et al. 1999), which only allowed relative quantification. Moreover, this measurement method does not provide any information about the mono- or diphosphate form of the deoxyribonucleotides, limiting its use for studying the entire metabolic pathway leading to dTTP with all its intermediates.

Consequently, for the detection and quantification of all the relevant deoxyribonucleotides, a more sensitive detection method such as mass spectrometry (MS) coupled with liquid chromatography (LC) has to be applied. In Straube et al, 2020a, a process for sample preparation and detection by LC-MS is described that allows for a robust yet sensitive detection as well as quantification of nucleotides and nucleosides in plants (Figure 2). Key aspects of the sample preparation include the use of 15% trichloroacetic acid during sample disruption, which leads to a rapid arrest of all enzymatic activities. These enzymes include phosphatases (Bieleski 1964; Ikuma and Tetley 1976), which can otherwise cause an alteration in metabolite concentrations and their composition. As a result, stabilization of the metabolites allows determination of *in vivo* concentrations. Another important aspect is a liquid/liquid extraction, in which the sample is treated with a nonpolar solvent, removing all soluble nonpolar components from the sample as well as the acid. The removal of unwanted components from the sample leads to a less complex matrix, which is an important

prerequisite for higher sensitivity in the later measurement, decreasing the so called matrix effect (Nieman et al. 1978; Straube et al. 2021b). A final important aspect here is the application of solid phase extraction (SPE). The usage of a weak anion exchange resin enables both the enrichment of nucleotides and the further minimization of the matrix by subsequent washing steps. Previous enrichment methods by using more sample material without subsequent SPE were also directly associated with a stronger matrix effect and therefore hardly led to better signals (Straube, unpublished). Thus, the possibility to enrich the nucleotides via SPE not only leads to a more robust signal in the measurement, but also enables the detection of less abundant nucleotides.

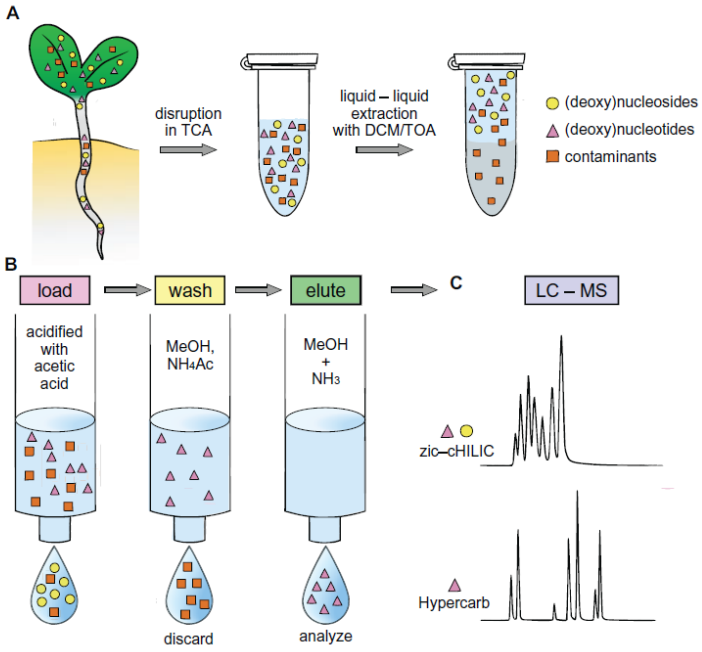

Figure 2. Schematic overview of the method for the extraction and analysis of nucleotides and nucleosides. (**A**) Plant material is disrupted and quenched with with trichloroacetic acid (TCA), which is removed together with apolar contaminants by liquid-liquid extraction with dichloromethane (DCM) and trioctylamine (TOA). (**B**) The extract is loaded onto a weak-anion exchange SPE cartridge, the flow-through contains nucleosides for the analysis. Subsequently contaminants are depleted by washing with methanol (MeOH) and ammonium acetate (NH_4AC), resulting in elution of nucleotides with MeOH and ammonia (NH_3). (**C**) Isolated fractions are analyzed by LC-MS using a porous graphitized black column or a polar endcapped C18 column. Reproduced from Straube et al., 2020a with permission from Oxford University Press.

Using the protocol described in Straube et al. 2021a for sample preparation and measurement employing the so-called Hypercarb method, it was possible to measure and quantify all relevant nucleotides except for the deoxyuridylates in plant cell extracts of different developmental stages (Niehaus et al., 2022).

1.3 *De Novo* Synthesis of Deoxyribonucleotides

Nucleotides are the building blocks of RNA and DNA. Therefore, they are required in every cell compartment, which has its own replication, transcription and translation mechanisms, namely the cytosol, mitochondria and chloroplast. Nucleotides are composed of three components (Figure 3). A pentose, in the case of RNA a ribose and in the case of DNA a 2-deoxyribose. A heterocyclic nucleobase, which can be divided into two groups: the purines adenine (A) and guanine (G) and the pyrimidines cytosine (C), thymine (T) and uracil (U). These nucleobases are also referred to as canonical nucleobases. In the case of RNA, A, G, C and U are required; in the case of DNA, U is replaced by T. The nucleobase is linked to the C1-atom of pentose via an N-glycosidic bond, this molecule is called a nucleoside. And last the phosphate group, which can consist of one to three phosphate residues. It is connected to the C5-atom of the pentose via an ester bond. These nucleotides are then referred to as nucleoside mono-, di- or triphosphates.

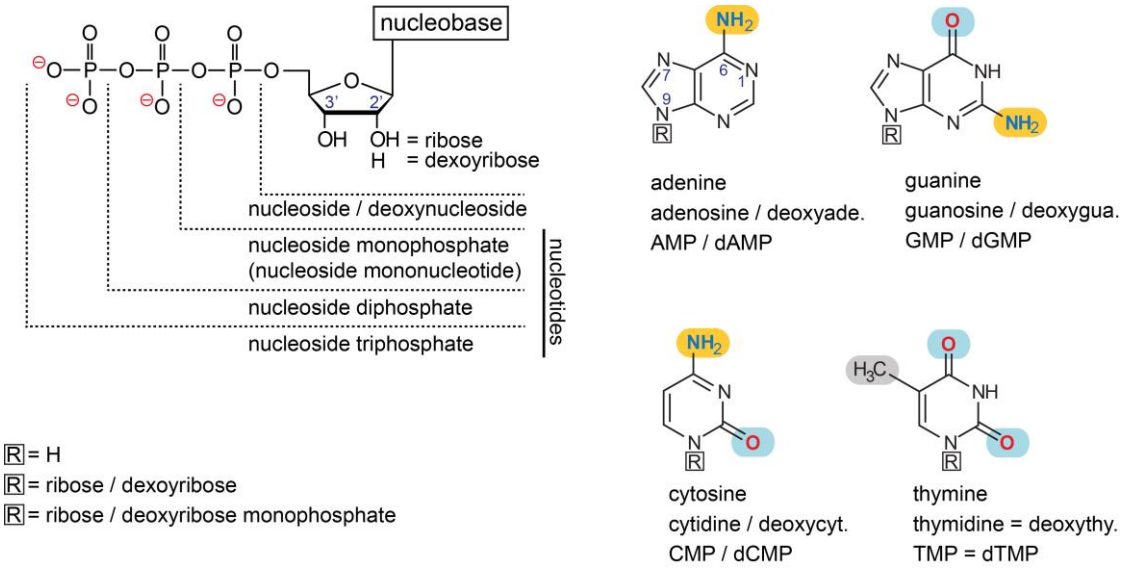

Figure 3. Structural composition of nucleobases, nucleosides, and nucleotides. For the nucleobases, "R" is simply a proton. For the nucleosides, "R" is a sugar moiety that can be ribose or deoxyribose (carrying a proton instead of a hydroxyl group at the 2' carbon of the ribose). Nucleotides have up to three phosphate groups esterified to the hydroxyl group of the 5'-carbon of the nucleoside sugar determining the prefix mono-, di-, or tri- in the name of the molecule. The terminal phosphate always carries two charges, irrespective of the number of phosphates present. The purine nucleobases are shown in the upper row and the pyrimidine nucleobases in the lower row. Groups attached to the heterocycles highlighted in red (oxo groups), blue (amino groups), and gray (methyl group). Reproduced and modified from Herde and Witte, 2019 (www.plantphysiol.org, Copyright American Society of Plant Biologists).

1.3 *De novo* Synthesis of Deoxyribonucleotides

The *de novo* synthesis of all deoxyribonucleotides starts with ribonucleotides. More specifically, the ribonucleoside diphosphates ADP, GDP, CDP and UDP, which are required as substrates for the entry reaction and represent intermediate steps in the course of the *de novo* biosynthesis of the ribonucleotides and salvage (Witte and Herde 2020; Zrenner et al. 2006; Ashihara et al. 2020). During the entry reaction, the hydroxyl group on the C2-atom of the ribose moiety of the dinucleotide is reduced, resulting in a 2-deoxyribose. Products of this reaction are dADP, dGDP, dCDP and dUDP. The enzyme responsible for this is the Ribonucleotide Reductase (RNR), which is localized in the cytosol (Lincker et al. 2004).
The further *de novo* synthesis can happen either in the cytosol, mitochondrion and chloroplast, for the synthesis in the organelles these reaction products first have to be imported. The necessary transport processes have been little studied so far, so that on the one hand it is not clear in which phosphorylation state the deoxynucleotides are transported and on the other hand the transporters involved are not known. A prominent family of transporters, some of which are well studied, are the so-called Equilibrative Nucleoside Transporters (ENTs). This group includes 8 members that are predominantly associated with the transport of purines and pyrimidines in the ribonucleoside form. However, there is evidence *in vitro* that some of them are also capable of transporting the deoxyribonucleoside form, including thymidine (Wormit et al. 2004; Hirose et al. 2005; Chen et al. 2006). Although most ENTs are localized in the plasma membrane or tonoplast, ENT2 and ENT5 are predicted to be located in membranes of the mitochondrion or chloroplast (Wormit et al. 2004). A study on rice with the transporter *Os*ENT2, which has a high sequence homology to ENT2, shows that this transporter is particularly expressed during germination. It is thought to be involved in the retrieval of nucleosides from the endosperm (Hirose et al. 2005). In total, the presence of the RNR in the cytosol and genetic studies (Clausen et al. 2012; Clausen et al. 2014), see later chapter) suggest a transport of deoxyribonucleotides and deoxyribonucleosides across the membrane of chloroplasts and mitochondria.

1.3.1 Deoxypurine Synthesis

The substrates dADP and dGDP can be phosphorylated by members of the multisubstrate enzyme family of Nucleoside Diphosphate Kinases (NDPKs) to dATP and dGTP, respectively. This family comprises 5 members, none of which shows high substrate specificity. Consequently, NDPKs are able to phosphorylate all nucleosides diphosphates (Zrenner et al.

2006). Members of this protein family are localized in different compartments. In the case of NDPK1, cytosolic localization has been observed (Dorion et al. 2006), whereas chloroplast localization has been described for NDPK2 (Bölter et al. 2007). Dual localization in chloroplasts and mitochondria has been described for NDPK3 (Sweetlove et al. 2001; Spetea et al. 2004; Luzarowski et al. 2017).

1.3.2 Deoxypyrimidine Synthesis

As in the case of purines, the further synthesis of dCDP to dCTP is carried out by the enzyme NDPK, whereas the synthesis of dTTP proceeds in a different and more complex way, which is shown in Figure 4. The RNR is not able to synthesize dTDP because the corresponding ribonucleotide disphosphate counterpart (TDP) is not a regular metabolite. Instead, the synthesis of dTTP occurs via dUDP.

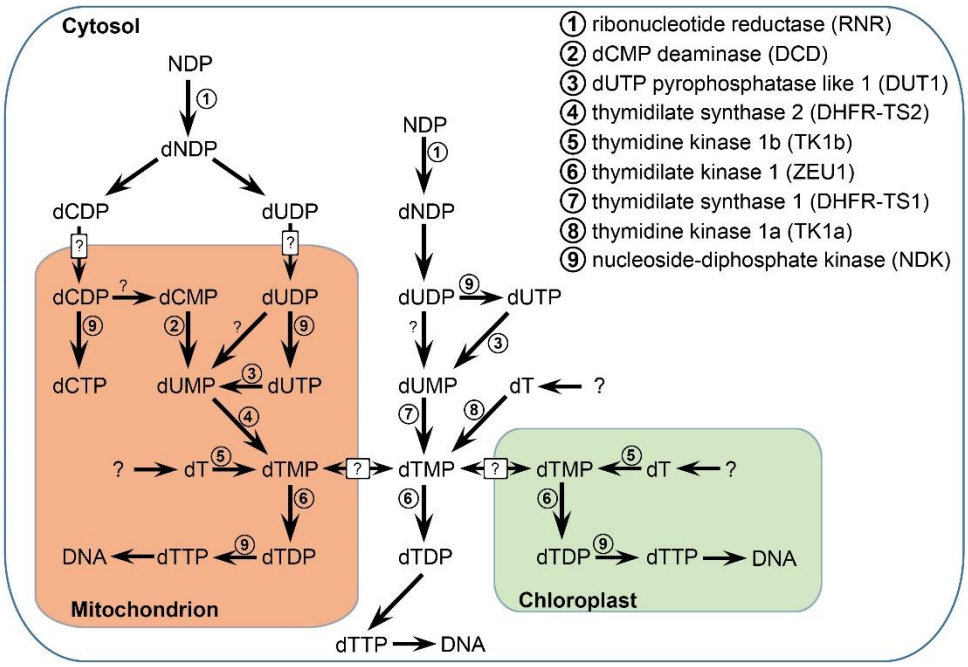

Fig. 4: Proposed model of thymidylate metabolism in *Arabidopsis thaliana*. Enzymes putatively involved in the formation of thymidylate pools and their subcellular localization are shown. Studies of loss-of-function mutants suggest the presence of currently unknown transporters allowing an exchange of metabolite pools between the cytosol, the chloroplast and the mitochondrion.

For the following step of *de novo* biosynthesis, however, dUMP is required. This can be made either by dephosphorylation of dUDP but the identity of an enzyme catalyzing this step is unknown. A possible candidate for this would be an organic pyrophosphatase, for example from the family of NUDIX hydrolases, of which some representatives are known to also accept

nucleoside diphosphates as substrates. Based on protein sequence analysis, representatives of this family are predicted to reside in the cytosol, the chloroplasts as well as in the mitochondria (Yoshimura and Shigeoka 2015). Alternatively, dUDP is first phosphorylated to dUTP by NDPK and in a further step is dephosphorylated to dUMP by dUTP Pyrophosphatase 1 (DUT1). It has been shown, that the gene encoding for DUT1 contains two open reading frames, one encoding a cytosolic and nuclear variant, and one encoding a version dual-localized to both the mitochondria and the chloroplasts (Niehaus et al. 2022).

Another source of dUMP is the deamination of dCMP by dCMP Deaminase (DCD), which hydrolytically cleaves off the amino group from the nucleobase moiety. In plants, this protein has been localized exclusively to the mitochondria (Xu et al. 2014; Niehaus et al. 2022), whereas in humans it occurs in the cytosol and nucleus, respectively (Somasekaram et al. 1999). Also a salvage pathway can function as a source for dNMPs. Deoxyribonucleosides derived from degradation processes serve as substrates and are phosphorylated to dNMPs via a kinase. In the case of all canonical deoxyribonucleosides except deoxythymidine (dT) and deoxyuridine (dU), this reaction is catalyzed by the enzyme Deoxynucleoside Kinase (dNK) which presumably localizes in the mitochondrion (Clausen et al. 2012; Clausen et al. 2014). The enzymes responsible for the salvage of dT and dU are the Thymidine Kinases (TKs) TK1a and TK1b, one of which is located in the cytosol and the other in the chloroplast as well as in the mitochondrion (Xu et al. 2015). Furthermore, it is possible that also deoxycytidine (dC) metabolism contributes to dUMP biosynthesis. It has been shown that the cytosol-localized enzyme Cytidine Deaminase (CDA) not only deaminates cytidine but also dC *in vitro* (Chen et al. 2016) and also *in vivo* (Straube et al. 2021a). The dU generated in this way may be phosphorylated by cytosolic TK1a contributing to the dUMP pool.

In the next reaction, dUMP is methylated to dTMP. The responsible enzyme is Dihydrofolate Reductase-Thymidilate Synthase (DHFR-TS), which transfers a methyl group from methylene-tetrahydrofolate to the C5-atom of uracil in the course of the reaction, resulting in dihydrofolate and 5-methyl-2'deoxyuridine monophosphate, also known as dTMP. For Arabidopsis thaliana, three isoforms are known, which are called DHFR-TS due to their dual function, dihyrodolate reductase and thymidylate synthase. Of these, only the first two isoforms show activity. DHFR-TS3 acts as an inhibitor of the other isoforms and could therefore have a regulatory effect on them (Gorelova et al. 2017). Subcellular localization in various tissues suggests that DHFR-TS1 is localized in the cytosol (Gorelova et al. 2017; Corral

et al. 2018), DHFR-TS2 in the mitochondrion (Gorelova et al. 2017; Corral et al. 2018; Niehaus et al. 2022), and DHFR-TS3 predominantly in the cytosol, with the exception that in a few cells, the localization was also observed in the nucleus as well as in the mitochondrion (Gorelova et al. 2017). However, none of the homologs are localized in the plastid, implying that the plastid relies on the import of dTMP or its derivatives (dT, dTDP, dTTP) for the further *de novo* biosynthesis.

Another source of dTMP is the salvage pathway. In the cytosol as well as in mitochondria and chloroplasts, dT can be phosphorylated to dTMP by the thymidine kinases TK1a and TK1b. The source of dT is not yet known, but possible sources could be degradation of DNA or the dephosphorylation of dTMP. An important determinant for the regulation of dT availability is the Nucleoside Hydrolase 1 (NSH1), which is exclusively localized in the cytosol. This enzyme catalyzes the hydrolytic cleavage of a nucleoside into its nucleobase and pentose. It is capable of cleaving not only ribonucleosides (Jung et al. 2009; Baccolini and Witte 2019) but also deoxyribonucleosides including dT (Straube et al. 2021a).

In addition to considering the individual compartments on their own, the interaction of the compartments must also be considered. Since chloroplasts do not contain a DHFR-TS for the synthesis of dUMP to dTMP, but all other required enzymes are present, it can be concluded that thymidine can be imported and subsequently phosphorylated by TK1b. However, also thymidylates may be imported by chloroplasts, leaving the possibility of a potential synergistic interplay regarding the supply with the cytosol open. Although the data on deoxyribonucleoside and deoxyribonucleotide transporters is currently quite limited, there is evidence that the transporters required for chloroplastic dT import belong to the ENTs, as described above, or in the case of the deoxyribonucleotides to the Mitochondrial Carrier Family (MCF). It was shown that NDT1 is localized in the chloroplast, whereas NDT2 is localized in the mitochondrion, and that both can transport dTMP *in vitro*. Moreover, they also facilitate the transport of dTDP as well as dTTP *in vitro*, although the latter is much weaker in NDT2 compared to NDT1. Although they have been characterized as NAD^+ carrier proteins it is possible that they are also involved in the transport of thymidylates (Palmieri et al. 2009).

The next step in the synthesis of dTTP is catalyzed by Thymidylate Kinase (TMPK), which phosphorylates dTMP to dTDP. From the gene encoding TMPK two alternative transcripts of different length in the 5’-end are generated. The shorter of the two encodes a cytosolic

variant, while the longer variant encodes a version previously assigned only to mitochondria (Ronceret et al. 2008) but is also localized in chloroplasts (Niehaus et al. 2022).

The final step, as described earlier, is carried out by enzymes of the NDPK family, which phosphorylates dTDP to dTTP in the cytosol, chloroplast and mitochondrion. The dTTP produced in each compartment can now be used for the synthesis of DNA and damage repair.

1.4 Thymidylate Synthesis during Germination

In this chapter and the following I will not only present and discuss the aspects described in the publication Niehaus et al., 2022 (see Chapter 2.4), but also add and discuss additional considerations that in my opinion are important and noteworthy. To make it easier for the reader to follow, I will refer to the figures of the publication.

Germination plays a unique role in plant development and presents many challenges for the plant. In addition to the start of plant growth and the associated increasing demand for a wide variety of building blocks, germination also involves the change from a heterotrophic to an autotrophic mode of life. The latter involves the rapid maturation of the heterotrophic etioplasts present in the seed into autotrophic chloroplasts (Waters and Langdale 2009). This maturation is accompanied by a massive duplication of the plastid genome, whereas the nuclear and mitochondrial genomes are replicated to a noteworthy degree only to a later stage (Fujie et al. 1994; Masubelele et al. 2005; Sliwinska et al. 2009; Paszkiewicz et al. 2017). Chloroplasts therefore represents the main sink for deoxyribonucleotides at this stage, making their supply particularly important for chloroplast development.

To gain a better general understanding of the availability and development of canonical nucleosides and nucleotides during germination, a time course experiment was performed with *Arabidopsis thaliana* Col-0 wild type plants with subsequent metabolite measurements. On this basis, three time points were selected representing important points during the early stages of plant growth: First, a time point at which the concentrations of deoxyribonucleosides and deoxyribonucleotides are at a constant and stable level representing the baseline before germination (3 hours after transfer to growth conditions, 3 h). Second, a time point in which deoxyribonucleosides and deoxyribonucleotides concentrations increase and the plastid genome is being replicated (48 hours after transfer to growth conditions, 48 h). And third, a time point at which germination is complete and the seedling is established (144 hours after transfer to growth conditions, 144 h) (see Niehaus et al., 2022 Figure 4). For these time points, experiments were performed to examine mutants for enzymes involved in thymidine und thymidylate metabolism (DHFR-TS, TK, DCD, $DUT1_{org}$) for their effect on nucleoside and nucleotide concentration as well as their influence on plastid and mitochondrial DNA. The special aspect of the here selected single and double mutants is that they not only give us a basic indication of the synthesis of dTTP in the cell and its compartments, but also allow

conclusions to be drawn about which compartments are more relevant for the overall supply at the respective times of observation. In the following, I will focus on three aspects: *De novo* biosynthesis of thymidylates, conversion of C to T, and the role and importance of the dT salvage pathway. The respective roles of these pathways in the formation of the thymidylate pools during germination is evaluated based on the experiments performed in this work and discussed in the context of the literature.

1.4.1 *De novo* Biosynthesis

Enzymes critical for the *de novo* biosynthesis of dTTP include RNR, DUT1, DHFR-TS1 as well as DHFR-TS2 and TMPK (Figure 4). In this work, only $DUT1_{org}$, DHFR-TS1 and DHFR-TS2, as well as TMPK, were investigated from the enzymes mentioned above.

De novo biosynthesis of all canonical deoxyribonucleotides starts with the reduction of ribonucleotides diphosphates by the RNR. This enzyme is composed of a total of 4 subunits, two large subunits (R1) harboring the regulatory function and two small subunits (R2) holding the catalytic function (Sauge-Merle et al. 1999; Wang and Liu 2006). Complete knockout of the gene encoding the R1 subunit is lethal, while plants with reduced activity are viable at least in some cases. RNAi plants have a phenotype indistinguishable from wild type at the cotyledon stage, but whose first true leaves show large peripheral chlorotic white areas and in some cases die shortly after. By contrast, a plant line cls8-2 isolated from an EMS population, which has a point mutation in the regulatory domain, shows a distinct phenotype at the cotyledon stage. Already in the heterozygous stage, this mutant has white spots on the cotyledons and subsequent leaves, but is able to generate seeds. In the homozygous mutant, the white areas are much more pronounced and the plant dies shortly after cotyledon stage. A PCR-based quantification of dATP and dTTP, performed with viable RNAi plants, shows a reduction in both metabolites relative to the wild type. Furthermore, at a later stage of development, it was found that the amount of chloroplastic DNA (cpDNA) is reduced compared to the wild type (Garton et al. 2007). A similar picture as for the R1 subunit is found for the R2 subunits. Due to the presence of three genes encoding the small subunits and the resulting redundancy of some of them, homozygous single knockouts are viable. In the case of the *TSO2* mutant, also smaller white areas appear in leaf tissue but later in development than in the *R1* mutants. In terms of effects on the dNTP pools, these are decreased in all cases as well (Wang and Liu 2006).

1.4 Thymidylate Synthesis during Germination

The RNR plays an essential role in providing deoxyribonucleotide diphosphates for *de novo* deoxyribonucleotide metabolism at every stage of plant development for all canonical deoxyribonucleotides. Even during germination, the seed's reserves are not sufficient to meet the seedling's need for deoxyribonucleotides and *de novo* synthesis via RNR is needed.

The product of RNR relevant for further synthesis of dTTP is dUDP. How exactly dTTP is made from dUDP is not known, but it is conceivable, that dUDP is phosphorylated to dUTP by NDPK. This process can occur in all compartments. In the subsequent step, dUTP can be dephosphorylated to dUMP by the pyrophosphatase DUT1. Mutation of both DUT1 variants, the cytosolic and mitochondrial/chloroplast version, in Arabidopsis is lethal (Dubois et al. 2011). The orthologous genes in *Saccharomyces cerevisiae* (Gadsden et al. 1993) and *Escherichia coli* (el-Hajj et al. 1988) are also essential for survival. However, the mutation of the mitochondrial and plastid variant alone (*DUT1$_{org}$*) is viable in Arabidopsis, with no noticeable growth phenotype throughout development. At the metabolite level, though, this mutant shows a significantly reduced dT pool at the 3 h time point as well as at 48 h time point. (see Niehaus et al., 2022 Figure 5A and 7A). The earlier reduced amounts of dT in *dut1$_{org}$* might be caused by an increase in TK activity. Consistently, the amount of dT is higher in *dut1$_{org}$ tk1b* background than in the single mutant (see Niehaus et al., 2022 Figure 5A). Together the data indicate that in early germination salvage is boosted when organellar DUT1 is compromised suggesting that DUT1$_{org}$ participates in *de novo bio*synthesis.

The influence on dT content is also reflected, at least in tendency, in the relative abundance of cpDNA, which is the main sink of dTTP at this developmental stage. At time points 3 h and 144 h, a slight decrease in the relative abundance of cpDNA can be observed in the *DUT1$_{org}$* mutant (see Niehaus et al., 2022 Figure 6 and 9). Whereas, a significant decrease in cpDNA is observed in *dut1$_{org}$ tk1b* at time point 48 h compared to *tk1b* alone (see Niehaus et al., 2022 Figure 8).

The effect of *dut1$_{org}$* on dT levels as well as the effects of this mutation together with compromised salvage on cpDNA, indicate that DUT1$_{org}$ is involved in the *de novo* biosynthesis of dTTP. Nevertheless, there may be additional alternative pathways to dUMP, such as via a NUDIX hydrolase, which could dephosphorylate dUDP. Indeed, there are organisms for which it has been described that DUT1 is the sole source of dUMP and thus represents an essential enzyme in thymidylate synthesis (Chan et al. 2004; Varga et al. 2008). Considering the minor phenotype of *dut1$_{org}$*, it seems however unlikely that DUT1, including its cytosolic counterpart,

in plants are the sole source of dUMP. Taking into consideration *dhfr-ts2*, which represents a complete knock out of the organellar *de novo* biosynthesis, the hypothesis that $DUT1_{org}$ is not the only enzyme leading to dUMP can be supported. If $DUT1_{org}$ was the sole pathway to dUMP in mitochondria, *dhfr-ts2* and $dut1_{org}$ would have to be phenocopies of each other. In comparison, however, it is evident that the observed effects on metabolic level and the decreased abundance of cpDNA in *dhfr-ts2* are more severe (see Niehaus et al., 2022 Figure 7B and 8). The fact that the complete knockout is nevertheless lethal is presumably due to the main function of DUT1. It keeps the concentration of dUTP low in the cell, as it is a cytotoxic agent for the plant. Polymerases are unable to distinguish between dUTP and dTTP during synthesis, so a low U:T ratio is critical for proper DNA replication (Vértessy and Tóth 2009). This is probably why chloroplasts also possess DUT1, although they do not contain a DHFR-TS for *de novo* biosynthesis of dTMP.

The two DHFR-TS enzymes convert dUMP to dTMP. The respective mutants *dhfr-ts1* and *dhfr-ts2* show no visible phenotype (see Niehaus et al., 2022 Figure 3), but the double mutant is lethal. Lethality occurs during early embryonic development and is reflected by small white seeds with no discernible embryo, indicating that both enzymes are essential during seed development (Gorelova et al. 2017; Corral et al. 2018). As soon as only one allele of one of the active isoforms is present, the plant shows normal growth again (Gorelova et al. 2017). When considering metabolite levels, however, it is noticeable that *dhfr-ts2* has slightly decreased dT levels at the 3 h time point (see Niehaus et al., 2022 Figure 5A). This observation also holds true for the 48 h time point, when also a significant decrease in dTMP levels is also observed (see Niehaus et al., 2022 Figure 7 A, B). These effects are no longer evident after 144 h (see Niehaus et al., 2022 Figure 10 E). Comparable effects on dT are observed in *dhfr-ts1*, but in this case the significant effect on dTMP is present only at the last time point (see Niehaus et al., 2022 Figure 10 E), indicating a more prominent role for DHFR-TS1 in later stages after germination. Again, the decrease in dT in both mutants is an indication for an increased activity of the thymidine kinases, i.e. increased salvage activity. This idea is supported by the alteration of the dT pools in the double mutants *dhfr-ts2 tk1b* and *dhfr-ts1 tk1a*. Both have higher dT amounts than the corresponding *DHFR-TS* mutants. It is remarkable that as in $dut1_{org}$ *tk1b* the dT levels reached in *dhfr-ts2 tk1b* are higher than those of the wild type (see Niehaus et al., 2022 Figure 5A and 7A). A possible explanation for this overcompensation in the case of *dhfr-ts2 tk1b* apart from boosted salvage might be reduced dT degradation. This idea is

supported by higher xanthosine concentrations in the corresponding *dhfr-ts2* mutant at the 3 h time point (see Niehaus et al., 2022 Figure S8). Next to dT, xanthosine is a substrate of the purine nucleoside catabolic enzyme NSH1. How the mitochondrion relays a possible inhibiting signal to NSH1 is unknown.

The overall decrease in dTMP levels in the *DHFR-TS* mutants can be explained simply by the absence of the biosynthetic reaction in combination with the constant demand for thymidylates. The data suggests that DHFR-TS2 plays a more important role at an earlier stage than its cytosolic counterpart DHFR-TS1, whereas DHFR-TS1 has a more important role later at 144 h. Similar effects can also be found when looking at the relative abundance of cpDNA. In *dhfr-ts2* the cpDNA content is lower than in wild type already at the 3 h time point (see Niehaus et al., 2022 Figure 6), whereas in *dhfr-ts1* such an effect is only observed in tendency at the 144 h time point (see Niehaus et al., 2022 Figure 9). In summary, the biosynthetic reactions catalyzed by DHFR-TS1 and DHFR-TS 2 are as the reaction of RNR, essential for plant development. In contrast to RNR, the mitochondrial and cytosolic pathways of DHFR-TS can substitute each other. Each compartment by itself is capable of covering the cellular demand for dTMP which is derived from *de novo* biosynthesis. However, over time the importance of the two DHFR-TS enzymes shifts from predominant role of the mitochondrial pathway at the beginning of germination to a more equal role for both enzymes later.

The last enzyme to be discussed in this context is TMPK, which catalyzes the phosphorylation of dTMP to dTDP. This enzyme has been studied little in plants so far. It is known that the gene encodes two alternative transcripts of different length in the 5'-end. The mutation of both variants leads to plant death at the zygote stage, demonstrating the critical role of this enzyme (Ronceret et al. 2008). The protein encoded by the longer transcript was previously shown to be located in the mitochondria. In this thesis it was additionally demonstrated that the protein is also localizing in the chloroplast. Here it is likely responsible for phosphorylating the dTMP from the salvage pathway since *de novo* synthesis is like not present in chloroplasts (Niehaus et al. 2022). To further evaluate the role of TMPK in the organelles, mutating only the organellar TMPK with CRISPR was attempted similar to the strategy used for DUT1, however in contrast to $dut1_{org}$ the corresponding *TMPK* mutant is lethal. Evaluation of the pods in the segregating population shows that about 25% of the seeds shrivel and turn brown about 2 to 3 weeks after pollination. From this, embryo lethality can be assumed. A similar picture emerges when looking at a cytosolic knockout variant, which has a 30 base pair deletion

affecting the start codon of the cytosolic variant and the 9 amino acids towards the N-terminus. Therefore, it cannot be completely ruled out that the observed embryo lethality of the cytosolic *TMPK* mutant is due to a decreased enzymatic activity of the organellar TMPK variant (Niehaus, unpublished; B.Sc. thesis Lukas Wiechmann). Nevertheless, one conclusion from these phenotypic observations is that the cytosolic and organelle pathways can substitute for each other, at least during the development of the zygote, because the single mutants die at a later stage compared to a mutant lacking both variants. Autonomy of each compartment in respect to thymidylate supply, on the other hand, becomes more important during embryo development. This could be due to the availability of suitable transporters for dTMP or dTDP, which, depending on their expression, allow exchange between compartments. Indeed, a look at the expression profile of the potential nucleotide transporters NDT1 and NDT2 during seed maturation shows that they are differentially expressed at this stage and thus, at least in this case, cooperation between the compartments is possible.

In comparison to mitochondria, chloroplasts do not possess DHFR-TS for *de novo* biosynthesis but they do contain all other enzymes required for thymidylate synthesis, which is a strong indication that chloroplasts do rely on supply from the cytosol or mitochondrion, at least with respect to this enzyme. Considering the *TK1b* mutant, which is abolished in the organellar salvage of dT to dTMP, having a chlorotic phenotype during early germination but not at later stages (see chapter 1.4.3), it can be assumed that dT can be transported, at least later in development. In addition, the *DHFR-TS2* mutant has in tendency a lower content of cpDNA 3 h after transfer to growth conditions. This tendency is strengthened in *dhfr-ts2 tk1b*, which shows a significant additive effect on cpDNA of *dhfr-ts2* on *tk1b* alone (see Niehaus et al., 2022 Figure 6). This suggests a limited transport during early germination of thymidylates synthesized by DHFR-TS2 in mitochondria to chloroplasts where is contributes to DNA synthesis in the chloroplast.

1.4.2 Conversion of C to T

DCD has a mitochondrial localization and is responsible for the deamination of dCMP to dUMP which then can be further used for thymidylate synthesis. It thus creates a link between the deoxycytidilate pools and thymidylate pools and helps to adjust the balance between them.

1.4 Thymidylate Synthesis during Germination

We tested the hypothesis that deamination of dCMP by DCD has an impact on the thymidylate synthesis by increasing the dUMP pool. The mutant of *DCD* shows a wild type phenotype (see Niehaus et al., 2022 Figure 3). At the metabolite level, an increase in dCTP content can be observed 48 h and 144 h after transfer to growth conditions (see Niehaus et al., 2022 Figure 7 E and 10 B). In addition, a lower concentration of dTMP and in tendency for dATP and dGTP (see Niehaus et al., 2022 Figure 10 A, C and E), as well as a reduced amount of cpDNA is evident for the 144 h time point (see Niehaus et al., 2022 Figure 9). However, an influence on dTTP is not detectable for any time points.

By contrast, the *DCD* mutant in rice shows a clear aberrant phenotype with reduced growth, smaller seeds and chlorotic leaves. The analysis on metabolite level of 10 days old seedlings shows that this mutant has more dCTP and less dTTP among other effects. Furthermore, it could be shown that the altered dNTP ratios and the decrease of dTTP are responsible for the phenotype. In the affected plant chloroplasts, cpDNA replication is affected, transcription is reduced, and their division is inhibited, ultimately leading to a chlorotic phenotype of the plant. It is therefore concluded, that DCD plays a critical role for the synthesis of dTTP in rice (Niu et al. 2017).

Considering these contrasting phenotypic observations, the question of the biological significance of DCD in Arabidopsis arises. It appears that DCD plays a minor role in dTTP synthesis in Arabidopsis and is rather involved in the control of the dCTP pool. It was previously suggested that another enzyme, CDA may compensate for a lack of DCD (Niu et al. 2017). This enzyme is capable of deaminating both cytidine and dC (Faivre-Nitschke et al. 1999; Chen et al. 2016; Straube et al. 2021a). It is conceivable that there is an accumulation of dC in *dcd*, which is then converted to dU by CDA and followed up by a phosphorylation to dUMP by TK (Clausen et al. 2012). This could minimize the effect of DCD in Arabidopsis, as compared to rice. However, *CDA* loss-of-function seedlings were shown to have increased levels of dTTP compared to the wild type (Straube et al. 2021a) and thus it does not seem likely that CDA and DCD fulfill redundant functions in Arabidopsis.

Another observation regarding the potential importance of DCD is demonstrated when looking at *dhfr-ts2 dcd*. Currently it was not possible to isolate a double mutant. So far, only variants were found that were homozygous for one mutation and heterozygous for the other, but did not exhibit a phenotype different from wild type. However, more plants need to be analyzed to claim that a *DHFR-TS2 DCD* double mutant is lethal. One hypothesis is that DCD

supplies dUMP in the cytosol as substrate for DHFR-TS1, thus a loss-of-function in *DCD* abolishes the cytosolic *de novo* biosynthesis. Therefore, a *DHFR-TS2 DCD* double mutant would have a completely abolished *de novo* synthesis similar to the *DHFR-TS1 DHFR-T2* double mutant that is lethal as well (Gorelova et al. 2017). This is consistent with the observation that the DCD is not localized in the matrix of the mitochondrion but is located in the outer or inner membrane or in the intermembrane space (see Niehaus et al., 2022 Figure S3 F). When comparing *dcd* and *dhfr-ts1* at the metabolic level, it was noticed that a reduction in dTMP concentration is only observed at time point 144 h for both. However, this effect tends to be stronger for *dcd* (see Niehaus et al., 2022 Figure 10 E), which also applies to the effect on cpDNA at this time point (see Niehaus et al., 2022 Figure 9). Implying, that DCD not only provides dUMP to the cytosol but also to some extent to the mitochondrion.

Based on the available data the relevance of DCD for *Arabidopsis thaliana* remains unclear. When Arabidopsis DCD is compared with the rice ortholog, it effects on the balance of the C:T ratio and also its effects on the biosynthesis of dTTP do not seem to be of crucial importance. However, it is possible that it plays an important role in maintaining dNTP ratios by fine-tuning these through the RNR via dTTP, which is indicated by the lower concentrations of dATP and dGTP in the *DCD* mutant at the 144 h time point (see Niehaus et al., 2022 Figure 10 A, C). The most important enzyme for adjusting these ratios is the RNR, which can be activated and inhibited in various ways by dATP, dGTP and dTTP, but not dUTP and dCTP. In this way, the *de novo* biosynthesis of the building blocks is feedback regulated to adjust the preferred ratios of the dNTP pools. In addition to RNR, however, it is feasible that the DCD not only brings an additional level of control for the dNTP ratios by catalyzing one of the reactions necessary for the conversion of C to T. But also enables a putative indirect involvement of dCTP via dTTP, which then can be used for allosterically regulation of the RNR. If DCD therefore ensures a low mutation rate was not tested in this work. Including CDA in the consideration of the weak influence of *dcd* on thymidylate pools, a putative existing functional redundancy between the two enzymes could be an explanation for the only small effects on thymidylates of *dcd*, as postulated before (Niu et al. 2017). Consequently, both enzymes combined would be responsible for the deamination of dCMP to dUMP. When this is taken into account together with the potential lethality of *dhfr-ts2 dcd,* a new picture of DCD emerges. In this DCD appears to have a critical function in the supply of dUMP for the cytosol, with possible support in part from CDA.

1.4.3 Salvage Pathway

De novo biosynthesis of dTTP is an energy-intensive process. To generate dTMP from UDP, 3 reduction equivalents are needed. Therefore, it is advantageous that there is a pathway that can return free dT and dU to the biosynthesis, the salvage pathway. The enzymes responsible for this process are the thymidine kinases TK1a and TK1b. However, not all deoxyribonucleosides are recycled because they can also be hydrolytically cleaved by NSH1 into their nucleobase and 2-deoxyribose followed by further degradation (Straube et al. 2021a). One putative source for free deoxyribonucleosides is the degradation of DNA, for example in the course of DNA damage repair (DDR). DDR plays an important role in the course of germination. During the dormant phase of the seed, various mutations may have occurred in the DNA that need to be repaired at an early stage to ensure optimal development of a healthy plant (Waterworth et al. 2016). Looking at the development of the dT level during germination, it can be observed that after transport to growth conditions, dT increases very rapidly and continuously. Interestingly, this trend does not hold true for dC (see Niehaus et al., 2022 Figure 4A). If DNA damage is the primary source of deoxyribonucleosides, the levels of all canonical deoxyribonucleosides should behave identically, unless their respective salvage enzyme activities are different. To test this idea, mutant lines for five enzymes relevant for DDR, UV Radiation 1 (RAD1), Ataxia-Telangiectasia Mutated 1 (ATM-1), Ataxia-Telangiectasia Mutated and RAD3-Related (ATR-2), Centrin 2 (CEN2) and Damaged DNA Binding Protein 1A (DDB1-A), were examined 48 h after transfer to growth conditions. Among all DDR mutants no dT concentration lower than wild type was observed and in the case of *rad-1* and *atm-2* there was even a higher dT concentration (see Niehaus et al., 2022 Figure 12). These observations suggest that, at least during germination, the main source of dT is not DDR.

To date, no direct synthesis pathway for dT is known. Therefore, a possible alternative source of dT could be dTMP, which is dephosphorylated to dT by an unknown phosphatase. This hypothesis is supported by observing the development of the dTMP pool during germination. Immediately at the beginning of the transfer to growth conditions there is a slight decrease and only after about 36 hours a significant increase of the pool size. By this time, however, the concentration of dT has approximately doubled and is now around 8 times higher than dTMP (see Niehaus et al., 2022 Figure 4 A, B). This supports the idea that, on the one hand, the dTMP stored in the seed is first dephosphorylated to dT, which would explain the immediate

increase in dT and the initial stagnation of the dTMP level. On the other hand, it also suggests that the dTMP newly synthesized via *de novo* biosynthesis is first dephosphorylated as well. Such seemingly pointless metabolic pathways that run in opposite directions are called futile cycles. In many cases they serve for heat generation, i.e in the bumblebee (Newsholme et al. 1972). However, in the context of DNA, another explanation might be more appropriate. As already described, it is important to keep the mutation rate low. This includes not only repairing damage that occurs in existing DNA, but also preventing errors during DNA synthesis. Such errors can be caused by aberrant deoxyribonucleotides that are not recognized as such by the polymerase and are therefore incorporated into the DNA. The origin of these faulty deoxyribonucleotides could be, among other things, the degradation of DNA with epigenetic markers (Zauri et al. 2015) or could be caused by oxidative stress (Yu et al. 2016), a concept that has been researched predominantly in humans so far. This leads to the idea that there has to be a quality control of the deoxyribonucleotides. In the case of the DNA building block dTTP, this could proceed in such a way that the entire pool of dTMP, including modified variants, is dephosphorylated to dT by a non-specific phosphatase, and phosphorylated again to dTMP by TK1a and TK1b. To be effective for purifying the dTMP pool both TKs would need to exhibit high substrate specificity for unmodified dT. Furthermore, this model implies that the original and the purified dTMP pool can be somehow distinguished. This could be achieved by substrate channeling between the TK and the TMPK preventing the release of purified dTMP.

Independent of a potential role in quality control, TKs have an important and already proven function for thymidylate synthesis, the phosphorylation of dT to dTMP. Looking at the phenotypes of *tk1a* and *tk1b*, it is noticeable that *tk1a* does not differ from the wild type, whereas *tk1b* exhibits chlorotic cotyledons (see Niehaus et al., 2022 Figure 3) and reduced root growth in the early germination phase. By contrast, the *TK1a TK1b* double mutant has white cotyledons and greatly reduced growth (Clausen et al. 2012; Xu et al. 2015; Pedroza-García et al. 2019). Survival of this mutant is only possible with the addition of sugar during the first two weeks of development. The addition of sugar leads to activation of *de novo* biosynthesis, which can partially substitute for the role of salvage. In these plants, there is partial greening of some leaf areas but no seed formation (Pedroza-García et al. 2019). Closer examination of the chlorotic cotyledons of *tk1b* show that they exhibit the strongest differences from the wild type 3 days after transfer to growth conditions and slowly turn green

over time until they are indistinguishable 6 days after transfer to growth (see Niehaus et al., 2022 Figure 3 and S6 A).

These observations on the individual mutants are also reflected at the level of metabolism. While *tk1a* shows a reduced dTMP concentration compared to the wild type only at time point 144 h, this is true for *tk1b* at every time point examined. Here, the effect on dTMP is least pronounced at time point 3 h which coincides with no differences in dT concentrations. However, at the 48 h time point *tk1a* and *tk1b* both have a higher dT concentration (see Niehaus et al., 2022 Figure 5 A, B, Figure 7 A, B and Figure 10 A, B), which implies that both enzymes are active during this stage. This result for *tk1a* is in contrast to the measured dTMP concentrations, which are comparable to wild type concentrations during this time. Based on this the question arises why the concentration of dTMP in the *TK1b* mutant decreases, whereas this does not occur in *tk1a* until time point 144 h, although both enzymes have been shown to be already active and a demand for dTMP is present. The likely answer to this question lies in the subcellular separation of the two enzymes and the location of the major sink of deoxyribonucleotides at the time of germination. As described earlier, replication of cpDNA is the major sink at this time, and therefore TK1b, which is localized in the chloroplast, has an important function as a supplier of dTMP. Salvage is the only direct source of dTMP for chloroplasts, as they lack a DHFR-TS for *de novo* biosynthesis. The cytosol, on the other hand, can synthesize dTMP both by *de novo* biosynthesis via DHFR-TS1 and by salvage realized by TK1a. However, at this stage of germination, the requirement for thymidylates in the cytosol is minimal because ncDNA synthesis has not yet started (Masubelele et al. 2005; Sliwinska et al. 2009). In principle the plastid could benefit from the cytosolic dTMP synthesis capacity but the respective chloroplastic transporters seem to be not fully available at this early stage. These are formed later in development. This is consistent with the expression profile of the potential thymidylate transporter NDT1 in chloroplasts, which shows low expression during early germination but is strongly induced around 48 h after transfer to growth conditions. This idea is also supported by the fact that the cotyledons of *tk1b* turn green over time. By contrast, the candidate for the mitochondrial thymidylate transporter, NDT2, is already well expressed at an early stage, which would enable the supply of the chloroplast by the mitochondrion.

It can be assumed that the dTMP made by TK1b or arriving in the chloroplast is rapidly converted to dTTP and directly used for the synthesis of cpDNA. According to this idea, the dTMP that can be measured in *tk1b* therefore represents the level of dTMP that is not

accessible for the chloroplast, the cytosolic and mitochondrial dTMP pool. For these pools the concentration of dTMP remains stable, because the need for thymidylates in the respective compartments is low. This would explain why *dhfr-ts2 tk1b* has the same dTMP concentration as *tk1b*, although both single mutants have a significant influence on their own.

Looking at cpDNA, *tk1b* already has an effect 3 hours after transfer to growth conditions, with this effect being stronger at the two subsequent time points. By contrast *tk1a* has an effect on cpDNA only at time point 144 h. In the case of *dhfr-ts2 tk1b*, a significant reduction is evident at the 3 h time point compared with *tk1b* (see Niehaus et al., 2022 Figure 6, 8 and 9), which supports the idea that the mitochondrion is involved in supplying the chloroplast. This observation could also be the explanation for the more drastic phenotype of this double mutant. Compared to *tk1b* alone, the double mutant *dhfr-ts2 tk1b* exhibits more severe chlorosis, and white leaf areas form within the cotyledons after a short time, which are persistent (see Niehaus et al., 2022 Figure 3A and S6 A).

The salvage pathway plays a crucial role especially in the early phase of germination. TK1b, which is mainly responsible for supplying the chloroplast with dTMP, is particularly important here. The cytosolic and mitochondrial salvage does not contribute significantly to the thymidylate pools in this stage of germination, as also shown by a hemicomplementation of TK1b. Here, TK1b was specifically complemented in the background of a *TK1b* mutant only in mitochondria or chloroplasts using a mitochondrial or plastid transit peptide, respectively. Recovery of plastid TK1b function in the *dhfr-ts2 tk1b* background resulted in the absence of the chlorotic phenotype. In the case of mitochondrial TK1b complementation, development of a plant with fewer chlorosis also occurred, but they still exhibited a higher degree of chlorosis than plastid complementation (see Niehaus et al., 2022 Figure 11). Nevertheless, this also supports the idea that the mitochondrion is involved, at least in part, in supplying the chloroplasts at early stages. However, at later time points, the chloroplast can be completely supplied with thymidylates by the cytosol and the mitochondrion.

The plastid phenotype observed in *tk1b* is primarily due to an undersupply of dTTP in the chloroplast. In this mutant, there is not only a reduction in cpDNA (Le Ret et al. 2018), but effects on the cellular pools of canonical dNTP are also evident. At the 48 h time point, an enrichment of all dNTPs except dTTP can be observed here (see Niehaus et al., 2022 Figure 7). Due to the strongly inhibited synthesis of cpDNA by the dTTP deficiency, the remaining dNTPs are accumulated. It can also be concluded that the measurable level of dTTP in *tk1b*, which

show no difference from wild type, represents the pool of cytosolic and mitochondrial dTTP that is not accessible for the chloroplast. The amount of cpDNA in the chloroplast is a critical factor for the maturation of the same. First, during development from plastid over etioplast to chloroplast, many plastid genes, such as photosystems, must be transcribed, which can be accelerated by high cpDNA copy number. This becomes clear when considering gene expression of plastid genes in the *TK1b* mutant background. In these cases, there is a strong reduction of the corresponding mRNAs and the associated proteins in the respective mutants (Le Ret et al. 2018). Since mRNAs are not made all canonical ribonucleotides pools are higher in the *tk1b* background (see Niehaus et al., 2022 Figure S10). The genome copy number also plays an important role in chloroplast division. Division only occurs when a certain copy number is reached. Depending on the cell type and developmental stage, there are about 40 to 120 chloroplasts in a plant cell, each of which in turn contains about 40 to 80 copies of its genome, making the chloroplast to a major sink for thymidylates during germination (Dobrogojski et al. 2020).

1.5 References

Agius, Stephanie C.; Rasmusson, Allan G.; Møller, Ian M. (2001): NAD(P) turnover in plant mitochondria. In *Functional Plant Biol.* 28 (6), p. 461. DOI: 10.1071/PP00155.

Ashihara, Hiroshi; Ludwig, Iziar A.; Crozier, Alan (2020): Plant Nucleotide Metabolism - Biosynthesis, Degradation, and Alkaloid Formation: Wiley.

Avery, O. T.; Macleod, C. M.; McCarty, M. (1944): Studies on the chemical nature of the substance inducing transformation of pneumococcal types: induction of transformation by a desoxyribonucleic acid fraction isolated from pneumococcus type III. In *The Journal of Experimental Medicine* 79 (2), pp. 137–158. DOI: 10.1084/jem.79.2.137.

Baccolini, Chiara; Witte, Claus-Peter (2019): AMP and GMP Catabolism in Arabidopsis Converge on Xanthosine, Which Is Degraded by a Nucleoside Hydrolase Heterocomplex. In *The Plant Cell* 31 (3), pp. 734–751. DOI: 10.1105/tpc.18.00899.

Behrens, M.; Thalaker, R. (1957): Gewinnung von Chloroplasten in nichtwässrigem Milieu. In *Die Naturwissenschaften* (44), p. 621.

Bieleski, R. L. (1964): The problem of halting enzyme action when extracting plant tissues. In *Analytical Biochemistry* 9 (4), pp. 431–442. DOI: 10.1016/0003-2697(64)90204-0.

Bölter, Bettina; Sharma, Rita; Soll, Jürgen (2007): Localisation of Arabidopsis NDPK2--revisited. In *Planta* 226 (4), pp. 1059–1065. DOI: 10.1007/s00425-007-0549-4.

Buckland, Robert J.; Watt, Danielle L.; Chittoor, Balasubramanyam; Nilsson, Anna Karin; Kunkel, Thomas A.; Chabes, Andrei (2014): Increased and imbalanced dNTP pools symmetrically promote both leading and lagging strand replication infidelity. In *PLoS Genetics* 10 (12), e1004846. DOI: 10.1371/journal.pgen.1004846.

CAVALIER-SMITH, T.; LEE, JOHN J. (1985): Protozoa as Hosts for Endosymbioses and the Conversion of Symbionts into Organelles 1,2. In *The Journal of Protozoology* 32 (3), pp. 376–379. DOI: 10.1111/j.1550-7408.1985.tb04031.x.

Chan, Sum; Segelke, Brent; Lekin, Timothy; Krupka, Heike; Cho, Uhn Soo; Kim, Min-Young et al. (2004): Crystal structure of the Mycobacterium tuberculosis dUTPase: insights into the catalytic mechanism. In *Journal of Molecular Biology* 341 (2), pp. 503–517. DOI: 10.1016/j.jmb.2004.06.028.

Chen, Kun Ling; Xu, Min Xin; Li, Guang Yong; Liang, Hui; Xia, Zong Liang; Liu, Xin et al. (2006): Identification of AtENT3 as the main transporter for uridine uptake in Arabidopsis roots. In *Cell Research* 16 (4), pp. 377–388. DOI: 10.1038/sj.cr.7310049.

Chen, Mingjia; Herde, Marco; Witte, Claus-Peter (2016): Of the Nine Cytidine Deaminase-Like Genes in Arabidopsis, Eight Are Pseudogenes and Only One Is Required to Maintain Pyrimidine Homeostasis in Vivo. In *Plant Physiology* 171 (2), pp. 799–809. DOI: 10.1104/pp.15.02031.

Clausen, Anders R.; Girandon, Lenart; Ali, Ashfaq; Knecht, Wolfgang; Rozpedowska, Elzbieta; Sandrini, Michael P. B. et al. (2012): Two thymidine kinases and one multisubstrate deoxyribonucleoside kinase salvage DNA precursors in Arabidopsis thaliana. In *The FEBS journal* 279 (20), pp. 3889–3897. DOI: 10.1111/j.1742-4658.2012.08747.x.

Clausen, Anders R.; Mutahir, Zeeshan; Munch-Petersen, Birgitte; Piškur, Jure (2014): Plants salvage deoxyribonucleosides in mitochondria. In *Nucleosides, nucleotides & nucleic acids* 33 (4-6), pp. 291–295. DOI: 10.1080/15257770.2013.853782.

Corral, Maxime G.; Haywood, Joel; Stehl, Luca H.; Stubbs, Keith A.; Murcha, Monika W.; Mylne, Joshua S. (2018): Targeting plant DIHYDROFOLATE REDUCTASE with antifolates and mechanisms for genetic resistance. In *The Plant journal : for cell and molecular biology*. DOI: 10.1111/tpj.13983.

Dahm, Ralf (2005): Friedrich Miescher and the discovery of DNA. In *Developmental biology* 278 (2), pp. 274–288. DOI: 10.1016/j.ydbio.2004.11.028.

Dietz, Karl-Josef (2017): Subcellular metabolomics: the choice of method depends on the aim of the study. In *Journal of experimental botany* 68 (21-22), pp. 5695–5698. DOI: 10.1093/jxb/erx406.

Dobrogojski, Jędrzej; Adamiec, Małgorzata; Luciński, Robert (2020): The chloroplast genome: a review. In *Acta Physiol Plant* 42 (6). DOI: 10.1007/s11738-020-03089-x.

Dorion, Sonia; Matton, Daniel P.; Rivoal, Jean (2006): Characterization of a cytosolic nucleoside diphosphate kinase associated with cell division and growth in potato. In *Planta* 224 (1), pp. 108–124. DOI: 10.1007/s00425-005-0199-3.

Dubois, Emeline; Córdoba-Cañero, Dolores; Massot, Sophie; Siaud, Nicolas; Gakière, Bertrand; Domenichini, Séverine et al. (2011): Homologous recombination is stimulated by a decrease in dUTPase in Arabidopsis. In *PloS one* 6 (4), e18658. DOI: 10.1371/journal.pone.0018658.

el-Hajj, H. H.; Zhang, H.; Weiss, B. (1988): Lethality of a dut (deoxyuridine triphosphatase) mutation in Escherichia coli. In *Journal of bacteriology* 170 (3), pp. 1069–1075. DOI: 10.1128/jb.170.3.1069-1075.1988.

Fairhead, Michael; Howarth, Mark (2015): Site-specific biotinylation of purified proteins using BirA. In *Methods in molecular biology (Clifton, N.J.)* 1266, pp. 171–184. DOI: 10.1007/978-1-4939-2272-7_12.

Faivre-Nitschke, S. E.; Grienenberger, J. M.; Gualberto, J. M. (1999): A prokaryotic-type cytidine deaminase from Arabidopsis thaliana gene expression and functional characterization. In *European journal of biochemistry* 263 (3), pp. 896–903. DOI: 10.1046/j.1432-1327.1999.00591.x.

Fujie, Makoto; Kuroiwa, Haruko; Kawano, Shigeyuki; Mutoh, Shoshi; Kuroiwa, Tsuneyoshi (1994): Behavior of organelles and their nucleoids in the shoot apical meristem during leaf development in Arabidopsis thaliana L. In *Planta* 194 (3). DOI: 10.1007/BF00197541.

Gadsden, M. H.; McIntosh, E. M.; Game, J. C.; Wilson, P. J.; Haynes, R. H. (1993): dUTP pyrophosphatase is an essential enzyme in Saccharomyces cerevisiae. In *The EMBO journal* 12 (11), pp. 4425–4431.

Garton, Sarah; Knight, Heather; Warren, Gareth J.; Knight, Marc R.; Thorlby, Glenn J. (2007): crinkled leaves 8--a mutation in the large subunit of ribonucleotide reductase—leads to defects in leaf development and chloroplast division in Arabidopsis thaliana. In *The Plant journal : for cell and molecular biology* 50 (1), pp. 118–127. DOI: 10.1111/j.1365-313X.2007.03035.x.

Gilar, Martin; DeLano, Mathew; Gritti, Fabrice (2021): Mitigation of analyte loss on metal surfaces in liquid chromatography. In *Journal of chromatography. A* 1650, p. 462247. DOI: 10.1016/j.chroma.2021.462247.

Gorelova, Vera; Lepeleire, Jolien de; van Daele, Jeroen; Pluim, Dick; Meï, Coline; Cuypers, Ann et al. (2017): Dihydrofolate Reductase/Thymidylate Synthase Fine-Tunes the Folate Status and Controls Redox Homeostasis in Plants. In *The Plant cell* 29 (11), pp. 2831–2853. DOI: 10.1105/tpc.17.00433.

Gray, M. W.; Burger, G.; Lang, B. F. (1999): Mitochondrial evolution. In *Science (New York, N.Y.)* 283 (5407), pp. 1476–1481. DOI: 10.1126/science.283.5407.1476.

Griffith, F. (1928): The Significance of Pneumococcal Types. In *The Journal of hygiene* 27 (2), pp. 113–159. DOI: 10.1017/S0022172400031879.

Heber, U. (1957): Über die Lokalisation von löslichen Zuckern in der Pflanzenzelle. In *Berichte der Deutschen Botanischen Gesellschaf* (70), pp. 371–382.

Hirose, Naoya; Makita, Nobue; Yamaya, Tomoyuki; Sakakibara, Hitoshi (2005): Functional characterization and expression analysis of a gene, OsENT2, encoding an equilibrative nucleoside transporter in rice suggest a function in cytokinin transport. In *Plant physiology* 138 (1), pp. 196–206. DOI: 10.1104/pp.105.060137.

Ikuma, H.; Tetley, R. M. (1976): Possible Interference by an Acid-stable Enzyme during the Extraction of Nucleoside Di- and Triphosphates from Higher Plant Tissues. In *Plant physiology* 58 (3), pp. 320–323. DOI: 10.1104/pp.58.3.320.

Jung, Benjamin; Flörchinger, Martin; Kunz, Hans-Henning; Traub, Michaela; Wartenberg, Ruth; Jeblick, Wolfgang et al. (2009): Uridine-ribohydrolase is a key regulator in the uridine degradation pathway of Arabidopsis. In *The Plant cell* 21 (3), pp. 876–891. DOI: 10.1105/tpc.108.062612.

Ku, Chuan; Nelson-Sathi, Shijulal; Roettger, Mayo; Garg, Sriram; Hazkani-Covo, Einat; Martin, William F. (2015): Endosymbiotic gene transfer from prokaryotic pangenomes: Inherited chimerism in eukaryotes. In *Proceedings of the National Academy of Sciences of the United States of America* 112 (33), pp. 10139–10146. DOI: 10.1073/pnas.1421385112.

Kumar, Dinesh; Abdulovic, Amy L.; Viberg, Jörgen; Nilsson, Anna Karin; Kunkel, Thomas A.; Chabes, Andrei (2011): Mechanisms of mutagenesis in vivo due to imbalanced dNTP pools. In *Nucleic acids research* 39 (4), pp. 1360–1371. DOI: 10.1093/nar/gkq829.

Kunz, B. A.; Kohalmi, S. E. (1991): Modulation of mutagenesis by deoxyribonucleotide levels. In *Annual review of genetics* 25, pp. 339–359. DOI: 10.1146/annurev.ge.25.120191.002011.

Le Ret, Monique; Belcher, Susan; Graindorge, Stéfanie; Wallet, Clémentine; Koechler, Sandrine; Erhardt, Mathieu et al. (2018): Efficient Replication of the Plastid Genome Requires an Organellar Thymidine Kinase. In *Plant physiology* 178 (4), pp. 1643–1656. DOI: 10.1104/pp.18.00976.

Lincker, Frédéric; Philipps, Gabriel; Chabouté, Marie-Edith (2004): UV-C response of the ribonucleotide reductase large subunit involves both E2F-mediated gene transcriptional regulation and protein subcellular relocalization in tobacco cells. In *Nucleic acids research* 32 (4), pp. 1430–1438. DOI: 10.1093/nar/gkh310.

Luzarowski, Marcin; Kosmacz, Monika; Sokolowska, Ewelina; Jasinska, Weronika; Willmitzer, Lothar; Veyel, Daniel; Skirycz, Aleksandra (2017): Affinity purification with metabolomic and proteomic analysis unravels diverse roles of nucleoside diphosphate kinases. In *Journal of experimental botany* 68 (13), pp. 3487–3499. DOI: 10.1093/jxb/erx183.

Masubelele, Nompumelelo H.; Dewitte, Walter; Menges, Margit; Maughan, Spencer; Collins, Carl; Huntley, Rachael et al. (2005): D-type cyclins activate division in the root apex to promote seed germination in Arabidopsis. In *Proceedings of the National Academy of Sciences of the United States of America* 102 (43), pp. 15694–15699. DOI: 10.1073/pnas.0507581102.

McFadden, Geoffrey I.; van Dooren, Giel G. (2004): Evolution: red algal genome affirms a common origin of all plastids. In *Current biology : CB* 14 (13), R514-6. DOI: 10.1016/j.cub.2004.06.041.

Meyer, Reiner; Wagner, Karl G. (1985): Determination of nucleotide pools in plant tissue by high-performance liquid chromatography. In *Analytical biochemistry* 148 (2), pp. 269–276. DOI: 10.1016/0003-2697(85)90228-3.

Newsholme, E. A.; Crabtree, B.; Higgins, S. J.; Thornton, S. D.; Start, C. (1972): The activities of fructose diphosphatase in flight muscles from the bumble-bee and the role of this enzyme in heat generation. In *The Biochemical journal* 128 (1), pp. 89–97. DOI: 10.1042/bj1280089.

Niehaus, Markus; Straube, Henryk; Künzler, Patrick; Rugen, Nils; Hegermann, Jan; Giavalisco, Patrick et al. (2020): Rapid Affinity Purification of Tagged Plant Mitochondria (Mito-AP) for Metabolome and Proteome Analyses. In *Plant physiology* 182 (3), pp. 1194–1210. DOI: 10.1104/pp.19.00736.

Niehaus, Markus; Straube, Henryk; Specht, André; Baccolini, Chiara; Witte, Claus-Peter; Herde, Marco (2022): The nucleotide metabolome of germinating Arabidopsis thaliana seeds reveals a central role for thymidine phosphorylation in chloroplast development. In *The Plant cell*. DOI: 10.1093/plcell/koac207.

Nieman, Richard H.; Pap, Dennis L.; Clark, Robert A. (1978): Rapid purification of plant nucleotide extracts with xad-2, polyvinylpolypyrrolidone and charcoal. In *Journal of Chromatography A* 161, pp. 137–146. DOI: 10.1016/S0021-9673(01)85221-3.

Niu, Mei; Wang, Yihua; Wang, Chunming; Lyu, Jia; Wang, Yunlong; Dong, Hui et al. (2017): ALR encoding dCMP deaminase is critical for DNA damage repair, cell cycle progression and plant development in rice. In *Journal of experimental botany* 68 (21-22), pp. 5773–5786. DOI: 10.1093/jxb/erx380.

NYGAARD, P. E.R. (1972): Deoxyribonucleotide Pools in Plant Tissue Cultures. In *Physiol Plant* 26 (1), pp. 29–33. DOI: 10.1111/j.1399-3054.1972.tb03541.x.

Palmieri, Ferdinando; Rieder, Benjamin; Ventrella, Angela; Blanco, Emanuela; Do, Phuc Thi; Nunes-Nesi, Adriano et al. (2009): Molecular identification and functional characterization of Arabidopsis thaliana mitochondrial and chloroplastic NAD+ carrier proteins. In *The Journal of biological chemistry* 284 (45), pp. 31249–31259. DOI: 10.1074/jbc.M109.041830.

Paszkiewicz, Gaël; Gualberto, José M.; Benamar, Abdelilah; Macherel, David; Logan, David C. (2017): Arabidopsis Seed Mitochondria Are Bioenergetically Active Immediately upon Imbibition and Specialize via Biogenesis in Preparation for Autotrophic Growth. In *The Plant cell* 29 (1), pp. 109–128. DOI: 10.1105/tpc.16.00700.

Pedroza-García, José-Antonio; Nájera-Martínez, Manuela; Mazubert, Christelle; Aguilera-Alvarado, Paulina; Drouin-Wahbi, Jeannine; Sánchez-Nieto, Sobeida et al. (2019): Role of pyrimidine salvage pathway in the maintenance of organellar and nuclear genome integrity. In *The Plant journal : for cell and molecular biology* 97 (3), pp. 430–446. DOI: 10.1111/tpj.14128.

Roberts, JKM.; Aubert, S.; Gout, E.; Bligny, R.; Douce, R. (1997): Cooperation and Competition between Adenylate Kinase, Nucleoside Diphosphokinase, Electron Transport, and ATP Synthase in Plant Mitochondria Studied by 31P-Nuclear Magnetic Resonance. In *Plant physiology* 113 (1), pp. 191–199. DOI: 10.1104/pp.113.1.191.

Ronceret, Arnaud; Gadea-Vacas, Jose; Guilleminot, Jocelyne; Lincker, Frédéric; Delorme, Valérie; Lahmy, Sylvie et al. (2008): The first zygotic division in Arabidopsis requires de novo transcription of thymidylate kinase. In *The Plant journal : for cell and molecular biology* 53 (5), pp. 776–789. DOI: 10.1111/j.1365-313X.2007.03372.x.

Roy, B.; Beuneu, C.; Roux, P.; Buc, H.; Lemaire, G.; Lepoivre, M. (1999): Simultaneous determination of pyrimidine or purine deoxyribonucleoside triphosphates using a polymerase assay. In *Analytical biochemistry* 269 (2), pp. 403–409. DOI: 10.1006/abio.1999.4051.

Sauge-Merle, S.; Falconet, D.; Fontecave, M. (1999): An active ribonucleotide reductase from Arabidopsis thaliana cloning, expression and characterization of the large subunit. In *European journal of biochemistry* 266 (1), pp. 62–69. DOI: 10.1046/j.1432-1327.1999.00814.x.

Sawert, Axel; Backer, Anke; Plank-Schumacher, Karin-Heide; Wagner, Karl G. (1987): Determination of Nucleotides and Nucleosides in Cereal Leaves by High Performance Liquid Chromatography. In *Journal of Plant Physiology* 127 (1-2), pp. 183–186. DOI: 10.1016/S0176-1617(87)80054-8.

Sliwinska, Elwira; Bassel, George W.; Bewley, J. Derek (2009): Germination of Arabidopsis thaliana seeds is not completed as a result of elongation of the radicle but of the adjacent transition zone and lower hypocotyl. In *Journal of experimental botany* 60 (12), pp. 3587–3594. DOI: 10.1093/jxb/erp203.

Solter, Alan W.; Handschumacher, R. E. (1969): A rapid quantitative determination of deoxyribonucleoside triphosphates based on the enzymatic synthesis of DNA. In *Biochimica et Biophysica Acta (BBA) - Nucleic Acids and Protein Synthesis* 174 (2), pp. 585–590. DOI: 10.1016/0005-2787(69)90288-3.

Somasekaram, A.; Jarmuz, A.; How, A.; Scott, J.; Navaratnam, N. (1999): Intracellular localization of human cytidine deaminase. Identification of a functional nuclear localization signal. In *The Journal of biological chemistry* 274 (40), pp. 28405–28412. DOI: 10.1074/jbc.274.40.28405.

Spetea, Cornelia; Hundal, Torill; Lundin, Björn; Heddad, Mounia; Adamska, Iwona; Andersson, Bertil (2004): Multiple evidence for nucleotide metabolism in the chloroplast thylakoid lumen. In *Proceedings of the National Academy of Sciences of the United States of America* 101 (5), pp. 1409–1414. DOI: 10.1073/pnas.0308164100.

Straube, Henryk; Niehaus, Markus; Zwittian, Sarah; Witte, Claus-Peter; Herde, Marco (2021a): Enhanced nucleotide analysis enables the quantification of deoxynucleotides in

plants and algae revealing connections between nucleoside and deoxynucleoside metabolism. In *The Plant cell* 33 (2), pp. 270–289. DOI: 10.1093/plcell/koaa028.

Straube, Henryk; Witte, Claus-Peter; Herde, Marco (2021b): Analysis of Nucleosides and Nucleotides in Plants: An Update on Sample Preparation and LC-MS Techniques. In *Cells* 10 (3). DOI: 10.3390/cells10030689.

Sureshkumar, Sridevi; Todesco, Marco; Schneeberger, Korbinian; Harilal, Ramya; Balasubramanian, Sureshkumar; Weigel, Detlef (2009): A genetic defect caused by a triplet repeat expansion in Arabidopsis thaliana. In *Science (New York, N.Y.)* 323 (5917), pp. 1060–1063. DOI: 10.1126/science.1164014.

Sweetlove, L.J; Mowday, B.; Hebestreit, H.F; Leaver, C.J; Millar, A.H (2001): Nucleoside diphosphate kinase III is localized to the inter-membrane space in plant mitochondria. In *FEBS Letters* 508 (2), pp. 272–276. DOI: 10.1016/S0014-5793(01)03069-1.

Varga, Balázs; Barabás, Orsolya; Takács, Eniko; Nagy, Nikolett; Nagy, Péter; Vértessy, Beáta G. (2008): Active site of mycobacterial dUTPase: structural characteristics and a built-in sensor. In *Biochemical and biophysical research communications* 373 (1), pp. 8–13. DOI: 10.1016/j.bbrc.2008.05.130.

Vértessy, Béata G.; Tóth, Judit (2009): Keeping uracil out of DNA: physiological role, structure and catalytic mechanism of dUTPases. In *Accounts of chemical research* 42 (1), pp. 97–106. DOI: 10.1021/ar800114w.

Wang, Chunxin; Liu, Zhongchi (2006): Arabidopsis ribonucleotide reductases are critical for cell cycle progression, DNA damage repair, and plant development. In *The Plant cell* 18 (2), pp. 350–365. DOI: 10.1105/tpc.105.037044.

Waters, Mark T.; Langdale, Jane A. (2009): The making of a chloroplast. In *The EMBO journal* 28 (19), pp. 2861–2873. DOI: 10.1038/emboj.2009.264.

Waterworth, Wanda M.; Footitt, Steven; Bray, Clifford M.; Finch-Savage, William E.; West, Christopher E. (2016): DNA damage checkpoint kinase ATM regulates germination and maintains genome stability in seeds. In *Proceedings of the National Academy of Sciences of the United States of America* 113 (34), pp. 9647–9652. DOI: 10.1073/pnas.1608829113.

WATSON, J. D.; CRICK, F. H. (1953): Molecular structure of nucleic acids; a structure for deoxyribose nucleic acid. In *Nature* 171 (4356), pp. 737–738. DOI: 10.1038/171737a0.

Witte, Claus-Peter; Herde, Marco (2020): Nucleotide Metabolism in Plants. In *Plant physiology* 182 (1), pp. 63–78. DOI: 10.1104/pp.19.00955.

Wormit, Alexandra; Traub, Michaela; Flörchinger, Martin; Neuhaus, H. Ekkehard; Möhlmann, Torsten (2004): Characterization of three novel members of the Arabidopsis thaliana equilibrative nucleoside transporter (ENT) family. In *The Biochemical journal* 383 (Pt 1), pp. 19–26. DOI: 10.1042/bj20040389.

Xu, Jing; Deng, Yiwen; Li, Qun; Zhu, Xudong; He, Zuhua (2014): STRIPE2 encodes a putative dCMP deaminase that plays an important role in chloroplast development in rice. In *Journal of genetics and genomics = Yi chuan xue bao* 41 (10), pp. 539–548. DOI: 10.1016/j.jgg.2014.05.008.

Xu, Jing; Zhang, Lin; Yang, Dong-Lei; Li, Qun; He, Zuhua (2015): Thymidine kinases share a conserved function for nucleotide salvage and play an essential role in Arabidopsis thaliana

growth and development. In *The New phytologist* 208 (4), pp. 1089–1103. DOI: 10.1111/nph.13530.

Yoshimura, Kazuya; Shigeoka, Shigeru (2015): Versatile physiological functions of the Nudix hydrolase family in Arabidopsis. In *Bioscience, biotechnology, and biochemistry* 79 (3), pp. 354–366. DOI: 10.1080/09168451.2014.987207.

Yu, Yang; Cui, Yuxiang; Niedernhofer, Laura J.; Wang, Yinsheng (2016): Occurrence, Biological Consequences, and Human Health Relevance of Oxidative Stress-Induced DNA Damage. In *Chemical research in toxicology* 29 (12), pp. 2008–2039. DOI: 10.1021/acs.chemrestox.6b00265.

Zauri, Melania; Berridge, Georgina; Thézénas, Marie-Laëtitia; Pugh, Kathryn M.; Goldin, Robert; Kessler, Benedikt M.; Kriaucionis, Skirmantas (2015): CDA directs metabolism of epigenetic nucleosides revealing a therapeutic window in cancer. In *Nature* 524 (7563), pp. 114–118. DOI: 10.1038/nature14948.

Zrenner, Rita; Stitt, Mark; Sonnewald, Uwe; Boldt, Ralf (2006): Pyrimidine and purine biosynthesis and degradation in plants. In *Annual review of plant biology* 57, pp. 805–836. DOI: 10.1146/annurev.arplant.57.032905.105421.

2 Publications and Manuscripts

2.1 Rapid affinity purification of tagged plant mitochondria (Mito-AP) for metabolome and proteome analyses

Niehaus, M.[a], Straube, H.[a], Künzler, P.[b], Rugen, N.[b], Hegermann, J.[b], Giavalisco, P.[c], Eubel, H.[b], Witte, C-P.[a], Herde, M.[a]

[a] Leibniz Universität Hannover, Department of Molecular Nutrition and Biochemistry of Plants, 30419 Hannover, Germany
[b] Leibniz Universität Hannover, Institute of Plant Genetics, 30419 Hannover, Germany
[c] Research Core Unit Electron Microscopy, Hannover Medical School (MHH), 30625 Hannover, Germany
[d] Max-Planck-Institute for Biology of Aging, 50931 Köln, Germany

Type of authorship:	First author
Type of article:	Research Article
Share of work:	75 %
Contribution to publication:	cloned the constructs and performed and optimized the affinity purification of tagged plant mitochondria and the Seahorse analysis, analyzed the data, prepared the figures and participated in writing the manuscript
Journal:	Plant Physiology
Impact factor:	8.005 (2021)
Date of publication:	07.01.2020
Number of citations: (Google Scholar, 28.09.22)	28
DOI:	10.1104/pp.19.00736

Rapid Affinity Purification of Tagged Plant Mitochondria (Mito-AP) for Metabolome and Proteome Analyses[1]

Markus Niehaus,[a] Henryk Straube,[a] Patrick Künzler,[b] Nils Rugen,[b] Jan Hegermann,[c] Patrick Giavalisco,[d] Holger Eubel,[b] Claus-Peter Witte,[a] and Marco Herde[a,2,3]

[a]Leibniz Universität Hannover, Department of Molecular Nutrition and Biochemistry of Plants, 30419 Hannover, Germany
[b]Leibniz Universität Hannover, Institute of Plant Genetics, 30419 Hannover, Germany
[c]Research Core Unit Electron Microscopy, Hannover Medical School (MHH), 30625 Hannover, Germany
[d]Max-Planck-Institute for Biology of Aging, 50931 Köln, Germany

ORCID IDs: 0000-0003-3057-7823 (M.N.); 0000-0001-9286-7784 (H.S.); 0000-0002-9686-5126 (P.K.); 0000-0002-9297-4560 (N.R.); 0000-0002-4636-1827 (P.G.); 0000-0001-7065-178X (H.E.); 0000-0002-3617-7807 (C.-P.W.); 0000-0003-2804-0613 (M.H.).

The isolation of organelles facilitates the focused analysis of subcellular protein and metabolite pools. Here we present a technique for the affinity purification of plant mitochondria (Mito-AP). The stable ectopic expression of a mitochondrial outer membrane protein fused to a GFP:Strep tag in Arabidopsis (*Arabidopsis thaliana*) exclusively decorates mitochondria, enabling their selective affinity purification using magnetic beads coated with Strep-Tactin. With Mito-AP, intact mitochondria from 0.5 g plant material were highly enriched in 30–60 min, considerably faster than with conventional gradient centrifugation. Combining gradient centrifugation and Mito-AP techniques resulted in high purity of >90% mitochondrial proteins in the lysate. Mito-AP supports mitochondrial proteome analysis by shotgun proteomics. The relative abundances of proteins from distinct mitochondrial isolation methods were correlated. A cluster of 619 proteins was consistently enriched by all methods. Among these were several proteins that lack subcellular localization data or that are currently assigned to other compartments. Mito-AP is also compatible with mitochondrial metabolome analysis by triple-quadrupole and orbitrap mass spectrometry. Mito-AP preparations showed a strong enrichment with typical mitochondrial lipids like cardiolipins and demonstrated the presence of several ubiquinones in Arabidopsis mitochondria. Affinity purification of organelles is a powerful tool for reaching higher spatial and temporal resolution for the analysis of metabolomic and proteomic dynamics within subcellular compartments. Mito-AP is small scale, rapid, economic, and potentially applicable to any organelle or to organelle subpopulations.

One challenge in science is to shift the scale in which observations can be made. From tissues via cells to compartments within a cell (e.g. organelles), the scale of scientific observation becomes progressively smaller, and the resolution must increase drastically to allow ever deeper insights into the details of biological processes.

Mitochondria are essential for cellular metabolism, because they are the major ATP-exporting organelles in plants, harbor central biochemical pathways such as the citrate cycle and the respiratory chain, represent a central hub of amino acid metabolism, and support photosynthesis and photorespiration. Objectives in plant mitochondria research are inter alia to create an inventory list of proteins and metabolites residing in these organelles as well as to investigate the dynamics of these molecules, for example upon exposure to different treatments and stresses. To address these objectives, the enrichment of mitochondria relative to other components of the cell is required. The reduction of complexity concomitant with purification also fosters the detection of proteins and metabolites with low abundances, because background and interfering matrix are removed prior to analysis.

To accomplish the isolation of mitochondria from leaf material, centrifugation-based methods have been developed that achieve a high degree of purity (Day et al., 1985; Keech et al., 2005). Nevertheless, a full overview of all mitochondrial proteins is still needed. To generate an inventory of proteins from a particular compartment, proteomic profiling of samples differentially enriched in this compartment was shown to

[1]This work was supported by the Deutsche Forschungsgemeinschaft (HE 5949/3-1 to M.H. and EU 54/4-1 to H.E.).

[2]Author for contact: mherde@pflern.uni-hannover.de.
[3]Senior author.

The author responsible for distribution of materials integral to the findings presented in this article in accordance with the policy described in the Instructions for Authors (www.plantphysiol.org) is: Marco Herde (mherde@pflern.uni-hannover.de).

M.N. cloned the constructs and performed and optimized the affinity purification of tagged plant mitochondria and the Seahorse analysis; H.S. did the analysis of polar metabolites and the phenotyping; P.K. and N.R. performed the differential and density gradient centrifugation and the proteomic analysis; J.H. performed the electron microscopy study and interpreted the results; P.G. provided the lipid analysis; H.E. analyzed the proteomic data and supervised P.K. and N.R.; C.-P.W. and M.H. designed the study and wrote the article; M.H. supervised M.N. and H.S. and did the correlation analysis.

www.plantphysiol.org/cgi/doi/10.1104/pp.19.00736

 © 2020 American Society of Plant Biologists. All Rights Reserved.

Downloaded from https://academic.oup.com/plphys/article/182/3/1194/6116177 by Institute of Horticultural Economics user on 10 December 2021

be a powerful technique (Eubel et al., 2007; Kraner et al., 2017). An even greater challenge is the analysis of subcellular metabolite pools, for example the mitochondrial pools, in particular if the same metabolites are present in several compartments, maybe even in grossly different amounts. Highly purified organelles (mitochondria) are needed to ensure that detected metabolites are truly derived from this organelle and not from other copurified compartments.

To capture the mitochondria as close as possible to their in vivo state, the swiftness of the isolation procedure is even more important than the purity. After removing the mitochondria from their cellular context during cell rupture, posttranslational protein modifications are expected to change quickly within the organelle. Steady-state concentrations of metabolites will also be altered by metabolite conversion, degradation, or leakage from the mitochondria (Roberts et al., 1997; Agius et al., 2001).

Currently, the state-of-the-art technology for large scale mitochondrial isolation is a combination of differential and density gradient centrifugation (DGC) of extracts from cell or callus cultures (Klein et al., 1998) or green leaves (Day et al., 1985; Keech et al., 2005). Although this technique provides comparatively high amounts of mitochondria with reasonably high purity, the procedure is laborious and time-consuming, and it requires a large amount of starting material. A centrifugation-based method on a smaller scale is less time consuming, but yield and purity of the obtained mitochondrial preparation were not reported (Boutry et al., 1984). Following isolation by DGC, mitochondria can be further purified by free-flow electrophoresis using the surface charge on the organelles as an alternative handle for differential isolation (Eubel et al., 2007). Additionally, a fractionation technique using rapid filtration has been employed to swiftly separate plant organelles, including mitochondria, for metabolite analysis, thus minimizing leakage or conversion of metabolites (Lilley et al., 1982; Gardeström and Wigge, 1988). This method requires specialized equipment and the preparation of protoplasts prior to isolation, which might have an undesired impact on the cells. Nonaqueous fractionation is another method for the separation of subcellular metabolite pools and proteins (Gerhardt and Heldt, 1984; Arrivault et al., 2014). This technique has the advantage of rapidly quenching biological activities in the material prior to fractionation, allowing the assessment of metabolites and proteins close to their native state. Whether nonaqueous fractionation can reproducibly separate cytosolic from mitochondrial proteins and metabolites is still under debate (Arrivault et al., 2014; Fürtauer et al., 2019).

Alternative approaches for mitochondria isolation have been developed more recently that do not rely on the general physicochemical characteristics of the organelle, but rather use affinity purification techniques targeting specific proteins present on the mitochondrial surface. An antibody coupled to magnetic beads directed against TOM22, a mitochondrial import receptor subunit in the outer membrane, allowed the isolation of native mitochondria from mammalian cells (Hornig-Do et al., 2009; Afanasyeva et al., 2018). Recently, an innovative approach employing a recombinant protein for the isolation of mitochondria from mammalian cells with affinity purification was established and used to quantify metabolites and proteins (Chen et al., 2016). The key feature of this technology is the heterologous expression of a chimeric protein with a C-terminal domain integrated into the outer mitochondrial membrane and an N-terminal cytosolic domain consisting of a GFP for microscopic localization and a hemagglutinin-tag (HA) for immunoprecipitation. Employing magnetic beads coupled to anti-HA antibodies, mitochondria decorated with this fusion protein can be affinity purified.

Here, we established an affinity purification scheme for mitochondria from Arabidopsis (*Arabidopsis thaliana*), which we call Mito-AP. Plants pose several unique challenges for Mito-AP, because they possess chloroplasts, which need to be selected against during purification, and because plant extracts are a difficult matrix for any purification method. Mito-AP yields highly enriched mitochondria, requires only a fraction of the starting material typically used for conventional mitochondrial isolation, is scalable, and can be performed considerably faster than the classical centrifugation-based methods. The protocol described here introduces several innovations, which substantially lower the cost of this technique and allow the nondestructive removal of the mitochondria from the magnetic beads.

RESULTS

The Locus At1g55450 Encodes a Suitable Adapter Protein for Mito-AP

The expression of a recombinant chimeric protein on the mitochondrial surface enabling affinity purification is a key feature of Mito-AP. The C-terminal domain of such a protein should be integrated into the outer mitochondrial membrane and the N-terminal domain, including a GFP and an affinity tag, should face the cytosol as a handle for the affinity purification employing magnetic beads (Fig. 1). In contrast to Chen et al. (2016), who used a similar approach for HA-tagged mammalian mitochondria employing a magnetic affinity resin decorated with anti-HA antibodies, we aimed to use the Strep-tag/Strep-Tactin interaction to reduce procedure costs and to potentially allow for mild affinity elution. The Twin-Strep tag (IBA Lifesciences) was chosen, because it supposedly binds more strongly to Strep-Tactin than the single Strep tag.

We did not employ the chimeric protein described by Chen et al. (2016), because plant cells have an elaborate organelle targeting system preventing the misimport of mitochondrial proteins into the chloroplast and vice versa. It therefore cannot be excluded that the mammalian adapter protein may be partially mistargeted

Downloaded from https://academic.oup.com/plphys/article/182/3/1194/6116177 by Institute of Horticultural Economics user on 10 December 2021

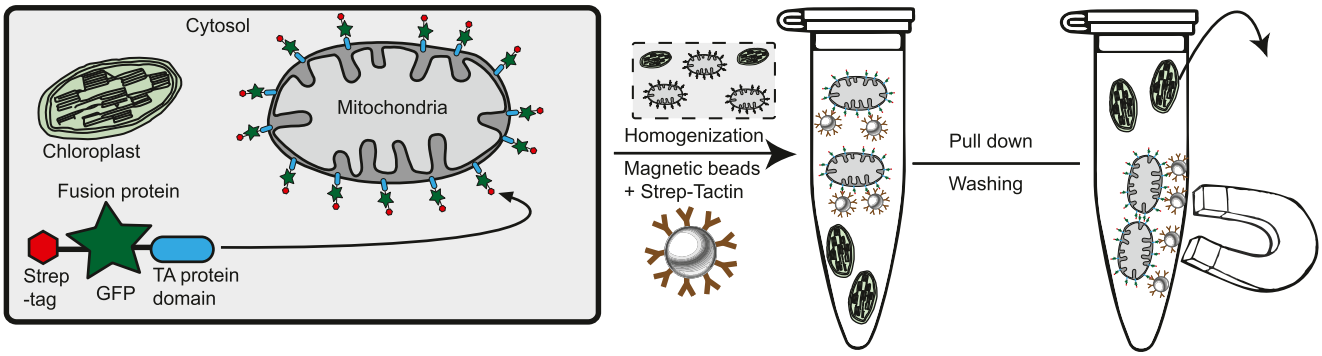

Figure 1. Workflow of Mito-AP. An ectopically expressed protein, which integrates into the outer mitochondrial membrane, fused with an N-terminal Strep-tag and a GFP-tag facing the cytosol can be used as an anchor for affinity purification of mitochondria with Strep-Tactin-coated magnetic beads.

to chloroplasts. In fact, plants ectopically producing mammalian mitochondrial proteins sometimes erroneously direct these proteins into chloroplasts (Maggio et al., 2007). We performed a literature survey to identify plant proteins that are specifically integrated with their C-terminal domain in the outer mitochondrial membrane and feature an N-terminal domain facing the cytosol. Three candidate proteins belonging to the class of tail-anchored proteins were identified: (1) Cb5-D described by Maggio et al. (2007); (2) a putative methyltransferase encoded at locus At1g55450 and described by Marty et al. (2014); and (3) TOM22-V encoded at locus At5g43970.

In the case of Cb5-D, the C-terminal sequence conferring mitochondrial localization has been well defined (Hwang et al., 2004). Therefore, this domain was tested, whereas for the other candidates, full-length proteins were used for the construction of fusion proteins. The expression of the constructs and the subcellular location of the three resulting N-terminal Twin-Strep-tag-GFP fusion variants were assessed in transient assays performed in *Nicotiana benthamiana*. Despite the use of a strong 35S promoter for the respective constructs, Cb5-D and TOM22-V expression were barely detectable by confocal microscopy. By contrast, a clear and strong signal consistent with a mitochondrial location was observed for the protein belonging to the S-adenosyl-L-Met-dependent methyltransferase superfamily encoded at At1g55450. We selected this protein, herein referred to as ADAPTER, for our approach (Supplemental Fig. S1).

A homozygous transgenic Arabidopsis line with intermediate expression (line 11) of the 35S:Twin-Strep-tag:GFP:ADAPTER construct was generated. Confocal microscopy analysis suggested that the mitochondrial membrane was exclusively decorated by this chimeric protein, whereas signals from other organelles, in particular from chloroplasts, were not observed (Fig. 2A). To verify this localization, we created Arabidopsis plants expressing the 35S:Twin-Strep-tag:GFP:ADAPTER construct as well as a construct for mCherry directed to the mitochondria by the *Sc*CoxIV peptide fused to the N terminus (Maarse et al., 1984). In these plants (line 1), GFP fluorescence from the ADAPTER:GFP fusion surrounded the mCherry signal located in the mitochondrial matrix (Fig. 2B).

Continuous GFP fluorescence from the whole rosette was observed in the Twin-Strep-tag:GFP:ADAPTER line 11, which was selected for all further experiments (Fig. 3A). The highly uniform expression in this line indicates that gene silencing did not occur, which would have resulted in individuals with patchy fluorescence. Silencing was probably prevented by the use of a GFP gene with an intron and by selecting a line with only moderate fluorescence.

Ectopic production of the ADAPTER fusion protein did not change the normal physiological appearance of the plant at any stage during development (Fig. 3, B–E). A recent study demonstrated that a short photoperiod enhances growth phenotypes caused by mutations in a mitochondrial protein (Pétriacq et al., 2017). Therefore, we asked the question whether a potential impact of the ADAPTER fusion protein on mitochondrial function is revealed under short-day conditions. Leaf surface and weight did not differ significantly between the wild-type and the Twin-Strep-tag:GFP:ADAPTER plants (Supplemental Fig. S2, A and B), suggesting that ectopic production of the ADAPTER fusion protein does not interfere with mitochondrial function. Additionally, we did not observe any effect on the root length of seedlings and the germination rate (Supplemental Fig. S2, C and D). Therefore, mitochondria isolated from the transgenic lines are likely representative of mitochondria from the wild type.

Outer Mitochondrial Membranes Can Be Isolated Together with the Mitoplast by Mito-AP

Stable homozygous 35S:Twin-Strep-tag:GFP:ADAPTER plants also possessing a transgene expressing the *Sc*CoxIV:mCherry protein (line 1) were used for affinity purification of mitochondria with commercially available magnetic beads carrying the Strep-Tactin

Downloaded from https://academic.oup.com/plphys/article/182/3/1194/6116177 by Institute of Horticultural Economics user on 10 December 2021

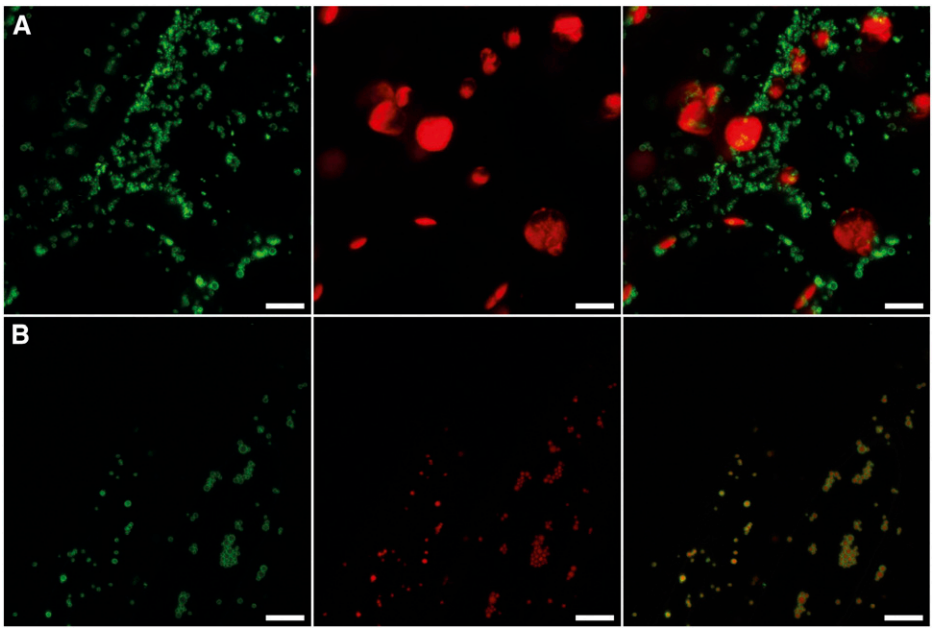

Figure 2. Subcellular localization of the Twin-Strep-tag:GFP:ADAPTER protein in stable transformed Arabidopsis. A, Confocal fluorescence microscopy images of the vascular tissue in leaves expressing the 35S:Twin-Strep-tag:GFP:ADAPTER construct. Shown are GFP (left) and autofluorescence (middle) of chloroplasts, and an overlay of both channels (right). B, Images from leaf vascular tissue coexpressing 35S:Twin-Strep-tag:GFP:ADAPTER (GFP, left) and 35S:*Sc*CoxIV:mCherry (mCherry, middle), and an overlay of both channels (right). Scale bars = 8 μm.

protein (IBA Lifesciences) on their surface. The beads were washed and then analyzed by confocal microscopy. Circular fluorescent structures were observed (Fig. 4) that were not detected on control beads incubated with extracts from wild-type plants. The fluorescence had the spectral emission characteristics of mCherry, suggesting that (1) mitochondria from total cell extracts had been isolated; and (2) these mitochondria maintained their integrity, still confining the mCherry protein to the mitochondrial matrix (Fig. 4). This analysis does not provide a quantitative assessment of mitochondrial integrity, and the presence of outer membranes without a mitoplast or otherwise damaged mitochondria cannot be ruled out (for a more quantitative assessment of intact mitochondria, see the last paragraph of the "Results" section).

For extracting and washing the beads, an ammonium bicarbonate/sodium chloride buffer previously suggested to be advantageous for downstream liquid chromatography-mass spectrometry (LC-MS) applications with mitochondria isolated from mammalian cells was used (Chen et al., 2016). To ensure that this buffer does not have a negative impact on mitochondrial integrity, we compared it to the mannitol buffer employed for the isolation of plant mitochondria by DGC (Klein et al., 1998). As a control, mitochondria were also exposed to pure water, resulting in hypoosmotic shock and mitochondrial rupture.

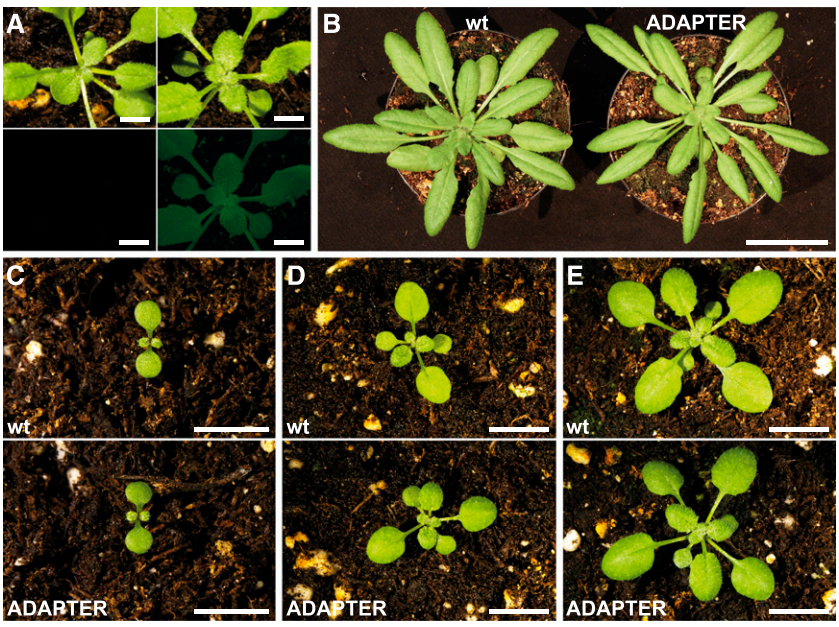

Figure 3. Comparison of growth and GFP fluorescence between the wild type (Col-0) and a stable transformed plant carrying the 35S:Twin-Strep-tag:GFP:ADAPTER construct. A, Photographs (top) and GFP fluorescence images (bottom) of wild-type (left) and transgenic plants (right) 21 d after imbibition (dai). Scale bars = 0.5 cm. B, Growth comparison of wild-type (wt) and transgenic (ADAPTER) plants at 35 dai (scale bar = 3.5 cm) and during development at 9 dai (C), 16 dai (D), and 21 dai (E). Pictures are representative of three plants within each experimental group. Scale bars = 1 cm (C–E).

Downloaded from https://academic.oup.com/plphys/article/182/3/1194/6116177 by Institute of Horticultural Economics user on 10 December 2021

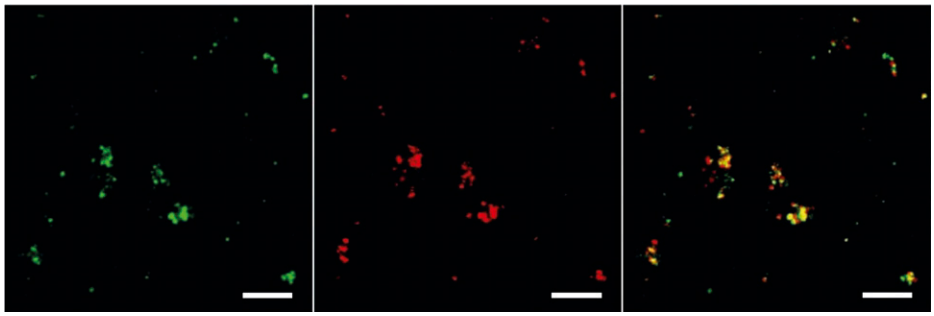

Figure 4. Colocalization of markers for mitochondrial outer membrane and matrix after affinity purification. Representative confocal fluorescence microscopy images of magnetic bead clusters with bound mitochondria originating from plants coexpressing 35S:Twin-Strep-tag:GFP:ADAPTER (GFP, left) and 35S:*Sc*CoxIV:mCherry (mCherry, middle), and an overlay of both channels (right). Scale bars = 10 μm.

Mitochondria were isolated using DGC, pelleted by centrifugation, and resuspended in either mannitol (original buffer from the DGC protocol), potassium chloride/bicarbonate, sodium chloride/bicarbonate, or water, and then incubated for 20 min on ice. The preparations were centrifuged, and both the pellet and the supernatant were analyzed by SDS gel electrophoresis. A high amount of protein in the supernatant was only observed from mitochondrial preparations that had been incubated in water (Supplemental Fig. S3), suggesting that mitochondrial integrity was compromised under these conditions. By contrast, all other mitochondrial treatments resulted in only minor amounts of protein in the supernatants. Since there was no difference between mitochondrial preparations exposed to mannitol or sodium chloride/bicarbonate buffer, we concluded that the sodium chloride/bicarbonate buffer is suitable for isolation of plant mitochondria.

The Surface Area of the Isolation Matrix Rather Than Its Loading with Strep-Tactin Limits the Yield of Mitochondria

Initial experiments were conducted with commercially available magnetic beads of 1-μm diameter decorated with Strep-Tactin (IBA Lifesciences), which were developed for the isolation of entire cells. Although the 1-μm beads are suitable for mitochondrial isolation in principle (Supplemental Fig. S4), it might be advantageous to use smaller beads, which have been suggested to increase the yield of mitochondria (Chen et al., 2016). However, Strep-Tactin-coated nanoparticles are not commercially available. Therefore, we generated Strep-Tactin-coated iron oxide particles in house by chemically linking Strep-Tactin (IBA Lifesciences) to iron oxide beads (Chemicell). When testing the separation of magnetic beads of different sizes from the liquid phase with an external magnet, we observed that beads with a 100-nm diameter were more difficult to separate than larger beads with a 200-nm diameter.

Magnetic beads are available either coated with starch, whose hydroxyl groups can be activated with cyanogen bromide, or coated with a sugar polymer possessing carboxyl groups, which can be activated with carbodiimide. Both activated groups react with the amino groups of Strep-Tactin, allowing coupling of the protein to the matrix. We performed both coupling regimes and compared the performance of the resulting matrices. With 200-nm starch-coated beads, a higher purity of mitochondria was obtained than with the other matrices. Purity was judged by the relative enrichment of proteins predicted to be located in mitochondria (SUBA4 database; Hooper et al., 2017). Proteins were identified and quantified using shotgun proteomics, where protein abundance was determined by a label-free quantification algorithm (Schwanhäusser et al., 2011) providing intensity-based absolute quantification (iBAQ) values (Supplemental Fig. S5). Compared to the commercial 1-μm beads, the 200-nm starch-coated beads performed only slightly better in terms of enrichment of mitochondrial proteins (Supplemental Fig. S5). However, with equal bead volumes used in the purification, a 3-fold higher protein yield in the samples derived from the 200-nm material was obtained, thus confirming the initial hypothesis that higher yields can be obtained with smaller beads (Supplemental Fig. S6).

We also quantified the amount of Strep-Tactin coupled to the surface of equal volumes of the commercial 1-μm and the in-house-made 200-nm matrices and observed ~20-fold more Strep-Tactin on the 1-μm beads (Supplemental Fig. S7). It appears that for isolation of mitochondria, the 5-fold greater surface area of the 200-nm beads is more important for the yield than is the absolute number of Strep-Tactin moieties on the surface.

Mitochondria Isolated by Affinity Purification Are Strongly Enriched

Next, we compared mitochondria preparations derived from Mito-AP to preparations made using DGC, currently accepted as the gold standard for mitochondria isolation from plants. Both methods were performed with 5-week-old 35S:Twin-Strep-tag:GFP:ADAPTER plants grown under short-day conditions, and both preparations were repeated on three different days. We used 220-fold more plant material for DGC than for Mito-AP (110 g versus 0.5 g; Supplemental Fig. S8, A and B). A similar or even slightly better relative protein yield was obtained with Mito-AP

Downloaded from https://academic.oup.com/plphys/article/182/3/1194/6116177 by Institute of Horticultural Economics user on 10 December 2021

(Supplemental Fig. S8C), but far less total protein was purified due to the lower amount of starting material used.

For the Mito-AP protocol, mitochondria bound to the magnetic beads were further processed in two different ways. In method 1, the beads were boiled in SDS loading buffer for elution of the proteins. In method 2, an affinity elution step with biotin was employed to potentially increase purity, because unspecific proteins bound to the bead surface will not be eluted and can be removed together with the affinity matrix by centrifugation. However, we observed that elution with biotin was not fully quantitative (Supplemental Fig. S9). Therefore, we supported the biotin elution by adding proteinase K to the elution buffer, subjecting all proteins outside of the mitochondria to proteolytic degradation, including the Twin-Strep-tag:GFP:ADAPTER fusion protein connecting the mitochondria to the beads as well as any remaining unspecific protein contaminants. We hypothesized that this step might improve elution and increase the enrichment of mitochondrial proteins in the preparation, but that proteins residing in the outer mitochondrial membrane might be lost.

As expected, most proteins in the crude extracts originated from plastids. The abundance of mitochondrial proteins was strongly increased by DGC as well as by Mito-AP (Fig. 5; Supplemental Table S1). Consistent with our expectation, mitochondrial proteins were not as highly enriched by method 1 as by method 2, which led to >70% of iBAQs originating from mitochondrial proteins. The ADAPTER protein, known to reside on the mitochondrial surface, was only detected in the sample derived from method 1 but not method 2, confirming the efficiency of proteinase K digestion. The addition of proteinase K improved the yield 1.7-fold (Supplemental Fig. S9). One can envisage that such a yield increase could also be achieved by upscaling the method without the proteinase K treatment, resulting in improved yield and purity. Most interestingly, mitochondrial proteins were enriched to a higher degree by Mito-AP (method 2) than by DGC (Fig. 5, A and B).

However, we had obtained a higher level of purity with DGC in the past (Klodmann et al., 2011; Senkler et al., 2017; Rugen et al., 2019). Also, the variation in mitochondrial protein enrichment across the replicates was high at ~8.5%, whereas the variation for Mito-AP replicates with both methods was considerably lower (3.3% for method 1 and 2.5% for method 2; Supplemental Fig. S10). Reasons for this are currently unknown. Most likely, the expression of the fusion protein has some impact on the sedimentation behavior of the mitochondria during centrifugation. Since the extraction of the mitochondrial band from the gradient is a manual process and subject to a certain degree of variation in terms of volume, position, and disturbance of the gradient, mitochondrial purity may suffer when the mitochondria of the transgenic line are extracted in the same way as previously performed for the wild type. Thus, minor adjustments to the DGC procedure are expected to yield organelle purities in the transgenic line that are comparable to those reported for wild-type mitochondria.

In a tandem purification experiment, we assessed whether purity might be further increased when mitochondria isolated via DGC are used as input for Mito-AP enrichment. With this approach, purities of >90%

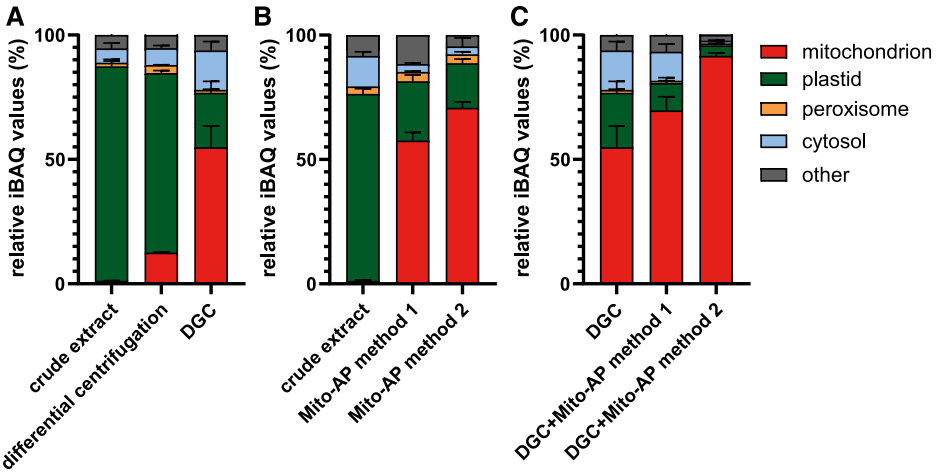

Figure 5. Enrichment of mitochondria by different purification methods. Plants were grown under short-day conditions for 4 weeks and subjected to either differential centrifugation, DGC, Mito-AP, or a combination of DGC and Mito-AP (DGC + Mito-AP). iBAQ values for every identified protein were assigned to their respective categories (mitochondrion, plastid, peroxisome, cytosol, or other), referred to total iBAQs of the corresponding sample, and plotted as percentages. The categories were defined by the SUBAcon annotation provided by SUBA4. Categorized iBAQ values are shown from crude extract, samples after only differential centrifugation, and samples after DGC (A); from crude extracts and samples after Mito-AP (method 1, boil-off; method 2, elution with biotin and proteinase K; B); and from samples after DGC and after tandem purification with DGC followed by the two different Mito-AP procedures (C). DGC data in A and C are the same. Error bars represent the SD (n = 3 biological replicates).

Downloaded from https://academic.oup.com/plphys/article/182/3/1194/6116177 by Institute of Horticultural Economics user on 10 December 2021

were achieved, suggesting that each method removes a different spectrum of contaminants (Fig. 5C).

Mito-AP can be performed considerably faster than DGC, requiring only about 30 min for method 1 and 60 min for method 2. The direct comparison of both methods shows that Mito-AP results in better purity than DGC and appears to be more reproducible. Mito-AP requires only comparatively small amounts of plant material and is quite economic when a Strep-Tactin affinity matrix is used. One Mito-AP employing 6.25 mg of Strep-Tactin-coated 200-nm beads and using 500 mg of Arabidopsis leaf material yields ~10 μg of mitochondrial protein and costs about 10 euros in consumables. The Strep-Tactin matrix is ~5-fold less expensive than comparable commercial beads coated with anti-HA antibody, which were employed by Chen et al. (2016) for the affinity purification of mammalian mitochondria.

Prediction of Mitochondrial Protein Localization by Correlation Analysis

Although many studies have contributed to a comprehensive inventory of the mitochondrial proteome, it is an ongoing challenge to compile a complete set of mitochondrial proteins. We hypothesize that this challenge can be addressed by monitoring and correlating the relative abundances of proteins in samples from distinct experimental approaches for enriching mitochondria. This study offered an opportunity to test this idea, because several different strategies were employed for generating samples enriched in mitochondria. In such samples, the relative abundances of proteins known to be located in mitochondria will strongly correlate, because their abundance directly reflects the ratio of mitochondria to other cellular components. By contrast, the relative abundance of a contaminant protein will depend on whether a particular enrichment strategy is suitable for its removal, and therefore, the relative abundance of contaminants may correlate to each other but not to proteins truly localized in mitochondria. Thus, correlation can be used as a tool to predict mitochondrial localization. Proteins that cluster with known mitochondrial proteins in such an analysis are likely to reside in mitochondria as well.

Because the combination of DGC and Mito-AP resulted in a higher mitochondrial purity (Fig. 5C) than any of these techniques alone, each method appears to remove different contaminants. Also, the two different versions of Mito-AP have distinct protein enrichment profiles. To increase the coverage of both mitochondrial and contaminating proteins, we employed a longer (4-h) liquid chromatography separation prior to shotgun MS analysis for all three biological replicates of (1) DGC alone, (2) Mito-AP method 1, (3) Mito-AP method 2, (4) DGC combined with Mito-AP method 1, and (5) DGC combined with Mito-AP method 2.

For the individual replicates of each method, the iBAQ value of each protein was normalized to the total number of iBAQs detected in the respective sample. For each of the five methods, a relative mean iBAQ value for each protein was calculated from the three replicates. With this data, a correlation matrix using Pearson's correlation coefficient was built. All correlations above a cutoff of 0.99 were displayed as a weighted network placing proteins with stronger correlation closer together.

The correlation analysis revealed one cluster containing 619 proteins that is highly enriched in proteins predicted by SUBAcon (Hooper et al., 2017) to be localized in mitochondria (517 of 619 [82%]; Fig. 6; Supplemental Table S2). Of these 517 proteins assigned to mitochondria, 491 (shown as black triangles in the cluster) have available supporting MS or fluorescence microscopy data. For the remaining 26 proteins, experimental evidence of their mitochondrial localization is provided here (Fig. 6, gray squares). For the other 102 proteins in the above-mentioned cluster of 619 proteins (18%), mitochondrial localization is not predicted according to SUBAcon. For 19 of these, no experimental data are available (Fig. 6, red circles). Therefore, this study provides evidence for mitochondrial location of these proteins despite a different SUBAcon prediction. For 83 of the 102 proteins not assigned to mitochondria by SUBAcon, either MS or fluorescent microscopy data are available (Fig. 6, orange diamonds), and 62 of these proteins have at least once been found in mitochondria by either technique. The remaining 21 proteins are not predicted by SUBAcon to be in mitochondria, nor is there current experimental evidence indicating their presence in mitochondria. Further analysis of these 21 proteins shows that only five were demonstrated by fluorescence microscopy to reside in another compartment. Although we cannot completely resolve this discrepancy, it is possible that in some instances protein variants arising from alternative transcripts might be differentially located. This might also be one possible explanation for the remaining 16 proteins, for which localization information is based on MS analysis of isolated cellular compartments. It is worth noting that for half of these proteins, the experimental evidence is limited to a single MS study.

In summary, in the mitochondrial cluster presented here, we have identified previously uncharacterized candidate proteins that exhibit mitochondrial localization as a starting point for further analysis and experimental assessment.

Mitochondrial Metabolites Can Be Detected and Quantified in Affinity-Purified Mitochondria

Our initial motivation to develop a purification protocol for mitochondria was to quantify nucleotide subpools in these organelles. Therefore, we tested whether nucleotides can be detected when mitochondria are enriched using method 1 and then directly

Downloaded from https://academic.oup.com/plphys/article/182/3/1194/6116177 by Institute of Horticultural Economics user on 10 December 2021

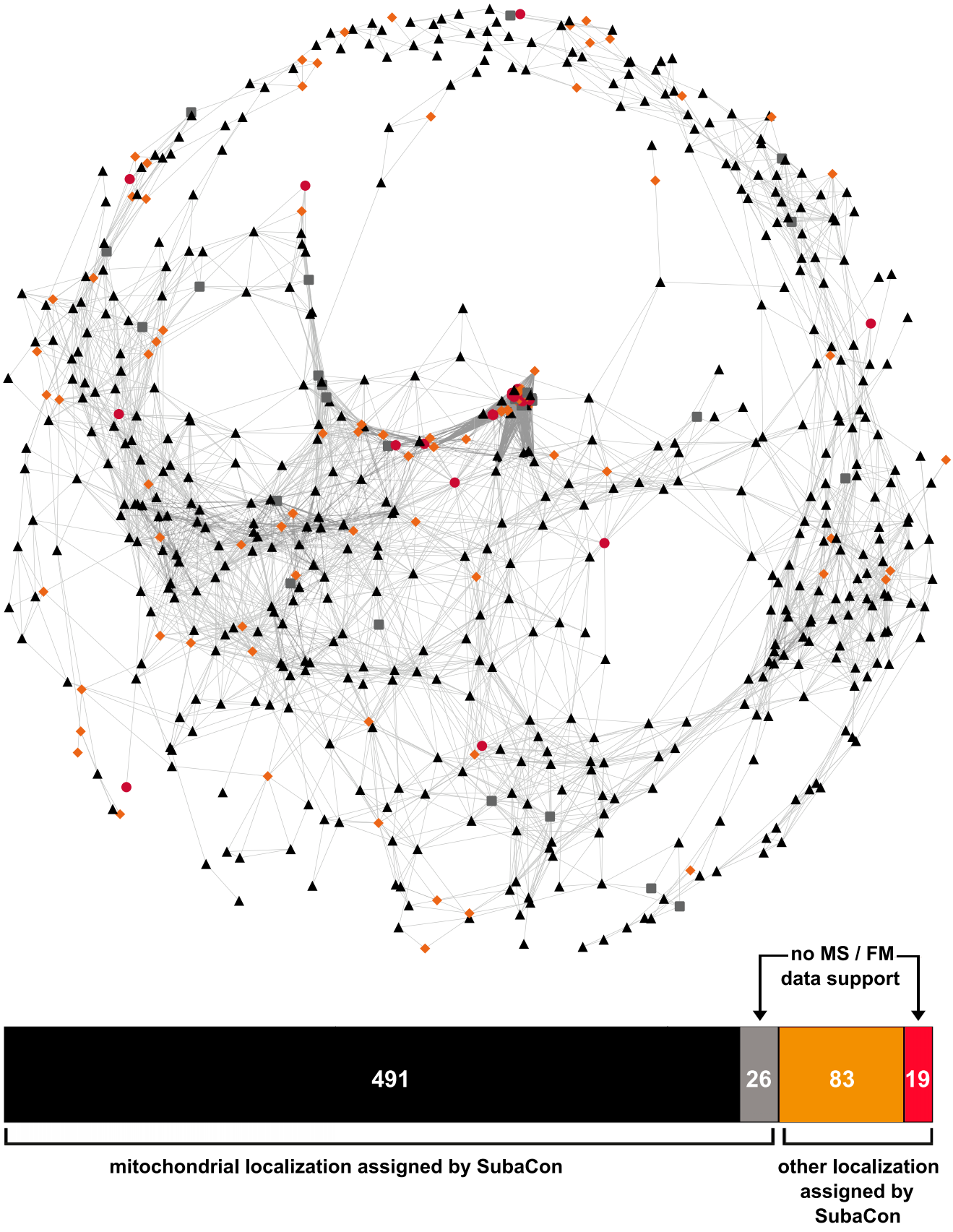

Downloaded from https://academic.oup.com/plphys/article/182/3/1194/6116177 by Institute of Horticultural Economics user on 10 December 2021

extracted on the beads. Unfortunately, metabolites could hardly be detected in these extracts. The addition of labeled nucleotide standards suggested that metabolites interact with the magnetic beads, preventing their detection in the mass spectrometer. We reasoned that the removal of the magnetic beads before metabolite extraction might alleviate the problem. To this end, method 2 was developed, in which the mitochondria are eluted and the affinity matrix is removed prior to extraction. Extracts from method 2 were analyzed for NAD, NADH, AMP, ADP, ATP, NADP, and nicotinamide mononucleotide (NMN). For all these metabolites, robust signals were recorded that were several orders of magnitude stronger than signals from the negative control, where beads had been incubated with extracts from wild-type plants and treated according to method 2 (Fig. 7).

The results demonstrate that with the protocol presented here, it is possible to obtain sufficient amounts of metabolites, aiding in the characterization of enriched mitochondria, as suggested before (Ikuma, 1970). However, from the NADH/NAD and ATP/ADP ratios, it is clear that the mitochondria lost activity during Mito-AP (Roberts et al., 1997, Agius et al., 2001). This strongly suggests that metabolite concentrations in vivo cannot be determined with Mito-AP, except in the case of stable metabolites, such as lipids, or for entire metabolite groups, such as the adenylates (Fig. 7).

Metabolites were also detected in the negative controls of the recently described Mito-AP from mammalian cells, but unfortunately the actual magnitude of this background noise was not shown (Chen et al., 2016). It is possible that this background arose from metabolites directly bound to the matrix, because Chen et al. (2016) extracted the metabolites from the mitochondria in the presence of the magnetic beads. We minimized such effects by removing the beads prior to extraction, but it cannot be fully excluded that a minor amount of matrix remained in our preparations, resulting in some background.

To assess whether there was any metabolite contamination of our mitochondrial preparations from intact plastids, we used ADP-Glc as a marker metabolite. It is generated by ADP-Glc pyrophosphorylase for starch biosynthesis, which normally occurs in the plastids. Under special circumstances, cytosolic starch biosynthesis might occur (Villand and Kleczkowski, 1994); however, the process has never been observed in mitochondria. Dilutions of ADP-Glc down to 0.67 fg on column were detected with a robust signal-to-noise ratio by our analytical platform (Supplemental Fig. S11), but ADP-Glc was not detected in any of the samples obtained with Mito-AP (Fig. 7), indicating that intact plastids were not present.

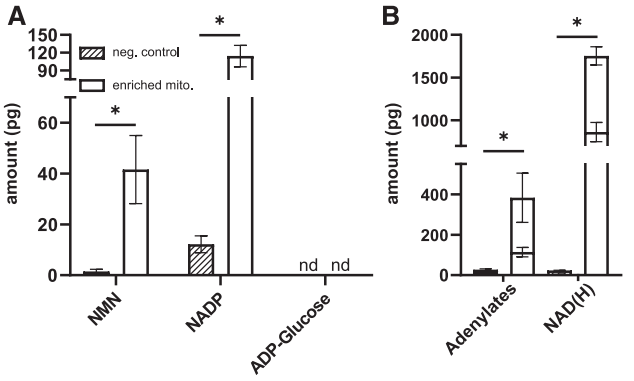

Figure 7. Polar metabolites in mitochondria enriched by Mito-AP. Seedlings carrying the 35S:Twin-Strep-tag:GFP:ADAPTER construct (enriched mito.) or Col-0 (neg. control) were grown for 10 d in liquid media and processed with Mito-AP (method 2). Polar metabolites were identified and quantified with a triple quadrupole MS in these preparations. A, NMN, NADP, and ADP Glc. The ADP-Glc content was below the detection limit of 0.65 fg (see Supplemental Fig. S10). B, Adenylates and reduced and oxidized NADH, each shown as a pool in one column, to emphasize that pools of these metabolites can be measured but that the concentrations of individual compounds within those pools do not represent the concentrations in vivo. For the adenylates the column is separated into AMP (lower), ADP (middle), and ATP (upper), whereas for the nicotinamides, NAD is shown in the lower part of the column and NADH in the upper part. The values for ATP were too low to be visualized. Error bars represent the SD ($n = 4$ biological replicates, derived from independent Mito-APs of distinct samples grown in parallel). Significant differences (at $P < 0.05$) were determined with Student's t test and marked with an asterisk. Calculation of the false discovery rate (FDR) was done using the two-stage linear step-up procedure described in Benjamini et al. (2006). The statistical analysis was done with a FDR of 1%. nd, Not detectable. Standard curves for different metabolite concentrations in water were used for absolute quantification.

Figure 6. (*Continued.*)
Correlation analysis of protein abundances in samples from DGC, the two Mito-AP methods, and tandem DGC-Mito-AP purifications. The normalized iBAQ values for all identified proteins from DGC and Mito-AP methods 1 and 2 as well as from tandem DGC + Mito-AP (methods 1 and 2) were determined. An average of the three biological replicates from each method was used to calculate Pearson's correlation coefficients for all possible combinations of two proteins. The correlations are displayed as an interaction graph using a cutoff value of 0.99. Proteins are nodes and the length of an edge is negatively correlated with the strength of the correlation. Black triangles and gray squares, proteins classified by SUBAcon as being located in mitochondria; gray squares, locations predicted only in silico, without experimental support (by MS or fluorescence microscopy [FM]); orange diamonds and red circles, proteins classified by SUBAcon as being located in other cellular compartments and not mitochondria; red circles, locations predicted only in silico, without experimental support; orange diamonds, experimental data are available. The same color scheme was used for the schematic below the interaction graph, representing the proportions of the respective protein groups.

Downloaded from https://academic.oup.com/plphys/article/182/3/1194/6116177 by Institute of Horticultural Economics user on 10 December 2021

Besides adenylates, the lipid composition of enriched mitochondria was also analyzed, and the abundances of individual lipids were compared between the Mito-AP and the negative control derived from magnetic beads incubated with the wild-type extract. Several cardiolipins, known to occur in mitochondria (Schlame et al., 1993; Zhou et al., 2016), were exclusively detected in extracts of the Mito-AP and absent in the control. Two cardiolipins were also detected in the control, but were over three orders of magnitude more abundant in the Mito-AP extracts (Fig. 8; Supplemental Table S3). Ubiquinone (Q), a membrane-soluble electron carrier in the electron transport chain of mitochondria, was strongly enriched in samples containing mitochondria. Qs are classified according to the number of isoprenoid side-chain units, which usually rank from 6 (for yeast [Q6]) to 10 (for humans [Q10]). Interestingly, Q7, Q8, Q9, and Q10 were detected (Fig. 8), although it has been reported that Q9 is the sole form of Q in Arabidopsis (Hirooka et al., 2003; Yoshida et al., 2010; Liu and Lu, 2016). The roles of these additional Qs in plant mitochondria are currently unknown, but it is tempting to speculate that they may function in nonrespiratory pathways, similar to the involvement of human Q10 in signaling (Schmelzer et al., 2007). The strong enrichment of mitochondria by Mito-AP in combination with the sensitive detection by MS probably explains why several Qs could be detected here, thus highlighting that resolution is indeed gained by the focused analysis of isolated mitochondria. Previous studies on cardiolipins (Zhou et al., 2016) and Qs (Yoshida et al., 2010) had the advantage of employing a rapid quenching of the sample, abolishing any possibility for metabolite conversion. The cardiolipin species we observed could previously only be detected using a solid-phase extraction protocol (Zhou et al., 2016), suggesting that Mito-AP maybe useful for the initial detection of metabolites in samples of enriched mitochondria without need for further sample preparation. However, such findings are pending confirmation from samples that are more efficiently quenched than is possible with Mito-AP.

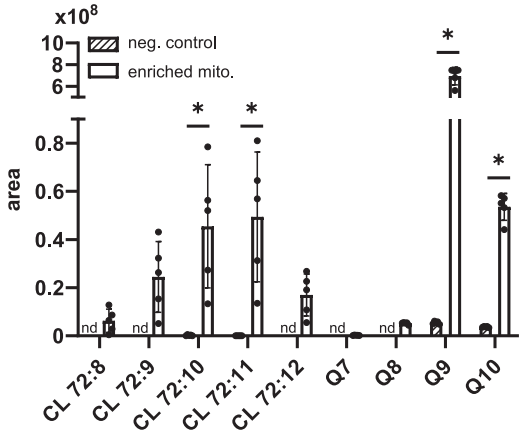

Figure 8. Enrichment of the mitochondrial cardiolipins (CL) and Qs in mitochondria enriched by Mito-AP. Seedlings carrying the 35S:Twin-Strep-tag:GFP:ADAPTER construct (enriched mito.) or Col-0 (neg. control) were grown for 10 d in liquid media for Mito-AP (method 2). Samples were extracted and lipids were identified and quantified with an orbitrap MS. Error bars represent the SD ($n = 5$ biological replicates, derived from independent Mito-APs of distinct samples grown in parallel). Significant differences (at $P < 0.05$) were determined with Student's t test and marked with an asterisk. Calculation of the FDR was done using the two-stage linear step-up procedure described in Benjamini et al. (2006). The statistical analysis was done with a FDR of 1%. nd, Not detectable.

Chlorophyll, associated with thylakoid membranes of the chloroplast, was also slightly enriched, by ~2-fold, in Mito-AP samples compared to controls (Supplemental Table S3). When mitochondria were bound to the beads, we observed that the beads became adhesive to each other, probably caused by mitochondria interconnecting several beads. This network of beads may occasionally trap thylakoid fragments which cannot be removed by washing. In fact, we occasionally observed some red auto-fluorescence in our mitochondria preparations, but never corresponding to the size of an intact chloroplast (Supplemental Fig. S12).

Interestingly, galactolipids, which are associated with the chloroplast, were also enriched in the Mito-AP samples. For the majority of these lipid species, only a slight enrichment of 10- to 20-fold was observed, but in one case a 200-fold enrichment was obtained (Supplemental Table S3). As for the chlorophylls, the physical entrapment of plastidic fragments during Mito-AP might explain this observation. It is also conceivable that some of these galactolipids actually reside in the mitochondria, because transfer of galactolipids from plastids to mitochondria has been observed, particularly in conditions of phosphate starvation (Jouhet et al., 2004). In summary, this proof-of-concept study demonstrates the feasibility of metabolite quantification in mitochondria upon isolation using the Mito-AP protocol, which paves the way for further studies addressing problems of metabolite conversion during the isolation procedure.

Mitochondria Isolated by Mito-AP Have a Membrane Potential, Respire, and Show Respiratory Control

Previous studies on mitochondria isolation techniques reported that the isolated organelles remained physiologically active (Keech et al., 2005). We also asked the question whether mitochondria isolated by Mito-AP maintain their membrane potential and respiratory control. However, this could not be addressed with the sodium chloride extraction buffer, because it was chosen for its compatibility with downstream LC-MS measurements and its reported potential to suppress metabolic activity (Kong et al., 2018). Different buffers containing either mannitol or Suc as osmotic agents were used instead.

First, we tested whether mitochondria in intact roots of the 35S:Twin-Strep-tag:GFP:ADAPTER plants have

Downloaded from https://academic.oup.com/plphys/article/182/3/1194/6116177 by Institute of Horticultural Economics user on 10 December 2021

membrane potential, which would indicate that the mitochondrial tag does not grossly disturb mitochondrial function or integrity. The fluorescent dye tetramethyl rhodamine methyl ester (TMRM) is only sequestered in mitochondria in the presence of a membrane potential (Brand and Nicholls, 2011; Schwarzländer et al., 2012). TMRM was found in mitochondria of the transgenic line as well as the wild type (Supplemental Fig. S13, A and B). The signal was quenched by adding carbonyl cyanide 3-chlorophenylhydrazone (CCCP), an uncoupling agent that abolishes the membrane potential. The same technique was applied to mitochondria isolated with the Mito-AP protocol using the modified extraction buffer containing 10 mM succinate. In these samples, the green fluorescence originating from the Twin-Strep-tag:GFP:ADAPTER protein coincided with the fluorescence of the TMRM dye in 73% of the cases. This rate dropped to 32% upon addition of the uncoupler CCCP (Supplemental Fig. S14). Moreover, the signal from these mitochondria was considerably weaker. These results suggest that >70% of the mitochondria enriched by Mito-AP are sufficiently intact to maintain a membrane potential.

Next, we assessed the respiration of mitochondria isolated by Mito-AP in a Seahorse Analyzer (Agilent; Rogers et al., 2011) and recorded the oxygen consumption rate (OCR) before and after addition of ADP, as well as in response to the inhibitors oligomycin and antimycin (Fig. 9). A basal respiration rate of 29 ± 3 nmol O_2 min^{-1} μg^{-1} protein was observed. Addition of ADP led to a 1.3-fold increase in OCR, which reverted to the basal level after addition of the ATP synthase inhibitor oligomycin. Furthermore, addition of antimycin, an inhibitor of complex III, reduced the OCR to background levels. These data demonstrate that mitochondria with respiratory activity can be isolated by Mito-AP, and that they maintain some degree of respiratory control, as indicated by the before-to-after OCR ratio upon addition of ADP or oligomycin (respiratory control ratio; Fig. 9).

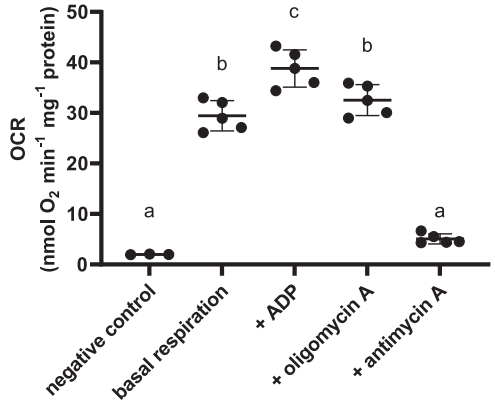

Figure 9. Activity of mitochondria isolated by Mito-AP from Arabidopsis. OCRs were measured for mitochondria bound to magnetic beads before (basal respiration) and after addition of ADP and in response to oligomycin A and antimycin A. In total, five replicates were analyzed for mitochondria bound to beads and three replicates for the negative control. The negative control represents the basal respiration of the empty beads. Error bars represent the SD. Statistical analysis was done using a one-way ANOVA with Tukey's honestly significant difference (HSD) mean-separation test. Lowercase letters indicate significant differences ($P < 0.05$).

These results were confirmed by the morphological assessment of Mito-AP-isolated organelles as deduced by electron microscopy. Mitochondria display outer and inner membranes as well as an ultrastructure consistent with intact organelles isolated in previous studies (Supplemental Fig. S15; de Virville et al., 1998; Logan and Leaver, 2000; Eubel et al., 2007). In some instances, a pronounced gap between the inner and outer membrane can be observed, suggesting either some shrinkage of the mitoplasts or an inflation of the outer membrane. Reasons for this are currently unknown. We also observed grana stacks and other unidentified compartments consistent with plastidic fragments observed in confocal microscopy and the presence of nonmitochondrial proteins in the preparations (Fig. 5; Supplemental Fig. S12).

DISCUSSION

Here we demonstrate that plant mitochondria can be enriched from small amounts of plant material in sufficient amounts to support proteome and metabolome analyses using affinity purification. The application and further development of this technique offers the potential to increase the resolution of proteome and metabolome experiments. Because comparatively little plant material is needed for Mito-AP, the biological context from which the mitochondria are obtained can be well defined. It can be envisioned that mitochondrial isolation may be restricted to only a certain tissue or only tissues in defined developmental states, for example leaves of different ages. Mito-AP also offers the prospect to exclusively decorate mitochondria of certain cell types or following environmental stimuli. For this, the Twin-Strep:ADAPTER protein would need to be expressed under the control of a cell-type-specific promoter or a promoter induced by a particular stimulus. Previous studies have shown the power of promoter-reporter fusions, for example for the elucidation of the root cell type-specific transcriptomes (Moussaieff et al., 2013) and for the isolation of cell-specific mitochondria from *Caenorhabditis elegans* as well as mouse (*Mus musculus*; Ahier et al., 2018; Bayraktar et al., 2019). Yet another possibility is the transfer of the affinity purification principle to other compartments of plant cells, for example to peroxisomes or chloroplasts. Along this line, an immunoprecipitation protocol has been developed for the enrichment of plant secretory vesicles to analyze their proteomes (Heard et al., 2015).

The affinity purification protocol presented here has several features that will facilitate its adaptation and use by other laboratories. First, the construct was

Downloaded from https://academic.oup.com/plphys/article/182/3/1194/6116177 by Institute of Horticultural Economics user on 10 December 2021

generated using the MoClo system (Patron et al., 2015), which is highly modular, allowing an independent exchange of different elements including the tags, the promoter, or the ADAPTER itself. Second, in contrast to DGC methods, no specialized equipment such as an ultracentrifuge is required to perform Mito-AP. Third, usage of the Strep-tag affinity system instead of a system based on antibodies (Chen et al., 2016) is cost effective. Mito-AP can be performed with a commercially available matrix already coated with Strep-Tactin. Alternatively, it is straightforward to attach Strep-Tactin to prepared iron oxide particles, further lowering the costs and increasing the yield (Supplemental Fig. S6).

Recently, a simple protocol was published for the economic production of iron oxide nanoparticles with carboxyl groups on the surface, called Bio on Magnetic Beads (Oberacker et al., 2019). We are currently investigating the suitability of these particles for Strep-Tactin loading. The availability of large quantities of affordable affinity matrix would permit an increase in the amount of beads used per preparation. This might improve the yield or accelerate the sample processing, because at high yields the magnetic separations do not need to be fully quantitative and can therefore be performed more swiftly. With shorter processing times, mitochondria could be isolated even closer to their native state. This is still a problem, because the ADP/ATP ratio (Fig. 6) showed that the mitochondria isolated by the current Mito-AP protocol are metabolically inactive (Stitt et al., 1982). An additional solution might be to prepare the mitochondria in the presence of buffers containing a broad selection of mitochondrial metabolite precursors suitable to maintain mitochondrial function during isolation. The successful reactivation of mitochondria with substrates for mitochondrial respiration was already demonstrated in this study (Fig. 9). In comparison to traditional isolation techniques, Mito-AP is performed in small volumes, which considerably reduces the costs of such an approach.

Conceptually, affinity elution from the matrix should increase the purity, because unspecifically bound contaminants will not be released and are removed together with the beads. Indeed, this was observed, because Mito-AP involving an elution step with biotin and proteinase K (method 2) resulted in higher purity than Mito-AP with method 1 (Fig. 5). However, it would be desirable to omit the proteinase K treatment, because it is time consuming and damages the mitochondrial surface proteins. Unfortunately, elution only with biotin is not efficient enough, probably because there are too many interactions between the Twin-Strep-decorated mitochondria and the Strep-Tactin on the matrix. The coating density of the matrix and the decoration density of the mitochondria should be further fine-tuned and optimized to develop a protocol that allows complete affinity elution. This might also reduce the number of beads connected to each other via mitochondria and thus limit the potential physical entrapment of contaminants in this network. Additionally, different bead surfaces should be tested with the aim to suppress the unspecific binding of metabolites, which would further reduce the background currently observed in the controls (Figs. 7 and 8). It is clear that metabolites can be interconverted in a very short period of time (Dietz, 2017) and that therefore the duration of the Mito-AP protocol is still too long to avoid such processes. However, the impact of mutants on the mitochondrial metabolome still can be studied by focusing on relative changes in metabolites rather than absolute amounts. Also, groups of metabolites that can be interconverted into each other can be combined and considered as pools. Alternatively, improved quenching techniques prior to the Mito-AP protocol may address this challenge. Furthermore, Mito-AP will allow the identification of low-abundance metabolites that cannot be detected in a crude extract (Fig. 8) because of ion suppression effects.

Plant mitochondria have been analyzed numerous times by proteomic approaches. However, definition of the complete set of proteins residing in this organelle and the discernment of these proteins from background and false positives is an ongoing struggle. Previous studies indicated an inconsistency between computational prediction for mitochondrial localization and experimental evidence from proteomic studies. Several nuclear-encoded proteins with a clear mitochondrial target peptide were not detected in mitochondria by proteomics (Heazlewood et al., 2005, 2007). To increase sensitivity and to eliminate more false positives, tandem purification strategies for mitochondria have been employed combining DGC with free-flow electrophoresis (Eubel et al., 2007). However, both methods are very time consuming and require specialized equipment and expertise. Here, we used a combination of DGC and Mito-AP and performed a correlation analysis for protein abundance integrating the data from all enrichment strategies. Irrespective of the technique used, true mitochondrial proteins should be enriched and form a closely correlated cluster. This was observed, and in addition to known mitochondrial proteins, previously uncharacterized candidate proteins were found in this cluster (Fig. 6). More detailed analyses are required to validate these mitochondrial protein candidates, which might provide clues about yet unknown processes taking place in plant mitochondria.

An important consideration is whether mitochondria isolated by Mito-AP are of the same quality as that described using centrifugation-based methods. Since the quantities of mitochondria isolated by Mito-AP are comparatively low, standard methods for quality control of mitochondria, for example an oxygen electrode assay to assess respiration, cannot be applied easily. Here, we demonstrate oxygen consumption of plant mitochondria using a Seahorse Analyzer, which is uniquely suited for minute sample amounts. Recently, the oxygen consumption of mammalian mitochondria bound to beads was observed using the same technique; however, in contrast to our study, the impact of

Downloaded from https://academic.oup.com/plphys/article/182/3/1194/6116177 by Institute of Horticultural Economics user on 10 December 2021

ADP on respiration was not reported (Ahier et al., 2018), suggesting that the methodology for assessing isolated mitochondria with this technology is still in its infancy. In our hands, the method required optimization of the amount of mitochondria and the concentration of ADP used. Currently, the minimum assay temperature in the Seahorse analyzer cannot fall below 29°C, which differs from previously described procedures for assessing the activity of plant mitochondria. The respiration rates and the respiratory control we report here (Fig. 9) are lower than that described previously for Arabidopsis (Kerbler et al., 2019). However, it is possible that these differences can in part be explained by the current imperfections of the assessment technology, which needs further optimization.

Electron microscopy pictures suggested the presence of predominantly intact mitochondria with an outer and inner membrane in the Mito-AP preparation (Supplemental Fig. S15), but the presence of strongly fragmented mitochondria cannot be excluded. In line with this result, we demonstrated that 73% of the isolated mitochondria showed a membrane potential (Supplemental Fig. S14). Although no abnormal phenotypes were observed in the Twin-Strep-tag:GFP:ADAPTER plants, another explanation for a lower respiration rate/respiratory control is that expression of the Twin-Strep-tag:GFP:ADAPTER protein has an impact on mitochondrial functionality. This potential effect might be attenuated by further reducing the abundance of the protein with a weaker promoter or by removing the catalytic domain of the ADAPTER protein.

In summary, this study shows that Mito-AP allows rapid enrichment of plant mitochondria from small amounts of plant material. This work should, however, be regarded as a proof-of-concept pilot study that requires further experimentation to determine whether tagging the mitochondria interferes with their function, especially under stress conditions. Using this protocol, the quantification of mitochondrial metabolite subpools in the absence of any significant contamination was achieved, and previously uncharacterized candidate proteins for the complete mitochondrial proteome were identified. We envisage that affinity purification of organelles will increase the sensitivity of metabolome and proteome approaches. The potential of this method to target particular organelle subpopulations, in combination with the short processing time required for affinity isolation, will increase the spatial and temporal resolution for the investigation of plant organelles in the future.

MATERIALS AND METHODS

Plant Material and Cultivation

For proteomic analysis, Arabidopsis (*Arabidopsis thaliana*) plants were cultivated in soil (Steckmedium, Klasmann-Deilmann) in a climate chamber under short-day conditions (8 h light/16 h darkness, 22°C, 85 μmol s^{-1} m^{-2} light, and 65% humidity), as described in Senkler et al. (2017). Plants were harvested after 6 weeks. For metabolome analysis, plants were cultivated at 22°C in sterile 100-mL flasks (10 mg seeds per flask) in liquid culture (0.5 × Murashige and Skoog, 0.125% [w/v] MES, pH 5.8) in a shaker with an artificial light source emitting 45 μmol s^{-1} m^{-2} light. For the first 3 d, the shaker (New Brunswick Innova 42, Eppendorf) was set to 30 rpm and subsequently changed to 50 rpm. Plants were harvested after 10 d. For phenotypical characterization, plants were cultivated in 8-cm pots filled with soil (Steckmedium, Klasmann-Deilmann) in a climate chamber under long-day conditions (16 h light/8 h darkness, 22°C day, 20°C night, 100 μmol s^{-1} m^{-2} light, and 70% humidity). For leaf surface area and rosette fresh weight analysis, plants were cultivated in trays with soil (Steckmedium, Klasmann-Deilmann) under short-day conditions as described above. For root length and germination assays, plants were grown on modified Murashige and Skoog medium (3 mM $CaCl_2$, 1.5 mM $MgSO_4$, 1.25 mM KH_2PO_4, 18.7 mM KNO_3, 0.1 mM $FeSO_4$, 0.1 mM Na_2EDTA, 0.13 mM $MnSO_4$, 0.1 mM BO_3, 0.03 mM $ZnSO_4$, 1 μM Na_2MoO_4, 0.1 μM $CuSO_4$, 0.1 μM $NiCl_2$, 0.5 g L^{-1} MES, and 8 g L^{-1} phytoagar, pH adjusted to 5.7 with KOH) under long-day conditions as described above.

Subcellular Localization and Confocal Microscopy

For subcellular localization, the constructs were coexpressed in *Nicotiana benthamiana* leaves for 4 d and analyzed by confocal microscopy as described by Dahncke and Witte (2013). For confocal microscopy, the Leica True Confocal Scanner SP8 microscope equipped with an HC PL APO CS2 40× 1.10 water immersion objective (Leica Microsystems) was used. Acquired images were processed using Leica Application Suite Advanced Fluorescence software.

Magnetic Bead Preparation

The activation of the polysaccharide resins was described previously (Kohn and Wilchek, 1984) and coupling of Strep-Tactin to the magnetic beads was performed according to a protocol provided by Chemicell, with minor modifications. In detail, 400 μL uncoated magnetic beads (25 mg mL^{-1}) with a GlcA polymer matrix (fluidMAG ARA, 4115-5, Chemicell) were mixed with 150 μL freshly prepared activation buffer containing 10 mg 1-ethyl-3-(3-dimethylaminopropyl) carbodiimide and mixed in a shaker for 10 min at room temperature (RT). Between the different steps, the beads were always pelleted using a magnetic separator. After activation, the beads were washed twice by suspending them in 1 mL water. For coating with Strep-Tactin, the bead pellet was resuspended in 250 μL water, 20 μL Strep-Tactin solution was added (5 mg mL^{-1} in phosphate-buffered saline [PBS]; 2-1204-005, IBA Lifesciences), and the slurry was incubated for 2 h under constant shaking. The beads were washed three times with 1 mL water and stored in 400 μL 0.05% (w/v) sodium azide solution.

500 μL beads with a starch polymer matrix (25 mg mL^{-1}; Chemicell, fluidMAG –D, 4101-5) were washed once with 1 mL freshly prepared activation buffer containing 0.2 M sodium hydrogen carbonate (pH range 8.4 to 8.7), pelleted, and resuspended in 500 μL activation buffer. After addition of 100 μL 5 M cyanogen bromide in acetonitrile, the beads were mixed and incubated for 10 min on ice, then washed twice with 1 mL PBS buffer and resuspended in 500 μL PBS. To ensure a homogenous coating, the beads were placed for 2 min in an ultrasonication bath. For coating, 500 μL magnetic beads were incubated with 20 μL Strep-Tactin solution (5 mg mL^{-1} in PBS; 2-1204-005, IBA Lifesciences) for 2 h under constant shaking. The beads were washed three times with 1 mL water and stored in 500 μL 0.05% (w/v) sodium azide solution.

Cloning

Cloning was performed using the MoClo system described by Engler et al. (2014). For this, several intermediate vectors in addition to already published vectors had to be created. The primers used are listed in Supplemental Table S4.

Turbo-GFP was amplified from pICSL50016 using P626 and P820 and cloned into pAGM1287, resulting in the vector pAGM1287_TurboGFP+Intron_without_Stop (V151). The TOM22-V fragment sequence was synthesized by Integrated DNA Technologies (IDT) and cloned into pAGM1301, resulting in the vector pAGM1301_level_1_TOM22-V (V152). The Cb5-D fragment sequence was synthesized by IDT and cloned into pAGM1301, resulting in the vector pAGM1301_level_0_Cb5-D (V153). The codon-optimized DNA sequence coding for the Twin-Strep-tag (28 amino acids: WSHPQFEK-GGGSGGGSGG-SA-WSHPQFEK) was synthesized by IDT and cloned into pAGM1276, resulting in the vector pAGM1276_Twin-Strep (V154). Amplification of the ADAPTER (encoded at locus At1g55450) using complementary DNA from

Downloaded from https://academic.oup.com/plphys/article/182/3/1194/6116177 by Institute of Horticultural Economics user on 10 December 2021

Arabidopsis was performed by using the primers P1023 + P1024 and P1025 + P1026, integrating a mutation to remove a *Bbs*I recognition site without changing the amino acid sequence. PCR products were digested, ligated, and cloned into pAGM1301, resulting in the vector pAGM1301_level_0_ADAPTER (V159).

The level_1 vector containing a phosphinothricin resistance for plant selection was generated by combining pICH87633, pICH43844, and pICH41421 with the recipient vector pICH47742 in a digestion/restriction reaction with *Bsa*I resulting in pICH47742_Basta_pos2_fwd (V166). For cloning the level_1 *Sc*CoxIV:mCherry vector, pICH45089, pAGM1482, pICSL80007, and pICH41432 were digested/ligated together with the recipient vector pICH47742, resulting in pICH47742 _pos2_fwd_ *Sc*CoxIV:mCherry (V168). For cloning the level_1 vector containing 35S:Twin-Strep-tag:GFP:TOM22-V, pICH41373, pAGT707, V154, V151, V152, and pICH41421 were combined with the recipient vector pICH47732 in a digestion/restriction reaction with *Bsa*I resulting in pICH47732_pos1_fwd_35S:Twin-Strep-tag:GFP:TOM22-V (H405). For cloning the level_1 vector containing 35S:Twin-Strep-tag:GFP:Cb5-D, pICH41373, pAGT707, V154, V151, V153, and pICH41421 and the recipient vector pICH47732 were combined in a digestion/restriction reaction with *Bsa*I resulting in pICH47732_pos1_fwd_35S:Twin-Strep-tag:GFP:Cb5-D (H407). For cloning the level_1 vector containing the 35S:Twin-Strep-tag:GFP:ADAPTER, pICH41373, pAGT707, V154, V151, V159, and pICH41421 were combined with the recipient vector pICH47732 in a digestion/restriction reaction with *Bsa*I resulting in pICH47732_pos1_fwd_35S:Twin-Strep-tag:GFP:ADAPTER (H433).

For the level_2 vector containing 35S:Twin-Strep-tag:GFP:ADAPTER and a Basta resistance gene, H433, V166, and pICH41744 were combined with the recipient vector pAGM4723 in a digestion/restriction reaction with *Bbs*I resulting in the vector pAGM4723_35S:Twin-Strep-tag:GFP:ADAPTER_Basta (H500). The level_2 vector pAGM4723_35S:Twin-Strep-tag:GFP:ADAPTER_*Sc*CoxIV:mCherry (H501) was cloned by combining H433, pICH41744, V168, and pAGM4723 in a digestion/restriction reaction with *Bpi*I. All materials (plants and vectors) are made available upon request.

Leaf Area Quantification

To quantify the leaf area, RGB (red/green/blue) pictures were taken from the same distance every day and loaded into ImageJ. To create a binary image, the pictures colors were split into separate channels (Image → color → split channels). The green channel image was then further processed to reduce background signal by minimum filtering with a radius of 50 pixels followed by maximum filtering with a radius of 50 pixels and a contrast enhancement with a saturation of 0.01%. Subsequently a binary picture was created by setting an auto-threshold. The binary picture was modified (euclidian distance map binary options → close [20 iterations]) and the region of interest was projected onto the scaled original picture to retrieve the leaf area of the respective sample.

Density Gradient Isolation of Mitochondria

A modified version of the protocol of Keech et al. (2005) was used. All steps were carried out at 4°C. Arabidopsis rosette leaves were ground for 10 min in disruption buffer using a mortar and pestle (0.3 M Suc, 60 mM TES, pH 8 [KOH], 25 mM sodium pyrophosphate, 10 mM KH_2PO_4, 2 mM EDTA, 1 mM Gly, 1% [w/v] PVP 40, 1% [w/v] bovine serum albumin [BSA], 50 mM sodium ascorbate, and 20 mM Cys) in the presence of sand. Two milliliters of disruption buffer was used for each gram of plant material. The homogenate was filtered through 4 layers of Miracloth and the dry cake was ground in disruption buffer for another 5 min before being filtered as outlined above. The pooled filtrate was centrifuged at 300*g* for 5 min and the resulting supernatant was centrifuged at 2,500*g* for 5 min once or twice, depending on the size of the pellet. A mitochondria-enriched pellet was produced by centrifuging the supernatant for 15 min at 15,100*g*. The pellet was subsequently resuspended in 1 mL washing buffer (0.3 M Suc, 10 mM TES, pH 7.5 [KOH], and 10 mM KH_2PO_4) and subjected to two strokes in a Dounce homogenizer. Mitochondria were further enriched on continuous Percoll gradients (50% [v/v] Percoll, 0.3 M Suc, 10 mM TES [pH 7.5 with KOH], 1 mM EDTA, 10 mM KH_2PO_4, and 1 mM Gly). Percoll gradients were established by centrifugation of the gradients at 69,400*g* for 40 min prior to loading. One milliliter of homogenized material was layered upon each of the 12 gradients, followed by centrifugation at 17,400*g* for 20 min. Mitochondria, concentrated near the bottom of the tube as a cloudy layer, were quantitatively removed using a glass pipette, resuspended in washing buffer, and centrifuged at 17,200*g* for 15 min. This was repeated two to four times until the pellets were solid. Finally, pellets of all gradients were pooled in a last washing step.

Isolation of Plant Mitochondria with Mito-AP

For Mito-AP, 500 mg plant material was ground using a mortar and pestle with some sand and 1 mL of ice cold, freshly prepared extraction buffer (32 μL mL^{-1} BioLock [IBA Lifesciences], 100 mM ammonium bicarbonate, and 200 mM NaCl, pH 8) on ice for 3 min. The extract was transferred to a 2-mL reaction tube and centrifuged at 4°C for 5 min at 1,000*g*. Aliquots of magnetic beads (25 mg mL^{-1}; 500 μL for metabolome analysis and 250 μL for proteome analysis) were prepared by washing beads twice with 1 mL washing buffer (100 mM ammonium bicarbonate and 200 mM NaCl, pH 8) followed by resuspension in 500 μL washing buffer. The supernatant of the extract (800 μL) was added to the beads and incubated for 5 min at 4°C with continuous inversion. The beads were separated from the remaining liquid with a magnetic separator for 2 min. The supernatant was discarded and 1 mL washing buffer was added. Beads were resuspended by inverting and gentle shaking of the reaction tube. The washing was repeated three times. For method 1, the beads were directly incubated with 20 μL 2× SDS loading buffer and heated for 5 min at 95°C. For method 2, the beads were further treated by resuspension in 1 mL elution buffer (50 mM biotin, 100 mM ammonium bicarbonate, and 200 mM NaCl, pH 8). The mixture was incubated for 5 min on ice and inverted every minute. Subsequently, 950 μL digest buffer (200 μg mL^{-1} proteinase K, 4 mM $CaCl_2$, 100 mM ammonium bicarbonate and 200 mM NaCl, pH 8) was added and the slurry incubated at RT for 10 min. Proteinase K was inhibited by the addition of 50 μL 100 mM phenylmethylsulfonyl fluoride (in pure isopropanol). The beads were separated for 2 min with a magnetic separator and the liquid was transferred with a cut tip, to prevent damaging the mitochondria, to a new 2-mL reaction tube followed by centrifugation at 4°C for 10 min at 14,500*g*. The supernatant was carefully removed and the pellet was stored at −80°C for further analysis.

Proteomic Analysis

Proteins from all crude extracts were first quantified with Bradford reagent to ensure a similar loading of SDS gels. Samples were resuspended in 20 μL 2× SDS loading buffer and heated for 5 min at 95°C. The proteins from all samples were additionally quantified by comparison with a BSA standard on the preparative SDS gel (Luo et al., 2006) employing a Li-cor Odyssey FC with Image Studio software. Sample preparation and proteomic analysis were performed according to Rugen et al. (2019). The volume used for resuspension of the peptides was adjusted for each sample to account for differences in the initial protein amounts. In fact, the total number of iBAQs in all samples with enriched mitochondria varied only by a factor of 3 (Supplemental Table S1). We found ~10-fold fewer iBAQs in crude extracts for differential and density gradient centrifugation (DGC), potentially indicating interference of the extraction buffer with in-gel quantification.

Correlation Analysis

Peptides from DGC, Mito-AP, and DGC combined with Mito-AP (method 1 and 2, respectively) were reanalyzed using a 4-h gradient for LC-MS/MS and otherwise treated as described above. All iBAQs were normalized to the total iBAQs in the respective sample and a correlation matrix, based on the Pearson correlation coefficient, was constructed in R (version 3.6.0; https://www.R-project.org). Correlations with a coefficient >0.99 were visualized by Cytoscape version 3.7.1 (Shannon, 2003), including an expression correlation plugin) with an edge-weighted spring-embedded layout, based on the correlation coefficient. Edges with a higher correlation coefficient are shorter.

Metabolome Analysis

The pellet of mitochondria derived from Mito-AP method 2 was solubilized with 0.5 mL 80:20 MeOH:5 mM ammonium acetate (pH 9.5, adjusted with NH_3), vortexed, and sonicated for 2 min at RT. Samples were centrifuged for 10 min at 40,000*g*, and supernatants were dried down in a vacuum centrifuge concentrator (RVC 2-25 CD plus, Thermo Fisher Scientific) until dry. The resulting metabolites were resuspended in 11 μL 5 mM ammonium acetate (pH 9.5, adjusted with NH_3). The chromatography of 10 μL solution was performed on a 1290 Infinity HPLC (Agilent Technologies) using a Hypercarb column (50 mm, 4.6-mm diameter; Thermo Fisher Scientific) with mobile phase A consisting of

Downloaded from https://academic.oup.com/plphys/article/182/3/1194/6116177 by Institute of Horticultural Economics user on 10 December 2021

5 mM ammonium acetate (pH 9.5, adjusted with NH_3) and mobile phase B consisting of pure acetonitrile. With a flow rate of 0.6 mL min^{-1}, the gradient was 0–7 min, 4% to 20% B; 7–11 min 10 s, 20% to 30% B; 11 min 10 s–15 min 10 s, 50% B; 15 min 10 s–15 min 20 s, 50% to 100% B; 15 min 20 s–17 min 42 s, 100% B; 17 min 42 s–18 min, 100% to 4% B; and 4% B until the end of the gradient (23 min). With this gradient, metabolites elute in the following order: NMN (4.6 min), ATP (6.1 min), ADP (6.33 min), AMP (6.35 min), NADP (9.1 min), and NAD/NADH (11.6 min). The masses for the metabolites were quantified on a 6470 triple quadrupole mass spectrometer (Agilent Technologies). The LC-Agilent Jet Stream-electrospray ionization-tandem MS measurements were conducted under multiple reaction monitoring in positive ion mode. Agilent Jet Stream-electrospray ionization source conditions were set as follows: gas temperature, 250°C; gas flow, 12 L min^{-1}; nebulizer gas, 20 psi; sheath gas temperature, 395°C; sheath gas flow, 12 L min^{-1}; capillary voltage, 3000 V; and nozzle voltage, 500 V. Absolute amounts were calculated by comparison with the respective external standard curves of known concentrations. Identification of compounds was confirmed by retention times identical with the external standards. For quantification, the multiple reaction monitoring with the highest signal was used as quantifier. Other transitions, if available, were used as additional qualifiers. Transitions, fragmentors, and collision energies for all compounds can be found in Supplemental Table S5. For quantification, the Agilent Mass Hunter Quantitative Analysis Software was used.

Lipidomic Analysis

The pellet of mitochondria from Mito-AP method 2 was extracted according to a described method for the extraction and analysis of lipids, metabolites, proteins, and starch (Salem et al., 2016). In brief, frozen beads were resuspended in 1 mL extraction buffer (methyl tert-butyl ether:MeOH, 3:1 [v/v]) and the samples were incubated on a shaker for 45 min before a 15-min sonication in an ice-cooled sonication bath was applied. Phase separation was achieved by adding 0.65 mL of water:MeOH (3:1). Lipids were analyzed from the organic (methyl tert-butyl ether) phase by ultra-performance LC-MS. For this purpose, an Acquity iClass (Waters) ultra-performance LC was connected to a Q-Exactive HF (Thermo Scientific) high-resolution MS. Samples were measured in positive ionization mode as described previously (Giavalisco et al., 2011; Hummel et al., 2011; Salem and Giavalisco, 2018;). Data analysis was performed using targeted peak extraction and integration using the Trace Finder software (Version 4.1, Thermo Scientific).

Visualization of the Mitochondrial Membrane Potential

Twelve-day-old seedlings originating from liquid culture were washed twice with water and incubated in 500 μL one-half strength Murashige and Skoog medium containing 40 nM TMRM (dissolved in dimethyl sulfoxide) for at least 15 min. For analyzing the decoupled state of the mitochondria, 40 μM CCCP (dissolved in dimethyl sulfoxide) was added additionally to the solution to a final concentration of 40 μM and incubated for 30 min.

Isolated mitochondria bound to magnetic beads were resuspended in 100 μL mitochondrial assay solution buffer (70 mM Suc, 219 mM mannitol, 5 mM HEPES, 1 mM EGTA, and 0.5% [w/v] BSA, pH 7.2) containing 10 mM succinate and treated as described.

The analysis of the samples was done by using confocal microscopy as described above. The TMRM dye was excited at 552 nm and the emission between 600 and 615 nm was visualized.

Respiratory Activity Measurement

For the respiratory activity, 500 mg plant material was ground up using a mortar and pestle with some sand and 1 mL ice cold, freshly prepared extraction buffer (32 μL mL^{-1} BioLock [IBA Lifesciences]; 5 mM dithiothreitol, 300 mM Suc, 5 mM KH_2PO_4, 10 mM TES, 10 mM NaCl, 2 mM $MgSO_4$, and 0.1% [w/v] BSA, pH 7.2) on ice for 2 min. The extract was transferred to a 2 mL reaction tube and centrifuged at 4°C for 5 min at 1,000*g*. Five hundred microliters of magnetic beads (25 mg mL^{-1}) was prepared by washing twice with 1 mL washing buffer (300 mM Suc, 5 mM KH_2PO_4, 10 mM TES, 10 mM NaCl, 2 mM $MgSO_4$, and 0.1% [w/v] BSA, pH 7.2), followed by resuspension in 500 μL washing buffer. The subsequent steps were performed as described in "Isolation of Plant Mitochondria with Mito-AP."

For the measurement of the respiration through succinate dehydrogenase (complex II), the beads were resuspended in respiration buffer 2 (300 mM Suc, 5 mM KH_2PO_4, 10 mM TES, 10 mM NaCl, 2 mM MgSO, and 0.1% [w/v] BSA, 10 mM succinate, 500 μM ATP, and 500 μM n-propyl gallate, pH 7.2) at RT.

The OCR measurements were performed using the Seahorse XFe 96 Analyzer (Agilent Technologies). The XFe96 Sensor Cartridge was prepared according to the manufacturer's instructions. The ports were filled as follows: port A, 20 μL 60 mM ADP, pH adjusted to 7.2 with KOH; port B, 22 μL 50 μg mL^{-1} oligomycin A; port C, 24 μL 80 mM antimycin A; port D, 26 μL buffer. All chemicals were prepared in the corresponding respiration buffer.

Resuspended beads were loaded into the XF96 cell culture microplate and the plate was subsequently centrifuged for 5 min at 2,200*g*. The wells were filled with the corresponding respiration buffer to a final volume of 200 μL. The four corners of the plate were not used for sample measurements.

The respiration assay was performed at 29°C (internal heater was turned off). After equilibration for 12 min, the baseline was measured by mixing for 30 s, waiting 10 s, and measuring for 2 min. The same procedure was done after the injection of the single ports. After the measurements, the protein amount was quantified for every sample.

Transmission Electron Microscopy

Samples, prepared as described above for the respiratory measurements, were fixed in 0.15 M HEPES, pH 7.35, containing 1.5% (w/v) formaldehyde and 1.5% (w/v) glutaraldehyde for 30 min at RT and overnight at 4°C. Samples were immobilized in 2% agarose (w/v) and then incubated in aqueous solutions of 1% (w/v) OsO4 (2 h at RT) and 1% (w/v) uranyl acetate (overnight at 4°C). After dehydration in acetone, samples were embedded in Epon, and 60-nm sections were stained with uranyl acetate and lead citrate (Reynolds, 1963). Images were recorded using a Morgagni transmission electron microscope (FEI) with a side-mounted Veleta charge-coupled device camera.

Accession Numbers

Sequences for the ADAPTER protein and TOM22-V are provided by Araport with the accession numbers At1g55450 and At5g43970, respectively. The Cb5-D sequence is available under the GenBank accession AY578730.

Supplemental Material

The following supplemental materials are available.

Supplemental Figure S1. Transient expression of different tail-anchored proteins fused to GFP in *N. benthamiana*.

Supplemental Figure S2. Quantitative comparison of phenotypical traits between the wild type (Col-0) and a stable 35S:Twin-Strep-tag:GFP:ADAPTER construct.

Supplemental Figure S3. Integrity of isolated mitochondria in different buffers.

Supplemental Figure S4. Plant mitochondria bound to a commercial matrix of 1-μm diameter.

Supplemental Figure S5. Different bead sizes and coating materials influence the enrichment of mitochondria.

Supplemental Figure S6. Quantification of the relative protein amounts from mitochondria enriched with different matrices.

Supplemental Figure S7. Quantification of Strep-Tactin bound to different magnetic matrices.

Supplemental Figure S8. Plant material needed for DGC and Mito-AP and relative mitochondrial protein yield obtained by both methods.

Supplemental Figure S9. Quantification of the total protein yield obtained from elution with and without proteinase K.

Supplemental Figure S10. Variation of mitochondrial purity from biological repeats processed by DGC or Mito-AP.

Supplemental Figure S11. ADP-Glc standard curve.

Supplemental Figure S12. Contamination with plastidic fragments.

Supplemental Figure S13. Visualization of the mitochondrial membrane potential in vivo.

Downloaded from https://academic.oup.com/plphys/article/182/3/1194/6116177 by Institute of Horticultural Economics user on 10 December 2021

Supplemental Figure S14. Visualization of the mitochondrial membrane potential in vitro.

Supplemental Figure S15. Electron micrographs of isolated mitochondria.

Supplemental Table S1. Proteins identified by proteomics for the determination of mitochondrial purity.

Supplemental Table S2. Proteins identified in a 4-h LC gradient for correlation analysis.

Supplemental Table S3. Lipids identified by LC-MS in Mito-AP (method 2) from 35S:Twin-Strep-tag:GFP:ADAPTER plants or Col-0 plants.

Supplemental Table S4. Primer sequences.

Supplemental Table S5. MRM parameters used for detection of polar metabolites with a triple quadrupole MS.

ACKNOWLEDGMENTS

The authors thank Hans-Peter Braun, Sascha Offermann (Leibniz University, Hannover), and Max Kraner (University Erlangen-Nürnberg) for helpful discussions, Nergis Özmen and Zachary Mullin-Bernstein (Leibniz University, Hannover) for the assistance with cloning and preliminary experiments, Jennifer Senkler for performing DGC-based mitochondria isolations, and Marianne Langer (Leibniz University, Hannover) for preparation of MS samples. The authors are deeply grateful to Guilhermina Carriche and Matthias Lochner (TWINCORE) for assisting with the Seahorse instrument. The authors also thank Werner Kammerloher and Daniel Gebhard (Agilent) for helpful advice on the Seahorse analyzer. We also express our gratitude to Sören Budig (Leibniz University, Hannover) for advice on the statistical analysis.

Received June 17, 2019; accepted December 16, 2019; published January 7, 2020.

LITERATURE CITED

Agius SC, Rasmusson AG, Møller IM (2001) NAD(P) turnover in plant mitochondria. Aust J Plant Physiol **28:** 461–470

Ahier A, Dai C-Y, Tweedie A, Bezawork-Geleta A, Kirmes I, Zuryn S (2018) Affinity purification of cell-specific mitochondria from whole animals resolves patterns of genetic mosaicism. Nat Cell Biol **20:** 352–360

Afanasyeva MA, Ustiugova AS, Golyshev SA, Kopylov AT, Bogolyubova AV, Demin DE, Belousov PV, Schwartz AM (2018) Isolation of large amounts of highly pure mitochondria for "omics" studies. Biochemistry (Mosc) **83:** 76–85

Arrivault S, Guenther M, Florian A, Encke B, Feil R, Vosloh D, Lunn JE, Sulpice R, Fernie AR, Stitt M, et al (2014) Dissecting the subcellular compartmentation of proteins and metabolites in Arabidopsis leaves using non-aqueous fractionation. Mol Cell Proteomics **13:** 2246–2259

Bayraktar EC, Baudrier L, Özerdem C, Lewis CA, Chan SH, Kunchok T, Abu-Remaileh M, Cangelosi AL, Sabatini DM, Birsoy K, et al (2019) MITO-Tag mice enable rapid isolation and multimodal profiling of mitochondria from specific cell types in vivo. Proc Natl Acad Sci USA **116:** 303–312

Benjamini Y, Krieger AM, Yekutieli D (2006) Adaptive linear step-up procedures that control the false discovery rate. Biometrika **93:** 491–507

Boutry M, Faber AM, Charbonnier M, Briquet M (1984) Microanalysis of plant mitochondrial protein synthesis products: Detection of variant polypeptides associated with cytoplasmic male sterility. Plant Mol Biol **3:** 445–452

Brand MD, Nicholls DG (2011) Assessing mitochondrial dysfunction in cells. Biochem J **435:** 297–312

Chen WW, Freinkman E, Wang T, Birsoy K, Sabatini DM (2016) Absolute quantification of matrix metabolites reveals the dynamics of mitochondrial metabolism. Cell **166:** 1324–1337

Dahncke K, Witte C-P (2013) Plant purine nucleoside catabolism employs a guanosine deaminase required for the generation of xanthosine in *Arabidopsis*. Plant Cell **25:** 4101–4109

Day DA, Neuburger M, Douce R (1985) Biochemical-characterization of chlorophyll-free mitochondria from pea leaves. Aust J Plant Physiol **12:** 219–228

de Virville JD, Alin MF, Aaron Y, Remy R, Guillot-Salomon T, Cantrel C (1998) Changes in functional properties of mitochondria during growth cycle of *Arabidopsis thaliana* cell suspension cultures. Plant Physiol Biochem **36:** 347–356

Dietz K-J (2017) Subcellular metabolomics: The choice of method depends on the aim of the study. J Exp Bot **68:** 5695–5698

Engler C, Youles M, Gruetzner R, Ehnert T-M, Werner S, Jones JDG, Patron NJ, Marillonnet S (2014) A golden gate modular cloning toolbox for plants. ACS Synth Biol **3:** 839–843

Eubel H, Lee CP, Kuo J, Meyer EH, Taylor NL, Millar AH (2007) TECHNICAL ADVANCE: Free-flow electrophoresis for purification of plant mitochondria by surface charge. Plant J **52:** 583–594

Fürtauer L, Küstner L, Weckwerth W, Heyer AG, Nägele T (2019) Resolving subcellular plant metabolism. Plant J **100:** 438–455

Gardeström P, Wigge B (1988) Influence of photorespiration on ATP/ADP ratios in the chloroplasts, mitochondria, and cytosol, studied by rapid fractionation of barley (*Hordeum vulgare*) protoplasts. Plant Physiol **88:** 69–76

Gerhardt R, Heldt HW (1984) Measurement of subcellular metabolite levels in leaves by fractionation of freeze-stopped material in nonaqueous media. Plant Physiol **75:** 542–547

Giavalisco P, Li Y, Matthes A, Eckhardt A, Hubberten H-M, Hesse H, Segu S, Hummel J, Köhl K, Willmitzer L (2011) Elemental formula annotation of polar and lipophilic metabolites using ^{13}C, ^{15}N and ^{34}S isotope labelling, in combination with high-resolution mass spectrometry. Plant J **68:** 364–376

Heard W, Sklenář J, Tomé DFA, Robatzek S, Jones AM (2015) Identification of regulatory and cargo proteins of endosomal and secretory pathways in *Arabidopsis thaliana* by proteomic dissection. Mol Cell Proteomics **14:** 1796–1813

Heazlewood JL, Tonti-Filippini J, Verboom RE, Millar AH (2005) Combining experimental and predicted datasets for determination of the subcellular location of proteins in Arabidopsis. Plant Physiol **139:** 598–609

Heazlewood JL, Verboom RE, Tonti-Filippini J, Small I, Millar AH (2007) SUBA: The Arabidopsis Subcellular Database. Nucleic Acids Res **35:** D213–D218

Hirooka K, Bamba T, Fukusaki E, Kobayashi A (2003) Cloning and kinetic characterization of *Arabidopsis thaliana* solanesyl diphosphate synthase. Biochem J **370:** 679–686

Hooper CM, Castleden IR, Tanz SK, Aryamanesh N, Millar AH (2017) SUBA4: The interactive data analysis centre for Arabidopsis subcellular protein locations. Nucleic Acids Res **45**(D1): D1064–D1074

Hornig-Do H-T, Günther G, Bust M, Lehnartz P, Bosio A, Wiesner RJ (2009) Isolation of functional pure mitochondria by superparamagnetic microbeads. Anal Biochem **389:** 1–5

Hummel J, Segu S, Li Y, Irgang S, Jueppner J, Giavalisco P (2011) Ultra performance liquid chromatography and high resolution mass spectrometry for the analysis of plant lipids. Front Plant Sci **2:** 54

Hwang YT, Pelitire SM, Henderson MPA, Andrews DW, Dyer JM, Mullen RT (2004) Novel targeting signals mediate the sorting of different isoforms of the tail-anchored membrane protein cytochrome b5 to either endoplasmic reticulum or mitochondria. Plant Cell **16:** 3002–3019

Ikuma H (1970) Necessary conditions for isolation of tightly coupled higher plant mitochondria. Plant Phys **45:** 773–781

Jouhet J, Marechal E, Baldan B, Bligny R, Joyard J, Block MA (2004) Phosphate deprivation induces transfer of DGDG galactolipid from chloroplast to mitochondria. J Cell Biol **167:** 863–874

Keech O, Dizengremel P, Gardestrom P (2005) Preparation of leaf mitochondria from *Arabidopsis thaliana*. Physiol Plant **124:** 403–409

Kerbler SM, Taylor NL, Millar AH (2019) Cold sensitivity of mitochondrial ATP synthase restricts oxidative phosphorylation in *Arabidopsis thaliana*. New Phytol **221:** 1776–1788

Klein M, Binder S, Brennicke A (1998) Purification of mitochondria from Arabidopsis. In JM Martinez-Zapater, and J Salinas, eds, Arabidopsis Protocols. Humana Press, Totowa, NJ, pp 49–53

Klodmann J, Senkler M, Rode C, Braun HP (2011) Defining the protein complex proteome of plant mitochondria. Plant Physiol **157:** 587–598

Kohn J, Wilchek M (1984) The use of cyanogen bromide and other novel cyanylating agents for the activation of polysaccharide resins. Appl Biochem Biotechnol **9:** 285–305

Kong Z, Jia S, Chabes AL, Appelblad P, Lundmark R, Moritz T, Chabes A (2018) Simultaneous determination of ribonucleoside and deoxyribonucleoside triphosphates in biological samples by hydrophilic

Downloaded from https://academic.oup.com/plphys/article/182/3/1194/6116177 by Institute of Horticultural Economics user on 10 December 2021

interaction liquid chromatography coupled with tandem mass spectrometry. Nucleic Acids Res **46:** e66

Kraner ME, Müller C, Sonnewald U (2017) Comparative proteomic profiling of the choline transporter-like1 (CHER1) mutant provides insights into plasmodesmata composition of fully developed *Arabidopsis thaliana* leaves. Plant J **92:** 696–709

Lilley RM, Stitt M, Mader G, Heldt HW (1982) Rapid fractionation of wheat leaf protoplasts using membrane filtration. Plant Physiol **70:** 965–970

Liu M, Lu S (2016) Plastoquinone and ubiquinone in plants: Biosynthesis, physiological function and metabolic engineering. Front Plant Sci **7:** 1898

Logan DC, Leaver CJ (2000) Mitochondria-targeted GFP highlights the heterogeneity of mitochondrial shape, size and movement within living plant cells. J Exp Bot **51:** 865–871

Luo S, Wehr NB, Levine RL (2006) Quantitation of protein on gels and blots by infrared fluorescence of Coomassie blue and Fast Green. Anal Biochem **350:** 233–238

Maarse AC, Van Loon AP, Riezman H, Gregor I, Schatz G, Grivell LA (1984) Subunit IV of yeast cytochrome c oxidase: Cloning and nucleotide sequencing of the gene and partial amino acid sequencing of the mature protein. EMBO J **3:** 2831–2837

Maggio C, Barbante A, Ferro F, Frigerio L, Pedrazzini E (2007) Intracellular sorting of the tail-anchored protein cytochrome *b*5 in plants: A comparative study using different isoforms from rabbit and *Arabidopsis*. J Exp Bot **58:** 1365–1379

Marty NJ, Teresinski HJ, Hwang YT, Clendening EA, Gidda SK, Sliwinska E, Zhang D, Miernyk JA, Brito GC, Andrews DW, et al (2014) New insights into the targeting of a subset of tail-anchored proteins to the outer mitochondrial membrane. Front Plant Sci **5:** 426

Moussaieff A, Rogachev I, Brodsky L, Malitsky S, Toal TW, Belcher H, Yativ M, Brady SM, Benfey PN, Aharoni A (2013) High-resolution metabolic mapping of cell types in plant roots. Proc Natl Acad Sci USA **110:** E1232–E1241

Oberacker P, Stepper P, Bond DM, Höhn S, Focken J, Meyer V, Schelle L, Sugrue VJ, Jeunen G-J, Moser T, et al (2019) Bio-On-Magnetic-Beads (BOMB): Open platform for high-throughput nucleic acid extraction and manipulation. PLoS Biol **17:** e3000107

Patron NJ, Orzaez D, Marillonnet S, Warzecha H, Matthewman C, Youles M, Raitskin O, Leveau A, Farré G, Rogers C, et al (2015) Standards for plant synthetic biology: A common syntax for exchange of DNA parts. New Phytol **208:** 13–19

Pétriacq P, de Bont L, Genestout L, Hao J, Laureau C, Florez-Sarasa I, Rzigui T, Queval G, Gilard F, Mauve C, et al (2017) Photoperiod affects the phenotype of mitochondrial complex I mutants. Plant Physiol **173:** 434–455

Reynolds ES (1963) The use of lead citrate at high pH as an electron-opaque stain in electron microscopy. J Cell Biol **17:** 208–212

Roberts J, Aubert S, Gout E, Bligny R, Douce R (1997) Cooperation and competition between adenylate kinase, nucleoside diphosphokinase, electron transport, and ATP synthase in plant mitochondria studied by ^{31}P-nuclear magnetic resonance. Plant Physiol **113:** 191–199

Rogers GW, Brand MD, Petrosyan S, Ashok D, Elorza AA, Ferrick DA, Murphy AN (2011) High throughput microplate respiratory measurements using minimal quantities of isolated mitochondria. PLoS One **6:** e21746

Rugen N, Straube H, Franken LE, Braun H-P, Eubel H (2019) Complexome profiling reveals association of PPR proteins with ribosomes in the mitochondria of plants. Mol Cell Proteomics **18:** 1345–1362

Salem MA, Giavalisco P (2018) Semi-targeted lipidomics of plant acyl lipids using UPLC-HR-MS in combination with a data-independent acquisition mode. Methods Mol Biol **1778:** 137–155

Salem MA, Jüppner J, Bajdzienko K, Giavalisco P (2016) Protocol: A fast, comprehensive and reproducible one-step extraction method for the rapid preparation of polar and semi-polar metabolites, lipids, proteins, starch and cell wall polymers from a single sample. Plant Methods **12:** 45

Schlame M, Brody S, Hostetler KY (1993) Mitochondrial cardiolipin in diverse eukaryotes. Comparison of biosynthetic reactions and molecular acyl species. Eur J Biochem **212:** 727–735

Schmelzer C, Lindner I, Vock C, Fujii K, Döring F (2007) Functional connections and pathways of coenzyme Q10-inducible genes: An in-silico study. IUBMB Life **59:** 628–633

Schwanhäusser B, Busse D, Li N, Dittmar G, Schuchhardt J, Wolf J, Chen W, Selbach M (2011) Global quantification of mammalian gene expression control. Nature **473:** 337–342

Schwarzländer M, Logan DC, Johnston IG, Jones NS, Meyer AJ, Fricker MD, Sweetlove LJ (2012) Pulsing of membrane potential in individual mitochondria: A stress-induced mechanism to regulate respiratory bioenergetics in *Arabidopsis*. Plant Cell **24:** 1188–1201

Senkler J, Senkler M, Eubel H, Hildebrandt T, Lengwenus C, Schertl P, Schwarzländer M, Wagner S, Wittig I, Braun H-P (2017) The mitochondrial complexome of *Arabidopsis thaliana*. Plant J **89:** 1079–1092

Shannon P (2003) Cytoscape: A software environment for integrated models of biomolecular interaction networks. Genome Res **13:** 2498–2504

Stitt M, Lilley RM, Heldt HW (1982) Adenine nucleotide levels in the cytosol, chloroplasts, and mitochondria of wheat leaf protoplasts. Plant Physiol **70:** 971–977

Villand P, Kleczkowski LA (1994) Is there an alternative pathway for starch biosynthesis in cereal seeds. Z Natforsch C J Biosci **49:** 215–219

Yoshida K, Shibata M, Terashima I, Noguchi K (2010) Simultaneous determination of in vivo plastoquinone and ubiquinone redox states by HPLC-based analysis. Plant Cell Physiol **51:** 836–841

Zhou Y, Peisker H, Dörmann P (2016) Molecular species composition of plant cardiolipin determined by liquid chromatography mass spectrometry. J Lipid Res **57:** 1308–1321

Downloaded from https://academic.oup.com/plphys/article/182/3/1194/6116177 by Institute of Horticultural Economics user on 10 December 2021

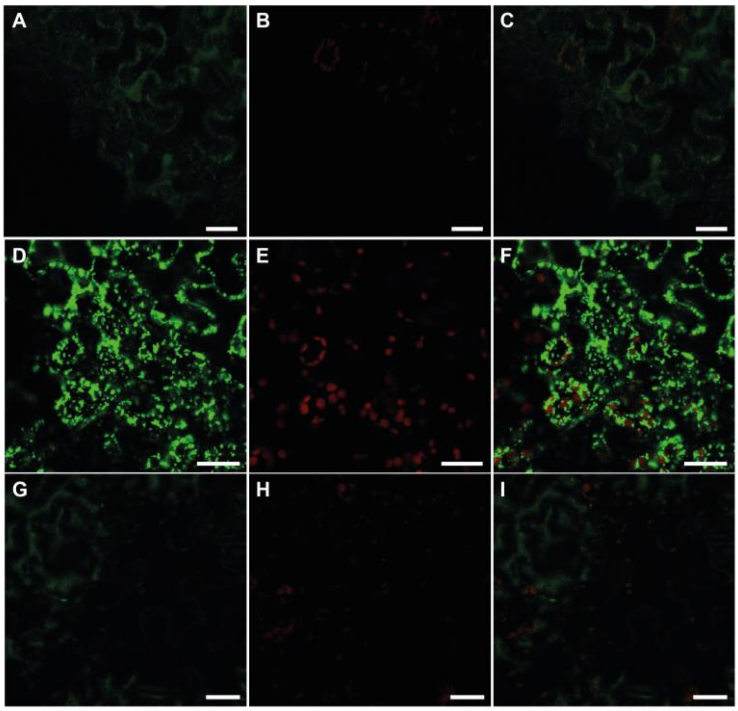

Supplemental Figure S1. Transient expression of different tail-anchored proteins fused to GFP in *Nicotiana benthamiana.* Confocal fluorescence microscopy images of *N. benthamiana* transiently expressing 35S:Twin-Strep-tag:GFP:TOM22-V (A to C), 35S:Twin-Strep-tag:GFP:ADAPTER (D to F), and 35S:Twin-Strep-tag:GFP:Cb5-D (G to I). GFP fluorescence (A, D, G), chlorophyll autofluorescence (B, E, H) and overlay of both channels (C, F, I). Scale bars, 25 µm.

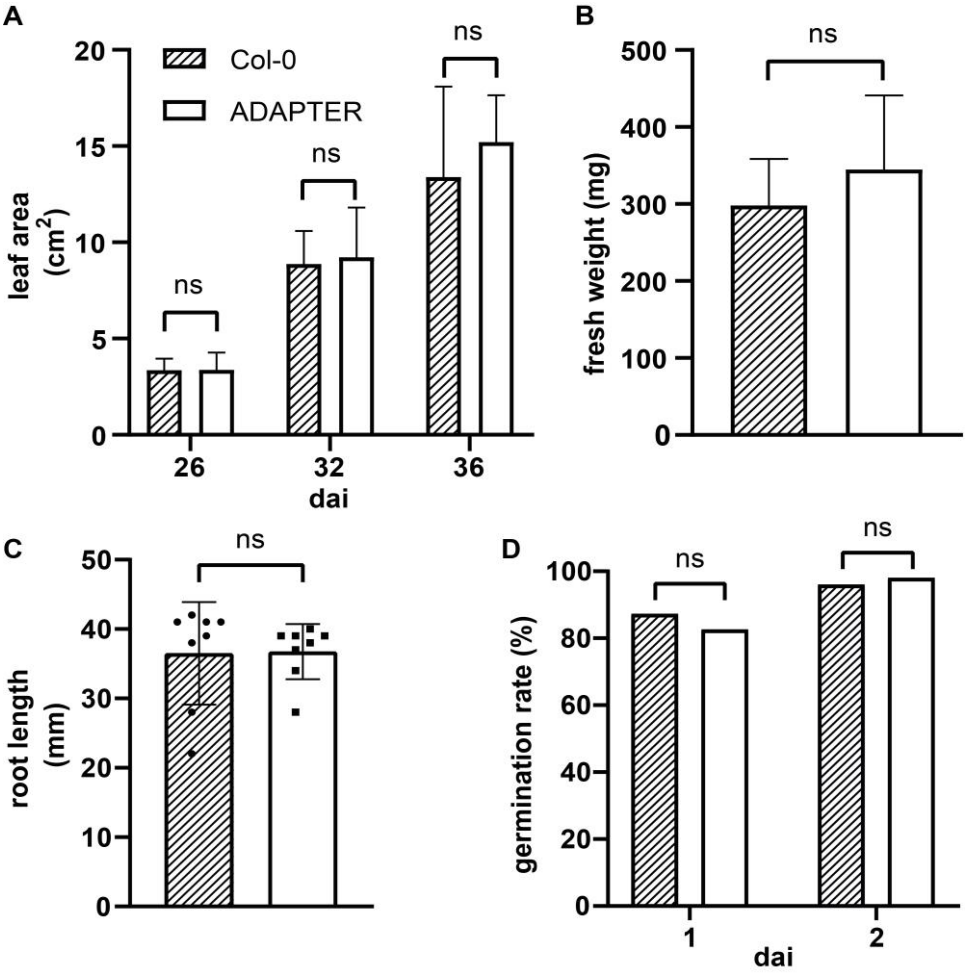

Supplemental Figure S2. Quantitative comparison of phenotypical traits between wild type (Col-0) and a stable transformed plant carrying the 35S:Twin-Strep-tag:GFP:ADAPTER. (A) Leaf area of plants at 26, 32 and 36 days after imbibition (dai) grown under short day conditions, n = 20. (B) Rosette fresh weight of plants 36 dai grown under short day conditions. (C) Root length of plants 12 dai grown on modified ½ MS media. Eight plants of each line were grown in parallel on one plate. The experiment was repeated three times with similar results. Error bars are SD. Significant differences (at $p < 0.05$) were determined with Student´s t-test and marked with a star. Calculation of the False Discovery Rate (FDR) was done using the two-stage linear step-up procedure described in Benjamini et al., 2006. The statistical analysis was done with a FDR of 1 %. (D) Germination rate of seeds on modified ½ MS media. In total 150 seeds were evaluated. For statistical evaluation the chi-square test X^2 was employed with (1, n = 150) = 1.281, $p = 0.257705$ for 1 dai and (1, n = 150) = 1.0309, $p = 0.309941$ for 2 dai. 'ns' denotes for 'not significant'.

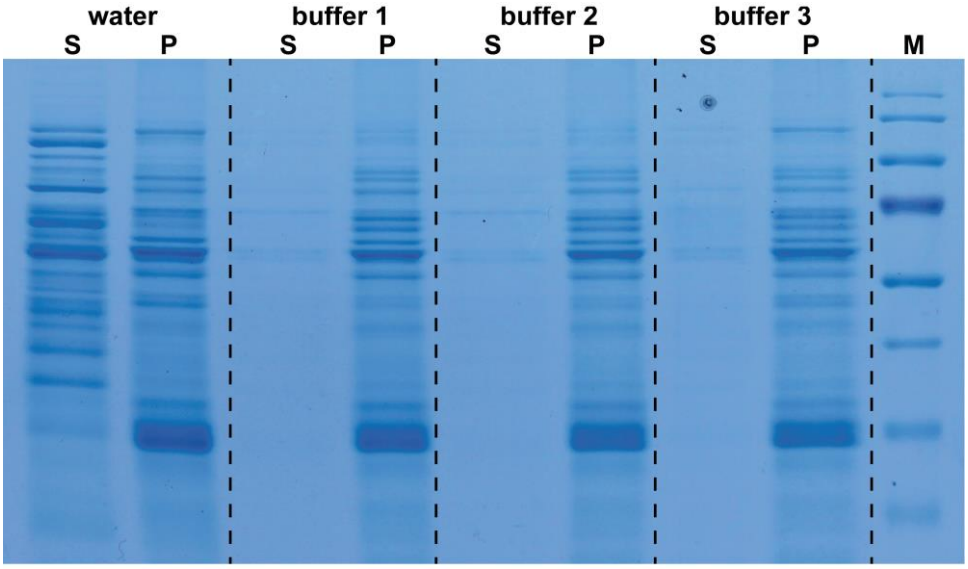

Supplemental Figure S3. Integrity of isolated mitochondria in different buffers. Plant mitochondria isolated from *Arabidopsis thaliana* with differential and density gradient centrifugation (DGC) were carefully resuspended in water, or buffer 1 (100 mM NaCl, 100 mM ammonium bicarbonate, pH 8), or buffer 2 (100 mM KCl, 100 mM ammonium bicarbonate, pH 8) or buffer 3 (400 mM mannitol, 1 mM EGTA, 10 mM Tricine, pH 7.2). These samples were centrifuged at 14500*g* for 10 minutes at 4°C and the supernatants were discarded. This procedure was rapidly repeated to ensure complete removal of the original buffer used for DGC. The resulting pellets were resuspended in the respective buffers and incubated on ice for 20 min and centrifuged again. SDS loading buffer was added to the supernatants (S) and pellets (P) and the samples were analyzed by SDS gel electrophoresis. For the marker (M) the PageRuler Prestained Protein Ladder (Thermo Fisher Scientific) was used. The gel was stained with colloidal Coomassie. For all proteome and metabolome analyses buffer 1 was employed, but the NaCl concentration was increased to 200 mM.

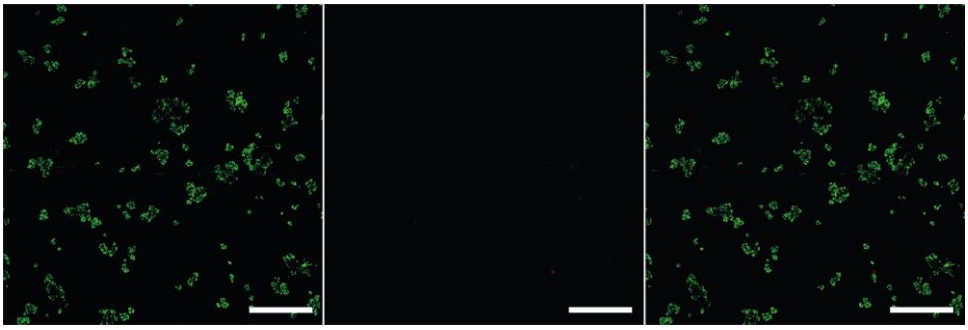

Supplemental Figure S4. Plant mitochondria bound to a commercial matrix of 1 µm diameter. Representative confocal fluorescence microscopy images of magnetic beads (1-µm diameter, IBA Lifesciences) with attached mitochondria extracted from *A. thaliana* carrying the 35S:Twin-Streptag: GFP:ADAPTER construct. GFP fluorescence (left panel), chloroplast autofluorescence (middle panel) and overlay of both channels (right panel). Scale bars, 25 µm.

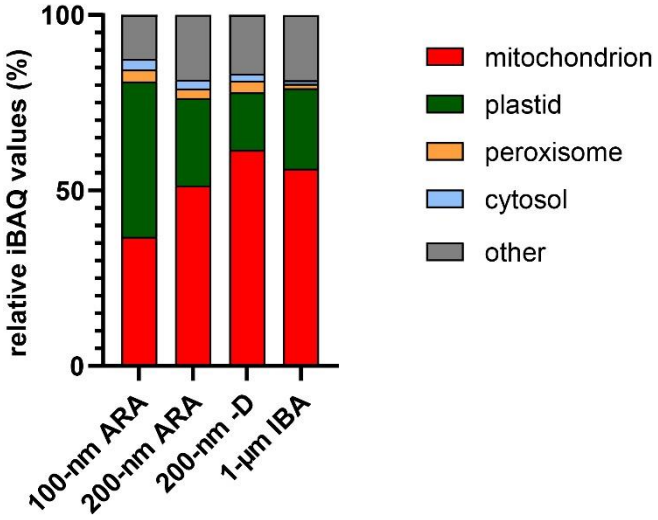

Supplemental Figure S5. Different bead sizes and coating materials influence the enrichment of mitochondria. 10-day-old seedlings of *A. thaliana* plants grown in liquid culture and expressing 35S:Twin-Strep-tag:GFP:ADAPTER were subjected to Mito-AP (method 1) with different bead types. Beads of 100-nm or 200-nm diameter coated in-house with Strep-Tactin using carboxyl (ARA; glucoronic acid as matrix polymer) or hydroxyl (-D; starch as matrix polymer) functional groups on the surface were used, or beads of 1-µm diameter already provided with a Strep-Tactin coating (IBA Lifesciences) were employed. iBAQ values for every identified protein were assigned to the respective categories (mitochondrion, plastid, peroxisome, cytosol, other), referred to total iBAQs of the corresponding sample, and plotted as a percentage. The categories were defined by the SUBAcon annotation provided by SUBA4.

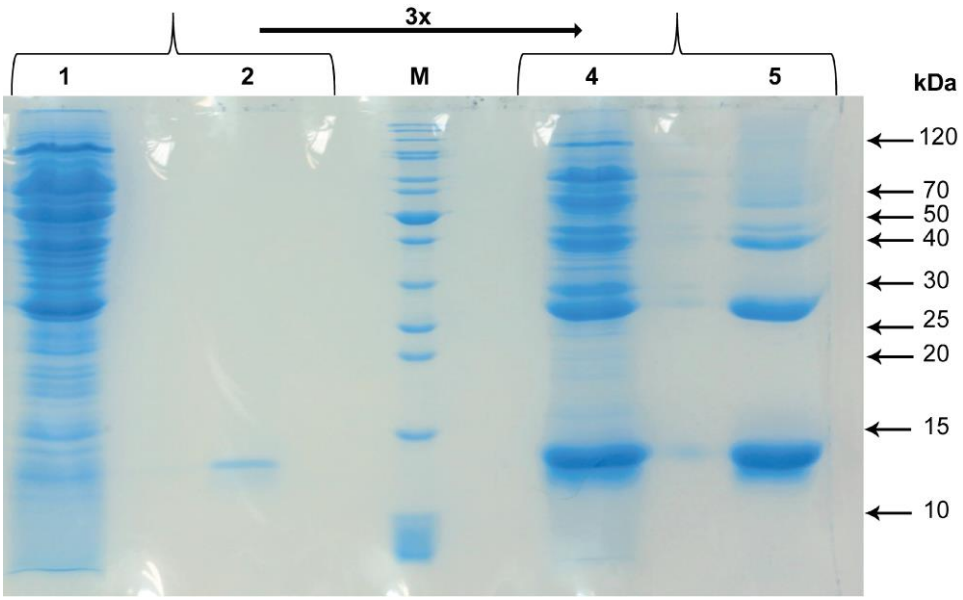

Supplemental Figure S6. Quantification of the relative protein amounts from mitochondria enriched with different matrices. 10-day-old seedlings of *A. thaliana* plants grown in liquid culture and expressing 35S:Twin-Strep-tag:GFP:ADAPTER were subjected to Mito-AP (method 1) with either 200-nm in-house-coated nanoparticles (lane 1) or 1-µm commercially available beads (lane 4). For all preparations, the same volume of beads was used. To assess which proteins originate from the bead coating and not from mitochondria, empty 200-nm and 1-µm beads were boiled in SDS buffer. The resulting proteins are shown in lanes 2 and 5, respectively. All bands were quantified with a Li-Cor Odyssee FC and signals from empty beads were subtracted from the corresponding loaded beads and the ratio between both signals was calculated. Three times more proteins were purified with the 200-nm beads compared to the 1-µm matrix. For the marker (M) the PageRuler Unstained Protein Ladder (Thermo Fisher Scientific) was used.

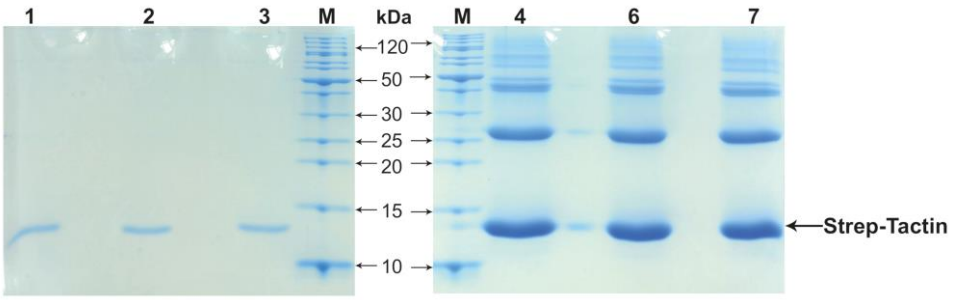

Supplemental Figure S7. Quantification of Strep-Tactin bound to different magnetic matrices. Strep-Tactin bound to in-house-coated 200-nm beads (left panel, lanes 1 to 3) and commercial 1-µm beads (right panel, lanes 4 to 6) was quantified. The same volumes of beads were treated with SDS loading buffer, incubated at 95°C, and samples were analyzed by SDS gel electrophoresis. The marked bands (Strep-Tactin monomer has a size of about 14 kDa) were quantified by analyzing BSA standards of defined concentrations on the same gel (not shown). On average 0.709 ± 0.027 µg Strep-Tactin was bound on the 200-nm beads (250 µl, 2.3% (v/v) slurry), whereas the 1-µm beads contained almost 20 times more Strep-Tactin (16.09 ± 0.32 µg in 115 µl 5% (v/v) slurry). For the marker (M) the PageRuler Unstained Protein Ladder (Thermo Fisher Scientific) was used.

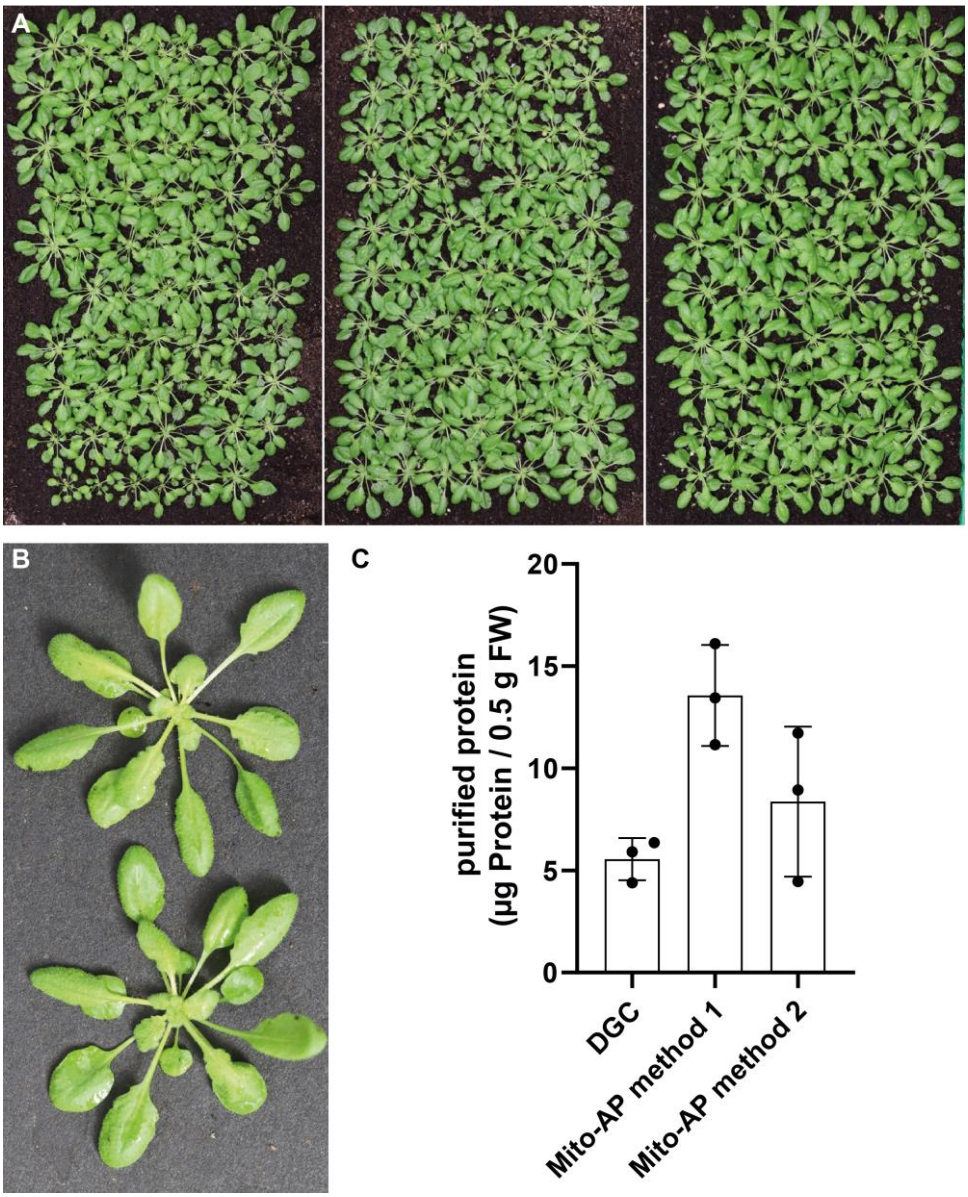

Supplemental Figure S8. Plant material needed for DGC and Mito-AP and relative mitochondrial protein yield obtained by both methods. *A. thaliana* plants were grown under short day conditions in a climate chamber for 5 weeks. (A) For the differential and density gradient centrifugation (DGC) around 110 g of plant material was used. (B) For Mito-AP (method 1 or method 2) 500 mg of plant material was used. (C) The total yield of protein referred to plant fresh weight input (FW) for all methods. Error bars are SD (n = 3 biological replicates)

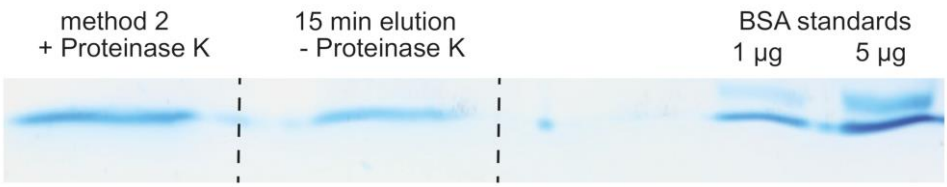

Supplemental Figure S9. Quantification of the total protein yield obtained from elution with and without proteinase K. 35S:Twin-Strep-tag:GFP:ADAPTER *A. thaliana* plants were subjected to either Mito-AP with proteinase K (method 2) or to the identical protocol but with omission of proteinase K and an extension of the time for elution to 15 min to match the incubation time of proteinase K (15 min elution). The resulting samples were analyzed by SDS gel electrophoresis. The observed band (stained with colloidal Coomassie) represents the total protein in the sample. These were quantified with a Li-Cor Odyssee FC and the total protein amounts were calculated by comparison with a BSA standard run on the same gel. 3.39 µg protein were present in lane 1 (method 2) and 1.97 µg protein were detected in lane 2 (15 min elution).

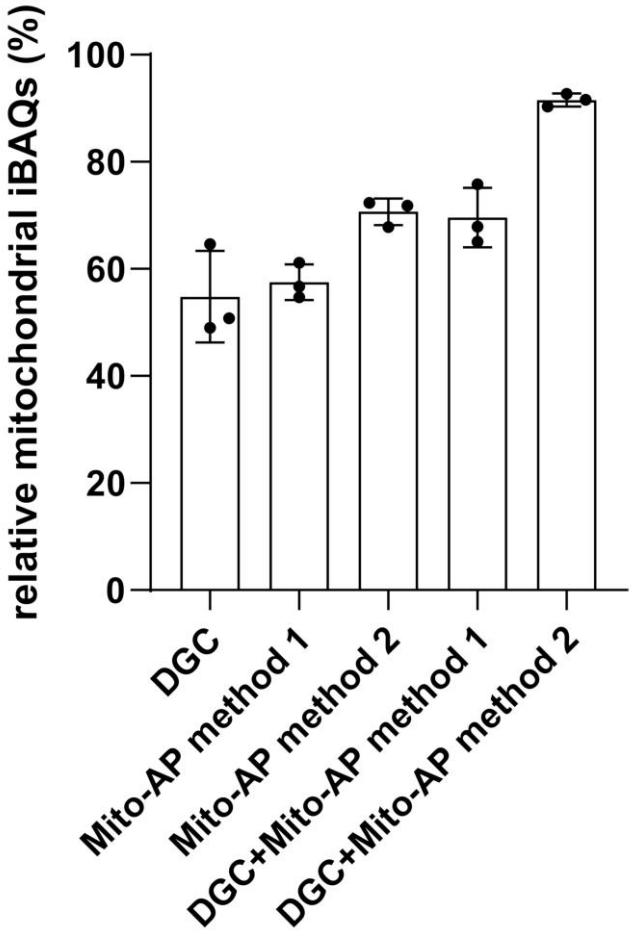

Supplemental Figure S10. Variation of mitochondrial purity from biological repeats processed by DGC or Mito-AP. The data for the mitochondrial category as described in Figure 5 is shown. Each of

the three replicates is a data point. Biological repeats were performed on consecutive days. Error bars are SD.

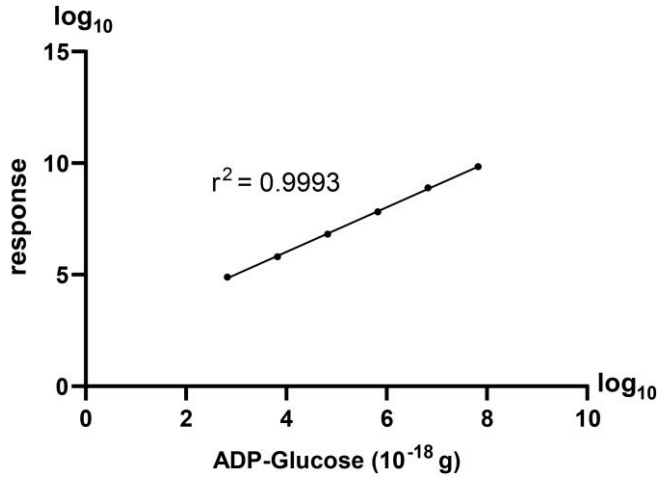

Supplemental Figure S11. ADP-glucose standard curve. ADP-glucose dissolved in different amounts in water were measured via LC-MS. The metabolite input in attogram was logarithmized. Linear regression was performed on non-logarithmized values with a response curve showing a linearity with $r^2 = 0.99$. The lowest detected amount of 0.67 fg on column was measured with a signal to noise ratio greater than 6.

Supplemental Figure S12. Contamination with plastidic fragments. Representative confocal microscopy overview pictures of 200-nm beads coated with Strep-Tactin bound to mitochondria derived from leaves of *A. thaliana* plants carrying the 35S:Twin-Strep-tag:GFP:ADAPTER construct. The mitochondria were purified using Mito-AP method 1. Bound mitochondria possess GFP fluorescence (GFP, left panel). Signals consistent with chloroplast autofluorescence (middle panel) and the overlay of both channels (right panel) are shown. Scale bars, 100 µm. Insert, higher magnification of several mitochondria bound to beads. Scale bar, 25 µm.

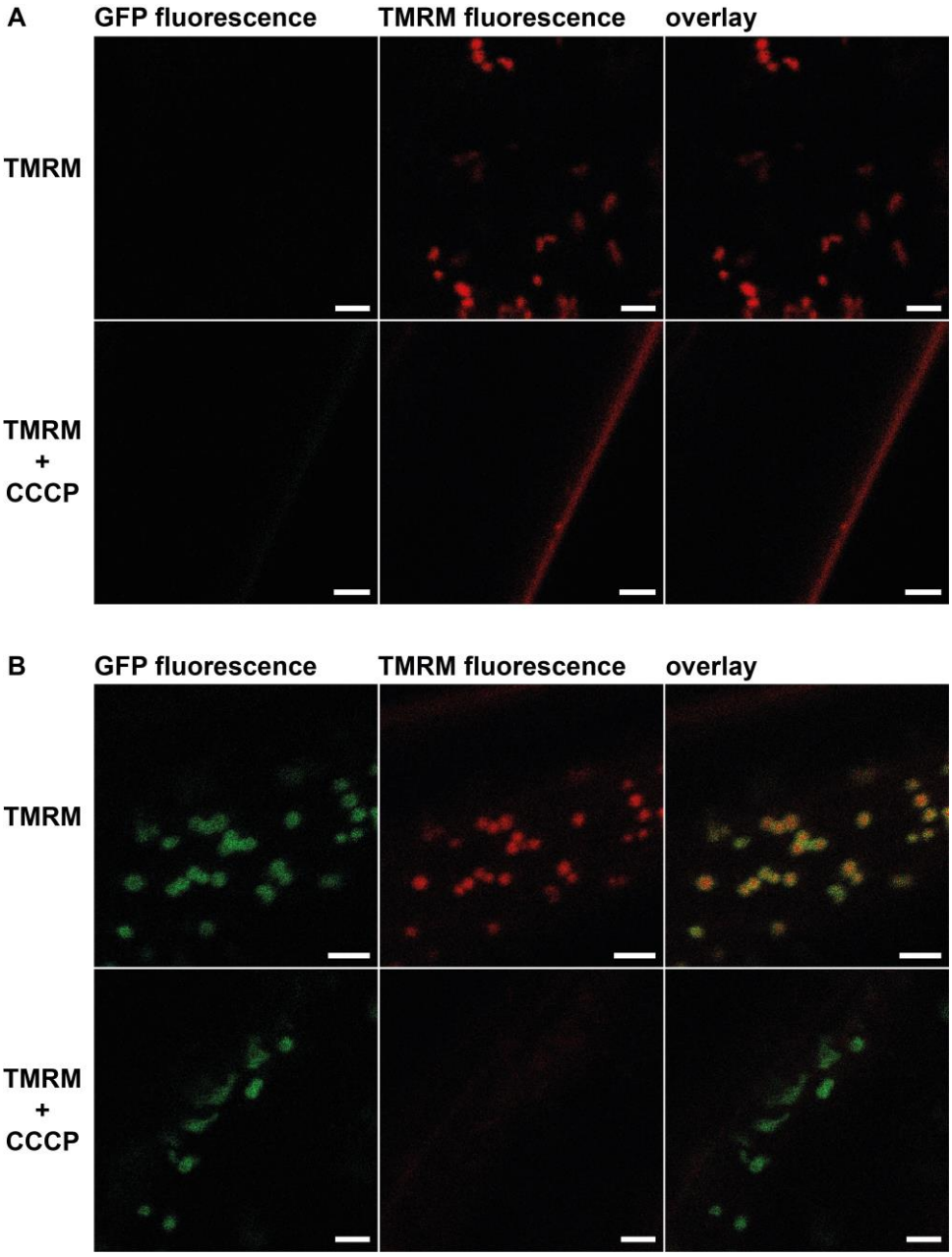

Supplemental Figure S13. Visualization of the mitochondrial membrane potential *in vivo*. Confocal fluorescence microscopy images of the root tissue of 12-day-old seedlings from a shaking culture. Seedlings were treated either with tetramethyl rhodamine methyl ester (TMRM) (upper panels) or a combination of TMRM and carbonyl cyanide 3-chlorophenylhydrazone (CCCP) (lower panels). The cell wall shows unspecific signal in the TMRM channel. (A) Wild type Col-0 and (B) plants expressing the 35S:Twin-Strep-tag:GFP:ADAPTER construct. In case of the 35S:Twin-Strep-tag:GFP:ADAPTER plants, a ring shaped structure surrounding the TMRM fluorescence signal was observed, indicating that this signal originates from mitochondria. Scale bars, 3 µm.

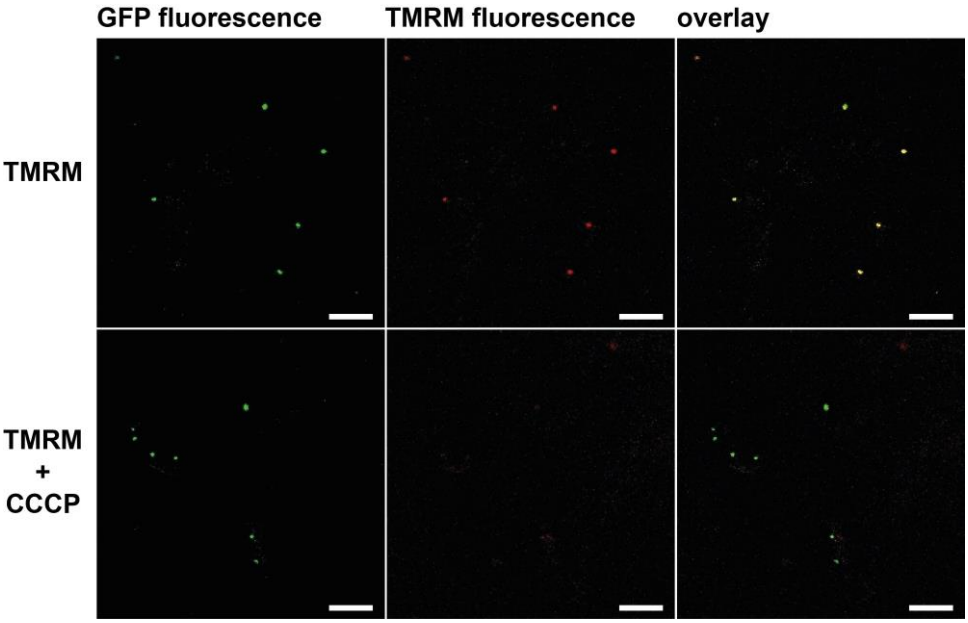

Supplemental Figure S14. Visualization of the mitochondrial membrane potential *in vitro.* Confocal fluorescence microscopy images of mitochondria bound to magnetic beads isolated from plants expressing the 35S:Twin-Strep-tag:GFP:ADAPTER construct. Isolated mitochondria were resuspended in MAS buffer containing 10 mM succinate and treated either with TMRM (upper panels) or a combination of TMRM and CCCP (lower panels). In total 219 GFP-fluorescent particles were counted for the TMRM treatment of which 160 showed a co-localization with the TMRM-fluorescence (73%). For the TMRM + CCCP treatment 183 GFP-fluorescent particles were counted of which 58 showed a co-localization with a weaker TMRM-fluorescence (31%). Scale bars, 10 µm.

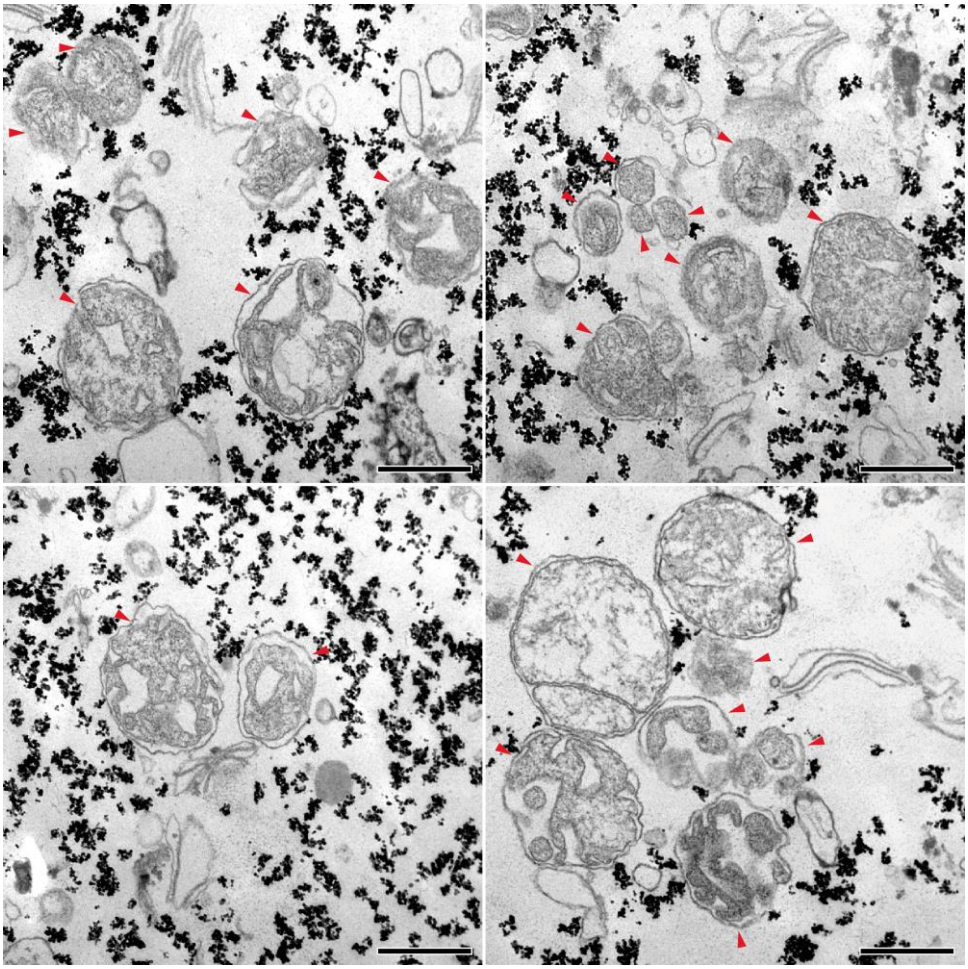

Supplemental Figure 15. Electron micrographs of isolated mitochondria. Representative transmission electron microscopy (TEM) images of mitochondria bound to magnetic beads isolated from plants expressing the 35S:Twin-Strep-tag:GFP:ADAPTER construct. Small dense particles are the iron oxide core of the magnetic beads. Mitochondria are indicated by red arrowheads. Scale bars, 400 nm.

Supplemental Table S4. Primer sequences

name	sequence
P1023	TTTGGTCTCAACATTTCGGCTGCCTTGTCGGATAAGTTAG
P1024	TTTGGTCTCAATCTTCGGACATTGTTGTGGGAG
P1025	TTTGGTCTCAAGATCAAATGGTTGCTCTAGTCGGCGGA
P1026	TTTGGTCTCAACAAAAGCCTAACTGTTCTTCCTTGCAGAG
P626	TTGAAGACAAAATGGAGTCTGATGAGTCT
P820	TTGAAGACAACGAACCTTCCTCACCAGCATC

Supplemental Table S5. MRM parameters used for the detection of polar metabolites with a triple quadrupole mass spectrometer. The precursor ion, the product ions (used for quantification, quant.; used for qualification, qual.), the fragmentor, and the collision energy (CV, in volt) is provided for every measured metabolite.

	Precursor Ion $[M+H]^+$ (m/z)	Product Ion (m/z)	Fragmentor	Collision Energy (V)
ADP	428	136 (quant.)	132	25
ADP-Glucose	590,1	136 (quant.)	105	49
		428 (qual.)	105	13
AMP	348,1	136 (quant.)	132	25
ATP	508	136 (quant.)	120	45
		410 (qual.)	120	15
NMN	335,07	123 (quant.)	101	13
		97 (qual.)	101	33
NAD^+	664,1	136 (quant)	144	48
		542,1 (qual.)	144	17
NADH	666,13	136 (quant.)	155	58
NADP	745,1	136 (quant.)	159	64

2.2 Enhanced nucleotide analysis enables the quantification of deoxynucleotides in plants and algae revealing connections between nucleoside and deoxynucleoside metabolism

Straube, H., Niehaus, M., Zwittian, S., Witte, C-P., Herde, M.

Leibniz Universität Hannover, Department of Molecular Nutrition and Biochemistry of Plants, 30419 Hannover, Germany

Type of authorship:	Co-author
Type of article:	Research Article
Share of work:	15 %
Contribution to publication:	acquired the experimental data together with H.S., S.Z. and M.H.
Journal:	The Plant Cell
Impact factor:	12.085 (2021)
Date of publication:	08.12.2020
Number of citations: (Google Scholar, 28.09.22)	10
DOI:	10.1093/plcell/koaa028

doi:10.1093/plcell/koaa028

THE PLANT CELL

THE PLANT CELL 2021: 33: 270–289

Research Article

Enhanced nucleotide analysis enables the quantification of deoxynucleotides in plants and algae revealing connections between nucleoside and deoxynucleoside metabolism

Henryk Straube ,[1] Markus Niehaus ,[1] Sarah Zwittian ,[1] Claus-Peter Witte [1] and Marco Herde [1,*]

1 Department of Molecular Nutrition and Biochemistry of Plants, Leibniz Universität Hannover, Hannover 30419, Germany

*Author for correspondence: mherde@pflern.uni-hannover.de

H.S. and M.H. designed the study. H.S., M.N., S.Z., and M.H. acquired the experimental data. H.S. analyzed the data and H.S., C.-P.W., and M.H. interpreted the data. H.S., C.-P.W., and M.H. wrote the manuscript. All authors read and revised the manuscript and agreed on the final version.

The author responsible for distribution of materials integral to the findings presented in this article in accordance with the policy described in the Instructions for Authors (https://academic.oup.com/plcell) is: Marco Herde (mherde@pflern.uni-hannover.de).

Abstract

Detecting and quantifying low-abundance (deoxy)ribonucleotides and (deoxy)ribonucleosides in plants remains difficult; this is a major roadblock for the investigation of plant nucleotide (NT) metabolism. Here, we present a method that overcomes this limitation, allowing the detection of all deoxy- and ribonucleotides as well as the corresponding nucleosides from the same plant sample. The method is characterized by high sensitivity and robustness enabling the reproducible detection and absolute quantification of these metabolites even if they are of low abundance. Employing the new method, we analyzed *Arabidopsis thaliana* null mutants of *CYTIDINE DEAMINASE*, *GUANOSINE DEAMINASE*, and *NUCLEOSIDE HYDROLASE 1*, demonstrating that the deoxyribonucleotide (dNT) metabolism is intricately interwoven with the catabolism of ribonucleosides (rNs). In addition, we discovered a function of rN catabolic enzymes in the degradation of deoxyribonucleosides in vivo. We also determined the concentrations of dNTs in several mono- and dicotyledonous plants, a bryophyte, and three algae, revealing a correlation of GC to AT dNT ratios with genomic GC contents. This suggests a link between the genome and the metabolome previously discussed but not experimentally addressed. Together, these findings demonstrate the potential of this new method to provide insight into plant NT metabolism.

Introduction

Metabolomics of nucleotides (NTs) and nucleosides (Ns) in plants is a notably understudied area, in part is due to technical challenges concerning sample preparation and chromatographic separation. In particular, research on deoxyribonucleotide (dNT) and deoxyribonucleoside (dN) metabolism would greatly benefit from methods allowing the comprehensive quantification of these metabolite classes in plant samples.

Several enzymes of plant dNT metabolism have been functionally characterized in *Arabidopsis thaliana*, but a direct impact of loss-of-function mutants on the dNT pools

Received September 4, 2020. Accepted November 12, 2020. Advance access publication December 8, 2020

© American Society of Plant Biologists 2020. All rights reserved. For permissions, please email: journals.permissions@oup.com

Downloaded from https://academic.oup.com/plcell/article/33/2/270/6026971 by Institute of Horticultural Economics user on 11 December 2021

was hitherto only proven in one case with a PCR-based approach that allows only relative quantification of dNT triphosphates (dNTPs) in vivo (Wang and Liu, 2006; Garton et al., 2007; Yoo et al., 2009). Severe phenotypes like aberrant leaf morphology, growth inhibition, white spots in leaves, and reduced seed yield result from mutation of plant dNT metabolism genes (Wang and Liu, 2006; Garton et al., 2007; Dubois et al., 2011; Pedroza-García et al., 2015, 2019; Le Ret et al., 2018). Although not shown, these mutations likely cause altered cellular dNT concentrations, which in turn are probably often the reason for the phenotypic alterations. Changes of NT quantities affecting DNA and RNA replication were observed in similar mutants of non-plant organisms (Nick McElhinny et al., 2010a, 2010b; Gon et al., 2011; Kumar et al., 2011). Furthermore, the catalytic function of plant dN kinases could so far only be validated in vitro (Stasolla et al., 2003; Clausen et al., 2012; Pedroza-García et al., 2015; Le Ret et al., 2018; Pedroza-García et al., 2019), because possible changes of dN concentrations in the corresponding mutants cannot be assessed with current methods (Pedroza-García et al., 2015, 2019; Le Ret et al., 2018). The inability to detect dNs is also the reason why the metabolic fate of dNs is currently unknown in plants. dNs might be degraded by the same enzymes that also catabolize ribonucleosides (rNs), because at least some of these enzymes were shown to catabolize both types of substrates in vitro (Dahncke and Witte, 2013; Chen et al., 2016).

In contrast to ribonucleotides (rNTs), dNTs, and dNs, the detection and quantification of rNs and their degradation products is less challenging; this spurred a comprehensive characterization of the rN degradation pathways in vivo (Baccolini and Witte, 2019; Witte and Herde, 2020). The catabolism of rNs is integrated into a complex network including the de novo biosynthesis of rNTs and the salvage (recycling) of rNs and nucleobases ultimately giving rise to ratios and amounts of rNTs suitable for all downstream processes (Zrenner et al., 2006; Ashihara et al., 2020; Witte and Herde, 2020).

Unlike most animals, plants are able to fully catabolize purine and pyrimidine rNs including the nucleobases, using the released nitrogen for amino acid biosynthesis (Werner et al., 2010; Werner and Witte, 2011; Ashihara et al., 2020; Witte and Herde, 2020). Three key enzymes participate in the initial steps of rN catabolism: cytidine deaminase (CDA; Vincenzetti et al. 1999; Kafer and Thornburg, 2000; Chen et al., 2016; Witte and Herde, 2020), guanosine deaminase (GSDA; Dahncke and Witte, 2013; Witte and Herde, 2020), and nucleoside hydrolase 1 (NSH1; Jung et al., 2009, 2011; Baccolini and Witte, 2019; Witte and Herde, 2020). CDA was shown to deaminate cytidine and deoxycytidine in vitro and mutants of *CDA* accumulate cytidine in vivo (Chen et al., 2016). GSDA deaminates guanosine and deoxyguanosine in vitro and the mutants accumulate guanosine in vivo (Dahncke and Witte, 2013; Baccolini and Witte, 2019), while NSH1 participates in the hydrolysis of uridine, xanthosine, and inosine in vitro and in vivo (Jung et al., 2009; Riegler et al., 2011; Baccolini and Witte, 2019).

Mutants of *GSDA*, *CDA*, and *NSH1* show phenotypical abnormalities (Jung et al., 2011; Dahncke and Witte, 2013; Chen et al., 2016; Baccolini and Witte, 2019) during germination, development, and dark stress. The abnormal phenotypes are thought to result from the accumulation and toxicity of rNs or the lack of degradation-derived metabolites (Stasolla et al., 2003; Schroeder et al., 2018; Baccolini and Witte, 2019). So far, only metabolomic data for rNs and their degradation products have been obtained in *gsda*, *cda*, and *nsh1* mutants, whereas rNT, dNT, and dN pools have not been investigated due to technical limitations. However, it would be interesting to quantify dNs in these mutants to clarify whether the corresponding enzymes are indeed involved in dN degradation in vivo. The substantial accumulation of rNs (and perhaps also dNs) in these mutants might also result in altered concentrations of rNTs and dNTs because plants possess kinases for the salvage of rNs and dNs (Witte and Herde, 2020).

The primary metabolome comprises four main classes of metabolites: the amino acids, the carbohydrates, the lipids, and the NTs. While the first three classes are routinely characterized comprehensively in plant metabolome studies using well-established methods (Salem et al., 2020), this does not apply to NTs and NT-derived metabolites, which are often not analyzed at all or are highly underrepresented. A main reason lies in the lack of suitable methods for a comprehensive analysis of NTs in plant samples with modern mass spectrometry (MS) techniques. So far, NT analysis in plants (see literature survey summarized in Supplemental Table S1) have employed either liquid chromatography (LC) combined with photometric detection (Meyer and Wagner, 1985; Dutta et al., 1991; Katahira and Ashihara, 2006), a polymerase assay (Castroviejo et al., 1979; Feller et al., 1980; Wang and Liu, 2006; Garton et al., 2007), or thin-layer chromatography (TLC; Nygaard, 1972). These methods suffer from different drawbacks, for example, low sensitivity (photometric detection), relative quantification of only dNTPs (polymerase), or the need for radiolabelled starting material (TLC). Some metabolome studies quantified rNTs but not dNTs employing ion-exchange chromatography–MS or LC–MS (Rolletschek et al., 2011; Souza et al., 2015); however, recovery rates of these methods were not reported. To improve dNT detection, some protocols remove rNTs by a periodate treatment (Dutta et al., 1991) that likely also affects dNT species such as dGTP, which reacts with dicarbonyl compounds resulting from the addition of periodate (Tanaka et al., 1984; Henneré et al., 2003). Focused rN extraction methods from plant material also exist (Kopecná et al., 2013) but these are not suitable for NT species. Ideally, a method coupling LC with modern MS would be needed.

Plant samples are particularly challenging for metabolomics employing LC–MS because plants contain a plethora of metabolites making extracts (the matrix) very complex.

Downloaded from https://academic.oup.com/plcell/article/33/2/270/6026971 by Institute of Horticultural Economics user on 11 December 2021

In fact, we previously quantified dNTPs in embryos of *Drosophila melanogaster* (Liu et al., 2019), but that same method failed to work for Arabidopsis tissues. So-called matrix effects can cause ion suppression greatly reducing the sensitivity of detection in the MS, which for dNTs is critical as they are not abundant in plant cells. Studies in human cells suggest that solid phase extraction (SPE), either employing a silica or an anion exchange resin, is uniquely suited to enrich NTs and reduce matrix effects for sensitive detection (Cohen et al., 2009; Pabst et al., 2010; Kong et al., 2018). Additionally, it has been pointed out that efficient quenching of enzymatic activities is essential to stabilize plant extracts, because they contain phosphatases displaying residual activity in mixed aqueous and organic solutions (Ullrich and Calvin, 1962; Bieleski, 1964; Ikuma and Tetley, 1976).

The LC of charged metabolites as front end for an MS analyzer is also not as straightforward as for moderately polar or hydrophobic compounds. For the LC–MS detection of NTs, various LC column materials have been used such as porous graphitized carbon in reverse-phase mode (Cohen et al., 2009) and resins carrying zwitterionic functional groups for hydrophilic interaction chromatography (Kong et al., 2018). A common problem with these chromatographies is that retention times can be unstable varying up to several minutes (Pabst et al., 2010). With the porous graphitized carbon stationary phase, this variation in chromatographic behavior is aggravated when crude plant extracts are used (our own observation) and might depend on the redox status of the column resin (Pabst et al., 2010). Taken together, these issues suggest that the detection and quantification of NTs in plant samples will require the development of a specially adapted protocol considering that methods of sample preparation and chromatography might interact to some extent.

In this study, we have established a sensitive and robust analytical method to simultaneously determine absolute concentrations of a comprehensive set of NTs and Ns in plants. The method works for a wide range of plant species including a moss (*Physcomitrium* [*Physcomitrella*] *patens*) and three algae (*Chlamydomonas reinhardtii*, *Mougeotia scalaris*, and *Volvox carteri*). We used the new protocol to analyze three Arabidopsis loss-of-function mutants in nucleoside catabolism lacking CDA, GSDA, and NSH1, respectively. We discovered that all three mutants harbor highly unbalanced rNTP and dNTP pools and we present evidence that CDA and NSH1 are not only required for rN but also for dN degradation in vivo.

Results

Optimization of sample preparation

The complex matrix of plant extracts notably complicates MS (Bieleski, 1964; Bieleski and Young, 1963; Nieman et al., 1978) preventing for example the straightforward detection of dNTs, which can be readily detected in non-plant samples (Kuskovsky et al., 2019). Additionally, plant samples must be efficiently quenched for NT analysis because plants possess stable phosphatases (Bieleski, 1964; Ikuma and Tetley, 1976) that are resistant to harsh conditions like organic solvents. A method (Figure 1) addressing these challenges was devised comprising tissue rupture and acid quenching, liquid/liquid extraction (LLE), weak anion SPE, and LC coupled to MS (LC–MS).

We evaluated different methods for sample preparation. In Table 1, we present the main findings of the optimization while the full detail of tested methods is shown in Supplemental Tables S2, S3. Consistent with previous studies, the NT triphosphates (NTPs) were more efficiently recovered upon extraction with strong acids like trichloroacetic acid (TCA) and perchloric acid (PCA) than with the organic solvent methanol (Bieleski, 1964; Dietmair et al., 2010) since the latter probably failed to inactivate all NT phosphatases. In our hands, recovery with PCA (Ashihara et al., 1987) was not as good as with TCA presumably because the PCA is removed by precipitation creating a bulky pellet, which traps liquid making quantitative sample recovery more difficult.

By contrast, TCA is removed by a LLE step in our method. Such a LLE has been developed over 40 years ago for mammalian systems (Khym, 1975) but has lost popularity, probably because the original protocol requires environmentally hazardous and expensive 1,1,2-trichlor-1,2,2-trifluorethan (Freon-113). We replaced Freon-113 with dichloromethane (DCM) and adopted the technology for plant extracts.

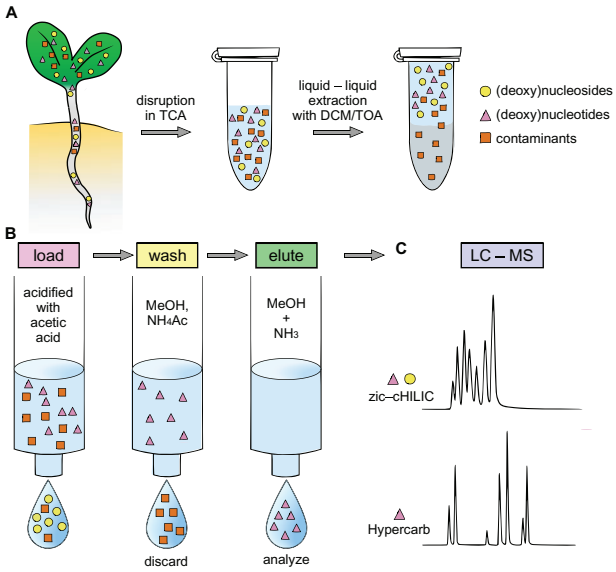

Figure 1 Schematic overview of the method for the extraction and analysis of NTs and Ns. Plant material is disrupted and quenched with TCA, which is removed together with apolar contaminants by LLE with DCM and TOA (A). The extract is loaded onto a weak-anion exchange SPE cartridge, the flow-through contains (deoxy)nucleosides for analysis. Subsequently, contaminants are depleted by washing with methanol (MeOH) and ammonium acetate (NH_4Ac), resulting in elution of (deoxy)ribonucleotides with MeOH and ammonia (NH_3; B). Isolated fractions are analyzed by LC–MS using a zic-cHILIC column (NTs and Ns) or a Hypercarb column (NTs; C).

Downloaded from https://academic.oup.com/plcell/article/33/2/270/6026971 by Institute of Horticultural Economics user on 11 December 2021

Table 1 Selection of tested methods and their combined effect on NT recovery

Method	Quenching	LLE/acid quenching	Dilution	Recovery (%) dTTP	Recovery (%) ATP	Recovery (%) dTMP
3	80/20 MeOH/10 mM NH_4Ac pH 4.5 (v/v)	–	–	10.2	10.3	107.8
7	6% PCA	20% KOH	–	92.3	61.6	26.8
8	15% TCA	DCM/TOA (78/22 v/v)	–	89.6	92.7	44.9
9	15% TCA	DCM/TOA (78/22 v/v)	1 mL water	87.8	90.0	88.4

Apart from removing the TCA in an elegant way resulting in little sample loss, the LLE additionally eliminates apolar metabolites from the extract. This is advantageous because it reduces the complexity of the matrix likely contributing to the improved NT recovery in comparison to the PCA method. An additional boost of recovery for NT monophosphates (NMPs) was achieved by diluting the sample with water prior to application to the SPE (Tables 1, 2). The dilution results in a reduced salt concentration in the sample fostering the binding of the NMPs to the anion-exchange matrix of the SPE. One can envisage that by fine-tuning the salt load of the sample, it will be possible to select against NMPs and other less-strongly bound ionic compounds. Such a reduction of matrix complexity could be advantageous when for example only the NTPs are in the analytical focus.

Interestingly, in the flow-through of the SPE loading step, we were able to detect deoxy- and rNs (dNs). Therefore, we included Ns in the evaluation of the final method (Table 2) determining the recovery rate of NMPs and NTPs in the eluate as well as Ns in the flow-through. Recovery rates for NTPs ranged from 41.2% to 104.0%, for NMPs from 85.8% to 113%, and for Ns from 82.6% to 96.4% (Table 2). Dinucleotides were not assessed because we reasoned that they will co-elute with NMPs and NTPs. This was later confirmed for ADP. In summary, the data show that the new method allows the simultaneous extraction and preparation for MS detection of NTs and Ns from the same plant sample.

Table 2 Relative recovery of Ns, NMPs, and NTPs

Relative recovery (%)					
NTPs		NMPs		Ns	
dATP 15N	100.2				
dCTP 15N	104.0	dCMP 13C, 15N	113.1		
dGTP 13C, 15N	64.6				
dTTP 13C, 15N	87.8	dTMP 13C, 15N	88.4	Deoxythymidine 13C, 15N	94.8
ATP 2H	90.0	AMP 15N	90.2	Adenosine 13C	82.6
CTP 2H	102.5	CMP 13C, 15N	75.5	Cytidine 15N	96.3
GTP 2H	41.2	GMP 15N	85.8	Guanosine 15N	86.4
UTP 2H	91.0	UMP 15N	103.5	Uridine 15N	82.6
				Inosine 15N	96.4

Comparison of chromatography methods and method validation

The chromatography method has a substantial impact on the sensitivity of the MS analysis because analytes and matrix are differentially separated and focused by distinct chromatographic techniques. Ion chromatography and capillary electrophoresis as well as hydrophilic interaction chromatography (HILIC) and porous graphitized carbon (PGC) chromatography have been used as front ends for NT analysis by MS (Ashihara et al., 1987; Riondet et al., 2005; Pabst et al., 2010; Kong et al., 2018). We used a zic-cHILIC (Merck) for HILIC (in the following called the cHILIC method) and a Hypercarb column (Thermo) for PGC chromatography (in the following called the Hypercarb method) and optimized the respective chromatographic and MS parameters (see the "Materials and methods" section, Supplemental Figures S1–S3, and Supplemental Tables S4–S6). Using the Hypercarb method, a lower limit of quantitation (LLOQ) of 0.1 pmol on column for NTs was determined, which was 5–50 times lower than the 0.5–5 pmol LLOQ on column measured by the cHILIC method (Table 3). For Ns, the LLOQ was 0.1 pmol on column (Table 4). These sensitivities are similar or even better than those previously described for the analysis of NTPs from mammalian cells (Kong et al., 2018). Thus, the sensitivity of our method is sufficient to allow for the first time the detection and quantification of dNTs in plant material by MS.

The quantification of isotope standards (ISTDs) spiked into matrix derived from SPE and resolved either by the Hypercarb or cHILIC method showed that standard amount and detector signal correlated with good linearity resulting in R^2 values equal or higher than 0.96 for all tested substances (Tables 3, 4). Different physiological conditions leading to changing NT or nucleoside concentrations can therefore be investigated.

Intra- and inter-day precision was evaluated for all used chromatography methods and three different concentrations of ISTDs in plant matrix (Supplemental Tables S7, S8). In general, the coefficient of variation (CV%) was higher for the cHILIC than for the Hypercarb method and inter-day variation was higher than intra-day variation. The values ranged

Downloaded from https://academic.oup.com/plcell/article/33/2/270/6026971 by Institute of Horticultural Economics user on 11 December 2021

Table 3 Calibration range, coefficient of determination (R^2), and LLOQ for NTPs using the Hypercarb or the cHILIC method

	Calibration range (pmol)	R^2 Hypercarb	Hypercarb LLOQ (pmol)	R^2 cHILIC	cHILIC LLOQ (pmol)
dATP	2.5–80	0.96	0.1	0.99	1
dCTP		0.98	0.1	0.99	1
dGTP		0.99	0.1	0.97	1
dTTP		0.99	0.1	0.98	0.5
ATP	25–800	0.99	0.1	0.98	1
CTP		0.96	0.1	0.98	1
GTP		0.99	0.1	0.99	5
UTP		0.99	0.1	0.98	1

Table 4 Calibration range, coefficient of determination (R^2), and LLOQ for Ns using the cHILIC method

	Calibration range (nmol)	R^2 cHILIC	cHILIC LLOQ (pmol)
Deoxythymidine	0.125–2	0.99	0.1
Adenosine		0.99	0.1
Cytosine		0.99	0.1
Guanosine		0.99	0.1
Inosine		0.99	0.1
Uridine		0.99	0.1

from 11% to 31% and are in good agreement with the variations determined for other SPE-based methods for NT analysis in non-plant organisms (Kong et al., 2018; Cohen et al., 2009).

In order to assess the effectiveness of the SPE method, we compared the matrix effect factor (MEF) of matrix obtained from the LLE step (before SPE) with the MEF of matrix obtained from the complete method (after SPE). The higher the MEF, the greater is the signal suppression by the respective matrix (see the "Materials and methods" section). Additionally, the comparison was made for both chromatographic techniques used, i.e. depending on whether the sample was separated via the Hypercarb or cHILIC method. Irrespective of the chromatography method, the SPE lowered the MEFs substantially and enabled the detection of several standards that were undetectable without SPE (Supplemental Tables S9, S10). Interestingly, the MEFs were generally lower when the samples were analyzed with the cHILIC method, showing that not only sample preparation but also the type of chromatography is important. For Ns, which are not retained by the SPE, the removal of charged metabolites from the matrix by the SPE nevertheless reduced the MEFs (Supplemental Table S10). The matrix after SPE even exerted a positive effect on sensitivity compared with buffer for some analytes (cytidine, inosine and uridine). Such ion enhancement effects have been reported previously (Zhou et al., 2017).

The robustness of the presented method, reflected in the LLOQs, variations, and MEFs, is equal to published SPE protocols for NT analysis of other organisms (Harmenberg et al., 1987; Cohen et al., 2009; Guo et al., 2013; Kong et al., 2018). Remarkably, for Ns, the method has a superior recovery and a similar MEF compared with SPE methods focusing exclusively on N analysis (Sawert et al., 1987; Farrow and Emery, 2012; Kopecná et al., 2013). Until now, the parallel quantification of Ns and NTs from plant samples was not possible—this robust method now allows this analysis and thus opens up new possibilities to investigate the NT metabolism of plants in greater depth.

For metabolite analysis, many laboratories have access to an LC system coupled with a photometric detector, whereas a MS detector is less common. Thus, it would be desirable that our sample preparation method also improves the photometric detection of NTs. After treating the samples with LLE alone, we were unable to detect any signals for NTs in the UV trace (at 254 nm) using the cHILIC method, but after SPE several peaks were detected (Supplemental Figure S4). For proof-of-concept, we showed that MS signals for the rNTs ATP, UTP, CTP, and GTP were associated with four of the photometric peaks. This demonstrates that the sample preparation via LLE and SPE improves NT detection also when a photometric detector is employed. However, in this case, it is recommendable to use other (non-MS-compatible) chromatographic separation techniques with increased resolution for NTs (see e.g. Meyer and Wagner, 1985). Our sample preparation method requires little plant material and allows inter alia the quantification of CTP and GTP in Arabidopsis leaves even without MS, which before has been difficult (Ashihara et al., 2020). Therefore, it might generally increase the sensitivity for NTs independent of the chosen detection method. Nonetheless, the analysis of less abundant NTs with photometric detection, for example dNTPs, would require significant upscaling.

dNTP pools in different plants are variable and correlate with the genomic GC content

We first applied the new method for the detection of NTs in the model plant *A. thaliana*. From as little as 100 mg of fresh material of either 7-day-old seedlings grown in liquid culture or leaves of 33-day-old plants grown on soil, not only all canonical rNTPs but also all of their dNTP counterparts were robustly detected (Figure 2, A and B). The concentrations of the rNTPs were in the nmol g^{-1} range, while dNTPs were 100- to 1000-fold less concentrated (Table 5). Data on the NTP contents in plants are scarce (Ashihara et al., 2020; Witte and Herde, 2020; Supplemental Table S1). However, our results on dNTPs are overall consistent with those from a previous study using radiolabelled plant cells and TLC (Nygaard, 1972). Because ATP and UTP are needed in higher amounts as energy carriers and for cell wall

Downloaded from https://academic.oup.com/plcell/article/33/2/270/6026971 by Institute of Horticultural Economics user on 11 December 2021

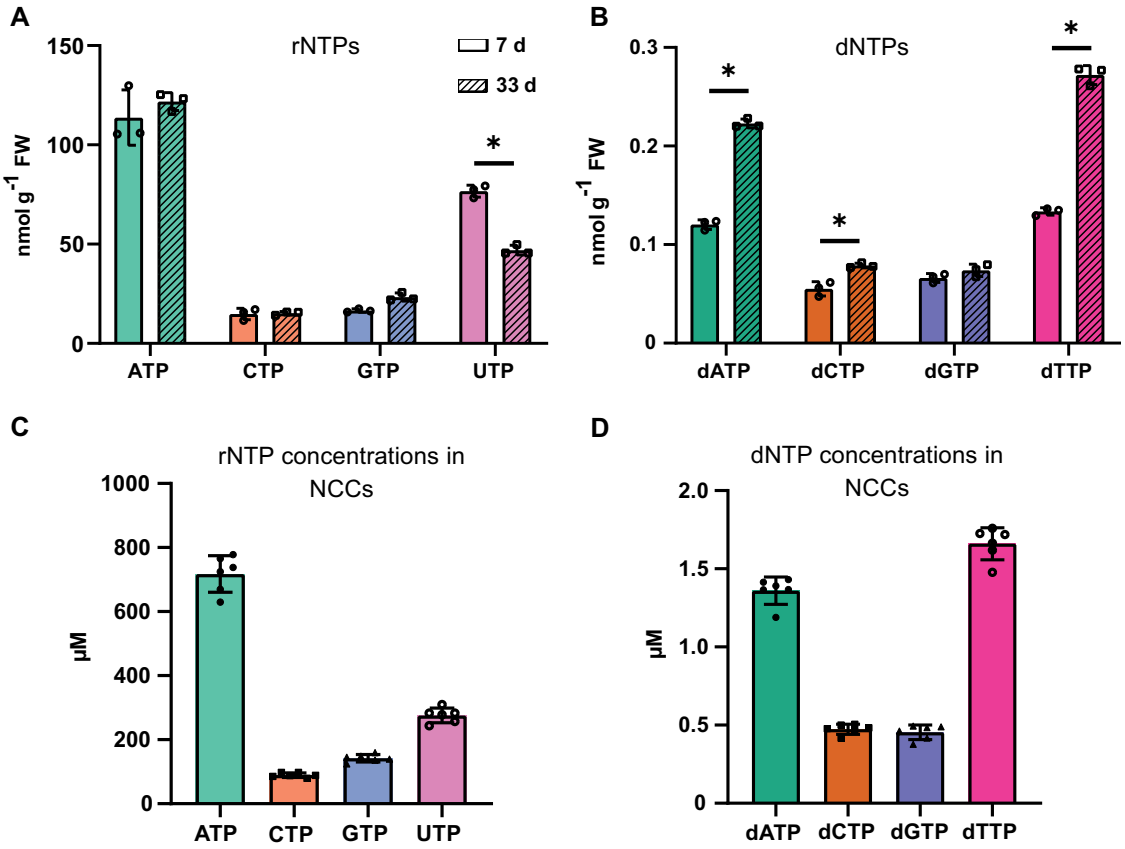

Figure 2 Cellular concentrations and absolute amounts of rNTs and dNTs in Arabidopsis leaves and seedlings. rNTs (rNTPs; A) and dNTs (dNTPs; B) were quantified in 7-day-old seedlings (unhatched bars) and 33-day-old rosette leaves (hatched bars). Each biological replicate represents a pool of several seedlings (A) or two leaves (B) which met the criteria outlined in the "Materials and methods" section from one individual plant. For seedlings, every replicate is a pool of seedlings grown together in one flask. Replicates were grown in parallel under identical conditions. Concentration of rNTPs (C) and dNTPs (D) in NT containing compartments of 33-day-old leaves. The concentration was calculated with the assumptions and formulas given in the "Materials and methods" section. Error bars indicate standard deviations (SD) for $n = 3$ biological replicates (A and B) or $n = 6$ biological replicates (C and D). * means $P < 0.05$ and was determined using a two-way ANOVA with Sidak's post test.

Table 5 Ratios of rNTP/dNTP in 7- and 33-day-old Arabidopsis plants

	ATP/dATP	CTP/dCTP	GTP/dGTP	UTP/dTTP
7 day	945	268	250	574
33 day	528	189	313	166

synthesis, respectively, the ratio of ATP/dATP and UTP/dTTP is higher than for CTP/dCTP and GTP/dGTP in seedlings (Table 5).

Interestingly, the dTTP and the dATP pools are increased and the UTP pool is decreased in older plants in comparison to seedlings (Figure 2, A and B). This may seem counterintuitive because one might expect more dNTPs in young growing tissue undergoing frequent cell divisions, but older tissues might require dNTPs for endoreduplication or for DNA damage repair. However, one needs to bear in mind that the growing conditions of the seedlings and the older plants were quite distinct, which may also account for the differences.

The immediate concentration of metabolites in a cell or cellular compartment influences enzyme activities or regulatory processes. It is therefore interesting to estimate the cellular concentrations of NTs. We used the cell and cell compartment volumes reported by Koffler et al. (2013) for leaves of 33-day-old plants. Based on the simplifying assumptions that NTs are equally distributed in the nucleus, cytoplasm, chloroplasts, and mitochondria, and largely absent from other cellular compartments, the average rNTP concentrations ranged from 100 to 750 µM whereas the concentrations of dNTPs were between 0.5 and 1.6 µM (Figure 2, C and D).

To ensure that the quenching in our method is suitable to preserve the phosphorylation status of the NTs, the adenylates (AMP, ADP, and ATP) in 33-day-old *A. thaliana* leaves were quantified (Table 6). The ratio of ATP/ADP was 15.2, while the ATP/AMP ratio was notably higher, resulting in an adenylate energy charge (AEC) of 0.97. We conclude that the phosphorylation status of these metabolites was maintained during the extraction, which is in line with the high recovery rates for these metabolites (Table 2). The ratios and the AEC are also consistent with results from other studies (Stitt et al., 1982; Guérard et al., 2011), although the

Downloaded from https://academic.oup.com/plcell/article/33/2/270/6026971 by Institute of Horticultural Economics user on 11 December 2021

Table 6 Absolute amounts of AMP, ADP, and ATP from 33-day-old Arabidopsis plants grown under long day conditions

Metabolite	nmol g^{-1} FW[a]
AMP	0.4 ± 0.04
ADP	7.6 ± 2.2
ATP	115.6 ± 7.8
Ratios	
ATP/ADP ratio	15.2
ATP/AMP ratio	286.4
AEC[b]	0.97 ± 0.01

[a]n = 6 biological replicates, where every replicate represents the oldest leaves of a different plant.
[b]AEC is defined as (ATP + 1/2ADP)/(ATP + ADP + AMP).

ATP/ADP and ATP/AMP ratio in 33 day-old-plants is higher than in other studies for unknown (Stitt et al., 1982; Savitch et al., 2001; Carrari et al., 2005). Additionally, the data show that also ADP as an example for the dinucleotides is co-eluted with the NMPs and NTPs from the SPE and can be quantified with this method.

We also identified NTs using an Orbitrap mass analyzer coupled to the Hypercarb chromatography providing exact masses for precursor and product ions as well as isotope patterns as additional evidence for the correct identification of the metabolites. In samples of 7-day-old seedlings, we identified all canonical NTPs with high confidence by MS/MS (Supplemental Table S11) except dGTP and dCTP for which the detection was not sensitive enough. Several NTPs were also detected in full MS mode suggesting that the samples provided by our method are in principle suitable to perform non-targeted analysis.

Plant species differ greatly in their metabolite composition in part due to variation in secondary metabolism. We wanted to assess if our method established in Arabidopsis is suitable for dNTP quantification in samples from diverse plant backgrounds. We extracted dNTPs from 11 different species encompassing monocotyledons, dicotyledons, a bryophyte, and three algae. In all tested species, the sensitivity was sufficient to detect and quantify dNTPs (Supplemental Figure S5) proving that our method is generally suitable for NT analysis of plants.

Because in DNA G pairs with C and A pairs with T, one might assume that the ratios of the corresponding dNTPs, i.e. the dGTP/dCTP and the dATP/dTTP ratios, are (i) close to unity and (ii) similar in different plants. Consistent with this concept, the dGTP/dCTP ratios were similar in the investigated species (with the exception of *C. reinhardtii*) but were general slightly lower than one, however the dATP/dTTP ratios were more variable, with *Avena sativa*, *Oryza sativa*, and *Solanum lycopersicum* containing notably more dATP than dTTP and *P. patens* having more dTTP than dATP (Supplemental Figure S5 and Figure 3). We additionally asked whether species with a high GC content in the DNA also have proportionally more dGTP and dCTP in their dNTP pool (GC content in dNTPs). Our results show that there is a moderate to strong positive correlation between these two parameters with a R^2 value of 0.67 (Figure 4) suggesting a link between the genome composition and the dNTP metabolome.

CDA and NSH1 metabolize dNs in vivo

The role of several enzymes in rN degradation is already well established, but to date it remains unclear whether dNs are also substrates of these enzymes in vivo, probably because these compounds are rather difficult to detect and quantify. We chose to investigate null mutants of genes encoding CDA (Vincenzetti et al. 1999; Faivre-Nitschke et al., 1999; Kafer and Thornburg 2000; Chen et al., 2016), GSDA (Dahncke and Witte, 2013; Baccolini and Witte, 2019), and NSH1 (Jung et al., 2009, 2011; Riegler et al., 2011) to address this issue with our newly established method. GSDA deaminates the purine nucleoside guanosine to xanthosine and CDA deaminates the pyrimidine nucleoside cytidine to uridine. NSH1 hydrolyzes the glycosidic bond of uridine generating uracil and ribose and is as well an essential component of a nucleoside hydrolase complex required for the hydrolysis of xanthosine to xanthine and ribose (Figure 5).

In seeds and seedlings of the Arabidopsis wild type, all rNs including the low abundant inosine but also deoxyadenosine in seeds and deoxythymidine in seedlings were reliably detected (Supplemental Figure S6 and Figure 6). Relative and absolute abundances of rNs in the *GSDA*, *CDA*, and *NSH1* loss-of-function mutants and in wild-type plants (Supplemental Figure S6) were consistent with concentrations reported in previous studies using a different extraction approach (Chen et al., 2016; Baccolini and Witte, 2019). In all mutants the abundance of adenosine, a metabolite not investigated previously in the context of these mutants, was elevated in seedlings (but not in seeds) compared with the wild type. With respect to the dNs, seeds contained a pool of deoxyadenosine that was not affected by any of the investigated mutations (Figure 6). By contrast, seeds of the *nsh1* and *cda* mutants showed an accumulation of deoxythymidine not observed in the Col-0 or *gsda* backgrounds (Figure 6, A). In seedlings, deoxythymidine additionally accumulated in the *GSDA* mutant, but was also detected at a lower level in Col-0 (Figure 6, B). However, in both tissues, the *nsh1* mutant accumulated by far the most deoxythymidine, suggesting that NSH1 is directly involved in the turnover of this metabolite. High concentrations of guanosine and cytidine occurring in the *gsda* and *cda* mutants, respectively (Supplemental Figure S3), are probably inhibiting NSH1 partially (Witte and Herde, 2020), leading to the intermediate deoxythymidine build-up observed in these backgrounds. Furthermore, deoxycytidine accumulated exclusively in the *cda* mutant (Figure 6) providing evidence for a role of CDA in the catabolism of this dN.

In summary, we provide evidence that NSH1 is involved in deoxythymidine hydrolysis and that CDA is responsible for deoxycytidine deamination in vivo, consistent with the ability of CDA to deaminate this dN in vitro (Chen et al., 2016). GSDA deaminates deoxyguanosine in vitro (Dahncke and Witte, 2013), but intriguingly deoxyguanosine was not

Downloaded from https://academic.oup.com/plcell/article/33/2/270/6026971 by Institute of Horticultural Economics user on 11 December 2021

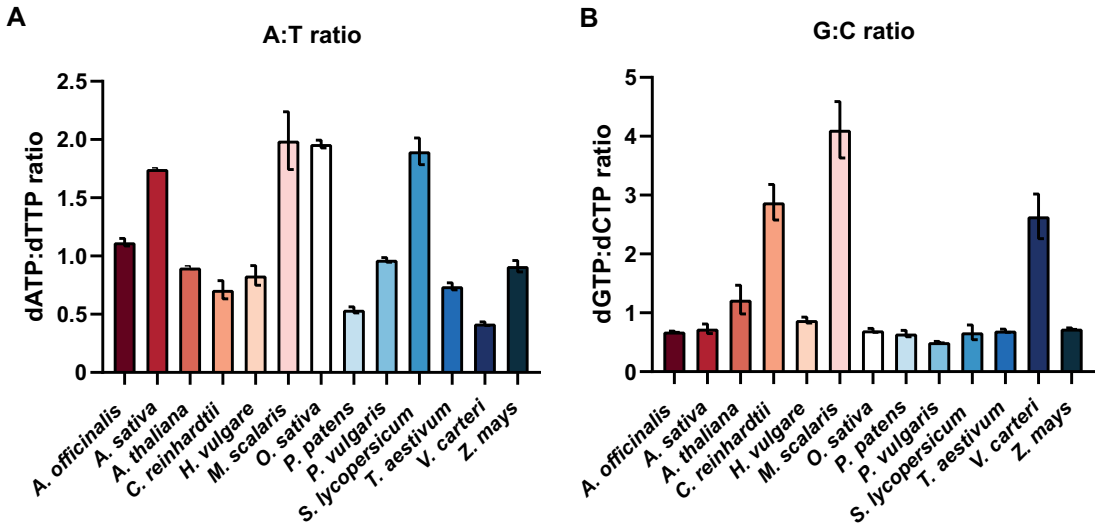

Figure 3 A/T and G/C ratios of dNTs (dNTPs) in different plant species. Ratios of dNTPs in *A. officinalis*, *A. sativa*, *A. thaliana*, *C. reinhardtii*, *H. vulgare*, *M. scalaris*, *O. sativa*, *P.* (*P.*) *patens*, *P. vulgaris*, *S. lycopersicum*, *T. aestivum*, *V. carteri*, and *Z. mays*. (A) Ratio of dATP to dTTP. (B) Ratio of dGTP to dCTP. Error bars indicate standard deviation (SD) for $n = 3$ biological replicates with each replicate representing a pool of several plants/seedlings all grown in parallel under the same environmental conditions.

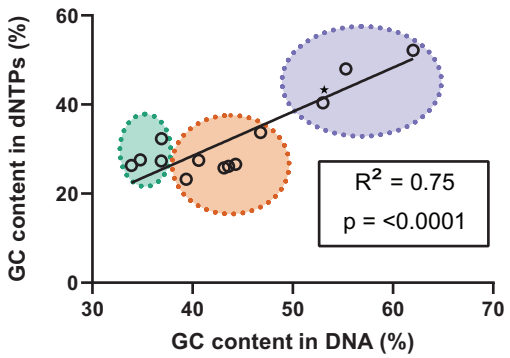

Figure 4 Regression analysis of the GC content in dNTPs and DNA. The GC content in the dNTPs (*y*-axis) is plotted against the genomic GC content (*x*-axis) and the Pearson correlation coefficient and the corresponding *P* value of a linear regression are calculated. Every white circle represents the average of three measurements. The green circle comprise all dicotyledonous species (*A. thaliana*, *P. vulgaris*, *S. lycopersicum*) and the bryophyte (*P. patens*), the orange circle encompasses the monocotyledonous species (*A. officinalis*, *A. sativa*, *H. vulgare*, *O. sativa*, *T. aestivum*, and *Z. mays*) and the purple circle alga (*C. reinhardtii*, *M. scalaris*, and *V. carteri*). * indicates an estimate of genomic GC content by extrapolation from known codon DNA sequences (R^2 without this datapoint is 0.73).

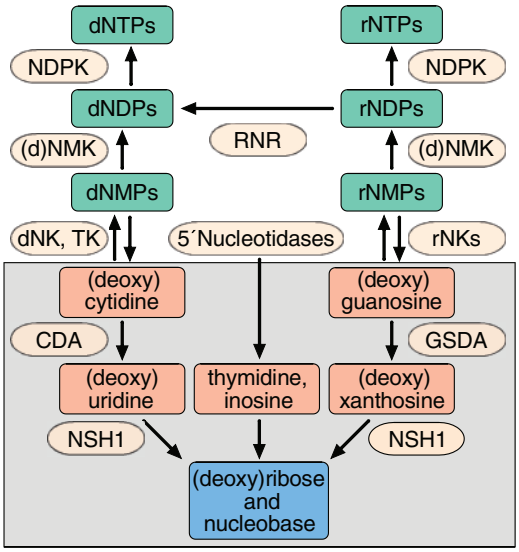

Figure 5 Scheme of nucleoside and NT metabolism. The (deoxy)nucleoside catabolism is highlighted with a gray background. NK, deoxynucleoside kinase; TK, thymidine kinase; rNK, ribonucleoside kinases; (d)NMK, (deoxy)nucleoside monophosphate kinases; and NDPK, nucleoside diphosphate kinases.

detectable in any of the analyzed genotypes (data not shown), although high concentrations of guanosine were detected in *gsda* seeds and seedlings (Supplemental Figure S6). Maybe for deoxyguanosine there is an additional metabolic escape route which is currently unknown.

CDA, GSDA, and NSH1 influence dNT and rNT pools

It is widely accepted that NT metabolism can be manipulated by the supply of extracellular Ns and nucleoside analogs, a concept exploited in chemotherapy (Galmarini et al., 2003; Robak and Robak, 2013). It is also established in plants that extracellular Ns can be taken up and interfere with plant metabolism (Traub et al., 2007; Chen et al., 2016; Ashihara et al., 2020). In plants, little is known about the impact of imbalanced intracellular N pools on the abundance of NTs. Therefore, we analyzed the NTs in the *cda*, *gsda*, and *nsh1* mutants, which have altered N pools. In seeds and seedlings lacking CDA and GSDA, the amounts of CTP and GTP are increased, respectively (Figure 7). Consistent with a previous study (Riegler et al., 2011), plants lacking NSH1

Downloaded from https://academic.oup.com/plcell/article/33/2/270/6026971 by Institute of Horticultural Economics user on 11 December 2021

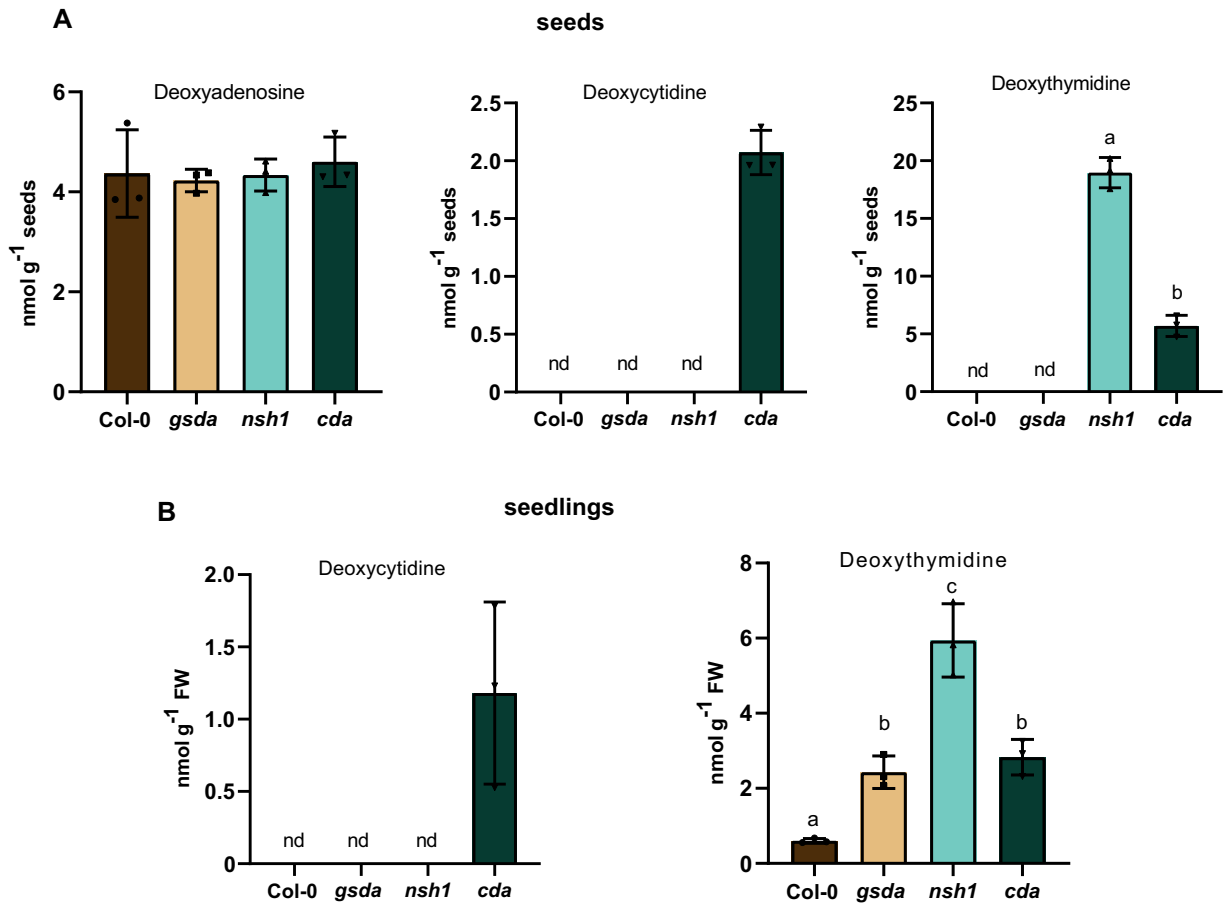

Figure 6 Absolute quantification of dNs in mutants impaired in the catabolism of rNs. Concentrations of dNs in seeds (A) and in 7-day-old seedlings (B) of *A. thaliana* wild type, as well as mutants in the degradation of purine and pyrimidine Ns (*gsda*, guanosin deaminase). Error bars are SD, $n = 3$ biological replicates, for seeds, three independent seed pools derived from different mother plants, for seedlings, three pools of seedlings from three independent liquid cultures were used. Statistical analysis was performed using one-way ANOVA with Tukey's post hoc test or in case of deoxythymidine by a two-tailed Student's *t* test. Different letters indicate $P < 0.05$. nd, not detected. FW, fresh weight.

accumulate more UMP and UTP compared with the wild-type (Figures 7, 8).

In general, the effects on NTP levels are also reflected by the respective NMPs (Figure 8). The accumulation of these NTs is probably a direct consequence of the increased pool sizes of the corresponding Ns (cytidine, guanosine, and uridine) in these mutants (Supplemental Figure S6), because the substrate availability for nucleoside and NT kinases (see scheme in Figure 5) is increased. However, some changes in the NT pools of the mutants cannot be explained by direct effects. The decrease of IMP concentrations in plants lacking GSDA or NSH1 (Figure 8, B) for example is puzzling because both contain much more inosine than the wild type (Supplemental Figure 3, B). Seeds and seedlings lacking GSDA have an increased content of ADP and ATP resulting in a higher AEC as well as more UMP and UTP. In *gsda* seedlings, there is also more CTP (Figures 7, 8). Thus, in seedlings, all measured NTP pools are strongly increased in the *gsda* background (Figure 7). The indirect changes in the *cda* and *nsh1* backgrounds are more subtle and are often similar. In seedlings, both mutants contain for example more GTP and ATP but in tendency less AMP than the wild type resulting in a higher AEC.

Except for the increased UTP level in *cda* seeds, all effects are more pronounced or even exclusively observed in seedlings compared with seeds. This also holds true for the Ns where for example adenosine only accumulates in mutant seedlings, but not in seeds (Supplemental Figure S6). As would be expected, these observations suggest that the flux through the NT metabolism is generally higher in growing seedlings compared with dormant seeds. Consistently, seeds harbor 5–10 times less rNTPs (and no detectable amounts of dNTPs), store adenylates mainly as AMP, display a lower ATP/ADP ratio, and have a lower AEC compared with seedlings which is in accordance with the literature (Raveneau et al., 2017; Figure 7).

Intriguingly, plants lacking enzymes of rN catabolism are not only impaired in the degradation of Ns (Figure 6 and Supplemental Figure S6) but also have elevated concentrations of dNTs, the substrates for DNA synthesis (Figure 9). The *CDA* mutant contains more dCTP similar to a human cancer cell line with reduced CDA activity (Chabosseau

Downloaded from https://academic.oup.com/plcell/article/33/2/270/6026971 by Institute of Horticultural Economics user on 11 December 2021

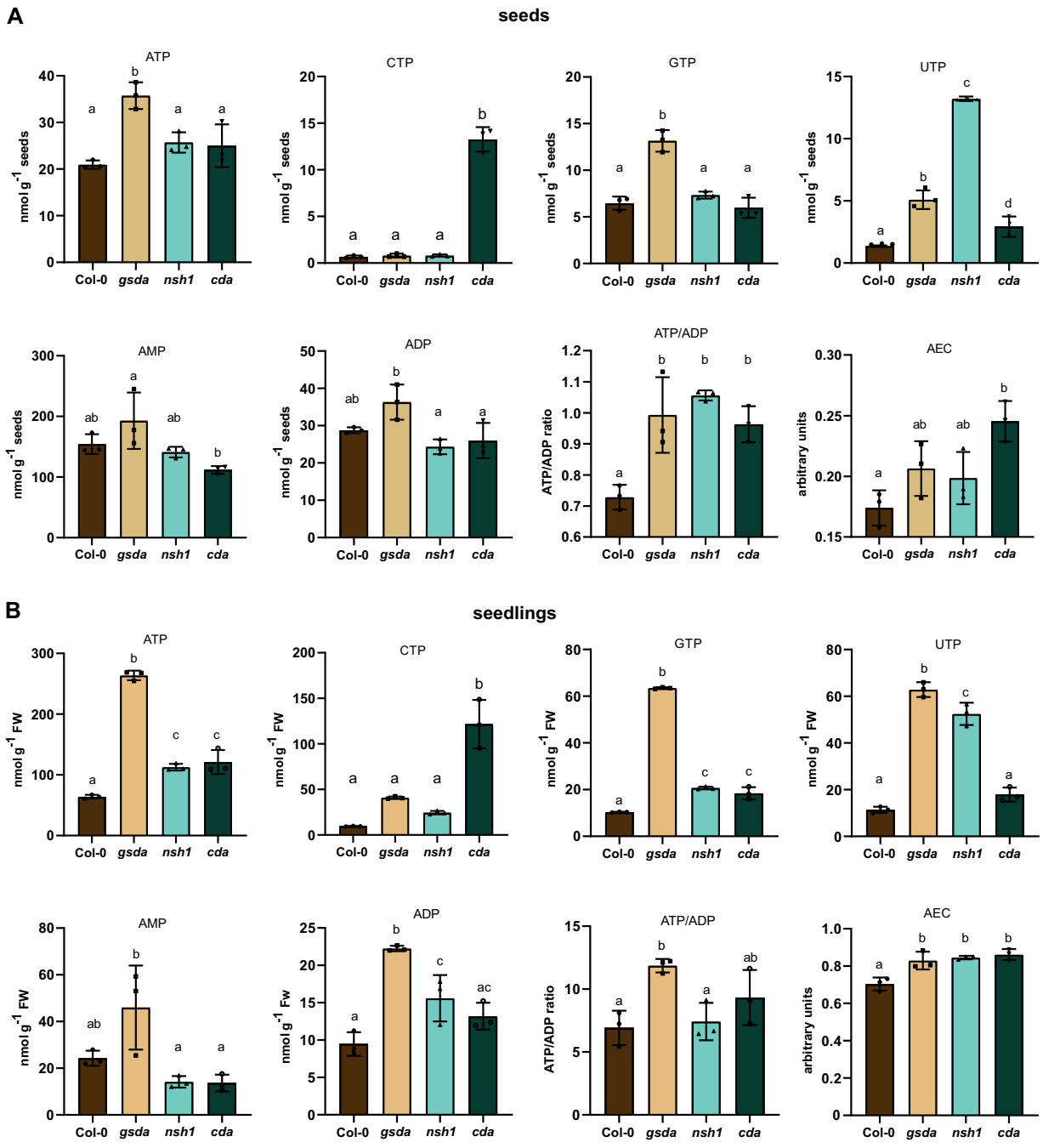

Figure 7 Comparison of the AEC, the ATP/ADP ratio, and the rNT concentrations between seeds and seedlings. Concentrations of rNTs, as well as ATP/ADP ratio and AEC in seeds (A) and in 7-day-old seedlings (B) of *A. thaliana* wild type, as well as mutants in the salvage and degradation of purine and pyrimidine Ns (*gsda*, guanosin deaminase) .Error bars are SD, $n = 3$ biological replicates, for seeds, three independent seed pools derived from different mother plants, for seedlings, three pools of seedlings from three independent liquid cultures were used. Statistical analysis was performed using one-way ANOVA with Tukey's post hoc test. Different letters indicate $P < 0.05$. FW, fresh weight.

et al., 2011). The high dCTP concentration may be a consequence of the high CTP concentration in *cda* seedlings. Interestingly, *gsda* seedlings accumulated the highest amounts of dGTP and dATP and also contained more dCTP and dTTP than the wild type. It seems as if the strongly elevated concentrations of ATP, GTP, and CTP in this mutant are mirrored in the corresponding dNTPs indicating that the pool sizes of these metabolites are directly linked. This also holds true for the higher dATP and dGTP concentrations mirroring the enlarged ATP and GTP pools in the *cda* and *nsh1* seedlings. In none of the mutants, deoxyguanosine was detected and deoxyadenosine concentrations were the same as in the wild type, whereas deoxycytidine was only found in *cda* background. It appears that the dN pool sizes of A,

Downloaded from https://academic.oup.com/plcell/article/33/2/270/6026971 by Institute of Horticultural Economics user on 11 December 2021

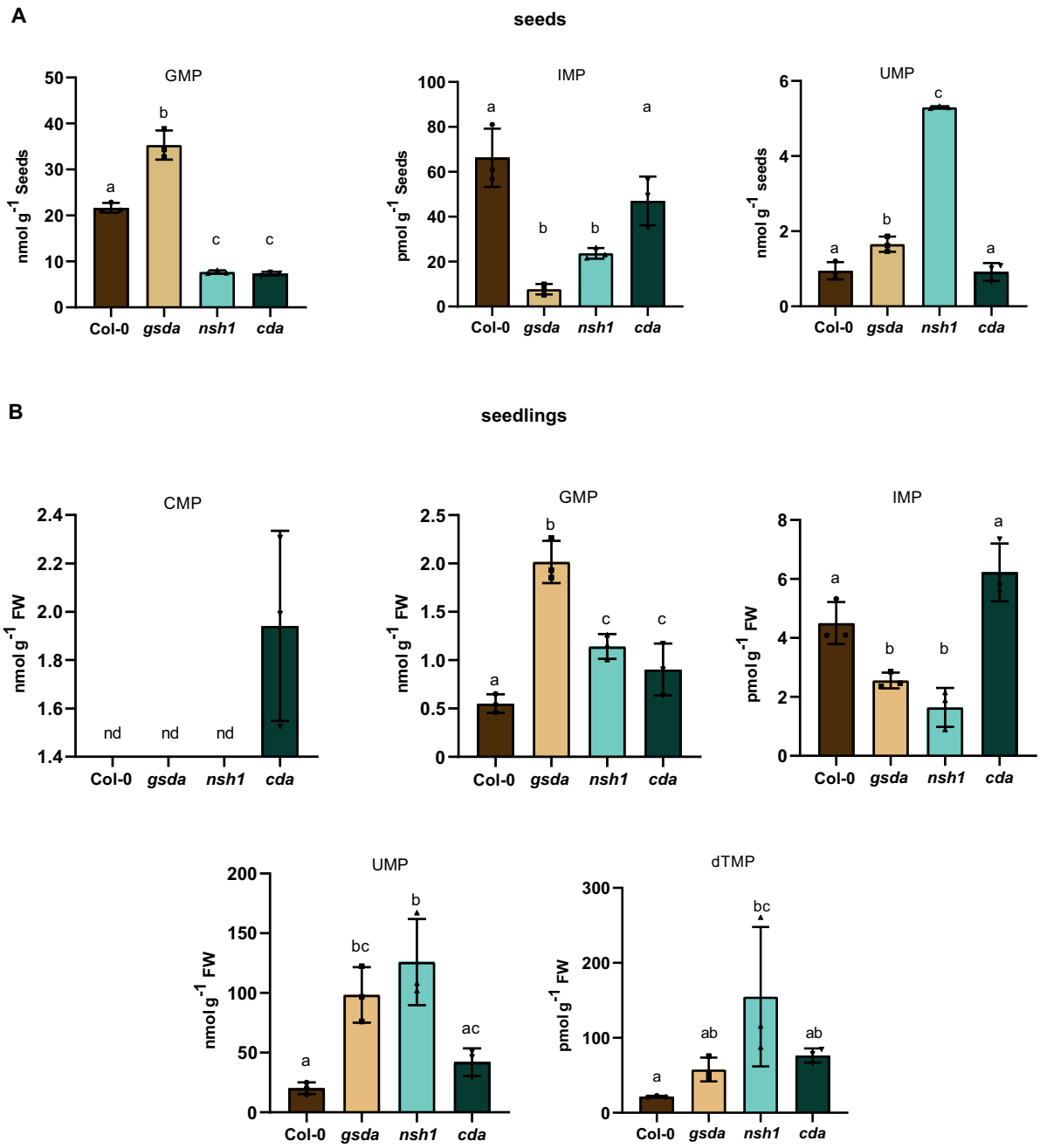

Figure 8 Absolute quantification of NMPs in seeds and seedlings of wild type and mutant plants impaired in nucleoside catabolism. Concentrations of NMPs in seeds (A) and in 7-day-old seedlings (B) of *A. thaliana* wild type, as well as mutants in the degradation of purine and pyrimidine Ns (*gsda*, guanosin deaminase) . Error bars are SD, $n = 3$ biological replicates, for seeds, three independent seed pools derived from different mother plants, for seedlings, three pools of seedlings from three independent liquid cultures were used. Statistical analysis was performed using one-way ANOVA with Tukey's post hoc test. Different letters indicate $P < 0.05$. nd, not detected. FW, fresh weight.

G, and C do not influence the corresponding dNTP amounts. By contrast, the deoxythymidine content seems to have a stronger influence on the dTTP pool size than the UTP concentration. Seedlings of the *cda* and the *gsda* mutants both have more deoxythymidine (Figure 6), more dTMP (Figure 8), and correspondingly more dTTP (Figure 9) than the wild type, but the UTP amounts are only elevated in the *gsda* and not in the *cda* background. However, the deoxythymidine and dTMP pools are largest in the *NSH1* mutant, but the dTTP concentration is only moderately increased, less than in *gsda* and *cda* seedlings. Although this seems contradictory, one needs to consider that uridine as well as deoxyuridine stemming from deoxycytidine deamination cannot be metabolized in *nsh1* background (uridine and resulting UMP accumulation are shown in Supplemental Figure S6 and Figure 8). The accumulation of

Downloaded from https://academic.oup.com/plcell/article/33/2/270/6026971 by Institute of Horticultural Economics user on 11 December 2021

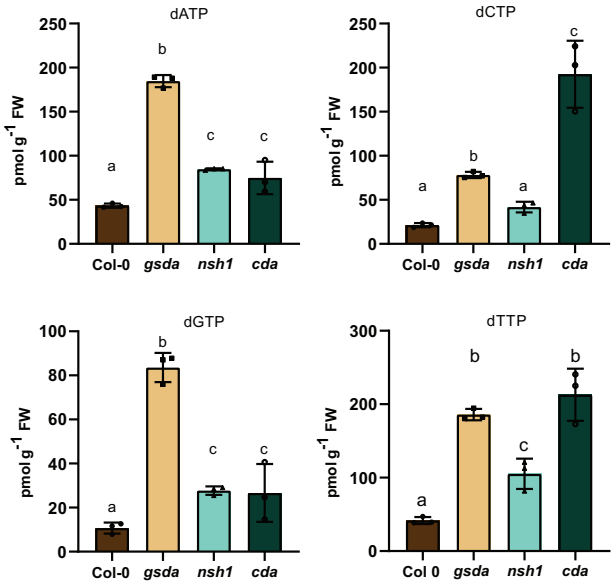

Figure 9 Absolute quantification of deoxynucleotide triphosphates in wild type and mutant seedlings impaired in nucleoside catabolism. Concentrations of dNTPs in 7-day-old seedlings of *A. thaliana* wild type, as well as mutants in the degradation of purine and pyrimidine Ns (*gsda*, guanosin deaminase). Error bars are SD, $n = 3$ biological replicates, for seedlings, three pools of seedlings from three independent liquid cultures were used. Statistical analysis was performed using one-way ANOVA with Tukey's post hoc test. Different letters indicate $P < 0.05$. FW, fresh weight.

these compounds may partially inhibit the thymidine kinases and maybe also thymidylate kinases known to be responsible for deoxythymidine (Clausen et al., 2012) and dTMP phosphorylation, respectively.

GSDA, CDA, and NSH1 were previously only considered to be involved in rN catabolism, but with our new method we can now show that they also play a role in dN degradation. By characterizing these mutants more in depth, we obtained a glimpse of the interconnection of deoxy- and rNT metabolism in plants. The data suggest that the ATP, GTP, and CTP pool sizes influence the amounts of dATP, dGTP, and dCTP, whereas the dTTP concentration seems to be more connected to the deoxythimidine than the UTP pool.

Discussion

A complex interplay of de novo synthesis, degradation, and salvage of rNTPs and dNTPs ensures that appropriate quantities of NTs are available for RNA and DNA synthesis as well as for signaling and energy metabolism (Zrenner et al., 2006; Witte and Herde, 2020). The fidelity of transcription and DNA replication is affected by altered ratios or changed total amounts of dNTPs (Nick McElhinny et al., 2010a, 2010b; Gon et al., 2011; Kumar et al., 2011; Buckland et al., 2014) emphasizing the importance of accurately balancing synthesis, degradation, and salvage of NTs and Ns. To gain a more comprehensive insight into these processes, a method allowing the parallel quantification of NTs and their respective Ns from one sample is a prerequisite. For the analysis of plants, such a method has not been available so far. Here, we fill this gap showing that the developed protocol is suitable for the analysis of NTs and Ns not only in seedlings and fully grown plants of Arabidopsis but also in a wide phylogenetic range of plants and even algae (Figure 2 and Supplemental Figure S5).

We found that the dGTP/dCTP ratios were quite similar between plant species, whereas the dATP/dTTP ratios (Figure 3) and the absolute contents of the dNTPs (Supplemental Figure S5) were more variable. Although clearly more evidence is needed, it is tempting to speculate that dNTPs produced in excess of their stoichiometric requirement in some plants might have an additional role in the respective species. The variation in dTTP contents for example might be related to the synthesis of dTDP-sugars and enzymes synthesizing dTDP-sugars are known to exist in plants (Neufeld, 1962; Frydman et al., 1963; Katan and Avigad, 1966).

Our data suggest that genome GC contents and the sum of dGTP and dCTP concentrations relative to all dNTPs are correlated (Figure 4). A dNTP-dependent evolution of the genomic GC content has been proposed (Vetsigian and Goldenfeld, 2008; Greilhuber et al., 2012; Šmarda et al., 2014) which may be an example of metabolism-driven evolution (de Lorenzo, 2014), but actually it is unknown if the dNTP abundances influence the DNA composition or vice versa. Certainly, more plant species need to be analyzed to test the validity of this correlation.

By analyzing well-characterized mutants of Arabidopsis impaired in rN catabolism (*nsh1*, *cda*, and *gsda*) with the new method, we obtained novel insights especially regarding the involvement of the corresponding enzymes in dN and dNT metabolism (Figures 6–9 and Supplemental Figure S6). We demonstrate that CDA and NSH1 partake in the catabolism of dNs in vivo (Supplemental Figure S3), showing that the known ability of CDA to deaminate deoxycytidine in vitro (Chen et al., 2016) is of relevance in the plant. Deoxythymidine accumulates in *nsh1* background suggesting that it is a NSH1 substrate in vivo, but so far this has not been investigated with the isolated enzyme in vitro.

The accumulation of dNs in seedlings of wild type and mutant plants indicates that even in this actively growing tissue some DNA or dNT degradation occurs (Figure 6). One needs to bear in mind that the dN accumulation in the mutants was observed despite the ability of the cells to salvage dNs. Salvage can strongly reduce accumulation as was shown for hypoxanthine which only accumulated when degradation and salvage were mutated (Baccolini and Witte, 2019). It is therefore possible that the flux through the dNs is much higher than one would assume from the relatively moderate levels of accumulation in the catabolic mutants. The origin of the dNs is currently unclear. They might be derived from DNA repair or from programmed cell death resulting in DNA degradation and release of dNMPs. Programmed cell death is a widespread process associated

Downloaded from https://academic.oup.com/plcell/article/33/2/270/6026971 by Institute of Horticultural Economics user on 11 December 2021

with many aspects of plant development such as endosperm degradation, tracheary element differentiation, senescence, or microbial interactions (Aoyagi et al., 1998; Sakamoto and Takami, 2014). It was even suggested that plants store NTs and phosphate for embryogenesis and germination in the DNA synthesized by endoreduplication within the endosperm (Wang et al., 1998; Leiva-Neto et al., 2004; Lee et al., 2009). Another putative source of dNs might be the continuous house-keeping dephosphorylation of NTs. It was previously hypothesized that the phosphorylation status especially of dNTs may be constantly changed to control dNTP quantity and to improve their quality, i.e. to ensure that the dNTP pools only contain dNTs with canonical bases (Rampazzo et al., 2010; Leija et al., 2016). Because nucleoside and NT kinases best recognize their canonical targets, they may serve to purify the dNT pools if the pools are simultaneously subject to continuous dephosphorylation (Chen et al., 2018; Chen and Witte, 2020). It follows from this idea that dN salvage must be an essential process, because without it the dNTP pools would be depleted. In agreement with this concept, salvage by thymidine kinase 1a and 1b (Pedroza-García et al., 2015, 2019; Xu et al., 2015; Le Ret et al., 2018) is crucial for plant development since plants lacking functional copies of both corresponding genes have etiolated seedlings that need carbohydrate supplementation for survival (Xu et al., 2015).

There is no doubt that salvage of deoxythymidine is important, but here we provide evidence that plants also degrade this compound employing NSH1. This raises the question of how degradation and salvage are coordinated. Partially this might be achieved by spatial separation of both processes because at least Tk1b is located in the mitochondria and the chloroplasts whereas NSH1 and Tk1a are found in the cytosol (Jung et al., 2009; Xu et al., 2015), suggesting a preference for salvage in the organelles and a competition of both processes in the cytosol.

Intriguingly, compromising N catabolism leads not only to N accumulation but results in increased and imbalanced NT pools (Figures 7–9). The N and NT pools are interconnected by kinases (Ashihara et al., 2020; Witte and Herde, 2020; Figure 5), thus the most straightforward way to explain the increases in rNTP abundances is the higher availability of rN substrates for these enzymes. By contrast, higher amounts of dNTPs in the mutants are in most cases probably not a result of phosphorylation of dNs, because their pool sizes are often not increased except for deoxythymidine. Instead increased dNTP levels might result from greater reduction of rN diphosphates by rNT reductase (RNR; Nordlund and Reichard, 2006).

The current literature on plant NT metabolism suggests a temporal or spatial separation of synthesis, salvage, and degradation to avoid futile cycles (Ashihara et al., 2020; Witte and Herde, 2020). However, the concomitant occurrence in the catabolic mutants of increased amounts of Ns and of NTs, indicative of salvage and biosynthetic processes, suggests that a seedling can realize all these processes simultaneously. The enzymes for synthesis, degradation, and salvage might all be present in the same metabolic space but the flux through the respective pathways might be coordinated by the regulation of key enzymes. Being able to detect and quantify Ns and NTs is a prerequisite to investigate such hypotheses for example by using metabolic flux analysis and conditional mutants.

In the *gsda* mutant not only the direct substrate (guanosine) and its phosphorylated counterpart (GTP) accumulate but also ATP suggesting a crosstalk between these metabolites. It has been shown biochemically that GTP severely inhibits the activity of plant AMP deaminase, an enzyme that is involved in the regulation of guanylate synthesis, adenylate catabolism, and AEC regulation (Yabuki and Ashihara, 1991; Sabina et al., 2007; Witte and Herde, 2020). Sabina et al. (2007) could not detect an effect on GTP pools when feeding AMP deaminase inhibitors, but detected a two–five-fold increase of all adenylates, similar to the effects we observed in the *GSDA* mutant. This suggests that GTP accumulation in the *gsda* background (Figure 7) inhibits AMP deaminase in vivo, thereby raising ATP levels. Because IMP is the product of AMP deaminase, the inhibition of this enzyme might reduce IMP concentrations. That is precisely what we observed in the *gsda* seeds and seedlings (Figure 8). UTP and CTP levels were also raised in *gsda* plants probably to balance the elevated ATP and GTP concentrations. How pyrimidine and purine NT concentrations are kept in balance is currently unknown, but with our new method this interesting question could be further investigated.

Several phenotypes have been described for *gsda*, *nsh1*, and *cda* mutants such as delayed germination, compromised growth, and reduced recovery from dark treatment along with chlorosis (Chen et al., 2016; Schroeder et al., 2018; Baccolini and Witte, 2019). It has been suggested that these phenotypes are directly caused by the accumulation of rNs (Schroeder et al., 2018). However, here we show that NT pools are also disturbed in these mutants, which is known or is easily conceivable to cause detrimental effects. An increase in rNTP pool sizes for example leads to the undesired incorporation of rNTPs into human mtDNA (Nick McElhinny et al., 2010a, 2010b; Berglund et al., 2017). An elevated GTP concentration as observed in *gsda* seedlings might interfere with signaling processes in plants, in which GTP plays an important role (Assmann, 2002; Johnston et al., 2007). The biosynthesis of dNTPs by RNR will be disturbed by changed NTP pool sizes because RNR is stimulated by ATP and inhibited by dATP. Such pool size changes are known to lead to mutations and even to apoptosis in non-plant organisms (Kumar et al., 2011). Also in Arabidopsis, a mutant lacking a subunit of the RNR has disturbed dNTP levels and displays severe defects like sensitivity to UV-C light, DNA damage, developmental abnormalities, and cell death (Wang and Liu, 2006). Furthermore, it was shown that feeding deoxyadenosine to bean roots results in chromosomal breakage which was suggested to be a result of an increased dATP pool (Odmark and Kihlman, 1965).

Downloaded from https://academic.oup.com/plcell/article/33/2/270/6026971 by Institute of Horticultural Economics user on 11 December 2021

In summary, it appears possible that the phenotypic alterations observed in the N catabolic mutants are at least partially caused by changed rNTP and dNTP pool sizes. It would be interesting to use these mutants to study the consequences of altered NT levels on transcriptional fidelity, DNA mutation rates, effects on the target of rapamycin (TOR) complex, and the involvement of dATP or ATP in plant immune signaling (Burdett et al., 2019; Nizam et al., 2019; Kazibwe et al., 2020).

NTs and Ns are not only involved in RNA and DNA metabolism but also play diverse roles for example in developmental processes and in plant pathogen interactions. The recently described *venosa4* mutant for example shows severe defects in chloroplast development and has a defect in an enzyme, which is likely involved in the dephosphorylation of dNTPs (Xu et al., 2020). In plant metabolome studies, NTs and Ns are strongly underrepresented hampering the discovery of novel functions for this major class of plant metabolites. The method described here will allow routine NT analysis to be performed in research focused on NT metabolism as well as in broad plant metabolomics surveys used in many plant research disciplines with the prospect of revealing so far unknown connections between the NT metabolome and other biological processes.

Materials and methods

Chemicals

Water, acetonitrile, methanol, ammonium acetate (all LC–MS grade), ethylenediaminetetraacetic acid (EDTA), and magnesium chloride were purchased from AppliChem. PCA and DCM were obtained from Carl Roth. 2′-Deoxyadenosine, 2′-deoxycytidine, 2′-deoxyguanosine, TCA, and trioctylamine (TOA) were purchased from Sigma–Aldrich. Twenty-five percent of ammonia solution and acetic acid (both LC–MS grade) were purchased from Merck. All ISTDs were from Eurisotope. The Strata-X-AW SPE cartridges, 30 mg, 33 µm were bought from Phenomenex.

Preparation of standard solutions

If not stated otherwise, all standards were measured in the matrix obtained after SPE. All stock solutions were stored at −80°C and dilutions were prepared fresh before analysis.

Plant culture

Arabidopsis thaliana plants were grown as previously stated in Niehaus et al. (2020) with slight modifications. Seeds were surface sterilized and cultivated in liquid culture (1.5 mM $MgSO_4 \times 7H_2O$, 1.25 mM KH_2PO_4, 3 mM $CaCl_2$, 18.7 mM KNO_3, 0.1 mM $FeSO_4 \times 7H_2O$, 0.1 mM $Na_2EDTA \times 2H_2O$, 0.13 mM $MnSO_4 \times H_2O$, 0.1 mM H_3BO_3, 30 µM $ZnSO_4 \times 7H_2O$, 1 µM $Na_2MoO_4 \times 2H_2O$, 0.1 µM $CuSO_4 \times 5H_2O$, 0.1 µM $NiCl_2 \times 6H_2O$, 0.125% [w/v] MES, pH 5.7 adjusted with KOH) in a shaker (New Brunswick Innova 42, Eppendorf) with six Sylvania e15t8 tubular fluorescent lamps emitting a photon flux of 45 µmol s^{-1} m^{-2} at 22°C in 100 mL flasks under sterile conditions (10 mg seeds per flask). The shaker was set to 80 rpm. The seedlings were harvested after 7 days. For the 33-day-old plants, Arabidopsis seeds were sown on soil and grown under long-day conditions (Binder KBFW 720 with Osram Lumilux lights,16-h light/8-h darkness, 22°C day, 20°C night, 100 µmol s^{-1} m^{-2} light, and 70% humidity).

T-DNA insertion mutants were obtained from our in-house collection. Their characterization is described in Dahncke and Witte (2013; *gsda*-2, GK432D08), Chen et al. (2016; *cda*-2, SALK036597), and Baccolini and Witte (2019; *nsh1*-1, SALK083120). The genotypes of all mutant lines were confirmed by PCR as described previously (Dahncke and Witte, 2013; Chen et al., 2016). A uniform seed batch was obtained from mutant and wild-type plants grown in parallel in a randomized fashion. The seeds were analyzed 2 weeks post-harvest. For the comparison of mutant seedlings, plants were grown in liquid culture as described above under constant light.

Seeds of asparagus (*Asparagus officinalis* cv. Ramires), barley (*Hordeum vulgare* cv. Golden Promise), common bean (*Phaseolus vulgaris* cv. Black Jamapa), oat (*A. sativa* cv. Fleuron), rice (*O. sativa* cv. Nipponbare), and wheat (*Triticum aestivum* cv. Thatcher) were surface sterilized and cultivated between sheets of filter paper placed in a container filled with some distilled water (Kirchner et al., 2018) and grown in a growth cabinet (Binder KBFW 720 with Osram Lumilux lights) at 22°C, 100 µmol s^{-1} m^{-2} light, and 70% humidity. Whole seedlings were collected 7 days after germination (dag) for all species except *A. officinalis* and *O. sativa* which needed 14 dag to accumulate enough biomass.

The moss *Physcomitrium* (*Physcomitrella*) *patens*, strain Grandsen 2004 (Kamisugi et al., 2008), was cultivated on Knoop medium (250 mg L^{-1} KH_2PO_4, 250 mg L^{-1} KCl, 250 mg L^{-1} $MgSO_4 \times 7H_2O$, 1 g L^{-1} $Ca(NO_3)$, 12.5 mg L^{-1} $FeSO_4 \times 7H_2O$, pH 5.8, and 1.2% [w/v] agar) in a climate chamber under long-day conditions (16-h light/8-h darkness, 22°C day, 20°C night, 100 µmol s^{-1} m^{-2} light, and 70% humidity). Plants were transferred to new plates every 4 weeks during cultivation. Plant material was collected 7 days after transferring to new plates.

Tomato plants (*S. lycopersicum* cv. Micro-Tom) were surface sterilized and transferred to germination medium (0.5 × Murashige and Skoog, 10 g L^{-1} sucrose, and 8 g L^{-1} phyto-agar). The seeds were placed in darkness at room temperature and moved to long-day conditions after 4 days (16-h light/8-h darkness, 22°C day, 20°C night, 100 µmol s^{-1} m^{-2} light, and 70% humidity). Seedlings were harvested 7 dag. Maize (*Zea mays* cv. Rafinio) was grown hydroponically between two plates in tap water wetted foam under long-day conditions (16-h light/8-h darkness, 22°C day, 20°C night, 100 µmol s^{-1} m^{-2} light, and 70% humidity) and harvested 7 dag. *C. reinhardtii* was cultivated for 7 days under the same conditions as the Arabidopsis seeds in liquid culture. *Volvox carteri* was cultivated for 7 days in Fernbach flasks (28°C, 16-h light/8-h dark and 100 µmol s^{-1} m^{-2} light), as described in Klein et al. (2017). *Mougeotia scalaris*

Downloaded from https://academic.oup.com/plcell/article/33/2/270/6026971 by Institute of Horticultural Economics user on 11 December 2021

strain SAG 164.80 was cultivated for 7 days (22–25°C, 16-h light/8-h dark, and 46 µmol s^{-1} m^{-2} light), as described in Regensdorff et al. (2018).

All plant and algae material was collected in the middle of the respective light period. Genomic GC-content of respective plant and algae species was acquired from the National Center for Biotechnology Information (NCBI, https://www.ncbi.nlm.nih.gov) or in the case of *M. scalaris* from Regensdorff et al. (2018).

Chromatography and MS parameters

An Agilent 1290 Infinity II LC System coupled with an Agilent 6470 triple quadrupole mass spectrometer was used. Chromatographic separations employed either a 150 × 2.1 mm zic-cHILIC column with 3-µm particle size (Merck) or a 50 × 4.6 mm Hypercarb column with 5-µm particle size (Thermo scientific). The zic-cHILIC column was operated at a flowrate of 0.2 mL min^{-1} and a temperature of 35°C. Mobile phase A was 90% 10 mM ammonium acetate pH 7.7 with 10% acetonitrile and mobile phase B was 10% 2.5 mM ammonium acetate pH 7.7 with 90% acetonitrile. In the following, we refer to chromatographies employing the zic-cHILIC column as cHILIC method. Depending on the analytes, different gradients were used (Tables 7, 8). The Hypercarb column was operated at a flow rate of 0.6 mL min^{-1} and a column temperature of 30°C. Mobile phase A was 5 mM ammonium acetate pH 9.5 and mobile phase B was acetonitrile (for the gradient see Table 9). In the following, we refer to the chromatography using the Hypercarb column as the Hypercarb method. The injection volume was 10 µL and analysis was carried out in positive mode for both methods employing the multiple-reaction-monitoring (MRM) mode. Transitions (precursor ions and product ions) as well as collision energies and fragmentor energies are listed in Supplemental Tables S4–S6. The in-source parameters for the cHILIC method were optimized according to Kong et al. (2018) as a starting point. The following adjustments to fit the plant matrix were made: gas temperature 290°C, gas flow 13 L min^{-1}, nebulizer pressure 25 psi, sheath gas temperature 320°C, sheath gas flow 11 L min^{-1}, capillary voltage 2,500 V, and nozzle voltage 2,000 V. The optimized in-source parameters for the Hypercarb method were: gas temperature 250°C, gas flow 12 L min^{-1}, nebulizer pressure 20 psi, sheath gas temperature 395°C, sheath gas flow 12 L min^{-1}, capillary voltage 3,000 V, and nozzle voltage 500 V. For the determination of exact masses, samples were separated with a Vanquish LC (Thermo Fisher) by the Hypercarb method. The metabolites were analyzed with an Orbitrap Q Exactive Plus mass spectrometer (Thermo Fisher) at a resolution of 70,000 when operated in full MS mode or 17,500 for detection of product ions in PRM (parallel reaction monitoring) mode with 35-V normalized collision energy or 140,000 using single-ion monitoring (SIM) in the positive polarity mode. Automatic gain control (AGC) target and maximum injection time were set to $3e^6$ and 200 ms, respectively. The heated ESI (electrospray-ionization) source was operated at 0-eV collision-induced dissociation (CID), sheath gas flow 45, auxiliary gas flow 10, sweep gas flow 2, spray voltage 3.5 kV, capillary temperature 250°C, S-lens RF level 45.0, and aux gas heater 400°C. All reported values were obtained with the Freestyle software (ver. 1.5, Thermo Fisher). For UV detection, samples were prepared as described in the respective section and identical to the procedure described for the analysis of the MEF. The detector was a VF-D40-A variable wavelength detector set to 254 nm. Identity of peaks was confirmed by MS as described before with an orbitrap mass analyzer in full MS mode.

Table 7 Gradient for NT chromatography on the zic-cHILIC column

Time (min)	Mobile phase A (%)	Mobile phase B (%)
0.0	20.0	80.0
7.0	20.0	80.0
12.0	40.0	60.0
17.0	40.0	60.0
19.0	20.0	80.0
23.0	20.0	80.0

Table 8 Gradient for nucleoside chromatography on the zic-cHILIC column

Time (min)	Mobile phase A (%)	Mobile phase B (%)
0.0	10.0	90.0
7.0	10.0	90.0
12.0	40.0	60.0
17.0	40.0	60.0
19.0	10.0	90.0
23.0	10.0	90.0

Table 9 Gradient for NT chromatography on the Hypercarb column

Time (min)	Mobile phase A (%)	Mobile phase B (%)
0.0	96.0	4.0
10.0	70.0	30.0
10.10	0.0	100.0
11.50	0.0	100.0
11.60	96.0	4.0
20.0	96.0	4.0

Sample preparation and SPE

Plant samples were harvested, briefly washed in tap water, and dried thoroughly with a paper towel. Approximately 100-mg plant material was weighed into a 2-mL safe-lock centrifuge-vial and frozen in liquid nitrogen together with five 5-mm steel beads (one 7-mm steel bead and five 5-mm steel beads in case of seeds). The exact sample weight was noted and used for calculating analyte concentrations. The tissue was disrupted using a MM 400 beadmill (Retsch, Germany) at 28 Hz for 2.30 min. Onto the frozen powder, 1 mL of ice-cold 15% TCA solution was added including the respective isotope standards. The samples were briefly vortexed, ground once more at 28 Hz for 2.30 min, and then centrifuged for 10 min at 4°C at 40,000 × *g*. To the supernatant 1 mL 78/22 DCM/TOA was added. Samples were vortexed for 12 s and centrifuged for 2 min at 4°C and 5,000 × *g*. The upper phase from each sample was transferred to a new tube and 1 mL water as well as 5 µL 0.5%

Downloaded from https://academic.oup.com/plcell/article/33/2/270/6026971 by Institute of Horticultural Economics user on 11 December 2021

acetic acid were added. This mixture was applied to a 30 mg/1 mL Strata X-AW cartridge that had been equilibrated sequentially with 1 mL methanol, 1 mL 2/25/73 formic acid/methanol/H_2O, and 1 mL 10 mM ammonium acetate pH 4.5. The sample solution was allowed to enter the cartridge for 2 min without suction and then percolated through the solid phase at a flowrate of about 1 mL min^{-1} using a vacuum manifold. The flow-through containing the nucleoside fraction was collected and evaporated in an Alpha 1–2 LDplus freeze dryer (Christ, Germany). The SPE cartridge was washed with 1 mL 1-mM ammonium acetate pH 4.5 and 1 mL methanol, dried shortly, and eluted two times with 0.5 mL 20/80 ammonia/methanol. The eluate was dried in a vacuum concentrator until no liquid was left. For the cHILIC method, the samples were reconstituted in 50 µL 30/9/1 acetonitrile/water/100 mM ammonium acetate pH 7.7. For the Hypercarb method, the samples were reconstituted in 50 µL 95/5 of 5-mM ammonium acetate (pH 9.5)/acetonitrile.

Method validation

We analyzed the developed method in terms of linearity, precision, LLOQ, relative recovery, and matrix effects. For calibration curves, peak area sums of ISTDs were plotted against their concentration. Concentrations were chosen in a range relevant in biological samples. Intra-day precision was calculated using the peak area sums of different concentrations of ISTDs in SPE-matrix, injecting the same sample three times a day. The inter-day precision was calculated using the peak area sums of different concentrations of ISTDs in SPE-matrix that have been injected on 3 days consecutively. Samples were stored at 4°C. The LLOQ was defined as the lowest concentrated standard with acceptable peak shape. The relative recovery was calculated as following:

$$\frac{\text{area of isotope standard added to extraction buffer}}{\text{area of isotope standard added after SPE}} \times 100 = \text{relative recovery } (\%).$$

The matrix effect was determined by comparing ISTDs with the same concentration separated either by the cHILIC method or the Hypercarb method in (i) matrix after extracting the TCA with the DCM/TOA, (ii) in matrix after the SPE procedure, and (iii) in pure buffer (for the cHILIC method 30/9/1 acetonitrile/water/100 mM ammonium acetate pH 7.7 and for the Hypercarb method 95/5 of 5-mM ammonium acetate [pH 9.5]/acetonitrile). The MEF was calculated according to Zhou et al. (2017):

$$\frac{\text{average area ISTD in buffer} - \text{average area of ISTD in matrix}}{\text{average area of ISTD in buffer}} \times 100 = \text{MEF}.$$

Quantification of metabolites

The amount of metabolites in plant samples was calculated either by the isotope dilution technique or with external calibration curves in SPE-matrix. ISTDs were added to the extraction buffer prior to extraction. Only calibration curves with a coefficient of determination (R^2) $>$ 0.99 were accepted.

Calculation of concentrations of metabolites in plant cell compartments

To determine the concentrations of rNTPs and dNTPs per unit NT-containing cell volume, we used the calculations of Koffler et al. (2013). They determined the total volume of the mesophyll cells in four sections of an Arabidopsis leaf and the volumes of the individual subcellular compartments in these sections. We grew plants until the leaves met the morphological criteria stated by Koffler and colleagues, i.e. to a size of approximately 1.5 × 3.0 cm, and then extracted them. We determined an average (i.e. not in sections but for the whole) leaf mesophyll volume per unit total fresh weight (AMV) of 600.0 µL g^{-1} fresh weight. We assumed that the nucleus, the cytoplasm, the mitochondria, and the plastids contain NTs (these are NT-containing compartments, NCC), whereas other cell compartments are likely devoid of relevant concentrations of NTs. An average of the percentile volumes of the compartments was calculated. Together, the NCCs accounted for 26.86% of the total mesophyll volume. We then calculated the concentrations of dNTPs and rNTPs in the NCC (Y in the formula), while X is the amount of metabolite in pmol g^{-1} fresh weight that was measured:

$$\frac{X\left[\frac{\text{pmol}}{\text{g}}\right]}{\text{AVM}\left[\frac{\mu\text{l}}{\text{g}}\right]} \times \frac{100\%}{26.86\%} = Y\ [\mu\text{M}].$$

Statistical analysis

Statistical analysis was performed using Prism 8 software. One-way analysis of variance (ANOVA) with Tukey's post test or two-way ANOVA with Sidak's post test were used. Different letters or a star indicate differences at significance level of $P < 0.5$. Statistical analysis results are shown in Supplemental File S1.

Accession numbers

Information regarding used mutants can be found in the GenBank/EMBL data libraries under the following accession numbers: *cda* (At2g19570), *gsda* (At5g28050), *nsh1* (At2g36310).

Supplemental data

Supplemental Figure S1. Chromatograms of all analyzed NTs by hypercarb chromatography.

Supplemental Figure S2. Chromatograms of all analyzed NTs by cHILIC chromatography.

Supplemental Figure S3. Chromatograms of all analyzed Ns by cHILIC chromatography.

Supplemental Figure S4. Analysis of NTs in Arabidopsis leaves by HPLC and UV detection.

Downloaded from https://academic.oup.com/plcell/article/33/2/270/6026971 by Institute of Horticultural Economics user on 11 December 2021

Supplemental Figure S5. SPE enables detection of dNTPs in several plant and algae species.

Supplemental Figure S6. SPE enables detection of rNs in Arabidopsis seeds and seedlings.

Supplemental Table S1. Literature survey on NT analysis in plants

Supplemental Table S2. Tested conditions for SPE optimization

Supplemental Table S3. Relative recovery of metabolites extracted by different methods.

Supplemental Table S4. Precursor, transitions (quantifier, qualifier), fragmentor, collision energy and retention times for NTP measurements

Supplemental Table S5. Precursor, transitions (quantifier, qualifier), fragmentor energy, collision energy and retention times for **NMP** measurements

Supplemental Table S6. Precursor, transitions (quantifier, qualifier), fragmentor energy, collision energy and retention times for nucleoside measurements

Supplemental Table S7. Intra-day variation and inter-day variation for different concentrations of NTs seperated by the Hypercarb or cHILIC method

Supplemental Table S8. Intra-day variation and inter-day variation for different concentrations of Ns seperated by the cHILIC method

Supplemental Table S9. Determination of MEF at 5- and 50-pmol dNTP and rNTP ISTDs, respectively, on column

Supplemental Table S10. Determination of MEF at 5-pmol nucleoside ISTD on column

Supplemental Table S11. NTPs analyzed with an Orbitrap mass spectrometer

Supplemental File S1. ANOVA tables.

Acknowledgments

The authors like to express their gratitude to Andreas Fricke, Jannis Rinne, Mareike Schallenberg-Rüdinger, Jennifer Senkler, and Jana Streubel for providing plant material and seeds and André Specht for technical assistance regarding LC and MS. They are very grateful to Henrik Buschmann, Armin Hallmann, and Benjamin Klein for growing and providing algae. They also like to thank Bernd Thierfelder and Chi Vinh Duong (Phenomenex) and Sascha Beutel for helpful discussion regarding sample preparation.

Funding

This work was supported by the Deutsche Forschungsgemeinschaft (grant no. HE 5949/3-1 to M.H.), (grant no. WI3411/4-1 to C-P.W.), and (grant no. INST 187/741-1 FUGG).

Conflict of interest statement. None declared.

References

Aoyagi S, Sugiyama M, Fukuda H (1998) BEN1 and ZEN1 cDNAs encoding S1-type DNases that are associated with programmed cell death in plants. FEBS Lett **429**: 134–138

Ashihara H, Crozier A, Ludwig IA (2020) Plant Nucleotide Metabolism: Biosynthesis, Degradation, and Alkaloid Formation. Wiley Blackwell, Chichester

Ashihara H, Mitsui K, Ukaji T (1987) A simple analysis of purine and pyrimidine nucleotides in plant cells by high-performance liquid chromatography. Z Naturforsch C **42**: 297–299

Assmann SM (2002) Heterotrimeric and unconventional GTP binding proteins in plant cell signaling. Plant Cell **14**: S355–S373

Baccolini C, Witte C-P (2019) AMP and GMP catabolism in arabidopsis converge on Xanthosine, which is degraded by a nucleoside hydrolase heterocomplex. Plant Cell **31**: 734–751

Berglund A-K, Navarrete C, Engqvist MKM, Hoberg E, Szilagyi Z, Taylor RW, Gustafsson CM, Falkenberg M, Clausen AR (2017) Nucleotide pools dictate the identity and frequency of ribonucleotide incorporation in mitochondrial DNA. PLoS Genet **13**: e1006628

Bieleski RL (1964) The problem of halting enzyme action when extracting plant tissues. Anal Biochem **9**: 431–442

Bieleski RL, Young RE (1963) Extraction and separation of phosphate esters from plant tissues. Anal Biochem **6**: 54–68

Buckland RJ, Watt DL, Chittoor B, Nilsson AK, Kunkel TA, Chabes A (2014) Increased and imbalanced dNTP pools symmetrically promote both leading and lagging strand replication infidelity. PLoS Genet **10**: e1004846

Burdett H, Bentham AR, Williams SJ, Dodds PN, Anderson PA, Banfield MJ, Kobe B (2019) The plant "resistosome": structural insights into immune signaling. Cell Host Microbe **26**: 193–201

Carrari F, Coll-Garcia D, Schauer N, Lytovchenko A, Palacios-Rojas N, Balbo I, Rosso M, Fernie AR (2005) Deficiency of a plastidial adenylate kinase in Arabidopsis results in elevated photosynthetic amino acid biosynthesis and enhanced growth. Plant Physiol **137**: 70–82

Castroviejo M, Tharaud D, Mocquot B, Litvak S (1979) Factors affecting the onset of deoxyribonucleic acid synthesis during wheat embryo germination: study of the changes in DNA polymerases A, B and C and the pool of DNA precursors. Biochem J **181**: 193–199

Chabosseau P, Buhagiar-Labarchède G, Onclercq-Delic R, Lambert S, Debatisse M, Brison O, Amor-Guéret M (2011) Pyrimidine pool imbalance induced by BLM helicase deficiency contributes to genetic instability in Bloom syndrome. Nat Commun **2**: 368

Chen M, Herde M, Witte C-P (2016) Of the nine cytidine deaminase-like genes in arabidopsis, eight are pseudogenes and only one is required to maintain pyrimidine homeostasis in vivo. Plant Physiol **171**: 799–809

Chen M, Urs MJ, Sánchez-González I, Olayioye MA, Herde M, Witte C-P (2018) m6A RNA degradation products are catabolized by an evolutionarily conserved N6-methyl-AMP deaminase in plant and mammalian cells. Plant Cell **30**: 1511–1522

Chen M, Witte C-P (2020) A kinase and a glycosylase catabolize pseudouridine in the peroxisome to prevent toxic pseudouridine monophosphate accumulation. Plant Cell **32**: 722–739

Clausen AR, Girandon L, Ali A, Knecht W, Rozpedowska E, Sandrini MPB, Andreasson E, Munch-Petersen B, Piškur J (2012) Two thymidine kinases and one multisubstrate deoxyribonucleoside kinase salvage DNA precursors in *Arabidopsis thaliana*. FEBS J **279**: 3889–3897

Cohen S, Megherbi M, Jordheim LP, Lefebvre I, Perigaud C, Dumontet C, Guitton J (2009) Simultaneous analysis of eight nucleoside triphosphates in cell lines by liquid chromatography coupled with tandem mass spectrometry. J Chromatogr B **877**: 3831–3840

Dahncke K, Witte C-P (2013) Plant purine nucleoside catabolism employs a guanosine deaminase required for the generation of xanthosine in Arabidopsis. Plant Cell **25**: 4101–4109

Dietmair S, Timmins NE, Gray PP, Nielsen LK, Krömer JO (2010) Towards quantitative metabolomics of mammalian cells:

Downloaded from https://academic.oup.com/plcell/article/33/2/270/6026971 by Institute of Horticultural Economics user on 11 December 2021

development of a metabolite extraction protocol. Anal Biochem **404**: 155–164

Dubois E, Córdoba-Cañero D, Massot S, Siaud N, Gakière B, Domenichini S, Guérard F, Roldan-Arjona T, Doutriaux M-P (2011) Homologous recombination is stimulated by a decrease in dUTPase in Arabidopsis. PLoS ONE **6**: e18658

Dutta I, Dutta PK, Smith DW, O'Donovan GA (1991) High-performance liquid chromatography of deoxyribonucleoside di- and triphosphates in tomato roots. J Chromatogr A **536**: 237–243

Faivre-Nitschke SE, Grienenberger JM, Gualberto JM (1999) A prokaryotic-type cytidine deaminase from *Arabidopsis thaliana* gene expression and functional characterization. Eur J Biochem **263**: 896–903

Farrow SC, Emery RN (2012) Concurrent profiling of indole-3-acetic acid, abscisic acid, and cytokinins and structurally related purines by high-performance-liquid-chromatography tandem electrospray mass spectrometry. Plant Methods **8**: 42

Feller W, Schimpf-Weiland G, Follmann H (1980) Deoxyribonucleotide biosynthesis in synchronous algae cells. Eur J Biochem **110**: 85–92

Frydman RB, Neufeld EF, Hassid WZ (1963) Thymidine diphosphate d-galactose pyrophosphorylase of *Phaseolus aureus*. Biochim Biophys Acta **77**: 332–334

Galmarini CM, Jordheim L, Dumontet C (2003) Pyrimidine nucleoside analogs in cancer treatment. Exp Rev Anticancer Ther **3**: 717–728

Garton S, Knight H, Warren GJ, Knight MR, Thorlby GJ (2007) Crinkled leaves 8—a mutation in the large subunit of ribonucleotide reductase—leads to defects in leaf development and chloroplast division in *Arabidopsis thaliana*. Plant J Cell Mol Biol **50**: 118–127

Gon S, Napolitano R, Rocha W, Coulon S, Fuchs RP (2011) Increase in dNTP pool size during the DNA damage response plays a key role in spontaneous and induced-mutagenesis in *Escherichia coli*. Proc Natl Acad Sci U S A **108**: 19311–19316

Greilhuber J, Dolezel J, Leitch IJ (2012) Plant Genomes, Their Residents, and Their Evolutionary Dynamics, Springer, Wien

Guérard F, Pétriacq P, Gakière B, Tcherkez G (2011) Liquid chromatography/time-of-flight mass spectrometry for the analysis of plant samples: a method for simultaneous screening of common cofactors or nucleotides and application to an engineered plant line. Plant Physiol Biochem **49**: 1117–1125

Guo S, Duan J-A, Qian D, Wang H, Tang Y, Qian Y, Wu D, Su S, Shang E (2013) Hydrophilic interaction ultra-high performance liquid chromatography coupled with triple quadrupole mass spectrometry for determination of nucleotides, nucleosides and nucleobases in *Ziziphus* plants. J Chromatogr A, **1301**: 147–155

Harmenberg J, Karlsson AHJ, Gilljam G (1987) Comparison of sample preparation methods for the high-performance liquid chromatographic analysis of cell culture extracts for triphosphate ribonucleosides and deoxyribonucleosides. Anal Biochem **161**: 26–31

Henneré G, Becher F, Pruvost A, Goujard C, Grassi J, Benech H (2003) Liquid chromatography–tandem mass spectrometry assays for intracellular deoxyribonucleotide triphosphate competitors of nucleoside antiretrovirals. J Chromatogr B **789**: 273–281

Ikuma H, Tetley RM (1976) Possible interference by an acid-stable enzyme during the extraction of nucleoside di- and triphosphates from higher plant tissues. Plant Physiol **58**: 320–323

Johnston CA, Taylor JP, Gao Y, Kimple AJ, Grigston JC, Chen J-G, Siderovski DP, Jones AM, Willard FS (2007) GTPase acceleration as the rate-limiting step in Arabidopsis G protein-coupled sugar signaling. Proc Natl Acad Sci U S A **104**: 17317–17322

Jung B, Flörchinger M, Kunz H-H, Traub M, Wartenberg R, Jeblick W, Neuhaus HE, Möhlmann T (2009) Uridine-ribohydrolase is a key regulator in the uridine degradation pathway of Arabidopsis. Plant Cell **21**: 876–891

Jung B, Hoffmann C, Möhlmann T (2011) Arabidopsis nucleoside hydrolases involved in intracellular and extracellular degradation of purines. Plant J Cell Mol Biol **65**: 703–711

Kafer C, Thornburg RW (2000) *Arabidopsis thaliana* cytidine deaminase 1 shows more similarity to prokaryotic enzymes than to eukaryotic enzymes. J Plant Biol **43**: 162–170

Kamisugi Y, von Stackelberg M, Lang D, Care M, Reski R, Rensing SA, Cuming AC (2008) A sequence-anchored genetic linkage map for the moss, *Physcomitrella patens*. Plant J Cell Mol Biol **56**: 855–866

Katahira R, Ashihara H (2006) Role of adenosine salvage in wound-induced adenylate biosynthesis in potato tuber slices. Plant Physiol Biochem **44**: 551–555

Katan R, Avigad G (1966) NADP dependent oxidation of TDP-glucose by an enzyme system from sugar beets. Biochem Biophys Res Commun **24**: 18–24

Kazibwe Z, Soto-Burgos J, MacIntosh GC, Bassham DC (2020) TOR mediates the autophagy response to altered nucleotide homeostasis in a ribonuclease mutant. J Exp Bot eraa410

Khym JX (1975) An analytical system for rapid separation of tissue nucleotides at low pressures. Clin Chem **21**: 1245–1252

Kirchner TW, Niehaus M, Rössig KL, Lauterbach T, Herde M, Küster H, Schenk MK (2018) Molecular background of pi deficiency-induced root hair growth in *Brassica carinata*—a fasciclin-like arabinogalactan protein is involved. Front Plant Sci **9**: 1372

Klein B, Wibberg D, Hallmann A (2017) Whole transcriptome RNA-Seq analysis reveals extensive cell type-specific compartmentalization in *Volvox carteri*. BMC Biol **15**: 1–22

Koffler BE, Bloem E, Zellnig G, Zechmann B (2013) High resolution imaging of subcellular glutathione concentrations by quantitative immunoelectron microscopy in different leaf areas of Arabidopsis. Micron **45**: 119–128

Kong Z, Jia S, Chabes AL, Appelblad P, Lundmark R, Moritz T, Chabes A (2018) Simultaneous determination of ribonucleoside and deoxyribonucleoside triphosphates in biological samples by hydrophilic interaction liquid chromatography coupled with tandem mass spectrometry. Nucl Acids Res **46**: e66

Kopecná M, Blaschke H, Kopecny D, Vigouroux A, Koncitíková R, Novák O, Kotland O, Strnad M, Moréra S, von Schwartzenberg K (2013) Structure and function of nucleoside hydrolases from *Physcomitrella patens* and maize catalyzing the hydrolysis of purine, pyrimidine, and cytokinin ribosides. Plant Physiol **163**: 1568–1583

Kumar D, Abdulovic AL, Viberg J, Nilsson AK, Kunkel TA, Chabes A (2011) Mechanisms of mutagenesis in vivo due to imbalanced dNTP pools. Nucl Acids Res **39**: 1360–1371

Kuskovsky R, Buj R, Xu P, Hofbauer S, Doan MT, Jiang H, Bostwick A, Mesaros C, Aird KM, Snyder NW (2019) Simultaneous isotope dilution quantification and metabolic tracing of deoxyribonucleotides by liquid chromatography high resolution mass spectrometry. Anal Biochem **568**: 65–72

Le Ret M, Belcher S, Graindorge S, Wallet C, Koechler S, Erhardt M, Williams-Carrier R, Barkan A, Gualberto JM (2018) Efficient replication of the plastid genome requires an organellar thymidine kinase. Plant Physiol **178**: 1643–1656

Lee HO, Davidson JM, Duronio RJ (2009) Endoreplication: polyploidy with purpose. Genes Dev **23**: 2461–2477

Leija C, Rijo-Ferreira F, Kinch LN, Grishin NV, Nischan N, Kohler JJ, Hu Z, Phillips MA (2016) Pyrimidine salvage enzymes are essential for de novo biosynthesis of deoxypyrimidine nucleotides in *Trypanosoma brucei*. PLoS Pathogens **12**: e1006010

Leiva-Neto JT, Grafi G, Sabelli PA, Dante RA, Woo Y-M, Maddock S, Gordon-Kamm WJ, Larkins BA (2004) A dominant negative mutant of cyclin-dependent kinase A reduces endoreduplication but not cell size or gene expression in maize endosperm. Plant Cell **16**: 1854–1869

Downloaded from https://academic.oup.com/plcell/article/33/2/270/6026971 by Institute of Horticultural Economics user on 11 December 2021

Liu B, Winkler F, Herde M, Witte C-P, Großhans J (2019) A Link between deoxyribonucleotide metabolites and embryonic cell-cycle control. Curr Biol **29**: 1187–1192.e3

de Lorenzo V (2014) From the selfish gene to selfish metabolism: revisiting the central dogma. BioEssays **36**: 226–235

Meyer R, Wagner KG (1985) Determination of nucleotide pools in plant tissue by high-performance liquid chromatography. Anal Biochem **148**: 269–276

Neufeld EF (1962) Formation and epimerization of dTDP-D-galactose catalyzed by plant enzymes. Biochem Biophys Res Commun **7**: 461–466

Nick McElhinny SA, Kumar D, Clark AB, Watt DL, Watts BE, Lundström E-B, Johansson E, Chabes A, Kunkel TA (2010a) Genome instability due to ribonucleotide incorporation into DNA. Nat Chem Biol **6**: 774–781

Nick McElhinny SA, Watts BE, Kumar D, Watt DL, Lundström E-B, Burgers PMJ, Johansson E, Chabes A, Kunkel TA (2010b) Abundant ribonucleotide incorporation into DNA by yeast replicative polymerases. Proc Natl Acad Sci U S A **107**: 4949–4954

Niehaus M, Straube H, Künzler P, Rugen N, Hegermann J, Giavalisco P, Eubel H, Witte C-P, Herde M (2020) Rapid affinity purification of tagged plant mitochondria (Mito-AP) for metabolome and proteome analyses. Plant Physiol **182**: 1194–1210

Nieman RH, Pap DL, Clark RA (1978) Rapid purification of plant nucleotide extracts with xad-2, polyvinylpolypyrrolidone and charcoal. J Chromatogr A **161**: 137–146

Nizam S, Qiang X, Wawra S, Nostadt R, Getzke F, Schwanke F, Dreyer I, Langen G, Zuccaro A (2019) *Serendipita indica* E5′NT modulates extracellular nucleotide levels in the plant apoplast and affects fungal colonization. EMBO Rep **20**

Nordlund P, Reichard P (2006) Ribonucleotide reductases. Annu Rev Biochem **75**: 681–706

Nygaard P (1972) Deoxyribonucleotide pools in plant tissue cultures. Physiol Plant **26**: 29–33

Odmark G, Kihlman BA (1965) Effects of chromosome-breaking purine derivatives on nucleic acid synthesis and on the levels of adenosine 5′-triphosphate and deoxyadenosine 5′-triphosphate in bean root tips. Mutat Res **2**: 274–286

Pabst M, Grass J, Fischl R, Léonard R, Jin C, Hinterkörner G, Borth N, Altmann F (2010) Nucleotide and nucleotide sugar analysis by liquid chromatography–electrospray ionization–mass spectrometry on surface-conditioned porous graphitic carbon. Anal Chem **82**: 9782–9788

Pedroza-García JA, Nájera-Martínez M, de La Paz Sanchez M, Plasencia J (2015) *Arabidopsis thaliana* thymidine kinase 1a is ubiquitously expressed during development and contributes to confer tolerance to genotoxic stress. Plant Mol Biol **87**: 303–315

Pedroza-García J-A, Nájera-Martínez M, Mazubert C, Aguilera-Alvarado P, Drouin-Wahbi J, Sánchez-Nieto S, Gualberto JM, Raynaud C, Plasencia J (2019) Role of pyrimidine salvage pathway in the maintenance of organellar and nuclear genome integrity. Plant J Cell Mol Biol **97**: 430–446

Rampazzo C, Miazzi C, Franzolin E, Pontarin G, Ferraro P, Frangini M, Reichard P, Bianchi V (2010) Regulation by degradation, a cellular defense against deoxyribonucleotide pool imbalances. Mutat Res **703**: 2–10

Raveneau M-P, Benamar A, Macherel D (2017) Water content, adenylate kinase, and mitochondria drive adenylate balance in dehydrating and imbibing seeds. J Exp Bot **68**: 3501–3512

Regensdorff M, Deckena M, Stein M, Borchers A, Scherer G, Lammers M, Hänsch R, Zachgo S, Buschmann H (2018) Transient genetic transformation of *Mougeotia scalaris* (Zygnematophyceae) mediated by the endogenous α-tubulin1 promoter. J Phycol **54**: 840–849

Riegler H, Geserick C, Zrenner R (2011) *Arabidopsis thaliana* nucleosidase mutants provide new insights into nucleoside degradation. New Phytol **191**: 349–359

Riondet C, Morel S, Alcaraz G (2005) Determination of total ribonucleotide pool in plant materials by high-pH anion-exchange high-performance liquid chromatography following extraction with potassium hydroxide. J Chromatogr A **1077**: 120–127

Robak P, Robak T (2013) Older and new purine nucleoside analogs for patients with acute leukemias. Cancer Treat Rev **39**: 851–861

Rolletschek H, Melkus G, Grafahrend-Belau E, Fuchs J, Heinzel N, Schreiber F, Jakob PM, Borisjuk L (2011) Combined noninvasive imaging and modeling approaches reveal metabolic compartmentation in the barley endosperm. Plant Cell **23**: 3041–3054

Sabina RL, Paul A-L, Ferl RJ, Laber B, Lindell SD (2007) Adenine nucleotide pool perturbation is a metabolic trigger for AMP deaminase inhibitor-based herbicide toxicity. Plant Physiol **143**: 1752–1760

Sakamoto W, Takami T (2014) Nucleases in higher plants and their possible involvement in DNA degradation during leaf senescence. J Exp Bot **65**: 3835–3843

Salem SA, Yoshida T, Perez de Souza L, Alseekh S, Bajdzienko K, Fernie AR, Giavalisco P (2020) An improved extraction method enables the comprehensive analysis of lipids, proteins, metabolites and phytohormones from a single sample of leaf tissue under water-deficit stress. Plant J **103**: 1614–1632

Savitch LV, Barker-Åstrom J, Ivanov AG, Hurry V, Öquist G, Huner NP, Gardeström P (2001) Cold acclimation of *Arabidopsis thaliana* results in incomplete recovery of photosynthetic capacity, associated with an increased reduction of the chloroplast stroma. Planta **214**: 295–303

Sawert A, Backer A, Plank-Schumacher K-H, Wagner KG (1987) Determination of nucleotides and nucleosides in cereal leaves by high performance liquid chromatography. J Plant Physiol **127**: 183–186

Schroeder RY, Zhu A, Eubel H, Dahncke K, Witte C-P (2018) The ribokinases of *Arabidopsis thaliana* and *Saccharomyces cerevisiae* are required for ribose recycling from nucleotide catabolism, which in plants is not essential to survive prolonged dark stress. New Phytol **217**: 233–244

Šmarda P, Bureš P, Horová L, Leitch IJ, Mucina L, Pacini E, Tichý L, Grulich V, Rotreklová O (2014) Ecological and evolutionary significance of genomic GC content diversity in monocots. Proc Natl Acad Sci U S A **111**: E4096–E4102

de Souza AP, Cocuron J-C, Garcia AC, Alonso AP, Buckeridge MS (2015) Changes in whole-plant metabolism during the grain-filling stage in sorghum grown under elevated CO_2 and drought. Plant Physiol **169**: 1755–1765

Stasolla C, Katahira R, Thorpe TA, Ashihara H (2003) Purine and pyrimidine nucleotide metabolism in higher plants. J Plant Physiol **160**: 1271–1295

Stitt M, Lilley RM, Heldt HW (1982) Adenine nucleotide levels in the cytosol, chloroplasts, and mitochondria of wheat leaf protoplasts. Plant Physiol **70**: 971–977

Tanaka K, Yoshioka A, Tanaka S, Wataya Y (1984) An improved method for the quantitative determination of deoxyribonucleoside triphosphates in cell extracts. Anal Biochem **139**: 35–41

Traub M, Flörchinger M, Piecuch J, Kunz H-H, Weise-Steinmetz A, Deitmer JW, Ekkehard Neuhaus H, Möhlmann T (2007). The fluorouridine insensitive 1 (fur1) mutant is defective in equilibrative nucleoside transporter 3 (ENT3), and thus represents an important pyrimidine nucleoside uptake system in *Arabidopsis thaliana*. Plant J Cell Mol Biol **49**: 855–864

Ullrich J, Calvin M (1962) Alcohol-resistant phosphatase activity in chloroplasts. Biochim Biophys Acta **63**: 1–10

Vetsigian K, Goldenfeld N (2008) Genome rhetoric and the emergence of compositional bias. Proc Natl Acad Sci U S A **106**: 215–220

Vincenzetti S, Cambi A, Neuhard J, Schnorr K, Grelloni M, Vita A (1999) Cloning, expression, and purification of cytidine deaminase from *Arabidopsis thaliana*. Protein Expr Purif **15**: 8–15

Downloaded from https://academic.oup.com/plcell/article/33/2/270/6026971 by Institute of Horticultural Economics user on 11 December 2021

Wang C, Liu Z (2006) Arabidopsis ribonucleotide reductases are critical for cell cycle progression, DNA damage repair, and plant development. Plant Cell **18**: 350–365

Wang M, Oppedijk BJ, Caspers MPM, Lamers GEM, Boot MJ, Geerlings DNG, Bakhuizen B, Meijer AH, Duijn BV (1998) Spatial and temporal regulation of DNA fragmentation in the aleurone of germinating barley. J Exp Bot **49**: 1293–1301

Werner AK, Romeis T, Witte C-P (2010) Ureide catabolism in *Arabidopsis thaliana* and Escherichia coli. Nat Chem Biol **6**: 19–21

Werner AK, Witte C-P (2011) The biochemistry of nitrogen mobilization: purine ring catabolism. Trends Plant Sci **16**: 381–387

Witte C-P, Herde M (2020) Nucleotide metabolism in plants. Plant Physiol **182**: 63–78

Xu D, Leister D, Kleine T (2020) VENOSA4, a human dNTPase SAMHD1 homolog, contributes to chloroplast development and abiotic stress tolerance. Plant Physiol **182**: 721–729

Xu J, Zhang L, Yang D-L, Li Q, He Z (2015) Thymidine kinases share a conserved function for nucleotide salvage and play an essential role in *Arabidopsis thaliana* growth and development. New Phytol **208**: 1089–1103

Yabuki N, Ashihara H (1991) Catabolism of adenine nucleotides in suspension-cultured plant cells. Biochim Biophys Acta **1073**: 474–480

Yoo S-C, Cho S-H, Sugimoto H, Li J, Kusumi K, Koh H-J, Iba K, Paek N-C (2009) Rice virescent3 and stripe1 encoding the large and small subunits of ribonucleotide reductase are required for chloroplast biogenesis during early leaf development. Plant Physiol **150**: 388–401

Zhou W, Yang S, Wang PG (2017) Matrix effects and application of matrix effect factor. Bioanalysis **9**: 1839–1844

Zrenner R, Stitt M, Sonnewald U, Boldt R (2006) Pyrimidine and purine biosynthesis and degradation in plants. Annu Rev Plant Biol **57**: 805–836

Downloaded from https://academic.oup.com/plcell/article/33/2/270/6026971 by Institute of Horticultural Economics user on 11 December 2021

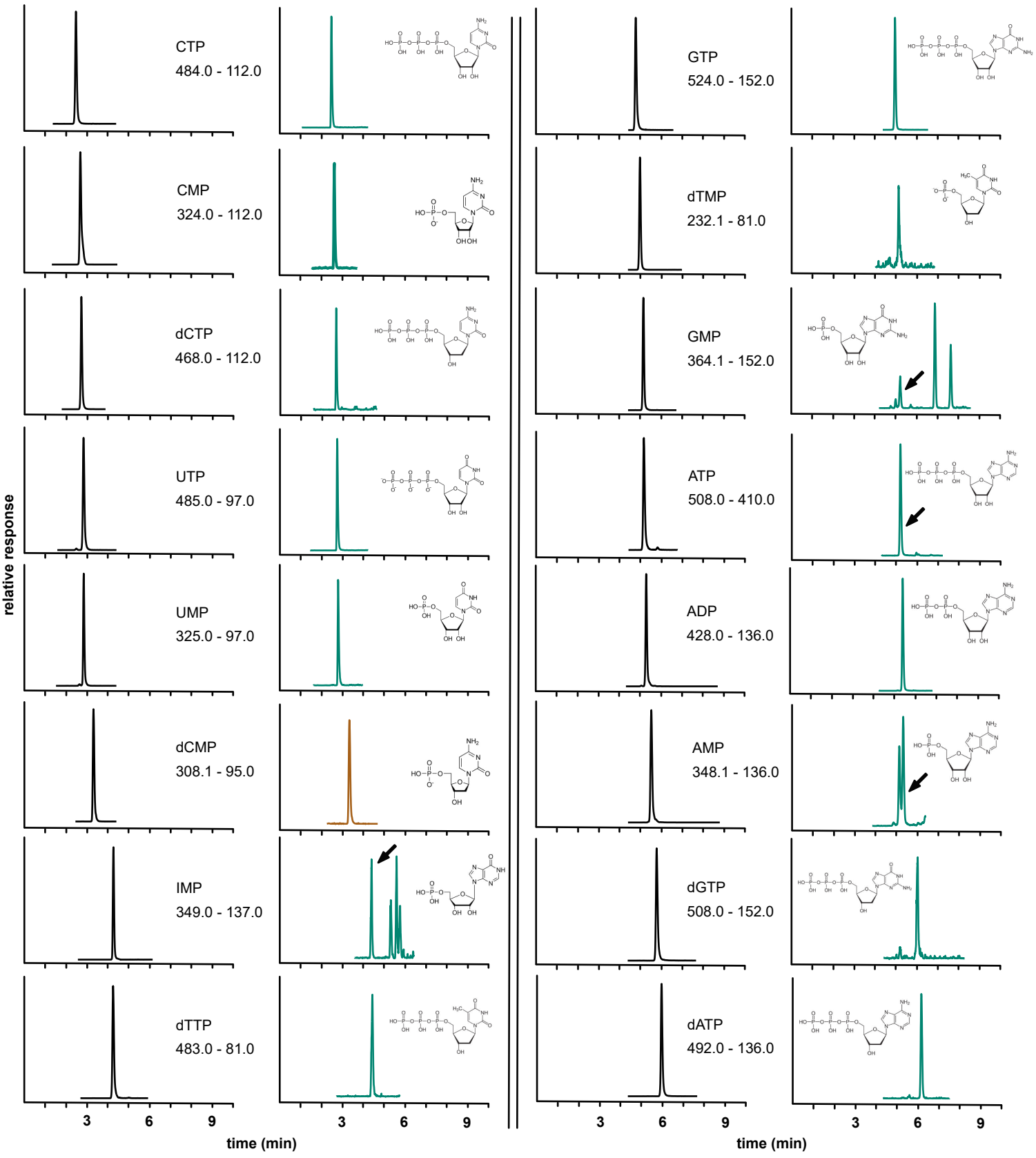

Supplemental Figure 1. Chromatograms of all analyzed nucleotides by hypercarb chromatography.

Representative depiction of Hypercarb multiple reaction monitoring (MRM) chromatograms of all analyzed (deoxy)nucleotides in buffer (left column) or in plant matrix (right column). Chromatograms shown in turquoise represent naturally occuring compounds, while chromatograms shown in brown indicates spiking of the respective analyte in plant matrix. MRM transitions used for quantification are given for the shown analytes. (Supports Figure 2,3,4,7,8 and 9)

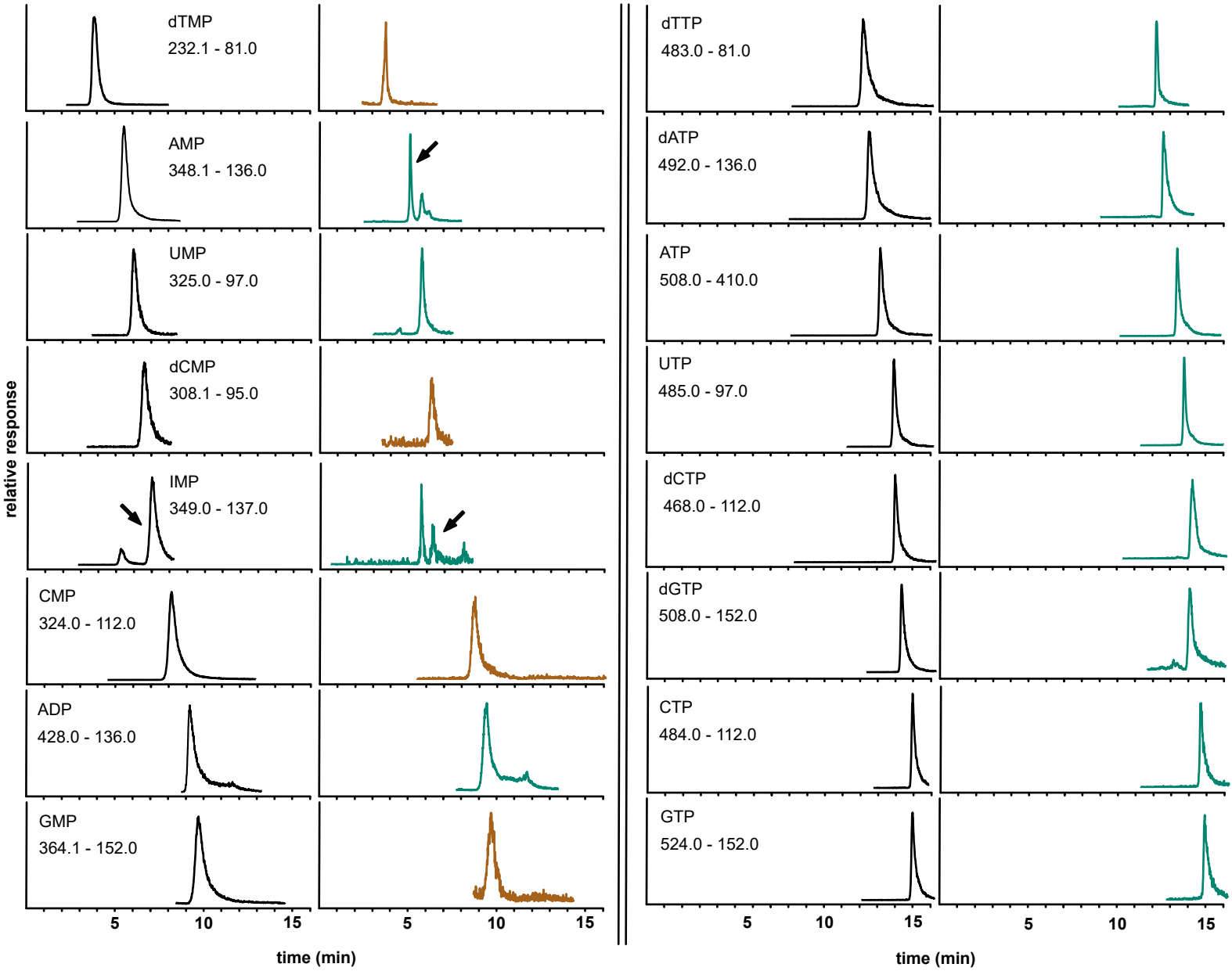

Supplemental Figure 2. Chromatograms of all analyzed nucleotides by cHILIC chromatography.

Representative depiction of cHILIC multiple reaction monitoring (MRM) chromatograms of all analyzed (deoxy)nucleotides in buffer (left column) or in plant matrix (right column). Chromatograms shown in turquoise represent naturally occuring compounds, while chromatograms shown in brown indicates spiking of the respective analyte in plant matrix. MRM transitions used for quantification are given for the shown analytes. (Supports Figure 2,3,4,7,8 and 9)

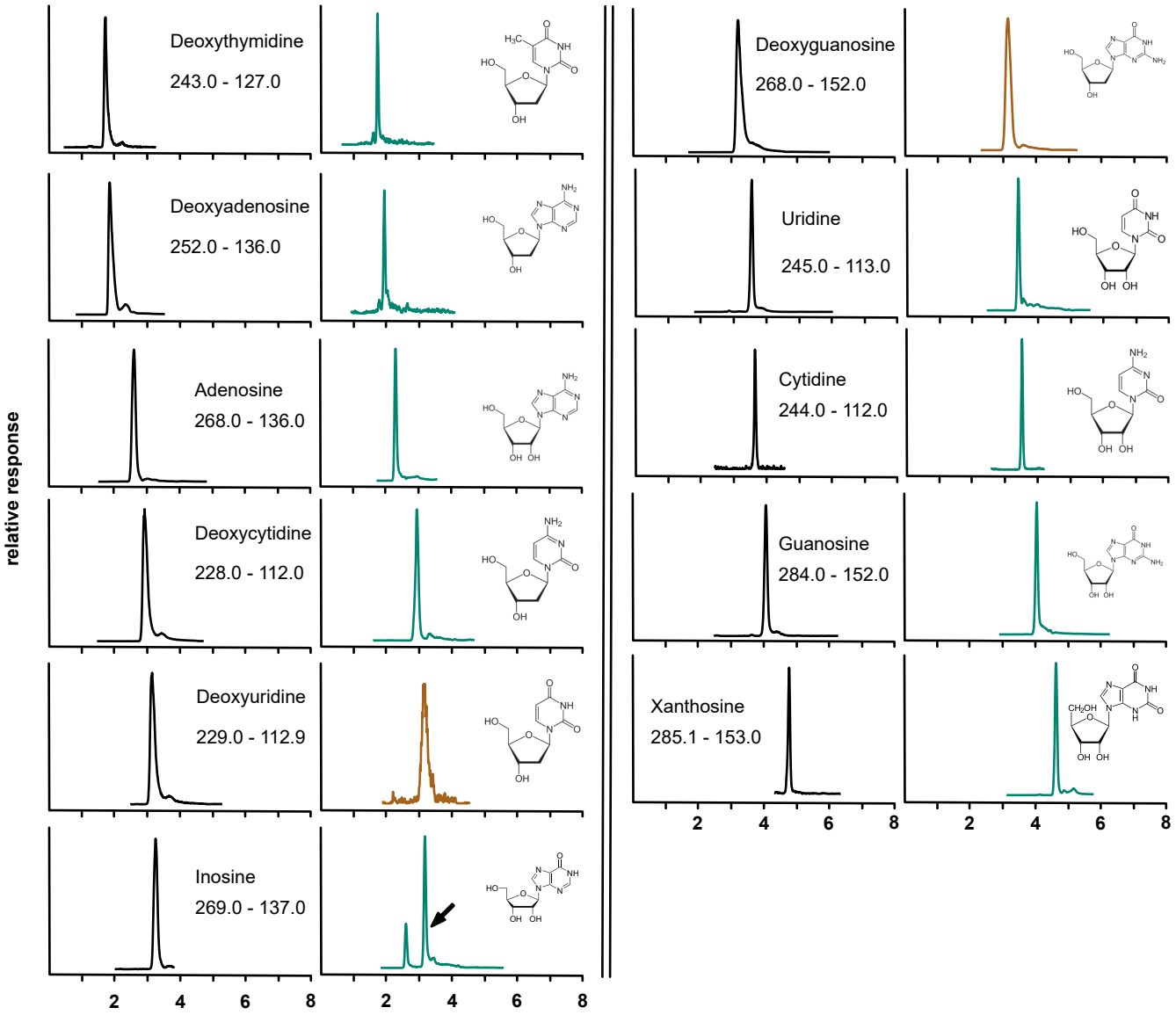

Supplemental Figure 3. Chromatograms of all analyzed nucleosides by cHILIC chromatography.

Representative depiction of cHILIC multiple reaction monitoring (MRM) chromatograms of all analyzed (deoxy)nucleosides in buffer (left column) or in plant matrix (right column). Chromatograms shown in turquoise represent naturally occuring compounds, while chromatograms shown in brown indicates spiking of the respective analyte in plant matrix. MRM transitions used for quantification are given for the shown analytes. (Supports Figure 6)

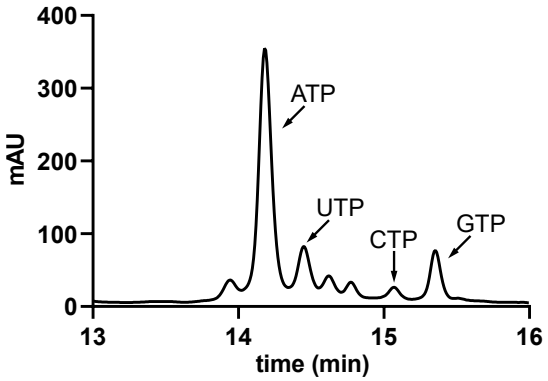

Supplemental Figure 4. Analysis of nucleotides in Arabidopsis leaves by HPLC and UV detection.

Analysis of extracts treated with LLE and SPE from 6-week-old Arabidopsis leaves by cHILIC LC using photometric detection at 254 nm. Major photometric peaks were associated with MS signals of NTs using an Orbitrap MS analyzer considering the delay volume between the photometric detector and the MS. mAU, milliabsorption

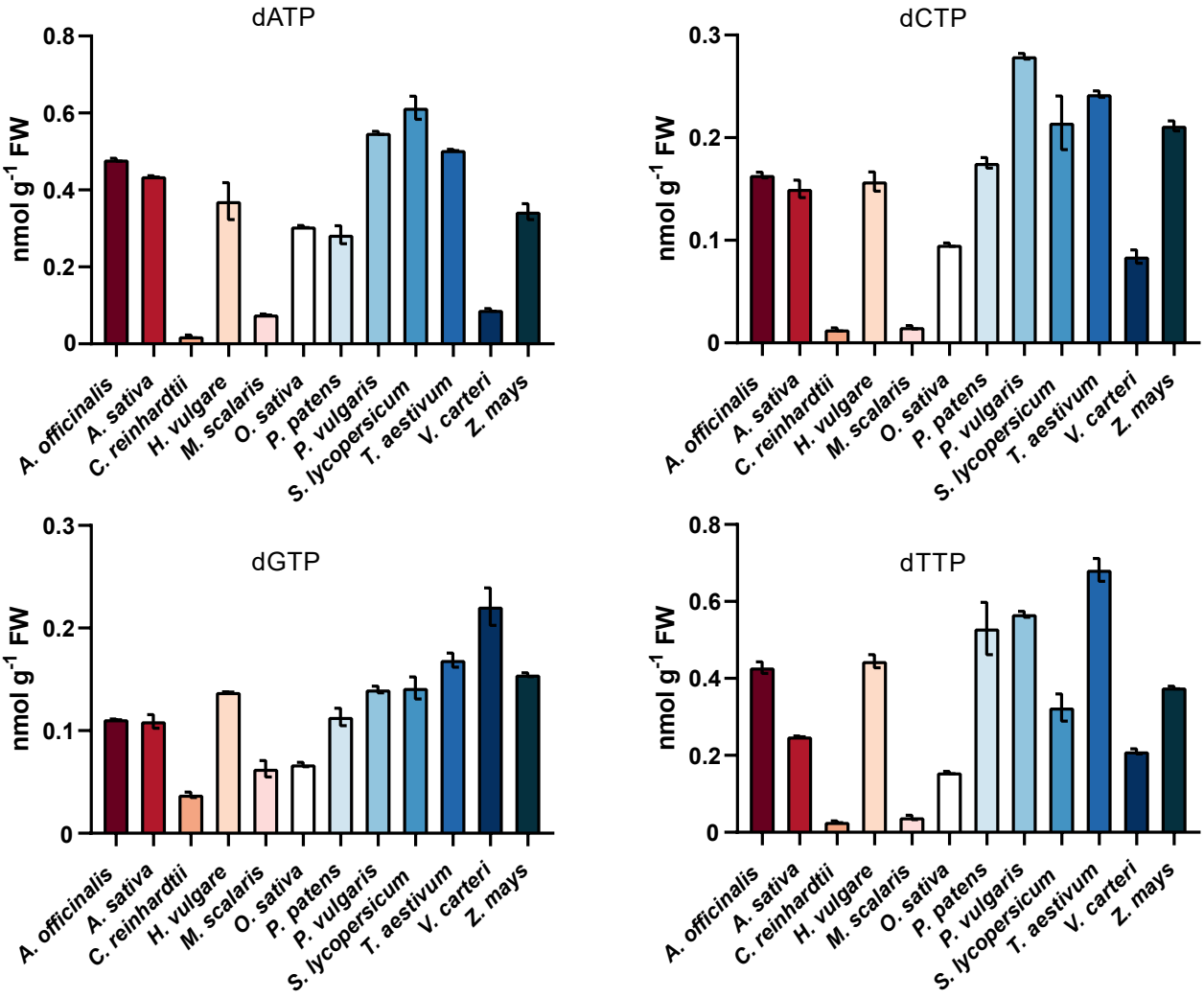

Supplemental Figure 5. SPE enables detection of deoxyribonucleotide triphosphates in several plant and algae species.

Determination of dNTP concentrations in *Asparagus officinalis, Avena sativa, Arabidopsis thaliana, Chlamydomonas reinhardtii, Hordeum vulgare, Mougeotia scalaris, Oryza sativa, Physcomitrella patens, Phaseolus vulgaris, Solanum lycopersicum, Triticum aestivum, Volvox carteri and Zea mays*. Error bars are SD. n = 3 biological replicates, consisting of several plants each. (Supports Figure 3)

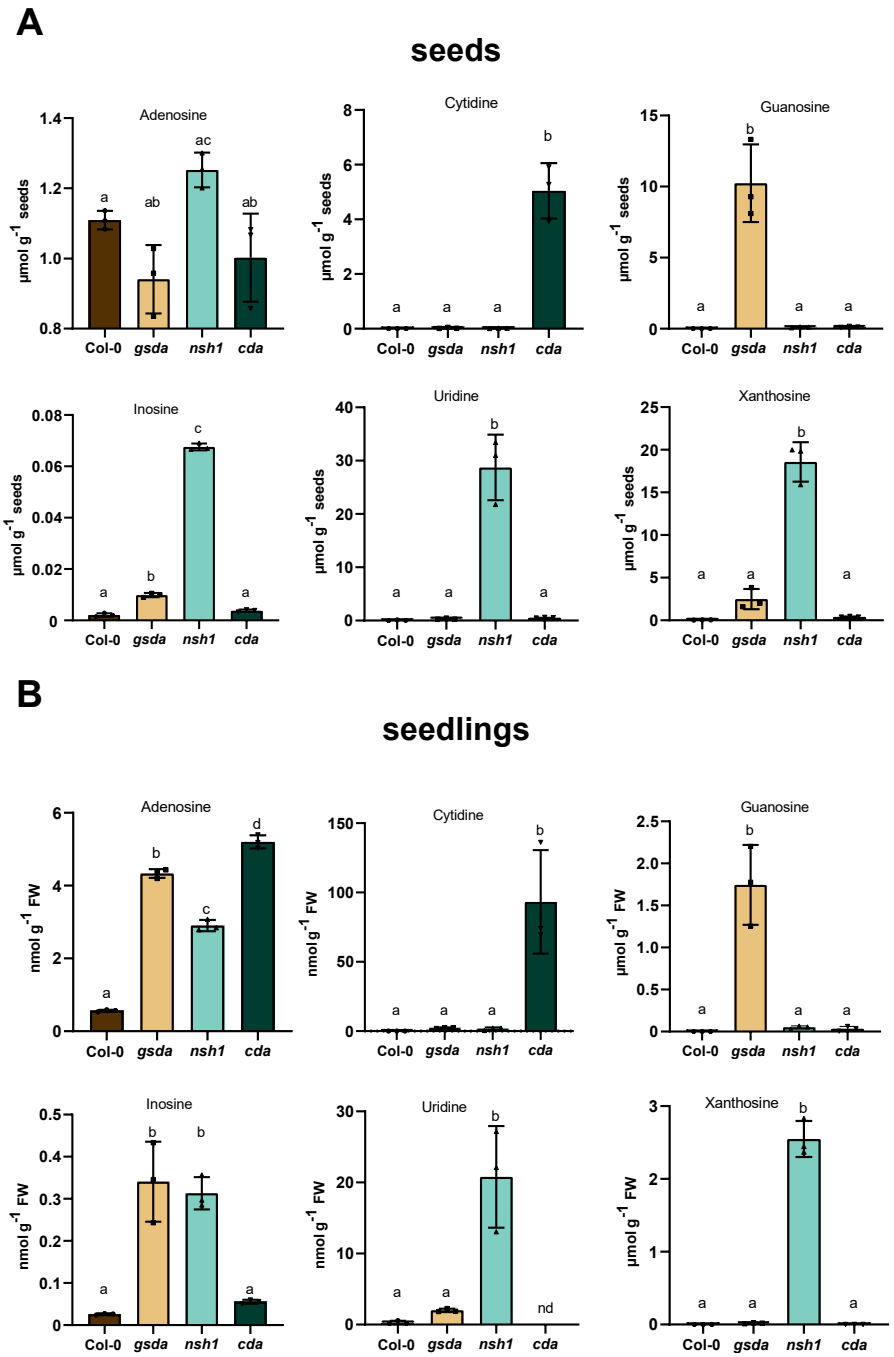

Supplemental Figure 6. SPE enables detection of ribonucleosides in Arabidopsis seeds and seedlings.

Concentrations of ribonucleosides in seeds (A) and seedlings (B) of *A. thaliana* wild type, as well as mutants in the salvage and degradation of purine and pyrimidine nucleosides (*gsda*, guanosin deaminase; *cda*, cytidine deaminase; *nsh1* nucleoside hydrolase 1). Error bars are SD, n = 3 biological replicates, for seeds, three independent seed pools derived from different mother plants were used; for seedlings, pools of seedlings from three independent liquid cultures were used. Statistical analysis was performed using one-way ANOVA with Tukey´s post test. Different letters indicate $P < 0.05$. nd, not detected. FW, fresh weight. (Supports Figure 6)

***Supplemental Table 1**: Literature survey on nucleotide analysis in plants*

sample material	measured metabolites	absolute/ relative	method	reference
Vicia faba root tips	dATP ATP	relative (ATP) and absolute (dATP)	acidic extraction/periodate treatment, spectroscopy	Odmark and Kihlman, 1965
Acer pseudoplatanus callus culture, *Pinus mugo* pollen	dNTPs rNTPs	absolute	PCA extraction, TLC	Nygaard, 1972
Gossypium barbadense radicle tips	dTTP	relative	polymerase based assay	Katterman *et al.*, 1975
Triticum aestivum embryos	dNTPs	absolute	TCA extraction, Polymerase based assay	Castroviejo *et al.*, 1978
Scenedesmus ohliquus	dNTPs	absolute	60% MeOH extraction, polymerase based assay	Feller *et al.*, 1980
Datura innoxia and Nicotiana tabacum cell culture, leaves and roots of *Nicotiana tabacum*	ribonucleosides ribonucleotides nucleotide-sugars NAD/NADP	absolute	PCA extraction, Phenylsilane-silica gel, LC-UV	Meyer and Wagner, 1985
Solanum lycopersicum root tips	dNTPs dNDPs	absolute	TCA extraction with PVP[a]/freon-amin/periodate treatment, LC-UV	Dutta *et al.*, 1991
plants and cell cultures of *Nicotiana tabacum*, *Arabidopsis thaliana*, *Solanum lycopersicum*	ribonucleotides cNMPs[c]	absolute	KOH[b] extraction, LC-UV	Riondet *et al.*, 2005
Arabidopsis thaliana	dNTPs	relative	polymerase based assay	Wang and Liu, 2006
Solanum tuberosum tubers	ribonucleotides	absolute	TCA extraction with EGTA[d]/diethylether-amin, LC-UV	Katahira and Ashihara, 2006
leaves of *Nicotiana benthamiana* and *Arabidopsis*	ribonucleotides nucleotide- sugars		sodium fluoride extraction, SPE, LC-MS	Pabst *et al.*, 2010

[a] polyvinylpyrrolidone; [b] potassium hydroxide; [c] cyclic nucleotide monophosphates, [d] ethylenglycol-bis(aminoethylether)-N,N,N,N-tetraaceticacid, [e]ion-exchange chromatography

Supplemental Table 2: *Tested conditions for SPE optimization*

	method 1	method 2	method 3	method 4	method 5	method 6	method 7	method 8	method 9
quenching	5% TCA, 5 mM EDTA	5% TCA, 5 mM EDTA	80/20 MeOH/ 10 mM NH_4AC pH 4.5 (v/v)	15% TCA, 30 mM $MgCl_2$	15% TCA, 30 mM $MgCl_2$	15% TCA, 30 mM $MgCl_2$	6 % PCA	15 % TCA	15 % TCA
LLE/ acid quenching	-	-	-	DCM/TOA (78/22 v/v)	DCM/TOA (78/22 v/v)	DCM/TOA (78/22 v/v)	20% KOH	DCM/TOA (78/22 v/v)	DCM/TOA (78/22 v/v)
dilution	1 ml water	1 ml 10 mM NH_4AC pH 4.5	-	-	1 ml 10 mM NH_4AC pH 4.5	1 ml MeOH	-	-	1 ml water
washing	1 ml MeOH, 1 ml 10 mM NH_4AC pH 4.5	1 ml MeOH, 1 ml 10 mM NH_4AC pH 4.5	1 ml MeOH, 1 ml 10 mM NH_4AC pH 4.5	1 ml MeOH, 1 ml 10 mM NH_4AC pH 4.5	1 ml MeOH, 1 ml 10 mM NH_4AC pH 4.5	1 ml MeOH, 1 ml 10 mM NH_4AC pH 4.5	1 ml MeOH, 1 ml 10 mM NH_4AC pH 4.5	1 ml MeOH, 1 ml 1 mM NH_4AC pH 4.5	1 ml MeOH, 1 ml 1 mM NH_4AC pH 4.5
elution					2 x 500 µl 5% NH_3 in MeOH				

Supplemental Table 3: *Relative recovery of metabolites extracted by different methods*

	relative recovery (%)								
	method 1	method 2	method 3	method 4	method 5	method 6	method 7	method 8	method 9
dATP; $_{15N}$	42.2	48.0	10.4	86.9	66.5	87.0	69.0	93.2	100.2
dCTP; $_{15N}$	55.7	54.0	14.1	97.7	49.9	69.6	84.0	106.4	104.0
dGTP; $_{13C, 15N}$	46.4	48.0	3.8	77.5	56.4	66.3	47.8	63.7	64.6
dTTP; $_{13C, 15N}$	57.9	57.8	10.2	96.7	53.4	90.5	92.3	89.6	87.8
ATP; $_{Deut.}$	45.6	49.7	10.3	81.2	69.4	92.0	61.6	92.7	90.0
CTP; $_{Deut.}$	55.7	54.8	19.4	78.57	66.5	96.1	68.0	84.7	102.5
GTP; $_{Deut.}$	42.5	53.4	16.4	59.0	28.4	36.8	23.6	51.8	41.2
UTP; $_{Deut.}$	58.9	49.0	16.1	47.0	47.6	95.2	72.6	78.0	91.0
dTMP; $_{13C, 15N}$	1.2	0.7	107.8	12.8	15.2	15.5	26.8	44.9	88.4

***Supplemental Table 4**: Prescursor, transitions (quantifier, qualifier), fragmentor, collision energy and retention times for nucleotide triphosphate measurements*

	precursor ion $[M+H]^+$ (m/z)	product ions* (m/z)	fragmentor	collision energy (V)	retention time cHILIC (min)	retention time Hypercarb (min)
ATP	508	410	30	15	13.8	5.1
		136	30	45		
ATP; Deut.	512	414	30	15	13.8	5.1
		136	30	45		
CTP	483.99	112	25	21	15.0	2.4
		97	25	40		
CTP; Deut.	488.99	113	25	21	15.0	2.4
		100	25	40		
dATP	492.01	81.1	55	40	13.2	6.0
		136	55	29		
dATP; 15N	497	81.1	55	40	13.2	6.0
		141	55	29		
dCTP	468	111.9	85	15	14.6	2.7
		81.1	85	15		
dCTP; 15N	471	114.9	85	15	14.6	2.7
		81.1	85	15		
dGTP	508	152	122	18	14.9	5.8
		81.1	122	18		
dGTP; 13C, 15N	523	162	122	18	14.9	5.8
		81.1	122	18		
dTTP	483	207	80	15	12.7	4.2
		81.1	80	15		
dTTP; 13C,15N	495	219	80	15	12.7	4.2
		86	80	15		
GTP	524	151.9	104	25	15.3	4.7
		97.1	104	25		
GTP; Deut.	528	151.9	104	25	15.3	4.7
		100	104	25		
UTP	485	227	135	25	14.2	2.7
		97	135	25		
UTP; Deut.	490	232	135	25	14.2	2.7
		100	135	25		

* The first product ion was used as the quantifier, while the second product ion (if stated) was used as the qualifier.

***Supplemental Table 5**: Prescursor, transitions (quantifier, qualifier), fragmentor energy, collision energy and retention times for nucleotide monophosphate measurements*

	precursor ion $[M+H]^+$ (m/z)	product ion* (m/z)	fragmentor	collision energy (V)	retention time cHILIC (min)	retention time Hypercarb (min)
AMP	348	136	132	25	5.4	5.5
AMP; 15N	353.1	141	132	25	5.4	5.5
CMP	324	112	90	12	8.7	2.6
		97	90	28		
CMP; 13C 15N	336	119	90	28	8.7	2.6
dCMP	308.1	112	60	9	6.9	3.3
		95	60	40		
		81	60	33		
dCMP; 15N	311.1	115	60	9	6.9	3.3
		97	60	40		
dTMP	323.1	126.9	60	25	4.2	5.0
		81	60	17		
dTMP; 13C 15N	335	134	60	25	4.2	5.0
		86.1	60	17		
GMP	364	152	80	13	10.0	5.1
		135	80	45		
GMP; 15N	369	157	80	13	10.0	5.1
		139	80	15		
UMP	325	212.9	98	3	6.0	2.8
		97	98	10		
UMP; 15N	327	212.9	98	3	6.0	2.8
		97	98	10		

* The first product ion was used as the quantifier, while the second product ion (if stated) was used as the qualifier.

Supplemental Table 6: *Prescursor, transitions (quantifier, qualifier), fragmentor energy, collision energy and retention times for nucleoside measurements*

	precursor ion $[M+H]^+$ (m/z)	product ion* (m/z)	fragmentor	collision energy (V)	retention time cHILIC (min)
Adenosine	268	136	86	15	2.6
		119	86	15	
Adenosine; 13C	273	136	86	15	2.6
		119	86	15	
Cytidine	244	133	20	150	3.7
		112	20	150	
Cytidine; 15N	247	133	20	150	3.7
		115	20	150	
Deoxyadenosine	252	136	59	19	2.0
		119	59	51	
Deoxycytidine	228	112	55	9	3.0
		95	55	40	
Deoxyguanosine	268	152	59	19	3.4
		135	59	39	
		110	59	43	
Deoxythymidine	243	127	60	9	1.9
		81	60	17	
Deoxythymidine; 13C 15N	255	134	60	9	1.9
	255	86	60	17	
Deoxyuridine	229	117	50	2	3.2
		113	50	10	
Guanosine	284	152	90	10	4.0
		135	90	45	
Guanosine; 15N	289	157	90	10	4.0
		139	90	45	
Inosine	269	137	55	14	3.3
		119	55	40	
Inosine, 15N	273	141	55	14	3.3
Uridine	245	133	85	14	3.6
		113	85	14	
Uridine; 15N	247	115	85	14	3.6

* The first product ion was used as the quantifier, while the second product ion (if stated) was used as the qualifier.

Supplemental Table 7. *Intra-day variation and inter-day variation for different concentrations of nucleotides seperated by the Hypercarb or cHILIC method*

	Hypercarb method[a]		*cHILIC method*[a]	
amount (pmol on column)	intra-day precision (CV%)	inter-day precision (CV%)	intra-day precision (CV%)	inter-day precision (CV%)
dATP				
5	6.4	10.4	14.1	14.9
10	8.7	14.7	10.3	12.5
20	10.8	17.4	9.5	21.5
dCTP				
5	3.0	2.5	19.7	26.3
10	1.6	1.3	11.0	22.1
20	12.7	3.7	10.7	18.2
dGTP				
5	4.5	5.1	22.3	26.2
10	1.1	5.8	16.5	12.4
20	1.3	6.2	12.3	30.8
dTTP				
5	6.7	5.1	5.8	2.3
10	2.5	1.4	14.0	3.5
20	1.7	0.6	10.0	10.4
ATP				
100	1.1	5.6	11.0	7.5
400	3.5	10.2	8.1	3.8
800	2.5	10.0	5.8	11.8
CTP				
50	13.4	10.9	26.6	11.5
100	10.2	8.6	27.5	14.5
200	8.7	6.5	14.0	23.3
GTP				
50	0.4	7.7	24.1	17.0
100	2.2	9.3	19.9	15.0
400	2.3	8.3	8.9	2.7
UTP				
50	7.0	9.0	17.8	13.3
100	1.9	9.6	13.3	6.3
400	2.3	10.8	6.7	5.8

[a] n = 3 replicates

Supplemental Table 8: *Intra-day variation and inter-day variation for different concentrations of nucleosides seperated by the cHILIC method*

	cHILIC method[a]	
amount (nmol on column)	intra-day precision (CV%)	inter-day precision (CV%)
Adenosine		
0.125	0.8	11.7
0.250	3.0	8.0
1.000	0.7	15.6
Cytdine		
0.125	6.6	9.8
0.250	6.6	4.6
1.000	0.9	16.1
Guanosine		
0.125	6.0	12.8
0.250	7.6	6.0
1.000	0.6	19.0
Inosine		
0.125	10.8	16.8
0.250	6.1	6.5
1.000	0.8	21.4
Uridine		
0.125	5.6	9.8
0.250	5.6	4.6
1.000	0.9	16.9
Deoxythymidine		
0.125	1.6	16.8
0.250	2.1	8.1
0.500	1.7	25.5

[a] n = 3 replicates

Supplemental *Table 9.* *Determination of matrix effect factor (MEF) at 5 and 50 pmol dNTP and rNTP ISTDs, respectively, on column*

metabolite	*Hypercarb*		*cHILIC*	
	MEF before SPE (%)	MEF after SPE (%)	MEF before SPE (%)	MEF after SPE (%)
dATP	97.0	43.9	96.0	3.7
dCTP	*nd*[a]	56.3	*nd*	13.7
dGTP	97.8	63.9	*nd*	14.0
dTTP	*nd*	65.3	93.3	10.3
ATP	99.8	65.1	91.1	12.2
CTP	*nd*	74.8	*nd*	16.8
GTP	98.0	72.7	*nd*	30.3
UTP	*nd*	73.1	*nd*	17.2

[a] *nd,* metabolite was not detected

Supplemental Table 10. *Determination of matrix effect factor (MEF) at 5 pmol nucleoside ISTD on column*

metabolite	cHILIC	
	MEF before SPE (%)	MEF after SPE (%)
Deoxythymidine	89.2	13.8
Adenosine	95.9	81.2
Cytidine	52.1	-111.2
Guanosine	58.8	36.5
Inosine	63.3	-122.0
Uridine	50.8	-111.2

***Table 11**: NTPs analyzed with an Orbitrap mass spectrometer*

nucleotides	elemental composition	measured exact mass	Δppm	masses of product ions	identified by full MS mode	matched isotopes/expected isotopes	RT
ATP	C10H16N5O13P3	508.0027	-0.72	136.0617 348.0702	yes	4/4	7.12
GTP	C10H16N5O14P3	523.9974	-0.95	97.0288 152.0566	yes	4/4	6.68
CTP	C9H16N3O14P3	483.9914	-0.81	97.0288 112.0508	no	2/4	4.31
UTP	C9H15N2O15P3	484.9742	-3.41	97.0288 227.0661	yes	2/3	4.4
dATP	C10H16N5O12P3	492.0078	-0.66	136.0617 103.0393	yes	3/3	9.1
dGTP	C10H16N5O13P3	*nd*[a]	*nd*	*nd*	no	*nd*	*nd*
dCTP	C9H16N3O13P3	*nd*	*nd*	*nd*	no	*nd*	*nd*
dTTP	C10H17N2O14P3	482.9965	-0.1	81.0340 112.0508	yes	3/3	6.75

[a] nd, not detected

Supplemental File 1: ANOVA analyses.

df = degrees of freedom; Sum sq = sum of squares; Mean sq = mean squares

Figure 2A

	Sum sq	df	Mean sq	F-value	P-value
Interaction	1416	3	471.9	15.52	<0.0001
Row Factor	40840	3	13613	447.7	<0.0001
Column Factor	76.36	1	76.36	2.511	0.1326
Residual	486.5	16	30.41		

Figure 2B

	Sum sq	df	Mean sq	F-value	P-value
Interaction	0.01764	3	0.005878	177.2	<0.0001
Row Factor	0.08753	3	0.02918	879.7	<0.0001
Column Factor	0.02782	1	0.02782	838.7	<0.0001
Residual	0.0005307	16	3.317e-005		

Figure 6A

Deoxyadenosine	Sum sq	df	Mean sq	F-value	P-value
Treatment	0.2220	3	0.07401	0.2550	0.8558
Residual	2.322	8	0.2903		
Total	2.544	11			

Deoxythymidine	Sum sq	df	Mean sq	F-value	P-value
Treatment	721.0	3	240.3	373.3	<0.0001
Residual	5.150	8	0.6438		
Total	726.1	11			

Figure 6B

Deoxythymidine	Sum sq	df	Mean sq	F-value	P-value
Treatment	44.20	3	14.73	43.00	<0.0001
Residual	2.741	8	0.3426		
Total	46.94	11			

Figure 7A

ATP	Sum sq	df	Mean sq	F-value	P-value
Treatment	356.3	3	118.8	13.70	0.0016
Residual	69.37	8	8.671		
Total	425.7	11			

CTP	Sum sq	df	Mean sq	F-value	P-value
Treatment	351.9	3	117.3	262.5	<0.0001
Residual	3.575	8	0.4468		
Total	355.5	11			

GTP	Sum sq	df	Mean sq	F-value	P-value
Treatment	99.50	3	33.17	42.21	<0.0001
Residual	6.286	8	0.7858		
Total	105.8	11			

UTP	Sum sq	df	Mean sq	F-value	P-value
Treatment	249.5	3	83.18	263.3	<0.0001
Residual	2.527	8	0.3159		
Total	252.1	11			

AMP	Sum sq	df	Mean sq	F-value	P-value
Treatment	10203	3	3401	5.352	0.0258
Residual	5083	8	635.4		
Total	15286	11			

ADP	Sum sq	df	Mean sq	F-value	P-value
Treatment	252.4	3	84.14	6.842	0.0134
Residual	98.38	8	12.30		
Total	350.8	11			

ATP/ADP	Sum sq	df	Mean sq	F-value	P-value
Treatment	0.1844	3	0.06147	12.25	0.0023
Residual	0.04014	8	0.005017		
Total	0.2245	11			

AEC	Sum sq	df	Mean sq	F-value	P-value
Treatment	0.007894	3	0.002631	7.176	0.0117
Residual	0.002933	8	0.0003667		
Total	0.01083	11			

Figure 7B

ATP	Sum sq	df	Mean sq	F-value	P-value
Treatment	66564	3	22188	180.1	<0.0001
Residual	985.6	8	123.2		
Total	67550	11			

CTP	Sum sq	df	Mean sq	F-value	P-value
Treatment	22509	3	7503	41.99	<0.0001
Residual	1429	8	178.7		
Total	23938	11			

GTP	Sum sq	df	Mean sq	F-value	P-value
Treatment	5151	3	1717	930.2	<0.0001
Residual	14.77	8	1.846		
Total	5166	11			

UTP	Sum sq	df	Mean sq	F-value	P-value
Treatment	5778	3	1926	176.5	<0.0001
Residual	87.30	8	10.91		
Total	5865	11			

AMP	Sum sq	df	Mean sq	F-value	P-value
Treatment	2055	3	684.9	7.761	0.0094
Residual	706.0	8	88.24		
Total	2761	11			

ADP	Sum sq	df	Mean sq	F-value	P-value
Treatment	260.4	3	86.79	22.49	0.0003
Residual	30.87	8	3.859		
Total	291.2	11			

ATP/ADP	Sum sq	df	Mean sq	F-value	P-value
Treatment	45.27	3	15.09	6.564	0.0150
Residual	18.39	8	2.299		
Total	63.66	11			

AEC	Sum sq	df	Mean sq	F-value	P-value
Treatment	0.04689	3	0.01563	14.12	0.0015
Residual	0.008853	8	0.001107		
Total	0.05574	11			

Figure 8A

GMP	Sum sq	df	Mean sq	F-value	P-value
Treatment	1599	3	533.1	186.4	<0.0001
Residual	22.87	8	2.859		
Total	1622	11			

IMP	Sum sq	df	Mean sq	F-value	P-value
Treatment	9332	3	3111	16.66	0.0008
Residual	1494	8	186.7		
Total	10825	11			

UMP	Sum sq	df	Mean sq	F-value	P-value
Treatment	39.38	3	13.13	349.5	<0.0001
Residual	0.3005	8	0.03756		
Total	39.68	11			

Figure 8B

GMP	Sum sq	df	Mean sq	F-value	P-value
Treatment	3.509	3	1.170	32.35	<0.0001
Residual	0.2893	8	0.03616		
Total	3.798	11			

IMP	Sum sq	df	Mean sq	F-value	P-value
Treatment	37.65	3	12.55	25.41	0.0002
Residual	3.952	8	0.4940		
Total	41.61	11			

UMP	Sum sq	df	Mean sq	F-value	P-value
Treatment	21536	3	7179	14.39	0.0014
Residual	3990	8	498.8		
Total	25527	11			

dTMP	Sum sq	df	Mean sq	F-value	P-value
Treatment	28493	3	9498	4.225	0.0458
Residual	17983	8	2248		
Total	46476	11			

Figure 9

dATP	Sum sq	df	Mean sq	F-value	P-value
Treatment	33594	3	11198	114.0	<0.0001
Residual	786.0	8	98.25		
Total	34380	11			

dCTP	Sum sq	df	Mean sq	F-value	P-value
Treatment	52576	3	17525	46.65	<0.0001
Residual	3006	8	375.7		
Total	55581	11			

dGTP	Sum sq	df	Mean sq	F-value	P-value
Treatment	9166	3	3055	54.02	<0.0001
Residual	452.5	8	56.56		
Total	9619	11			

dTTP	Sum sq	df	Mean sq	F-value	P-value
Treatment	54742	3	18247	41.30	<0.0001
Residual	3534	8	441.8		
Total	58276	11			

Supplemental Figure 6A

Adenosine	Sum sq	df	Mean sq	F-value	P-value
Treatment	0.1676	3	0.05587	7.865	0.0090
Residual	0.05683	8	0.007103		
Total	0.2244	11			

Cytidine	Sum sq	df	Mean sq	F-value	P-value
Treatment	56.87	3	18.96	73.77	<0.0001
Residual	2.056	8	0.2570		
Total	58.93	11			

Guanosine	Sum sq	df	Mean sq	F-value	P-value
Treatment	232.1	3	77.36	41.47	<0.0001
Residual	14.92	8	1.866		
Total	247.0	11			

Inosine	Sum sq	df	Mean sq	F-value	P-value
Treatment	0.008840	3	0.002947	3741	<0.0001
Residual	6.302e-006	8	7.877e-007		
Total	0.008847	11			

Uridine	Sum sq	df	Mean sq	F-value	P-value
Treatment	1815	3	605.0	63.96	<0.0001
Residual	75.67	8	9.459		
Total	1891	11			

Xanthosine	Sum sq	df	Mean sq	F-value	P-value
Treatment	707.2	3	235.7	139.5	<0.0001
Residual	13.52	8	1.690		
Total	720.8	11			

Supplemental Figure 6B

Adenosine	Sum sq	df	Mean sq	F-value	P-value
Treatment	36.99	3	12.33	691.7	<0.0001
Residual	0.1426	8	0.01782		
Total	37.13	11			

Cytidine	Sum sq	df	Mean sq	F-value	P-value
Treatment	19008	3	6336	18.23	0.0006
Residual	2781	8	347.6		
Total	21789	11			

Guanosine	Sum sq	df	Mean sq	F-value	P-value
Treatment	6.627	3	2.209	39.02	<0.0001
Residual	0.4529	8	0.05661		
Total	7.080	11			

Inosine	Sum sq	df	Mean sq	F-value	P-value
Treatment	0.2480	3	0.08267	31.39	<0.0001
Residual	0.02107	8	0.002634		
Total	0.2691	11			

Uridine	Sum sq	df	Mean sq	F-value	P-value
Treatment	908.7	3	302.9	23.66	0.0002
Residual	102.4	8	12.80		
Total	1011	11			

Xanthosine	Sum sq	df	Mean sq	F-value	P-value
Treatment	14.54	3	4.848	315.0	<0.0001
Residual	0.1231	8	0.01539		
Total	14.67	11			

2.3 Rapid Affinity Purification of Tagged Plant Mitochondria

Niehaus, M., Herde, M.

Leibniz Universität Hannover, Department of Molecular Nutrition and Biochemistry of Plants, 30419 Hannover, Germany

Type of authorship:	First author
Type of article:	Invited book chapter
Share of work:	90 %
Contribution to publication:	wrote and reviewed the manuscript together with M.H.
Journal:	Methods in Molecular Biology
Impact factor:	1.17 (2022)
Date of publication:	19.05.2022
Number of citations: (Google Scholar, 28.09.22)	0
DOI:	10.1007/978-1-0716-2176-9_9

Chapter 9

Rapid Affinity Purification of Tagged Plant Mitochondria (Mito-AP)

Markus Niehaus and Marco Herde

Abstract

This protocol describes the isolation of mitochondria by affinity chromatography using magnetic beads coated with Strep-Tactin in a timeframe of ca. 30 min. Compared to a classic differential and density gradient centrifugation this protocol enables a more rapid and efficient isolation of mitochondria even with small amounts of plant material. Transgenic plants with mitochondria that are decorated with a protein that is integrated into the outer mitochondrial membrane and fused to a green fluorescent protein (GFP) and a TwinStrep-tag facing the cytosol. This tag can bind to Strep-Tactin coated magnetic beads. Isolated mitochondria still bound to magnetic beads are uniquely suited for measuring oxygen consumption rates since this measurement needs mitochondria to be immobilized on the bottom of the measuring well. Furthermore, the isolated mitochondria can be used for downstream applications such as proteomics and metabolomics. This technique also allows for the isolation of mitochondria from specific cell types and tissues by altering the expression of the protein decorating the mitochondria.

Key words Arabidopsis, Mitochondria, Affinity chromatography, Metabolomics, Proteomics, Lipidomics, Respiratory activity measurement

1 Introduction

History of mitochondria isolation began 1934 when Bensley and Hoerr first described a protocol to enrich mitochondria originating from liver cells of rodents using differential centrifugation [1]. Over the following decades scientists further refined this method and combined it with a density gradient centrifugation. Nowadays, this dual approach is still used in the plant field to isolate mitochondria in large quantities from green tissue [2, 3] and cell or callus cultures [4]. This approach results in highly pure mitochondria with respiratory activity, but often requires a large amount of plant material, is time-consuming and needs experience as well as specialized equipment. Thus, in cases where material is limited and hands-on time is crucial alternatives for the current state-of-the-art method are required. Here we describe a technique that requires significantly

B. Vijayalakshmi Ayyar and Sushrut Arora (eds.), *Affinity Chromatography: Methods and Protocols*, Methods in Molecular Biology, vol. 2466, https://doi.org/10.1007/978-1-0716-2176-9_9, © Springer Science+Business Media, LLC, part of Springer Nature 2022

less starting material, is much faster and can be performed with basic lab equipment. This method is based on an approach using affinity chromatography with antibodies directed against an outer mitochondrial membrane protein [5] or by using antibodies against an outer mitochondrial membrane protein tagged with an HA tag, which requires a genetically modified organism [6, 7]. The construct used for the protocol presented here [8] is uniquely suited for a promotor exchange, allowing for tissue-specific isolation of mitochondria, since it is based on modular cloning [9–12]. In fact we observed successful ectopic expression, for example, in seeds, guard cells, and mesophyll cells (Niehaus, unpublished).

The central element for the presented method is the labelling of a protein located only in the outer mitochondrial membrane with a TwinStrep tag. Tagged mitochondria bind to magnetic beads covered with Strep-Tactin (commercial or self-made), which provides the advantage of rapidly pulling them on the side of the reaction tube with the help of a magnet. Thus, leaving unwanted cell material in solution, which can be subsequently removed (Fig. 1). After several quick washing steps mitochondria bound to the magnetic beads can be directly used for downstream applications, like metabolite/proteome analysis. Despite the shortened time needed for isolation, this protocol is not sufficient to completely halt all enzymatic activities (quenching). Therefore, it is important to note that the metabolite analysis may not reflect the in vivo abundance.

An important downstream application of mitochondrial isolation procedures are respiratory activity measurements. Affinity purification of mitochondria with magnetic beads is uniquely suited for respiration analysis in a seahorse analyzer since this technology benefits from the fact that mitochondria are immobilized and sink to the bottom of the measuring well.

Modifications of the protocol such as a treatment with biotin will elute the mitochondria from the beads potentially increasing specificity and thus purity, albeit with a lower recovery. Treatment with proteinase K significantly increases the yield and removes all

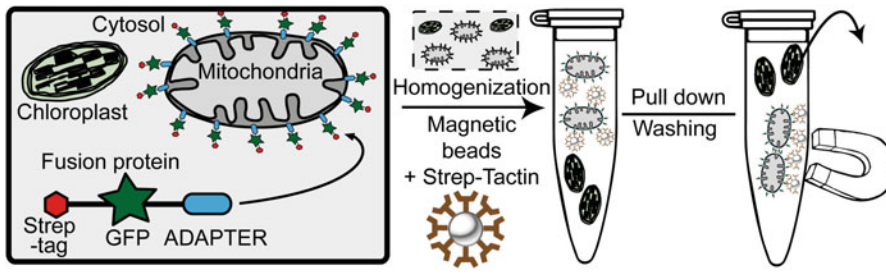

Fig. 1 Workflow of Mito-AP. An ectopically expressed protein, which integrates into the outer mitochondrial membrane, fused with an N-terminal Strep-tag and a GFP-tag facing the cytosol can be used as an anchor for affinity purification of mitochondria with Strep-Tactin-coated magnetic beads (reproduced and modified from [8] (www.plantphysiol.org), Copyright American Society of Plant Biologists)

proteins that are attached to the outside of the mitochondria or bind to the beads nonspecifically.

2 Materials

All buffers, solutions, and media are prepared using highly pure water (sensitivity of >18 MΩ cm) and analytical grade reagents and solvents. Buffers should be stored at room temperature, unless stated otherwise.

- Magnetic separator for 1.5 mL and/or 2 mL reaction tubes.
- Overhead shaker.
- Ultrasonication bath (*see* **Note 1**).
- Uncoated starch polymer matrix magnetic beads suspension, 25 mg mL^{-1}: Store at 4 °C (*see* **Note 2**).
- Activation Buffer: 0.2 M sodium hydrogen carbonate buffer, pH 8.4–8.7. Dissolve 1.68 g of sodium hydrogen carbonate in 100 mL water. No pH adjustment is necessary.
- CNBr solution: 5 M cyanogen bromide solution in acetonitrile. Weigh in 5.3 g of cyanogen bromide and dissolve in 10 mL acetonitrile. Store at 4 °C (shelf life several months) (*see* **Note 3**).
- 1× PBS Buffer (136.9 mM sodium chloride, 8.1 mM disodium hydrogen phosphate, 2.68 mM potassium chloride, 1.47 mM potassium dihydrogen phosphate), pH 7.4. Dissolve 8 g of sodium chloride, 200 mg potassium chloride, 1.44 g disodium hydrogen phosphate dehydrate and 200 mg potassium dihydrogen phosphate in 900 mL water. Adjust the pH to 7.4 using HCl and NaOH. Fill up to 1 L and store at 4 °C (shelf life 1 month).
- Strep-Tactin solution in 1× PBS buffer. Dissolve 2 mg lyophilized Strep-Tactin protein in 200 µL PBS Buffer. Store at −20 °C (shelf life up to 6 months).
- Storage Buffer: 1× PBS buffer with 0.05% (w/v) sodium azide. Dissolve 5 mg of sodium azide in 10 mL 1× PBS Buffer. Store at 4 °C (shelf life 1 month) (*see* **Note 4**).
- Sterile bench.
- Plant growth chamber/plant growth cabinet with a shaker option.
- 100 mL Erlenmeyer flasks
- Plant material: 10 days old seedlings of transgenic Arabidopsis thaliana plants carrying the ADAPTER-TwinStrep construct [8] (*see* **Note 5**).

- Culture media: 0.5× Murashige and Skoog (MS), pH 5.7, autoclaved: Dissolve 2.15 g of Murashige and Skoog Basal salt mixture in 900 mL of water, adjust the pH to 5.8 using HCl and NaOH, fill up to 1 L. Subsequently, 30 mL media was dispensed in 100 mL Erlenmeyer flasks, sealed and autoclaved.
- Precooled mortar and pestle.
- Cold centrifuge at 4 °C.
- Ice bucket big enough to hold the magnetic separator.
- Extraction Buffer A: 100 mM ammonium bicarbonate; 200 mM sodium chloride; 32 μL mL^{-1} BioLock (IBA Lifesciences); pH 8. Dissolve 790 mg ammonium bicarbonate and 1.17 g of sodium chloride in 80 mL water. Adjust the pH to 8 using HCl and NaOH. Fill up to 100 mL with water. Store at 4 °C (shelf life 2 days). Add 32 μL mL^{-1} BioLock shortly before use.
- Washing Buffer A: 100 mM ammonium bicarbonate; 200 mM sodium chloride. Dissolve 790 mg ammonium bicarbonate and 1.17 g of sodium chloride in 80 mL water. Adjust the pH to 8 using HCl and NaOH. Fill up to 100 mL with water. Store at 4 °C and use within 2 days.
- Elution Buffer: 100 mM ammonium bicarbonate; 200 mM sodium chloride, 50 mM D-biotin, pH 8. Dissolve 61.1 mg D-biotin in 3 mL Wash Buffer A and adjust the pH to 8 using HCl and NaOH (*see* **Note 6**). Fill up to 5 mL with Wash Buffer A. Store at 4 °C and use within 1 day.
- Digestion Buffer: 100 mM ammonium bicarbonate; 200 mM sodium chloride, 4 mM calcium chloride, 200 μg mL^{-1} proteinase K, pH 8. Dissolve 4.44 mg calcium chloride and 2 mg proteinase K in 5 mL Wash Buffer A, adjust the pH to 8 using HCl and NaOH. Fill up to 10 mL using Wash Buffer A. Store at 4 °C and use within 2 days.
- Inhibition Buffer: 100 mM phenylmethylsulfonyl fluoride in isopropanol. Dissolve 34.8 mg phenylmethylsulfonyl fluoride in 2 mL isopropanol. Store at −20 °C (shelf life several months).
- 2× SDS loading Buffer: 0.1% (w/v) bromophenol blue; 0.2 M dithiothreitol (DTT); 20% glycerol (v/v); 4% (w/v) sodium dodecyl sulfate (SDS); 0.1 M Tris–HCl, pH 6.8. Dissolve 5 mg bromophenol blue, 154.25 mg DTT and 200 mg SDS in 3 mL water, add 1 mL 100% Glycerol and 500 μL of a 1 M Tris–HCl, pH 6.8 solution. Fill up to 5 mL Store at −20 °C (shelf life several months).
- DTT 1 M stock solution. Dissolve 154.25 mg DTT in 1 mL water. Store at −20 °C (shelf life several months).

- Adenosine triphosphate (ATP) 100 mM stock. Dissolve 55.11 mg ATP in 1 mL water. Store at −20 °C (shelf life several months).
- n-propyl gallate (nPG) 100 mM stock. Dissolve 21.22 mg nPG in DMSO. Store at −20 °C (shelf life several months).
- Succinic acid 500 mM stock, pH 7.2. Dissolve 590.5 mg succinic acid in 8 mL water. Adjust the pH to 7.2 using 5 M KOH. Fill up to 10 mL. Store at −20 °C (shelf life several months).
- Extraction Buffer B: 5 mM DTT; 300 mM sucrose; 5 mM potassium dihydrogen phosphate; 10 mM TES, 10 mM sodium chloride; 2 mM magnesium sulfate; 0.1% (w/v) BSA; 32 μL mL^{-1} BioLock; pH 7.2. Dissolve 10.27 g sucrose, 68 mg potassium dihydrogen phosphate, 229.3 mg TES, 58.4 mg sodium chloride and 24.1 mg magnesium sulfate in 70 mL water. Adjust the pH to 7.2 using HCl and KOH. Fill up to 100 mL with water. Store at −20 °C (shelf life several weeks). Add 5 μL mL^{-1} of a 1 M DTT stock and 32 μL mL^{-1} BioLock shortly before use.
- Washing Buffer B: 300 mM sucrose; 5 mM potassium dihydrogen phosphate; 10 mM TES, 10 mM sodium chloride; 2 mM magnesium sulfate; 0.1% (w/v) BSA, pH 7.2. Dissolve 10.27 g sucrose, 68 mg potassium dihydrogen phosphate, 229.3 mg TES, 58.4 mg sodium chloride, and 24.1 mg magnesium sulfate in 70 mL water. Adjust the pH to 7.2 using HCl and KOH. Fill up to 100 mL with water. Store at −20 °C (shelf life several weeks).
- Respiration Buffer: 300 mM sucrose; 5 mM potassium dihydrogen phosphate; 10 mM TES, 10 mM sodium chloride; 2 mM magnesium sulfate; 0.1% (w/v) BSA, 10 mM succinic acid, 500 μM ATP, and 500 μM n-propyl gallate, pH 7.2. Add 100 μL mL^{-1} of a 500 mM succinic acid stock, 25 μL mL^{-1} of a 100 μM ATP stock, and 25 μL mL^{-1} of a 100 μM nPG stock to 4.85 mL Washing Buffer B at room temperature shortly before use.
- Seahorse XFe96 Analyzer (Agilent Technologies).
- XFe96 Sensor Cartridge (Agilent Technologies).
- Seahorse XF Calibrant (Agilent Technologies).
- 96-well plate centrifuge
- Non-CO_2 37 °C incubator.
- Adenosine diphosphate solution (ADP) 1 M stock. Dissolve 2.14 g ADP in 3 mL water. Adjust the pH to 7.2 using KOH (*see* **Note 7**). Fill up to 5 mL. Store at −20 °C (shelf life several months). Prepare 1 mL of a 60 mM working solution by mixing

60 µL of the 1 M stock and 940 µL Respiration Buffer. Store on ice and use within 1 day.

- Oligomycin A, 5 mg mL^{-1} stock. Dissolve 1 mg oligomycin A in 200 µL 95% EtOH (*see* **Note 8**). Store at −20 °C (shelf life several months). Prepare 1 mL of a 50 µg mL^{-1} solution by mixing 10 µL of the 5 mg mL^{-1} stock and 990 µL Respiration Buffer. Store on ice and use within 1 day.
- Antimycin A, 40 mM stock. Dissolve 25 mg Antimycin A in 1175 µL 95% EtOH. Store at −20 °C (shelf life several months). Prepare 1 mL of an 80 µM solution by mixing 2 µL of the 40 mM stock with 998 µL Respiration Buffer. Store on ice and use within 1 day.

3 Methods

3.1 Strep-Tactin Coating of Starch Polymer Matrix Coated Magnetic Beads (Modified from Manufacturer Instructions (Chemicell, Berlin, Germany)

1. Vortex the stock tube of the uncoated magnetic beads and transfer 500 µL to a new 2 mL tube. Add 1 mL of Activation Buffer, mix and spin down briefly (*see* **Note 9**) to assure that no beads are stuck in the lid of the tube.
2. Place the tube in the magnetic separator and allow the beads to settle on the side of the reaction tube for 2 min. While the tube is still in the magnetic separator, carefully discard the supernatant with a pipette (*see* **Note 10**). Add another 500 µL Activation Buffer and resuspend the beads by vortexing.
3. Add 100 µL cold CNBr solution to the suspension, mix by vortexing and place the tube in wet ice for 10 min. Mix the suspension by inverting twice every minute. After the incubation, briefly spin down the tube and place it in the magnetic separator for 1 min. Carefully discard the supernatant in a toxic waste disposal.
4. Add 1 mL 1× PBS Buffer, resuspend by vortexing, briefly spin down and place the tube in the magnetic separator for 1 min. Discard the supernatant in a toxic waste disposal. Repeat this washing step. Resuspend the beads in 500 µL 1× PBS Buffer.
5. Place the beads in an ultrasonication bath for 2 min.
6. Add 20 µL of the Strep-Tactin solution and incubate at room temperature for 2 h in an overhead shaker (*see* **Note 11**).
7. Place the tube in the magnetic separator for 2 min and remove the supernatant (*see* **Note 12**). Wash the beads by adding 1 mL of 1× PBS Buffer, resuspend by vortexing, briefly spinning down and magnetic separation for 2 min. Repeat this washing step 2 times.
8. Resuspend the beads in 500 µL Storage Buffer and store at 4 °C and use within 1 week.

3.2 Plant Material and Cultivation

1. Surface sterilize 10 mg seeds of transgenic Arabidopsis thaliana for 20 min using 70% EtOH at room temperature (*see* **Note 13**).
2. Under a sterile bench, dry the seeds on sterile filter paper and subsequently transfer them into a sterile 100 mL flasks containing 30 mL of culture media.
3. Store the prepared flasks for 24 h at 4 °C in the dark (*see* **Note 14**).
4. Place the flasks on a shaker in your plant growth chamber/plant growth cabinet with the desired growth conditions, for example, different light settings or temperatures. Set the shaker to 50 rpm.
5. Harvest the seedlings after 10 days by removing the media and wash the plants by briefly dipping them in distilled water (*see* **Note 15**).
6. Collect the seedlings and dry them by gently pressing them in between clean paper towels.

3.3 Affinity Purification of Plant Mitochondria for Proteomic, Metabolomic, and Lipidomic Analyses

1. Precool all the buffers, magnetic separator, centrifuge, and mortar and pestle to 4 °C.
2. For metabolomic and lipidomic analyses take an aliquot of the Strep-Tactin coated magnetic beads of 500 µL per sample, for proteomic analyses use 250 µL per sample. Place the aliquot in the magnetic separator and discard the Storage Buffer. Wash the magnetic beads 2× with 1 mL Washing Buffer A and resuspend in 500 µL Washing Buffer in a 2 mL tube. Store on ice for later use.
3. Weigh in 500 mg of seedlings, and combine them in a mortar with a spatula tip of sand and 1 mL Extraction Buffer A.
4. Grind the sample for 3 min on ice.
5. Transfer the crude extract to a new 2 mL tube using a pipette with a cut tip (*see* **Note 16**).
6. Centrifuge for 5 min at 1000 × *g*.
7. Transfer 800 µL of the supernatant to the 500 µL washed Strep-Tactin coated magnetic beads and let them incubate for 5 min on an overhead shaker at 4 °C.
8. Briefly spin down and place the tube in the magnetic separator in ice. Allow the particles to settle on the side of the reaction tube for 2 min. Carefully remove the supernatant. Add 1 mL of Washing Buffer A and resuspend by gently inverting and light flicking of the tube (*see* **Note 17**).
9. Repeat the previous step 3 times for a total of four washing steps.

10. For metabolomic analysis, remove the supernatant completely and use the mitochondria still attached to the magnetic beads as the starting material for metabolite extraction (*see* **Note 18**).
11. For proteomic or lipidomic analysis, either combine the mitochondria attached to the magnetic beads from step 10 with 20 µL 2× SDS loading buffer and heat for 5 min at 95 °C or continue with a further purification treatment described in the following steps (*see* **Note 19**).
12. Add 1 mL Elution Buffer, resuspend and incubate for 5 min on ice and invert the tube every minute.
13. Add 950 µL Digestion Buffer, mix by inverting and incubate for 10 min at room temperature.
14. Stop the digest by adding 50 µL Inhibition Buffer and mix again by inverting the tube several times.
15. Place the tube in the magnetic separator in ice and allow the beads to settle on the side of the reaction tube for 2 min.
16. Transfer the supernatant carefully to a new 2 mL tube and centrifuge for 10 min at 14,500 × *g*. Discard the supernatant and store the pellet at −80 °C until further analysis.

3.4 Affinity Purification of Plant Mitochondria for Respiratory Activity Measurements Through Complex II

The following steps are very similar to the steps described in Subheading 3.2. The main differences are the changes in buffers and time needed for the magnetic beads to settle on the side of the reaction tube during the magnetic separation, due to the higher viscosity of the buffers. All previous notes still apply.

3.4.1 Affinity Purification of Plant Mitochondria

1. Precool Extraction Buffer B and Washing Buffer B, the magnetic separator, centrifuge, and mortar and pestle to 4 °C.
2. In a 2 mL tube place an aliquot of 250 µL of the Strep-Tactin coated magnetic beads in the magnetic separator and discard the Storage Buffer. Wash the magnetic beads 2× with 1 mL Washing Buffer B and resuspend the beads in 500 µL Washing Buffer B by vortexing. Store on ice for later.
3. Weigh in 500 mg of seedlings and combine them in a mortar with a spatula tip of sand and 1 mL Extraction Buffer B.
4. Grind the sample for 3 min on ice.
5. Transfer the crude extract to a new 2 mL tube using a pipette with a cut tip.
6. Centrifuge for 5 min at 1000 × *g*.
7. Transfer 800 µL of the supernatant to the 500 µL washed Strep-Tactin coated magnetic beads and let them incubate for 5 min on an overhead shaker at 4 °C.
8. Briefly spin down and place the tube in the magnetic separator in ice. Allow the particles to settle on the side of the reaction

tube for 3 min. Carefully remove all of the supernatant. Add 1 mL of Washing Buffer B and resuspend by gently inverting and light flicking of the tube.

9. Repeat the previous step 3 times for a total of four washing steps.
10. Resuspend the beads carefully in 100 µL Respiration Buffer. Samples can be stored for a short time at room temperature while preparing **step 5** described in Subheading 3.4.2.

3.4.2 Respiratory Activity Measurements Through Complex II

1. On the day before the assay, place a 25 mL aliquot of Seahorse XF Calibrant in a non-CO_2 incubator overnight. Fill each well of the utility plate with 200 µL sterile water, carefully assemble the sensor cartridge on top of the filled utility plate and make sure that the sensors are submerged in the sterile water. Incubate this assembly in a non-CO_2 incubator at 37 °C overnight (*see* **Note 20**).
2. On the next day, remove the sensor cartridge from the utility plate and place it upside down. Discard the water from the utility plate completely and fill each well up again with 200 µL of prewarmed Seahorse CF Calibrant. Assemble the sensor cartridge on the utility plate again and place them in a non-CO_2 incubator for 60 min.
3. After incubation, fill the ports of the sensor cartridge while still attached to the utility plate as follows: port A, 20 µL 60 mM ADP working solution; port B, 22 µL 50 µg mL oligomycin A working solution; port C, 24 µL 80 µM antimycin A working solution; port D, 26 µL Respiration Buffer (*see* **Note 21**).
4. Start with setting up the Seahorse XFe96 Analyzer using the Wave Software. Define the used ports, plate setup and turn off the internal heater (*see* **Note 22**). Following instrument protocol was used:
   (a) Baseline measurement cycle: 12 min equilibration, 30 s mixing, 10 s waiting, 2 min measuring.
   (b) Injection of port A: 30 s mixing, 10 s waiting, 2 min measuring.
   (c) Injection of port B: 30 s mixing, 10 s waiting, 2 min measuring.
   (d) Injection of port C: 30 s mixing, 10 s waiting, 2 min measuring.
5. Start the run and place the sensor cartridge/utility plate assembly correctly into the machine and begin with the sensor cartridge calibration by pressing "I'm Ready."
6. Start loading the cell plate by carefully preparing different dilutions (*see* **Note 23**) of the resuspended beads:

(a) 50 µL resuspended beads +200 µL Respiration Buffer (1:5)

(b) 25 µL resuspended beads +225 µL Respiration Buffer (1:10)

(c) 12.5 µL resuspended beads +237.5 µL Respiration Buffer (1:20).

7. Mix carefully by gentle flicking the tube and pipet 5 technical replicates with 40 µL each to the bottom of the well. Keep one additional aliquot of 40 µL for later protein quantification.
8. Centrifuge at 2200 × *g* for 5 min. After centrifugation carefully take the plate with the precipitated beads. Add 160 µL of Respiration Buffer to each well, by slow and careful pipetting the solution on the side of each well (*see* **Note 24**).
9. After the successful sensor cartridge calibration, remove the utility plate by clicking "Open Tray) and place the cell plate without the lid in the machine.
10. Click "Load Cell Plate" and the assay will start.
11. After the assay is finished click "Eject" and carefully remove the assembly of the sensor cartridge and cell plate.
12. Check the cell plate for any dispersions of the magnetic beads and exclude these wells in your later analysis.

4 Notes

1. An ultrasonication bath is not strictly required. Vortexing the beads for 60 s at full speed is also possible, but yields in a lower homogeneity.
2. Magnetic beads should under no circumstances be stored at temperatures below 0 °C. Freezing leads to damage of the coating and exposure of the iron core. Oxidation of the iron core results in the loss of the paramagnetic property.
3. It is strongly recommended to perform all steps involving cyanogen bromide, including weighing, under a fume hood or a very well ventilated area and to treat all resulting leftovers as toxic waste.
4. It is possible to add 0.1% bovine serum albumin (BSA) to the Storage Buffer to achieve a blocking of nonspecific binding sites. In our hands BSA complicated the protein quantification after the affinity purification.
5. The method presented here is not limited to the described plant material and transgenic line. Affinity purification of plant mitochondria were already performed with Arabidopsis plants grown under various conditions (e.g., short day),

different time points and with tissue specific promoters (e.g., seeds, mesophyll, and guard cells). Additionally, *N. benthamiana* leaves, transiently expressing the ADAPTER-TwinStrep protein, can be used for purification.

6. Addition of D-Biotin results in a dramatic increase of the pH. A complete dissolution of the D-Biotin can only be achieved by compensating the pH decrease caused by D-Biotin dissolution with gradual addition of NaOH. Usage of 5 M NaOH is strongly recommended.
7. Adjusting the pH of the ADP stock solution is a crucial point for the following respiratory activity measurement and should be done with care.
8. 100% EtOH contains traces of benzene, which is harmful for mitochondrial function. It is necessary for this step to use 95% EtOH [13].
9. Avoid lengthy centrifugation steps. The sole purpose of the described centrifugation steps is to avoid liquids to be stuck in the lid of the tube. Alternatively, stuck liquids can be collected using a pipette.
10. During the magnetic separation, especially during the coating process, it is normal that some beads are not being pulled to the site of the tube and are lost during the washing steps.
11. Using a higher concentration of Strep-Tactin results in a matrix with a higher density of Strep-Tactin. But the amount of Strep-Tactin used in the reaction and the density of the resulting matrix is not linear.
12. The protein concentration of the supernatant can be quantified using Bradford to get an overview of the coating efficiency.
13. The use of 10 mg Arabidopsis seeds in 30 mL MS media filled in a 100 mL flask is suitable to grow plants for around 10 days without changing the media in between.
14. Storing the Arabidopsis seeds at 4 °C in the dark for 24 h under wet conditions leads to a more synchronized germination and enables a more precise determination and analysis of specific developmental stages.
15. If plants should be grown for longer than 10 days, a replenishment of the MS media is necessary.
16. All steps in which a solution containing mitochondria is transferred by using a pipette, the tip should be cut to minimize shearing forces.
17. It should be clearly visible that the beads will form bigger chunks due to cross connections of single magnetic beads with attached mitochondria. Do not mix too vigorously since

too strong shearing forces will disrupt the mitochondrial membrane.

18. While extracting your metabolites, be sure to mix the tube by vortexing and/or sonicating it for 2 min to ensure a complete disruption of the mitochondrial membranes. After extraction, the magnetic beads can be removed using the magnetic separator and/or centrifugation for 10 min at 40,000 × *g*.
19. The additional purification allows for the removal of the magnetic particles as a potential contamination source for nonspecifically bound proteins to the magnetic bead. The elution with D-Biotin is not quantitative, therefore we added a proteinase K digestion step to further increase the number of released mitochondria.
20. To ensure a complete hydration of the sensors, make sure to minimize the risk of evaporation by setting the incubator to a proper humidity.
21. Although port D is not needed in this assay, filling it up with Respiration Buffer ensures a flawless sensor cartridge calibration.
22. Turning off the internal heater of the Seahorse XFe96 Analyzer will result in the machine running the assay at the given room temperature.
23. The amount of resuspended beads to load is highly variable and strongly depends on the practitioner. Starting with preparing a series of dilutions is therefore a needed compromise. If you load too much the layer of precipitated beads is too thick and will clog the sensor. A good indicator for that are the 3 small elevations at the bottom of each well in the cell plate, on which the sensor is resting. If these are still visible after centrifugation, the amount of loaded beads will not lead to a clogging of the sensor.
24. Make sure not to disturb the precipitated beads during this or any other step. Disturbing the beads will otherwise lead to a clogging of the sensor during the assay.

Acknowledgments

We thank the Deutsche Forschungsgemeinschaft (HE 5949/3-1) for funding of the project.

References

1. Bensley RR, Hoerr NL (1934) Studies on cell structure by the freezing-drying method VI. The preparation and properties of mitochondria. Anat Rec 60:449–455. https://doi.org/10.1002/ar.1090600408

2. Day D, Neuburger M, Douce R (1985) Biochemical characterization of chlorophyll-free mitochondria from pea leaves. Funct Plant Biol 12:219. https://doi.org/10.1071/pp9850219
3. Keech O, Dizengremel P, Gardeström P (2005) Preparation of leaf mitochondria from Arabidopsis thaliana. Physiol Plant 124:403–409. https://doi.org/10.1111/j.1399-3054.2005.00521.x
4. Klein M, Binder S, Brennicke A (1998) Purification of mitochondria from Arabidopsis. Methods Mol Biol 82:49–53. https://doi.org/10.1385/0-89603-391-0:49
5. Hornig-Do H-T, Günther G, Bust M et al (2009) Isolation of functional pure mitochondria by superparamagnetic microbeads. Anal Biochem 389:1–5. https://doi.org/10.1016/j.ab.2009.02.040
6. Chen WW, Freinkman E, Wang T et al (2016) Absolute quantification of matrix metabolites reveals the dynamics of mitochondrial metabolism. Cell 166:1324–1337.e11. https://doi.org/10.1016/j.cell.2016.07.040
7. Kuhnert F, Stefanski A, Overbeck N et al (2020) Rapid single-step affinity purification of HA-tagged plant mitochondria. Plant Physiol 182:692–706. https://doi.org/10.1104/pp.19.00732
8. Niehaus M, Straube H, Künzler P et al (2020) Rapid affinity purification of tagged plant mitochondria (Mito-AP) for metabolome and proteome analyses. Plant Physiol 182:1194–1210. https://doi.org/10.1104/pp.19.00736
9. Weber E, Engler C, Gruetzner R et al (2011) A modular cloning system for standardized assembly of multigene constructs. PLoS One 6:e16765. https://doi.org/10.1371/journal.pone.0016765
10. Werner S, Engler C, Weber E et al (2012) Fast track assembly of multigene constructs using Golden Gate cloning and the MoClo system. Bioeng Bugs 3:38–43. https://doi.org/10.4161/bbug.3.1.18223
11. Engler C, Youles M, Gruetzner R et al (2014) A golden gate modular cloning toolbox for plants. ACS Synth Biol 3:839–843. https://doi.org/10.1021/sb4001504
12. Gantner J, Ordon J, Ilse T et al (2018) Peripheral infrastructure vectors and an extended set of plant parts for the modular cloning system. PLoS One 13:e0197185. https://doi.org/10.1371/journal.pone.0197185
13. Rogers GW, Murphy A, Elorza A et al Analyzing microgram quantities of isolated mitochondria in the Seahorse XFe/XF96 Analyzer. https://www.agilent.com/cs/library/applications/5991-7144EN.pdf. Accessed 14 Jan 2021

2.4 The nucleotide metabolome of germinating *Arabidopsis thaliana* seeds reveals a central role for thymidine phosphorylation in chloroplast development

Niehaus, M., Straube, H., Specht, A., Baccolini, C., Witte, C-P., Herde, M.

Leibniz Universität Hannover, Department of Molecular Nutrition and Biochemistry of Plants, 30419 Hannover, Germany

Type of authorship:	First author
Type of article:	Research Article
Share of work:	75 %
Contribution to publication:	designed the study together with M.H., cloned the constructs and performed the experiments together with H.S., A.S and C.B, analyzed the data together with H.S, prepared the figures and participated in writing the manuscript
Journal:	The Plant Cell
Impact factor:	12.085 (2021)
Date of publication:	21.07.2022
Number of citations: (Google Scholar, 28.09.22)	0
DOI:	10.1093/plcell/koac20

https://doi.org/10.1093/plcell/koac207 THE PLANT CELL 2022: 34: 3790–3813

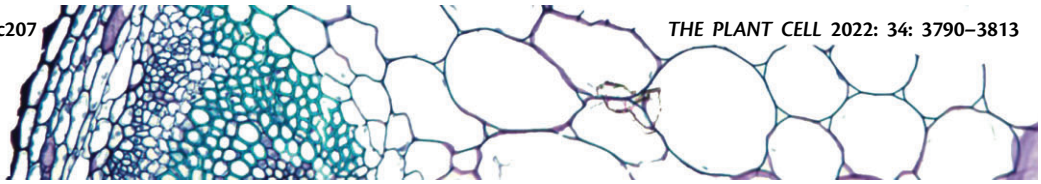

Research Article

The nucleotide metabolome of germinating *Arabidopsis thaliana* seeds reveals a central role for thymidine phosphorylation in chloroplast development

Markus Niehaus [1], Henryk Straube [1], André Specht [1], Chiara Baccolini [1,†], Claus-Peter Witte [1] and Marco Herde [1,*]

1 Department of Molecular Nutrition and Biochemistry of Plants, Leibniz Universität Hannover, Hannover 30419, Germany

*Author for correspondence: mherde@pflern.uni-hannover.de

†Present address: Max Planck Institute of Molecular Plant Physiology, Potsdam, 14476, Germany.

M.N. and M.H. designed the study. M.N., H.S., C.B., and A.S. acquired the experimental data. M.N. and H.S. analyzed the data and M.N., H.S., C.P.W., and M.H. interpreted the data. M.N., H.S., C.P.W., and M.H. wrote the manuscript. All authors read and revised the manuscript and agreed on the final version.

The author responsible for distribution of materials integral to the findings presented in this article in accordance with the policy described in the Instructions for Authors (https://academic.oup.com/plcell) is Marco Herde (mherde@pflern.uni-hannover.de).

Abstract

Thymidylates are generated by several partially overlapping metabolic pathways in different subcellular locations. This interconnectedness complicates an understanding of how thymidylates are formed in vivo. Analyzing a comprehensive collection of mutants and double mutants on the phenotypic and metabolic level, we report the effect of de novo thymidylate synthesis, salvage of thymidine, and conversion of cytidylates to thymidylates on thymidylate homeostasis during seed germination and seedling establishment in Arabidopsis (*Arabidopsis thaliana*). During germination, the salvage of thymidine in organelles contributes predominantly to the thymidylate pools and a mutant lacking organellar (mitochondrial and plastidic) thymidine kinase has severely altered deoxyribonucleotide levels, less chloroplast DNA, and chlorotic cotyledons. This phenotype is aggravated when mitochondrial thymidylate de novo synthesis is additionally compromised. We also discovered an organellar deoxyuridine-triphosphate pyrophosphatase and show that its main function is not thymidylate synthesis but probably the removal of noncanonical nucleotide triphosphates. Interestingly, cytosolic thymidylate synthesis can only compensate defective organellar thymidine salvage in seedlings but not during germination. This study provides a comprehensive insight into the nucleotide metabolome of germinating seeds and demonstrates the unique role of enzymes that seem redundant at first glance.

Introduction

The molecular processes of synthesis, degradation, and salvage of deoxyribonucleotides (dNTs; relevant abbreviations are also listed in Supplemental Table S1), the building blocks of DNA, are central to the maintenance of genetic information. In two ways dNTs are crucial for efficient and faithful DNA replication: (1) the absolute concentration of dNT

Received February 09, 2022. Accepted June 13, 2022. Advance access publication July 21, 2022

© American Society of Plant Biologists 2022. All rights reserved. For permissions, please email: journals.permissions@oup.com

Downloaded from https://academic.oup.com/plcell/article/34/10/3790/6647853 by Technische Informationsbibliothek (TIB) user on 28 September 2022

IN A NUTSHELL

Background: All living organisms, including plants, possess DNA and rely on the active synthesis of its building blocks, called deoxyribonucleotides (dNTs; A, G, C, and T). DNA is made not only in the nucleus but also in chloroplasts and mitochondria; thus, dNTs must be either made in or transported to these organelles. Several alternative pathways transport and synthesize one of these nucleotides (T) for the nucleus and the organelles. These processes are important during seed germination and seedling establishment since a dry seed does not contain any dNTs. Thus, they have to be made prior to DNA replication.

Question: What is the concentration of dNTs during germination and seedling establishment? What is the importance of every alternative pathway that results in the formation of the "T" nucleotide? What are the consequences of lacking "T" for DNA synthesis in the nucleus and the organelles during germination and seedling establishment?

Findings: The concentration of nucleotides in germinating Arabidopsis seeds is constantly rising. The ratio of the different nucleotides seems to be first tailored to support DNA synthesis within chloroplasts. Analyzing a collection of mutants which are impaired in processes for the formation of "T", we found that the phosphorylation of thymidine within organelles is the most important process. Plants that are unable to phosphorylate thymidine have a reduced amount of DNA in chloroplasts and seedlings are pale. Interestingly, this effect is weaker in established seedlings and we assume that transport processes that change during seedling establishment are responsible for this phenomenon.

Next steps: Although we found thymidine to be a crucial metabolite for "T" formation we do not know which process generates it. We think that the transport of precursors for "T" over the plastidic membrane changes during seedling establishment, and our aim now is to identify transporters and characterize the process further.

triphosphates (dNTPs) and the concentration ratios of dNTPs to each other affect the mutation rate and the rate of DNA synthesis (Kohalmi et al., 1991; Buckland et al., 2014; Le Ret et al., 2018) and (2) the abundance of noncanonical dNTPs that arise from enzymatic or nonenzymatic processes can cause mutations. Thus, sanitizing dNT pools prevents DNA damage (Nagy et al., 2014). In some cases, the effects of purity and size of dNTP pools on the DNA are tightly interconnected. In mammals, the usage of the noncanonical deoxyuridine triphosphate (dUTP) by DNA polymerases depends on the size of the deoxythymidine triphosphate (dTTP) pool; thus, enzymes involved in dTTP synthesis influence its pool size and thereby modulate the effect of noncanonical dNTPs (Anderson et al., 2011; Schmidt et al., 2019; Martínez-Arribas et al., 2020). Some enzymes are hypothesized to contribute to both dNTP purity and pool size. For example, the enzyme dephosphorylating dUTP (dUTP PYROPHOSPHATASE 1 [DUT1]) has a role in sanitizing the dNTP pool (Dubois et al., 2011) but also a function in dTTP synthesis, since the product of this reaction (deoxyuridine monophosphate, [dUMP]) is also a precursor of dTTP (Guillet et al., 2006; Vértessy and Tóth, 2009).

For reproduction, many plants form dormant seeds, which upon stimulus germinate to reestablish a plant. Seed vigor is of high economic importance, as it determines successful germination and crop yield (Rajjou et al., 2012; Waterworth et al., 2015). In the dormant seed, nucleic acids are damaged and need to be repaired during germination (Waterworth et al., 2015). Much research has focused on how RNA and DNA are repaired during germination, but little is known about the metabolism of nucleic acid precursors, besides its importance for proper seedling development (Ashihara et al., 2020). Furthermore, dNTPs are mostly discussed as fueling DNA repair, but little attention has been paid to the aspect that imbalanced or too low dNTP concentrations cause faulty DNA replication and mutations (Buckland et al., 2014; Pedroza-García et al., 2019). Dormant seeds of Arabidopsis (*Arabidopsis thaliana*) and wheat (*Triticum aestivum*) have been shown not to contain dNTPs (Schimpff et al., 1978; Castroviejo et al., 1979; Straube et al., 2021a). Therefore, dNTPs must be synthesized during germination, consistent with a strong rise of dNTP concentrations after imbibition. These dNTP concentrations quickly reach a plateau, coinciding with the onset of DNA synthesis (Castroviejo et al., 1979).

DNA synthesis not only occurs in the nucleus, but also in mitochondria and chloroplasts. The nuclear, mitochondrial, and plastidic replication machineries need access to dNTPs, either requiring the presence of enzymes synthesizing dNTPs at each of these cellular locations or transport of dNTPs. Furthermore, for the on-site synthesis of dNTPs, transport processes are required, namely of precursors like deoxyribonucleosides (dNs) or dNT monophosphates or diphosphates (dNMPs, dNDPs). Organellar (i.e. chloroplastic and mitochondrial) dNTPs are currently thought to be supplied by a combination of transport and organellar synthesis where different transport processes, as well as distinct biosynthetic routes, are functionally redundant. This model is supported by a lack of phenotypic alterations in mutant plants lacking only a single metabolic route (Gorelova et al., 2017;

Downloaded from https://academic.oup.com/plcell/article/34/10/3790/6647853 by Technische Informationsbibliothek (TIB) user on 28 September 2022

Pedroza-García et al., 2019). Because most of these single knockouts have no altered phenotype, in this study, we assessed the influence of the different metabolic processes that contribute to dNT formation and especially the dTTP pool in plants on a molecular level, analyzing the dNT metabolome as a more sensitive readout.

It is not only necessary to ensure the dNTP supply, but the dNTP pool sizes in the cytosol and the organelles must be tailored to the different demands of each replication machinery. In mammalian cells, dNTPs are more abundant at the onset of DNA synthesis in the S-phase, suggesting a coordination of dNTP supply and demand (Franzolin et al., 2013; Stillman, 2013). In germinating seeds, the replication of the different genomes is asynchronous. Strong replication of the plastid genome precedes the mitochondrial and nuclear replication for at least 24 h (Barroco et al., 2005; Paszkiewicz et al., 2017). Therefore, the demand for dNTPs also differs between the nucleus, mitochondria, and chloroplasts during germination.

All dNTs can be synthesized from the respective ribonucleotide diphosphates (NDPs) by the action of a RIBONUCLEOTIDE REDUCTASE (RNR) localized in the cytosol (Lincker et al., 2004; Wang and Liu, 2006). The dNDPs require phosphorylation by NUCLEOTIDE DIPHOSPHATE KINASES (NDKs) to form dNTPs. However, for the synthesis of thymidylates, the RNR generates deoxyuridine diphosphate (dUDP) (Zrenner et al., 2006; Witte and Herde, 2020), which is dephosphorylated to dUMP. Then dUMP is methylated to deoxythymidine monophosphate (dTMP) before being phosphorylated to dTTP. The transfer of the methyl moiety to dUMP is catalyzed by DIHYDROFOLATE REDUCTASE-THYMIDYLATE SYNTHASE (DHFR-TS). In Arabidopsis, three isoforms of DHFR-TS exist; DHFR-TS1 is located in the cytosol, DHFR-TS2 is present exclusively in mitochondria while the third isoform probably has no catalytic function (Gorelova et al., 2017; Corral et al., 2018). Mutants lacking single DHFR-TS isoforms are phenotypically normal, suggesting that they are functionally redundant and that thymidylates (dTMP, deoxythymidine diphosphate [dTDP], or dTTP) can be transported across the mitochondrial membrane. Combining *dhfr-ts1* and *dhfr-ts2* loss-of-function mutants results in albino seeds occurring at a frequency supporting Mendelian inheritance, which emphasizes the crucial role for both isoforms in embryo development (Gorelova et al., 2017). Interestingly, the molecular basis for the conversion of the RNR product dUDP to the DHFR-TS substrate dUMP is unknown. Two alternative scenarios for this conversion can be envisioned. Either dUDP is dephosphorylated by a so far unknown dUDP phosphatase or dUDP is first phosphorylated to dUTP by a nucleotide diphosphate kinase (Zrenner et al., 2006; Witte and Herde, 2020) and subsequently converted to dUMP by the pyrophosphatase DUT1. A direct dephosphorylation of dUDP by DUT1 in plants seems unlikely, because DUT1 belongs to a protein family that is generally unable to dephosphorylate dNDPs (Vértessy and Tóth, 2009). In contrast to other metabolic routes, the formation of dTMP by RNR and DHFR-TS does not require dNs or other dNTs; thus, we refer to this pathway here as de novo T synthesis.

A fine-tuning of deoxycytidilate and thymidylate pools was observed in rice (*Oryza sativa*), which has an endogenous DEOXYCYTIDINE MONOPHOSPHATE (dCMP) DEAMINASE (DCD) that converts dCMP to dUMP, the substrate for dTMP synthesis by DHFR-TS (Xu et al., 2014). The protein is exclusively localized in mitochondria and a mutation abolishing enzyme function causes a strong increase in deoxycytidine triphosphate (dCTP) and a moderate reduction of dTTP levels concomitant with chlorosis and white leaf areas in young and in fully grown plants (Xu et al., 2014; Niu et al., 2017). A homolog of DCD was identified in Arabidopsis but no altered phenotype was observed in the respective loss-of-function mutant and the subcellular localization is unknown (Niu et al., 2017).

The formation of dTMP by several processes is followed by phosphorylation of dTMP to dTDP catalyzed by dTMP KINASE (TMPK, previously referred to as ZEU1; Ronceret et al., 2008). The *TMPK* gene generates transcripts that contain a long and a short open reading frame (ORF) encoding two proteins localizing in mitochondria and the cytosol, respectively (Ronceret et al., 2008). A possible dual localization of TMPK not only in mitochondria but also in chloroplasts has not been investigated yet since localization experiments were performed in onion (*Allium cepa*) peels, an experimental system in which plastidic localization can be overlooked (Ronceret et al., 2008; Osaki and Kodama, 2017).

Most dNs can be salvaged by DEOXYNUCLEOSIDE KINASE phosphorylating deoxyguanosine (dG), deoxyadenosine (dA), and deoxycytidine (dC) while for thymidine (dT) a separate enzyme, THYMIDINE KINASE (TK1), is required, which can also phosphorylate deoxyuridine (dU; Clausen et al., 2012). One TK1 isoform (TK1a) is located in the cytosol (Xu et al., 2015) while the second isoform (TK1b) is present in mitochondria and chloroplasts (Xu et al., 2015; Pedroza-García et al., 2019). In contrast to *tk1a*, *tk1b* mutant seedlings have chlorotic cotyledons but later develop normally (Clausen et al., 2012; Pedroza-García et al., 2019). Interestingly, a *tk1a tk1b* double mutant shows an albino phenotype and development is arrested at the four-leaf stage (Clausen et al., 2012; Pedroza-García et al., 2019), suggesting that de novo T synthesis alone is not sufficient to sustain DNA synthesis but that the salvage of dT is required to support the thymidylate pools. It has been reported that this double mutant can be rescued with carbohydrates in the media, which was attributed to a stimulation of de novo T synthesis (Pedroza-García et al., 2019). In addition, we recently demonstrated that dT can also be degraded in Arabidopsis by NUCLEOSIDE HYDROLASE 1 (NSH1; Straube et al., 2021a), influencing thymidine and thymidylate pools.

The expression profiles of genes potentially involved in thymidylate formation (*TK1a*, *TK1b*, *DHFR-TS1*, *DHFR-TS2*, *DCD*, *DUT1*, and *TMPK*) were investigated during germination and seedling establishment (Narsai et al., 2011). While the

Downloaded from https://academic.oup.com/plcell/article/34/10/3790/6647853 by Technische Informationsbibliothek (TIB) user on 28 September 2022

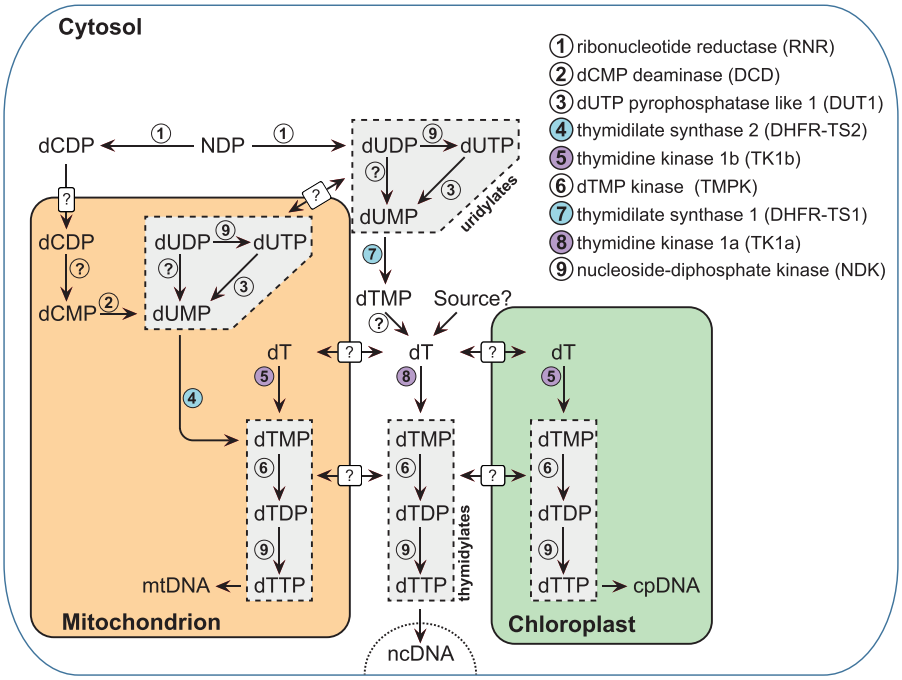

Figure 1 Proposed model of thymidylate metabolism in *A. thaliana* during germination and seedlings establishment. Enzymes putatively involved in the formation of thymidylate pools and their subcellular localization are shown. Question marks indicate currently unknown enzymes or transporters allowing an exchange of nucleosides and nucleotides between the cytosol, the chloroplast, and the mitochondrion. Enzymes of the de novo thymidylate synthesis pathway are colored in blue while enzymes of the salvage pathway are colored in purple. The localization of DUT1 in plastids is not shown. Deoxycytidine diphosphate (dCDP); thymidine (dT); deoxythymidine monophosphate (dTMP).

transcript of *TK1b* is abundant and present already in dry seeds, transcripts of all other genes are increased rapidly upon transfer to long-day growth conditions (Supplemental Figure S1). This observation suggests that the enzymes hypothesized to contribute to thymidylate formation (Figure 1) play a role during germination and seedling establishment.

Both de novo T synthesis of dNTPs via RNR (reductive pathway) and the salvage of dNs seem to be important during germination, with salvage activity preceding the activity of RNR in time. Several studies concerning the DNA synthesis during germination used the application of labeled dT, or sometimes dA and dC, and their incorporation into DNA as a readout for DNA synthesis (Castroviejo et al., 1979; Dellaquila et al., 1980; Strugala and Buchowicz, 1984; Marciniak et al., 1987; Stasolla et al., 2002). The reductive pathway was assessed with labeled cytidine and uridine whose incorporation into DNA requires the action of RNR (Schimpff et al., 1978; Stasolla et al., 2002). Soon after imbibition, salvage activity assessed by incorporation of dNs into DNA was already active, whereas activity of the reductive pathway was only observed at later stages of germination and depended on seed age (Schimpff et al., 1978). Fresh wheat (*T. aestivum*) seeds contained an unknown compound inhibiting the RNR, but dN incorporation (salvage) was not affected by this inhibitor (Schimpff et al., 1978; Baumann et al., 1984). Further evidence that the salvage pathway is active early on is derived from experiments utilizing hydroxyurea, an inhibitor of the RNR, showing a steady incorporation of labeled dT in the first hours of germination (Thornton et al., 1993). These experiments all rely on the exogenous feeding of nucleosides and demonstrate that germinating seeds have the capacity to incorporate dNs by salvage. However, it is not known whether salvage actually takes place under conditions where pool sizes are not manipulated. The contribution of salvage to the dNT pools in vivo remains unclear. Furthermore, little is known about the amounts and origins of dNs in dormant or germinating seeds (Straube et al., 2021a). Hitherto it was speculated that dNs are derived from DNA degradation or dNTP dephosphorylation, but no evidence has been presented so far (Bryant, 1980).

In this study, we monitored the nucleotide and nucleoside metabolome in germinating seeds and demonstrate that dNTs are synthesized very early in germination, long before the onset of DNA synthesis. Furthermore, we created and analyzed a collection of mutants abolished in enzymatic activities of all known processes for thymidylate formation. We conclude that thymidine salvage in organelles contributes predominantly in germinating seeds to the thymidylate pool and has a strong impact on other dNT pools as well as on chloroplast DNA (cpDNA) synthesis during early seedling establishment.

Results

An alternative ORF encodes a DUT1 version that localizes in mitochondria and chloroplasts

To investigate the impact of the different metabolic routes on the formation of the thymidylate pool, a collection of

Downloaded from https://academic.oup.com/plcell/article/34/10/3790/6647853 by Technische Informationsbibliothek (TIB) user on 28 September 2022

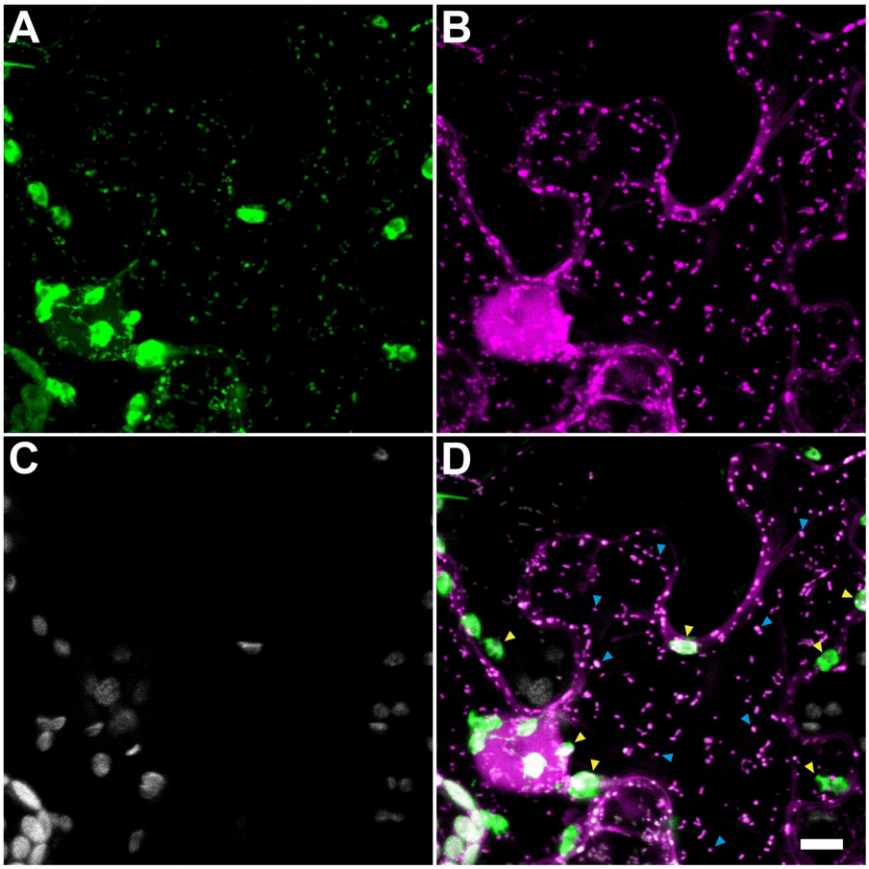

Figure 2 Subcellular localization of DUT1 translated from a full-length transcript. Confocal microscopy images of a *N. benthamiana* leaf transiently expressing DUT1 as C-terminal-tagged eYFP fusion protein (Pro_{35S}:*DUT1:eYFP*) from a longer transcript than previously annotated containing 5′-prolonged ORF encoding 41 additional amino acids at the N-terminal end. A mitochondrial marker protein (*Sc*COXIV:mCherry) was co-expressed. Images were taken 3 days after agrobacteria infiltration. A, eYFP:DUT1, B, mitochondrial marker Sc.COXIV:mCherry, C, chloroplast autofluorescence, and D, overlay of A, B, and C. Exemplary, selected mitochondria, and chloroplasts showing dual localization are marked with blue and yellow arrowheads, respectively. Scale bars = 10 μm.

mutants lacking these processes was created. Mutant plants lacking steps of salvage, C-to-T conversion, and de novo T synthesis (Figure 1) located in cytosol and organelles, were available from previous studies (Clausen et al., 2012; Gorelova et al., 2017; Niu et al., 2017). However, DUT1, which may be involved in the formation of dTMP via the generation of the DHFR-TS substrate dUMP (Figure 1), is less characterized and a complete loss-of-function mutant of *DUT1* is likely not viable (Dubois et al., 2011). We observed the presence of several RNA-seq reads mapping upstream of the 5′-UTR (untranslated region) predicted by The Arabidopsis Information Resource, version 10, suggesting the presence of an alternative transcription start site. This longer transcript contains an extended ORF that encodes the original protein plus 41 additional amino acids at the N-terminus that are predicted to constitute a transit peptide. The coding sequence (CDS) of enhanced yellow fluorescent protein (eYFP) was fused to the 3′-end of the extended ORF and the construct was transiently expressed under the control of a constitutive promoter (Pro_{35S}) in *Nicotiana benthamiana* leaves. A signal consistent with cytosolic and nuclear as well as mitochondrial and plastidic localization of the fusion protein was detected with confocal microscopy (Figure 2A). The mitochondrial and plastidic localization was corroborated by an overlay with the signal of a mitochondrial marker (yeast COXIV transit peptide fused to mCherry fluorescent protein; Nelson et al., 2007) and the chloroplast autofluorescence, respectively (Figure 2, B–D).

Since the mitochondrial localized DUT1 might alone provide the substrate for DHFR-TS2, whose loss-of-function does not lead to phenotypic alterations (Gorelova et al., 2017), we speculated that a mutant abolished in organellar DUT1 function is viable. We used a CRISPR (clustered regularly interspaced short palindromic repeats) approach to introduce a lesion between the first and second start codon of the respective ORFs (Supplemental Figure S2, A and B) that results in exclusive disruption of the ORF encoding the organellar localized DUT1. A homozygous $dut1_{org}$ mutant lacking the T-DNA used for its creation was isolated and is phenotypically inconspicuous (Supplemental Figure S2C). DNA from the $dut1_{org}$ mutant was used as a template to amplify the full-length CDS including the genetic lesion. A construct encoding this mutated variant of DUT1 fused to eYFP was generated. In contrast to the wild-type fusion

Downloaded from https://academic.oup.com/plcell/article/34/10/3790/6647853 by Technische Informationsbibliothek (TIB) user on 28 September 2022

protein, the mutant variant was exclusively found in the cytosol/nucleus (Supplemental Figure S2D), demonstrating that our approach to disrupt only the ORF encoding the organellar localized DUT1 was successful.

It has been reported that the subcellular localization of DHFR-TS may vary depending on the tissue (Gorelova et al., 2017). Therefore, we determined the localization of all organellar proteins involved in the formation of the thymidylate pool to demonstrate their subcellular location in an establishing seedling. The subcellular localization of DCD, DHFR-TS2, and TK1b in roots and cotyledons of germinating seeds (2 days after transfer to long-day growth conditions) was assessed using transgenic plants constitutively expressing the respective eYFP fusion proteins (Supplemental Figures S3 and S4). In line with previous studies, DHFR-TS2 was exclusively observed in mitochondria while TK1b was localized in mitochondria and chloroplasts (Supplemental Figures S3, A–D and S4, B and C; Gorelova et al., 2017; Corral et al., 2018; Pedroza-García et al., 2019). Consistent with results for the DCD in rice, we also observed a mitochondrial localization of the homolog in Arabidopsis (Supplemental Figures S3, E and F and S4A). We found that TMPK is present in chloroplasts in addition to the already described localization in mitochondria (Ronceret et al., 2008) by expressing the TMPK:eYFP fusion protein in *N. benthamiana* (Supplemental Figures S3G and S4E).

Only the disruption of organellar salvage and de novo T synthesis alters the phenotype of seedlings

While a complete blockage of either de novo T synthesis or salvage of dT in the cytosol and the organelles is lethal (*tk1a tk1b* or *dhfr-ts1 dhfr-ts2*), loss-of-function mutants of any single gene are phenotypically normal with the exception of the *tk1b* mutant whose cotyledons are chlorotic (Clausen et al., 2012; Xu et al., 2015; Gorelova et al., 2017; Pedroza-García et al., 2019). We performed a side-by-side comparison of seedlings grown on soil from all single mutants (*tk1a* cytosolic salvage; *tk1b* salvage in organelles, *dhfr-ts1* cytosolic de novo T synthesis, *dhfr-ts2* mitochondrial de novo T synthesis; $dut1_{org}$ putative function in de novo T synthesis in mitochondria; *dcd* C-to-T conversion in mitochondria). We photographed individual seedlings (Figure 3A) and quantified the green and yellow pixels (Figure 3B) in the respective micrographs from different time points to gain quantitative insight into the chlorosis previously observed for the *tk1b* mutant. Consistent with the previous reports, only *tk1b* mutants displayed chlorosis, further emphasizing the importance of dT salvage in mitochondria and chloroplasts for the fitness of the seedling. We also determined relative growth rates from 3 to 4 and 4 to 5 days after transfer to long-day growth conditions of plants from all genotypes and did not observe any significant differences between mutants and wild-type (Supplemental Figure S5).

We reasoned that the phenotype of the *tk1b* mutant is probably caused by increased thymidine and decreased thymidylate pools and that therefore visualizing the impact of other processes such as the de novo T synthesis might be facilitated in the *tk1b* mutant background. Plants of this background were thus crossed with *dhfr-ts1*, *dhfr-ts2*, *dcd*, and $dut1_{org}$ mutants, respectively. Interestingly, the *tk1b dhfr-ts2* double mutant displayed a markedly stronger chlorosis together with white areas on the cotyledons that are not observed in the *tk1b* single mutant (Figure 3A). While the cotyledons of the *tk1b* single mutant recover and accumulate more green pigment over time until they are indistinguishable from wild-type, the white areas in the *tk1b dhfr-ts2* double mutant do not recover (Supplemental Figure S6A). A pronounced fold difference between the cpDNA/nuclear DNA (ncDNA) ratios of wild-type and *tk1b* as well as *tk1b dhfr-ts2* mutants 2 days after transfer to long-day growth conditions is progressively reduced at later time points (6 and 10 days; Supplemental Figure S6B) concomitant with the visual recovery. At 10 days, the ratio of cpDNA/ncDNA in the *tk1b* mutant compared to the wild-type was not significantly different anymore while a small difference between wild-type and *tk1b dhfr-ts2* was still present (Supplemental Figure S6B). At early time points, dT salvage but not de novo T synthesis plays apparently the main role for supplying thymidylates for cpDNA synthesis. Interestingly, in dry seeds no significant differences in cpDNA can be observed, suggesting that TK1b and DHFR-TS2 are predominantly important during germination rather than embryo development (Supplemental Figure S6B). The synergistic effect of *tk1b* and *dhfr-ts2* on the chlorosis suggests that predominantly salvage in mitochondria and chloroplasts but also de novo T synthesis in mitochondria contribute to plant fitness. Rarely, but exclusively in the *tk1b dhfr-ts2* double mutant population, we also observed plants with completely albinotic sections (Supplemental Figure S6C) suggesting that abolished thymidine salvage and thymidylate de novo T synthesis together can sometimes also affect the phenotype of an adult plant. Overall, the data show that the lack of the organellar enzymes cannot be fully compensated by the cytosolic isoenzymes (TK1a and DHFR-TS1).

dNTs and dN pools increase rapidly during early seedling establishment

We hypothesized that the impact of *tk1b* and *tk1b dhfr-ts2* mutants on the phenotype of seedlings is the result of altered thymidine and thymidylate formation during germination. Since comprehensive data on the nucleotide metabolome of plants is scarce (Straube et al., 2021b, 2021a), our first objective was to monitor the (d)NT and (d)N pool formation during germination. We recently established a protocol to comprehensively monitor the nucleotide and nucleoside metabolome (Straube et al., 2021a) and used this technique to investigate germination and seedling establishment.

The treatment of the seeds was identical as described in transcriptome studies (Narsai et al., 2011; Law et al., 2014) and a study on nuclear, chloroplast, and mitochondria DNA

Downloaded from https://academic.oup.com/plcell/article/34/10/3790/6647853 by Technische Informationsbibliothek (TIB) user on 28 September 2022

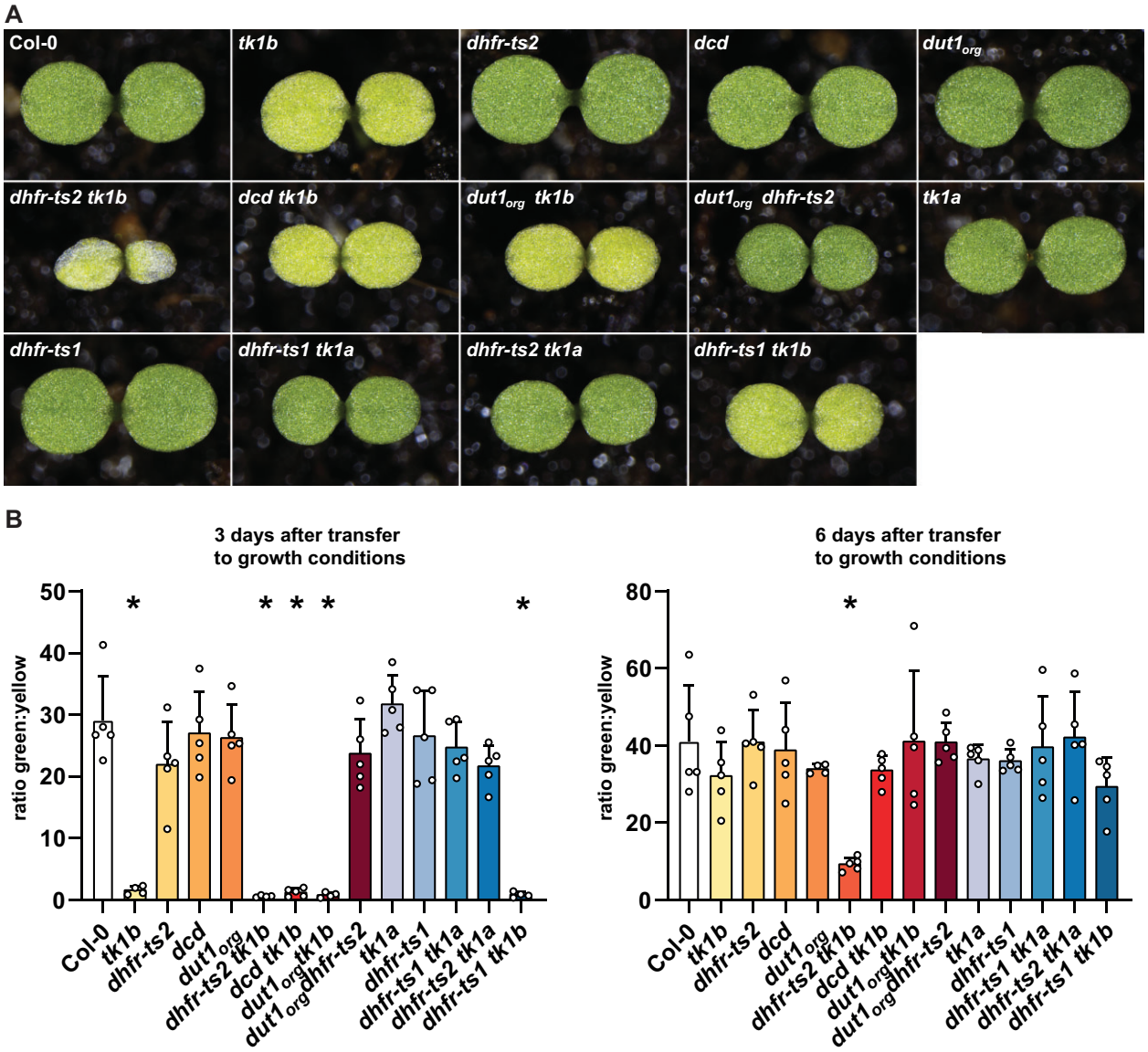

Figure 3 Phenotypes of wild-type and mutant seedlings lacking enzymes putatively involved in thymidylate homeostasis. Seedlings of all mutants and double mutants used in this study were grown on soil and photographed 3 days after transfer to long-day growth conditions. A, Images are representative for four to five individual plants. B, Quantification of the ratio between green and yellow pixels of each genetic variant. Images of seedlings 3 and 6 days after transfer to long-day growth conditions were analyzed. Two-sided Tukey's pairwise comparisons using the sandwich variance estimator were used for statistical analysis. Asterisks indicate significant differences ($P < 0.05$) to Col-0. Four to five biological replicates (individual plants) were analyzed. Error bars are SD. Adjusted *P*-values for multiple comparisons can be found in Supplemental Data Set 2.

replication (Paszkiewicz et al., 2017) to allow comparability. Seeds were imbibed at 4°C for 48 h in the dark and then transferred to long-day growth conditions (16-h light, 22°C) and monitored for 6 days (144 h). In our recent report (Straube et al., 2021a), we did not observe dT and dC in dry wild-type seeds, whereas small amounts of these nucleosides were quantified here (Figure 4B). This is likely due to an improved disruption of seed tissue and a refined metabolite separation in this study. While there was a slight increase of dNTP concentrations during the incubation at 4°C, dT, dC, and dTMP did not change. However, upon transfer to long-day growth conditions, dNTP and also dT concentrations increased rapidly within a few hours. Note that the dT pool was in general 10 times larger than the dC pool, whereas the dTTP concentration exceeded that of dCTP only two- to three-fold. The increase of the dTMP pool was delayed by 24 h compared to the dT and dNTP pools, suggesting that initially dTMP was consumed for dTTP production as rapidly as it was made (Figure 4, A and B).

Ribonucleotide mono and triphosphates, especially ATP (adenosine triphosphate) but also UMP (uridine monophosphate) and UTP (uridine triphosphate) (Supplemental Figure S7, A and B), were rising in concentration over time, similar to dNTPs, suggesting that pyrimidine de novo biosynthesis was creating the substrates for RNR and the subsequent de novo T synthesis of thymidylates.

Downloaded from https://academic.oup.com/plcell/article/34/10/3790/6647853 by Technische Informationsbibliothek (TIB) user on 28 September 2022

Interestingly, the dATP (deoxyadenosine triphosphate) and dTTP concentrations decreased after an initial burst but then rose again. This short-term reduction, more pronounced for dATP, corresponds with the onset of chloroplast DNA (cpDNA) replication at 6 h after transfer to long-day growth conditions (Paszkiewicz et al., 2017). The amount of dNTPs needed for cpDNA replication is substantial. In a conservative estimation, we calculated that at least 4.3-nmol dTTP is required per gram seed (see "Material and methods")—this amount is easily accessible with LC–MS (liquid chromatography–mass spectrometry). It is tempting to speculate that the pool size changes in this phase reflect a stronger consumption of dATP and dTTP than of dCTP and dGTP (deoxyguanosine triphosphate) because the chloroplast genome is rather A/T rich—the GC content of cpDNA is 36%.

One can calculate the GC content of the dNTPs that is the sum of dGTP and dCTP amounts as a percentage of the total amount of dNTPs. We previously suggested that this GC content of the dNTPs correlates with the GC content of genomes in plants and algae (Straube et al., 2021a). Because in germination the chloroplastic genome is replicated earlier than the nuclear genome, we wanted to assess whether the GC content of the dNTPs is specifically adjusted for the distinct phases of germination. Interestingly, we found that between 24 and 48 h after transfer to long-day growth conditions, when mainly cpDNA is made (Paszkiewicz et al., 2017), the GC content in dNTPs is higher (40%) than at later time points (30%; Figure 4C). We reported previously a content of 30% for adult Arabidopsis plants (Straube et al., 2021a). Indeed, it seems that the dNTP GC content is adjusted for cpDNA replication, but this does not relate to the GC contents of the chloroplastic and the nuclear genomes (both 36%). Maybe these adjustments of the dNTP GC content reflect different requirements of the evolutionarily unrelated polymerases (Mori et al., 2005; Parent et al., 2011) that replicate the cpDNA and ncDNA.

During germination the lack of organellar DUT1 reduces the dT pool, which is suppressed by an abolished organellar salvage of thymidine

The seedling phenotype of *tk1b* and *tk1b dhfr-ts2* mutants (Figure 3) and the rapid formation of dT and thymidylates during germination (Figure 4, A and B) prompted us to study the nucleotide metabolome of all available mutants (Figure 3A). Previously none of these mutants had been analyzed regarding the nucleotide metabolome, which may be disturbed although most of the mutants are phenotypically inconspicuous. Based on the results of the time course (Figure 4A), we chose one time point in the germination and two time points in the seedling establishment phase (3 h "germination," 48 h "early seedling establishment," 144 h "late seedling establishment" after transfer to long-day growth conditions). These reflect an initial phase of dNTP pool increase (3 h), a strong increase of pool sizes (48 h) and a last phase of decreasing dNTP pool sizes (144 h).

During germination (3 h), seeds from wild-type and all mutant plants contained roughly similar amounts of dNs and dNTs (Figure 5), suggesting that a lack of the investigated enzymes does not cause disturbances during embryogenesis that affect the thymidylate pools in the seed. The sink demand for dNTs is still low at 3 h because cpDNA biosynthesis is just beginning (Paszkiewicz et al., 2017). Thus, metabolic fluxes through the dNTP pools are probably small. We observed a decrease of the dT pool in the $dut1_{org}$ mutant compared to the wild-type. Assuming that $DUT1_{org}$ provides the substrate dUMP for dTMP biosynthesis and thus the lack of $DUT1_{org}$ interferes with dTMP production, the cytosolic and organellar dT salvage by the TKs compensate for the reduced dTMP synthesis resulting in depletion of the dT pool in the mutant. In fact, dT pools were restored to wild-type levels and even surpassed these in the $dut1_{org}$ *tk1b* double mutant, suggesting that dT salvage in organelles and the cytosol is indeed responsible for depletion of the dT pool in the $dut1_{org}$ mutant. Interestingly, no differences in dT pools were observed in mutants lacking de novo dTMP biosynthesis (*dhfr-ts1* and *dhfr-ts2*) compared to the wild-type, although DHFR-TS1 and DHFR-TS2 directly form dTMP from dUMP.

The observation that wild-type dT levels are surpassed in the $dut1_{org}$ *tk1b* double mutant suggests that yet another process might be involved—possibly reduced dT degradation. We showed recently that dT can be degraded by the NSH1 in seedlings (Straube et al., 2021a) and it is tempting to speculate that compromised dTMP biosynthesis, caused by a putatively reduced dUMP pool in the $dut1_{org}$ mutant, results in reduced dT degradation by inhibition of NSH1. We attempted to monitor xanthosine accumulation as an indicator for NSH1 inhibition; however, no effect in the $dut1_{org}$ mutant compared to the wild-type was observed (Supplemental Figure S8). Regarding dTTP, no significant effects other than a slightly increased level in the *dhfr-ts1* mutant were observed (Figure 5C). Furthermore, there is no contribution of C-to-U conversion by DCD to the formation of thymidylates during germination.

We also monitored the ratio of chloroplast/nuclear and mitochondrial/ncDNA in the wild-type and all mutants by qPCR (quantitative polymerase chain reaction). We observed a reduction of cpDNA, but not mitochondrial DNA (mtDNA; Figure 6; Supplemental Figure S9A), only in the *tk1b* mutant compared to the wild-type, indicating that already at this early time point in germination organellar dT salvage is crucial for the synthesis of cpDNA. A lack of the respective enzyme cannot be fully compensated by the cytosolic counterpart (TK1a). One needs to bear in mind that at this early time point only little cpDNA synthesis occurs, thus metabolic fluxes are probably small, but apparently thymidine salvage already contributes to the production of thymidylates.

Downloaded from https://academic.oup.com/plcell/article/34/10/3790/6647853 by Technische Informationsbibliothek (TIB) user on 28 September 2022

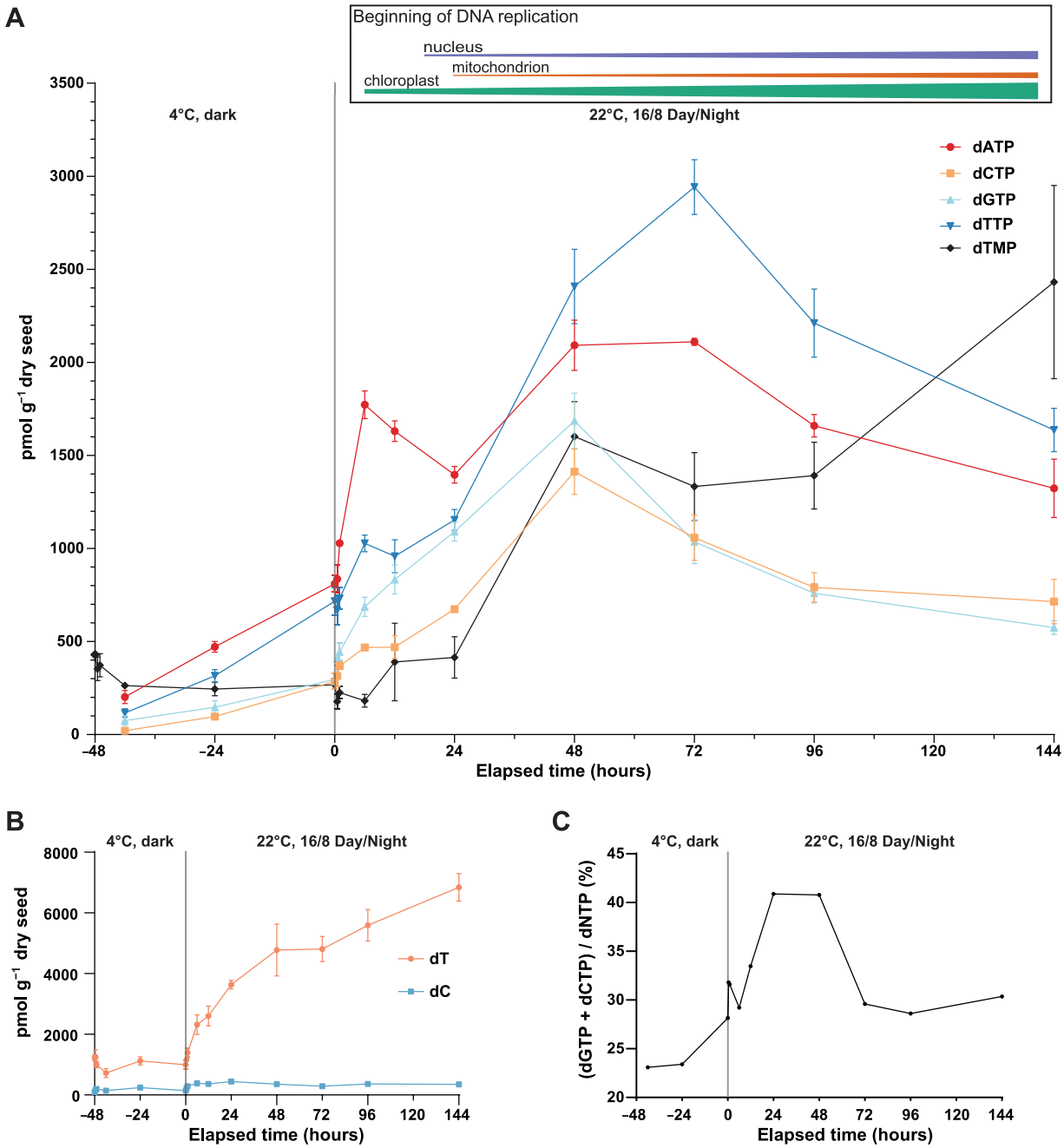

Figure 4 Concentration of dNTs and dNs at different time points during seed germination and in the establishing seedling. Concentrations of (A) all canonical dNTPs as well as dTMP and (B) dT and dC were quantified with LC–MS before transfer to long-day growth conditions (−48 h, −47.5 h, −42 h, −24 h; dark and 4°C), at transfer to long-day growth conditions (0 h, light and 22°C) and after the transfer to long-day growth conditions (0.5, 1, 6, 12, 24, 48, 72, 96, and 144 h). While seeds at the −48 h time point were dry all other samples were imbibed in water. At the −48, −47.5, and −42 h time points no reliable signal for dNTPs was detected. The onset of nuclear, plastid, and mtDNA replication, as reported by Paszkiewicz et al. (2017), Masubelele et al. (2005); and Sliwinska et al. (2009) is displayed by purple, green, and orange bars respectively in (A). C, Time course of the sum of dGTP and dCTP amounts as a percentage of the total amount of dNTPs. Four biological replicates (pooled seeds/seedlings) were analyzed. Error bars are SD.

During early seedling establishment, a lack of organellar dT salvage strongly interferes with chloroplast genome replication and globally affects the nucleotide metabolome

We tested the impact of mutants in the salvage, de novo T synthesis, and C-to-U conversion on the dN and dNT pools during early seedling establishment (48 h after transfer to long-day growth conditions) and observed the most severe effects at this time point (Figure 7). Mutants in the organellar salvage (*tk1b*; $P = 0.052$) and more pronounced in the cytosolic salvage (*tk1a*) showed an accumulation of dT, suggesting that both metabolic pathways are active

Downloaded from https://academic.oup.com/plcell/article/34/10/3790/6647853 by Technische Informationsbibliothek (TIB) user on 28 September 2022

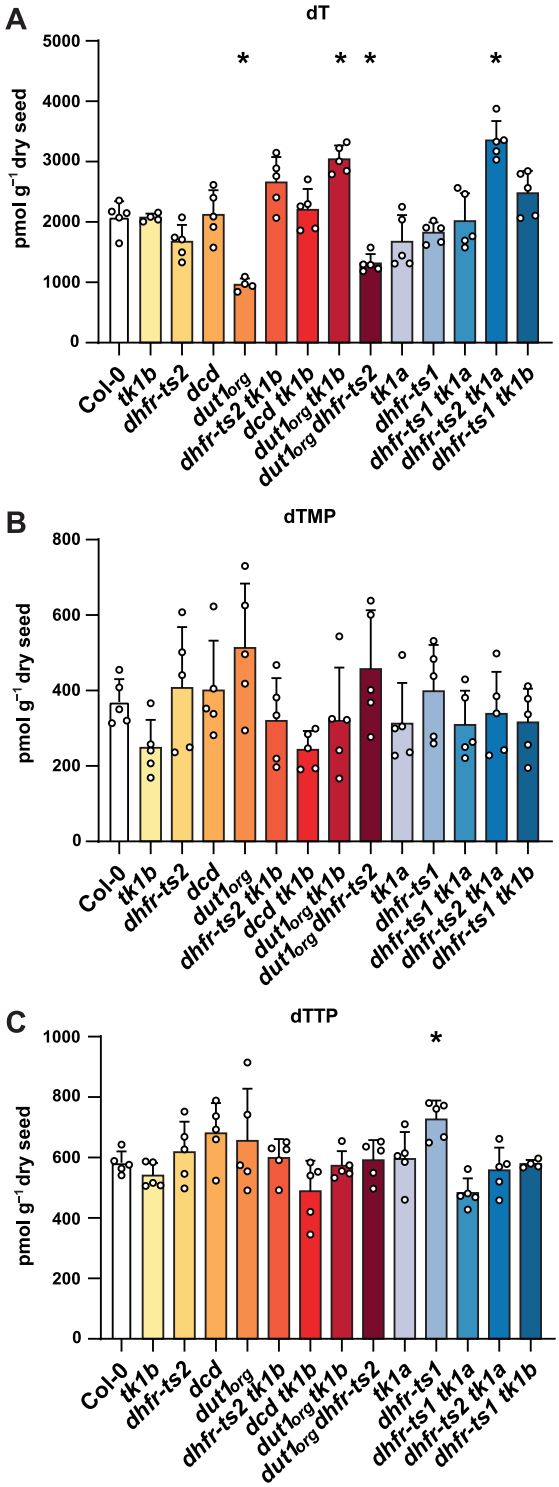

Figure 5 Concentration of thymidine and thymidylates in wild-type and mutant seeds lacking enzymes putatively involved in thymidylate homeostasis during germination. Seeds were imbibed in water for 48 h at 4°C in the dark, transferred for 3 h to long-day growth conditions and harvested for LC–MS analysis. Concentrations of (A) dT, (B) dTMP, and (C) dTTP in seeds are shown. Two-sided Tukey's pairwise comparisons using the sandwich variance estimator were used for statistical analysis. Asterisks indicate significant differences ($P < 0.05$) to Col-0. Four to five biological replicates (pooled seedlings) were analyzed. Error bars are SD. Adjusted *P*-values for multiple comparisons can be found in Supplemental Data Set 2.

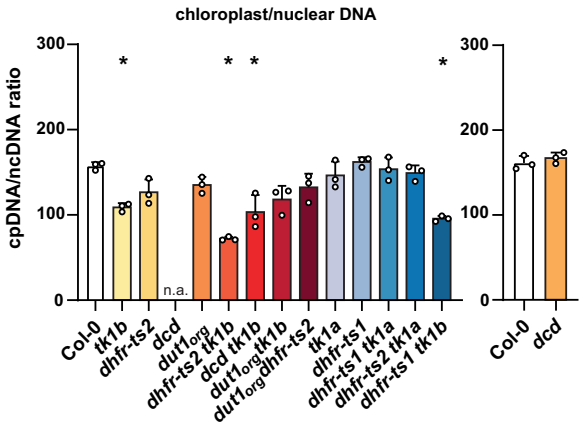

Figure 6 Abundance of the cpDNA relative to the ncDNA in wild-type and mutants lacking enzymes putatively involved in thymidylate homeostasis during germination. Seeds were imbibed in water for 48 h at 4°C in the dark then transferred for 3 h to long-day growth conditions and harvested. qPCR was performed with primers amplifying one gene from cpDNA (*RBCL*) and ncDNA (*UBC21*), respectively. The cpDNA/ncDNA ratios were calculated from Ct values for the respective genes. Ratios for the *dcd* mutant and the wild-type were analyzed in a separate experiment due to a technical error. Two-sided Tukey's pairwise comparisons using the sandwich variance estimator were used for statistical analysis. Asterisks indicate significant differences ($P < 0.05$) to Col-0. Three biological replicates (pooled seedlings) were analyzed. Error bars are SD, n.a. indicates that the value is not available. Adjusted *P*-values for multiple comparisons can be found in Supplemental Data Set 2.

(Figure 7A). These observations suggest that not only the organellar but also the cytosolic salvage pathway are active to form thymidylates at this developmental stage.

However, in the *tk1b* and *dhfr-ts2* single mutants, the amounts of dTMP were reduced (Figure 7B), demonstrating that during early seedling establishment not only organellar salvage but also mitochondrial de novo biosynthesis of dTMP contributes to the thymidylate pool. A reduction of dTMP was also observed in all double mutants with abolished *tk1b* function, while a *tk1b dhfr-ts2* double mutant has similar amounts of dTMP compared with the *tk1b* single mutant, suggesting that the impact of *dhfr-ts2* and *tk1b* on dTMP are not additive. While the *dhfr-ts2* single mutant has a reduced dTMP level compared to the wild-type, we do not observe this effect in the *dut1$_{org}$ dhfr-ts2* and *tk1a dhfr-ts2* double mutants for unknown reasons. We hypothesize that the observed reduction of total dTMP in the *tk1b* background reflects mainly a reduction of the chloroplast and mitochondrial dTMP pools because TK1b is located in these organelles. Total dTMP levels are neither altered in the *dhfr-ts1* and *tk1a* single mutants nor in the *dhft-ts1 tk1a* double mutant (Figure 7B). Apparently, dTMP generation in the organelles can compensate for a defect of dTMP production in the cytosol but not vice versa. Especially the salvage of dT in the organelles cannot be compensated by cytosolic dT salvage, which is nonetheless clearly active at this time point (see effect of *tk1a* mutation on dT in Figure 7A). This may

Downloaded from https://academic.oup.com/plcell/article/34/10/3790/6647853 by Technische Informationsbibliothek (TIB) user on 28 September 2022

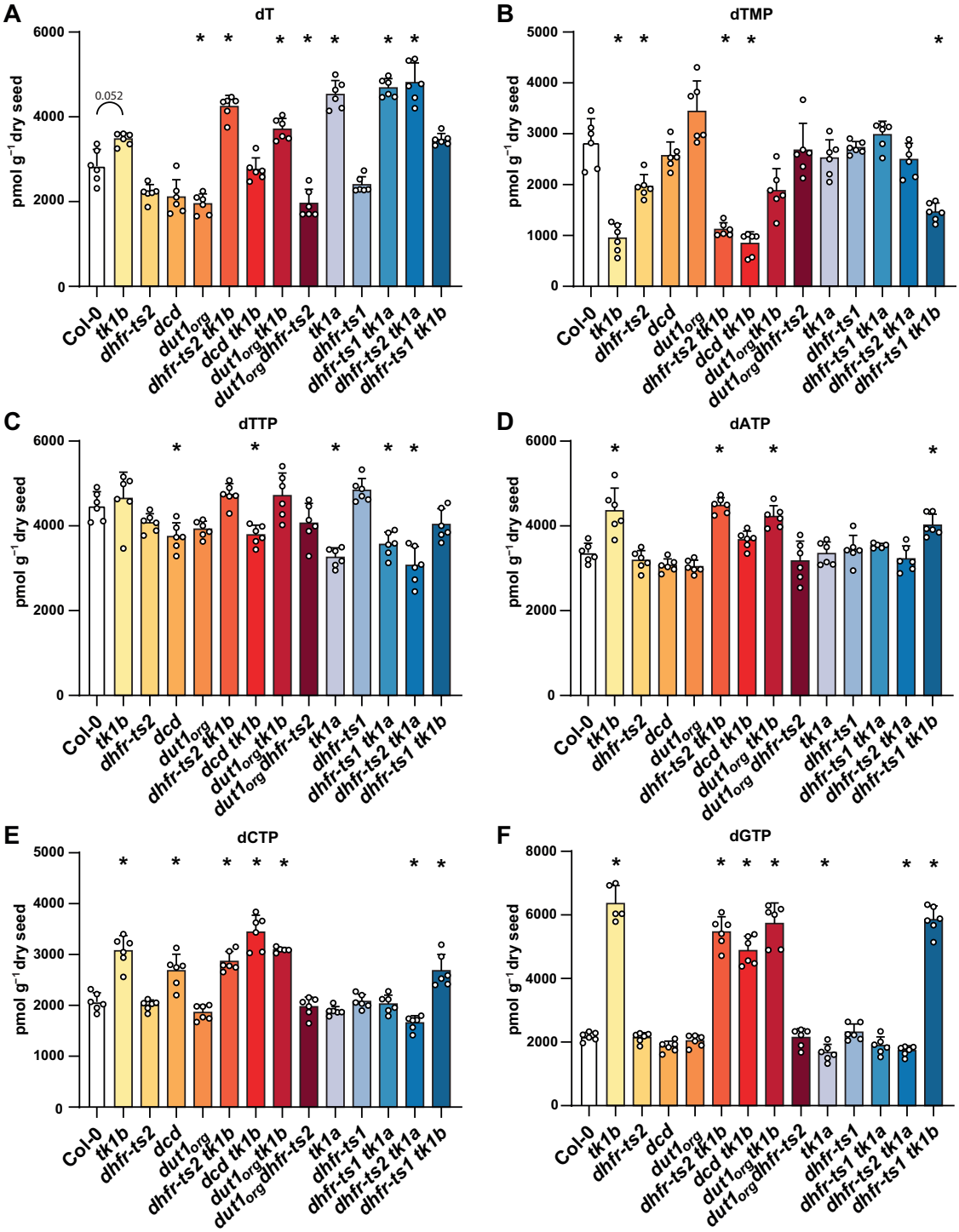

Figure 7 Concentrations of dT, dTMP, and dNTPs in wild-type and mutants lacking enzymes putatively involved in thymidylate homeostasis during early seedling establishment. Seeds were imbibed in water for 48 h at 4°C in the dark, transferred for 48 h to long-day growth conditions and harvested for LC–MS analysis. Concentrations of (A) dT, (B) dTMP, (C) dTTP, (D) dATP, (E) dCTP, and (F) dGTP in germinating seed are shown. Two-sided Tukey's pairwise comparisons using the sandwich variance estimator were used for statistical analysis. Asterisks indicate significant differences ($P < 0.05$) to Col-0; $P > 0.05$ are indicated if value comparisons are made in the text. Five to six biological replicates (pooled seedlings) were analyzed. Error bars are SD. Adjusted *P*-values for multiple comparisons can be found in Supplemental Data Set 2.

be explained by a low capacity for thymidylate import into the organelles.

Interestingly, the amounts of dTTP were not as different as those of dTMP between any of the mutants and the wild-type (Figure 7C). We showed that in the *tk1b* mutant, due to the lack of thymidylates, the replication of the chloroplast genome severely slowed down (Supplemental Figure S6B), probably because the plastidic dTTP pool is depleted.

Downloaded from https://academic.oup.com/plcell/article/34/10/3790/6647853 by Technische Informationsbibliothek (TIB) user on 28 September 2022

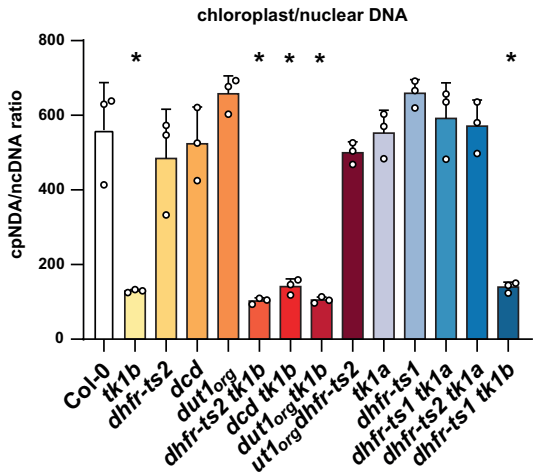

Figure 8 Abundance of the cpDNA relative to the ncDNA in wild-type and mutants lacking enzymes putatively involved in thymidylate homeostasis during early seedling establishment. Seeds were imbibed in water for 48 h at 4°C in the dark, transferred for 48 h to long-day growth conditions and harvested. qPCR was performed with primers amplifying one gene from cpDNA (*RBCL*) and ncDNA (*UBC21*), respectively. The cpDNA/ncDNA ratios were calculated from Ct values for the respective genes. Two-sided Tukey's pairwise comparisons using the sandwich variance estimator were used for statistical analysis. Asterisks indicate significant differences ($P < 0.05$) to Col-0. Three biological replicates (pooled seedlings) were analyzed. Error bars are SD. Adjusted *P*-values for multiple comparisons can be found in Supplemental Data Set 2.

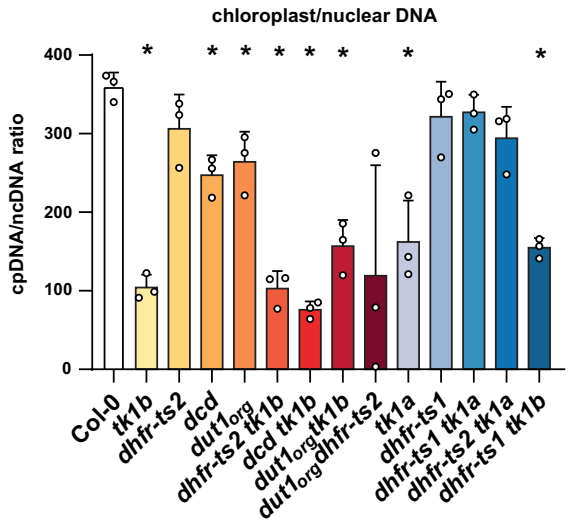

Figure 9 Abundance of the cpDNA relative to the ncDNA in wild-type and mutants lacking enzymes putatively involved in thymidylate homeostasis during late seedling establishment. Seeds were imbibed in water for 48 h at 4°C in the dark, transferred for 144 h to long-day growth conditions and harvested. qPCR was performed with primers amplifying one gene from cpDNA (*RBCL*) and ncDNA (*UBC21*), respectively. The cpDNA/ncDNA ratios were calculated from Ct values for the respective genes. Two-sided Tukey's pairwise comparisons using the sandwich variance estimator were used for statistical analysis. Asterisks indicate significant differences ($P < 0.05$) to Col-0. Three biological replicates (pooled seedlings) were analyzed. Error bars are SD. Adjusted *P*-values for multiple comparisons can be found in Supplemental Data Set 2.

The measured dTTP would, in this case, reflect the cytosolic and mitochondrial pools, but these are not consumed since ncDNA and mtDNA replication is negligible at this time point in germination (Paszkiewicz et al., 2017). In line with this hypothesis, no differences in dTTP concentrations were observed between *tk1b* and the wild-type. Consistent with a probable arrest of cpDNA replication in the *tk1b* mutant, we observed significantly elevated concentrations of the other DNA building blocks (dGTP, dATP, and dCTP) compared to the wild-type (Figure 7, D–F). These probably accumulate in *tk1b* because they are not consumed for cpDNA replication. Interestingly, the amount of building blocks that accumulate is about the same as that required for cpDNA synthesis during germination (see "Materials and methods" for an estimation). Furthermore, we observed elevated levels of NTPs (Supplemental Figure S10) in the *tk1b* background compared to the wild-type, suggesting that an arrest of cpDNA replication reduces the template required for transcription, resulting in the accumulation of RNA building blocks.

We also assessed the cpDNA copy number in mutant and wild-type plants at 48 h after transfer to long-day growth conditions. The ratio of cpDNA to ncDNA did not change significantly between the 3 and the 48-h time points in the *tk1b* mutant, whereas it increased almost 3.5-fold in the wild-type (Figures 6 and 8). The halt of cpDNA synthesis in the *tk1b* mutant combined with the ongoing synthesis in the wild-type resulted in a 4.3-fold difference of the cpDNA/ncDNA ratio between wild-type and *tk1b* and also all double mutants with *tk1b* background at 48 h, indicative of cpDNA replication arrest in *tk1b*. No differences were observed in the mtDNA/ncDNA ratios between the wild-type and mutants (Supplemental Figure S9B), which is in line with previous observations that mtDNA and ncDNA replication is negligible in this phase of germination (Paszkiewicz et al., 2017). We supported this result using additional loci on the chloroplast and mitochondrial genomes and confirmed our initial observation (Supplemental Figure S11).

In established seedlings, organellar salvage, and mitochondrial de novo T synthesis are still active but less important

Next, we investigated (d)N and (d)NT concentrations as well as cpDNA/ncDNA ratios in 6-day-old seedlings (144 h after transfer to long-day growth conditions). This time point was chosen, because the *tk1b* mutant appeared to have recovered as indicated by green pigmentation comparable to that of the wild-type (Supplemental Figure S6A). Nonetheless, a reduced cpDNA/ncDNA ratio was still detectable in *tk1b* compared to wild-type plants but it was only 3.5-fold smaller than that of the wild-type (Figure 9) in contrast to a 4.3-fold difference at the 48 h time point (Figure 8). Note that the ratios between the 48 and 144 h time points cannot be compared since ncDNA is

Downloaded from https://academic.oup.com/plcell/article/34/10/3790/6647853 by Technische Informationsbibliothek (TIB) user on 28 September 2022

synthesized at 144 h but not at 48 h (Barroco et al., 2005), causing a general decrease of the ratios. During late seedling establishment, mtDNA is likely replicated as well. Salvage by the organellar TK1b but also the cytosolic TK1a seems to support cpDNA and mtDNA synthesis because the respective mutants (*tk1a* and *tk1b*) tend to have a reduced cpDNA/ncDNA and mtDNA/ncDNA (tk1b; $P = 0.054$, tk1a; $P = 0.078$) ratio compared to the wild-type (Figure 9; Supplemental Figure S9C).

The accumulation of dATP, dCTP, and dGTP observed in the *tk1b* mutant during early seedling establishment (48 h) was not observed anymore in the established seedling (Figure 10, A–C), suggesting that cpDNA synthesis was now operative. Consistent with the greening of the *tk1b* seedlings (Supplemental Figure S6A), similar concentrations of NTs in wild-type compared to mutant seedlings were observed (Supplemental Figure S12), which suggests that transcription in the chloroplast was not halted anymore. It is tempting to speculate that in the established seedling (144 h), in contrast to the seedling during the early establishment phase (48 h), the transport of thymidylates to the chloroplast has sufficient capacity to allow cytosolic de novo T synthesis and salvage to partially compensate for the loss of these pathways in organelles. Interestingly, a reduction of dTMP and also dTTP was observed in the seedling not only in the *tk1b* but also in the *tk1a* mutant compared to the wild-type. This suggests that both corresponding enzymes contribute to the thymidylate pools in seedlings (Figure 10D). Loss-of-function of any of these genes cannot be fully compensated by the respective counterpart and causes an alteration of the nucleotide metabolome that does not affect the visible appearance. A small effect of DHFR-TS1 but not DHFR-TS2 on the dTMP concentration was also observed (Figure 10E), suggesting that additionally cytosolic de novo T synthesis contributes to the thymidylate pools. Similarly, an accumulation of dCTP and a reduction of dTMP was detected in the *dcd* mutant compared to the wild-type (Figure 10, C and E), suggesting that DCD has a role in equilibrating the dNTP pools, especially by reducing the dCTP concentration (already observed during early seedling establishment; Figure 7E), in addition to a role in thymidylate synthesis.

Chloroplast TK1b can complement the *dhfr-ts2 tk1b* double mutant

Native TK1b is localized in mitochondria and chloroplasts. We wondered whether an engineered targeting of TK1b in the *tk1b* background exclusively localized to either the mitochondria or the chloroplasts can complement the pigmentation phenotype of the mutant. We expressed TK1b fused to either a chloroplast transit peptide (CTP) or a mitochondrial transit peptide (MTP; Kohler et al., 1997; Shen et al., 2017), in the *tk1b dhfr-ts2* background because this mutant shows the strongest phenotype. The constructs were driven by a nopaline synthase promoter (Pro_{NOS}:*CTP:TK1b*, Pro_{NOS}:*MTP:TK1b*). To assess whether TK1b activity is required for complementation, transgenic plants expressing the corresponding inactive variants were also generated. Here the catalytically important amino acid Glu163 was exchanged to Gln ($TK1b_{E163Q}$), rendering the enzyme inactive (Welin et al., 2004). A quantification of green and yellow pixels in images from cotyledons of 5-day-old seedlings showed a reduced ratio of green/yellow pixels in the *dhfr-ts2 tk1b* double mutant compared to wild-type, as observed previously. The *CTP:TK1b* transgene fully restored the wild-type phenotype, whereas the *MTP:TK1b* transgene complemented the lack of *TK1b* only partially (Figure 11). The inactive TK1b version $TK1b_{E163Q}$ did not restore the wild-type phenotype independent of its localization. When targeted to the chloroplast, it even aggravated the phenotype, indicative of a dominant negative effect (Figure 11). The in vivo function of TK1b thus clearly requires its enzymatic activity. The observation that only the chloroplastic TK1b variant restores the wild-type phenotype fully further suggests that transport of thymidylates over the chloroplast membrane is limited. Nonetheless, mitochondrial TK1b can partially support the chloroplasts, indicating that transport of thymidylates occurs to some extent in the already established seedling.

Is global genome repair the source of dT during germination and seedling establishment?

The dT concentration is comparatively high and rises constantly during germination and seedling establishment (Figure 4B) but the source of this dT is unclear. Since this study highlights the importance of dT salvage for cpDNA replication in the process of germination, it is of interest to identify the source of dT. The phenotype of the *tk1b* mutant is aggravated by the application of genotoxic chemicals, suggesting that salvage of dT supports DNA repair processes by supplying building blocks (Pedroza-García et al., 2015, 2019). However, dNMPs produced during global DNA repair may be dephosphorylated and the resulting dNs require salvage; thus, DNA repair could also be a substantial source of dT. DNA repair is a prominent process during germination even in the absence of genotoxic stress (Bray and West, 2005; Weitbrecht et al., 2011). Therefore, we used five mutants crucial for global genome repair, that is, *rad1*, *atm-1*, *atr-2*, *cen2*, and *ddb1-A* (Garcia et al., 2003; Molinier et al., 2004, 2008; Yoshiyama et al., 2009), to assess whether they show reduced dT concentrations in seeds 48 h after transfer to long-day growth conditions. This was not the case for any of the mutants and some even contained more dT (Figure 12), suggesting that DNA repair is not a significant source for dT.

Discussion

Formation of the thymidylate pool during seedling establishment is crucial for cpDNA replication

Nucleotide metabolism, especially with respect to deoxynucleotides, is poorly understood compared to other metabolic pathways in plants, although it is of central importance (Ashihara et al., 2020; Straube et al., 2021a). In this study, we monitored dNT and dN concentrations at different time

Downloaded from https://academic.oup.com/plcell/article/34/10/3790/6647853 by Technische Informationsbibliothek (TIB) user on 28 September 2022

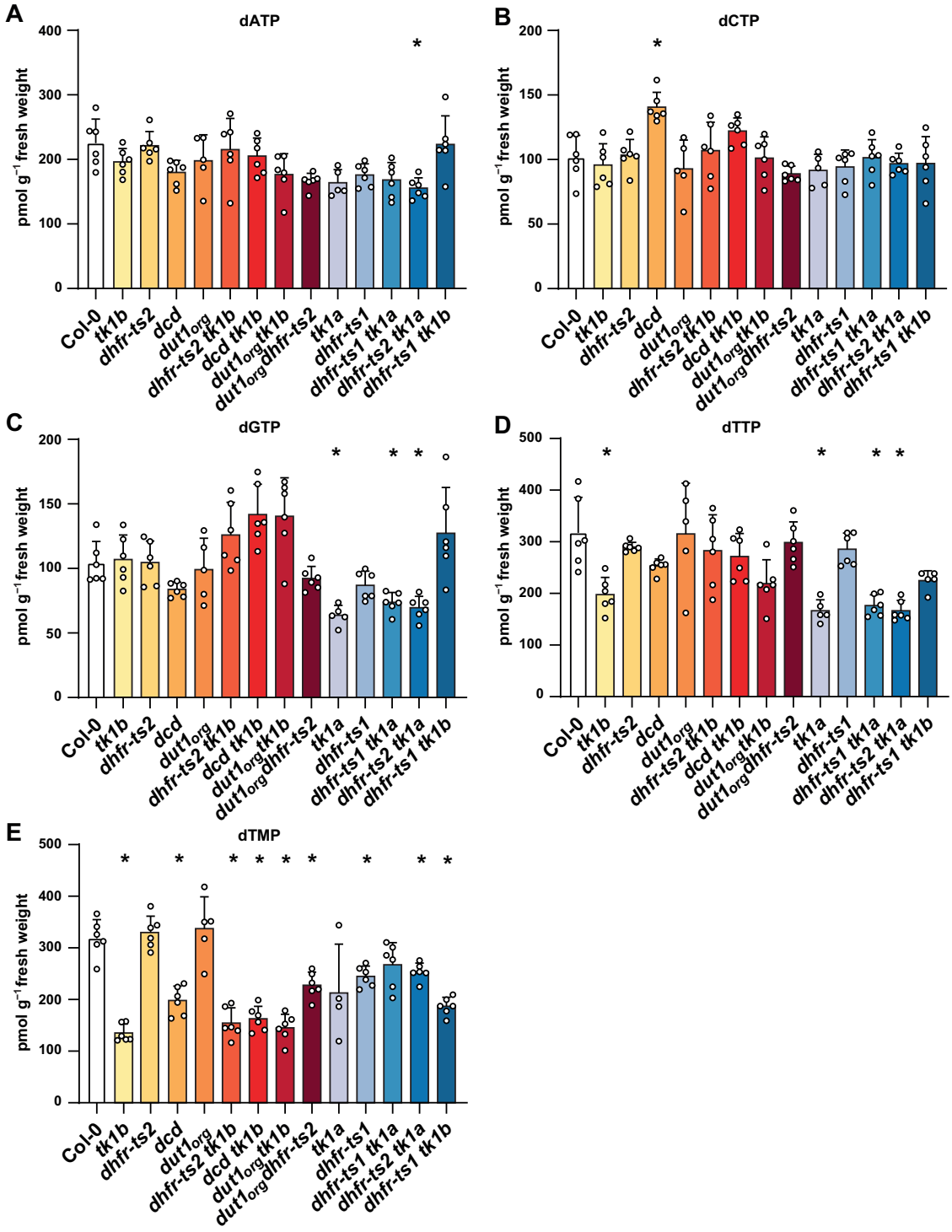

Figure 10 Concentrations of dNTPs and dTMP in wild-type and mutants lacking enzymes putatively involved in thymidylate homeostasis during late seedling establishment. Seeds were imbibed in water for 48 h at 4°C in the dark, transferred for 144 h to long-day growth conditions, and harvested for LC–MS analysis. Concentrations of (A) dATP, (B) dCTP, (C) dGTP, (D) dTTP, and (E) dTMP in germinating seed are shown. Two-sided Tukey's pairwise comparisons using the sandwich variance estimator were used for statistical analysis. Asterisks indicate significant differences ($P < 0.05$) to Col-0. Five to six biological replicates (pooled seedlings) were analyzed. Error bars are SD. Adjusted *P*-values for multiple comparisons can be found in Supplemental Data Set 2.

points during seed germination and observed a strong increase of dNTPs but also dT and with some delay dTMP (Figure 4, A and B) within the first hours of transferring seeds to long-day growth conditions. This coincides with the induction of nucleotide biosynthesis genes, which are among the first to be activated in germination (Law et al., 2014).

Downloaded from https://academic.oup.com/plcell/article/34/10/3790/6647853 by Technische Informationsbibliothek (TIB) user on 28 September 2022

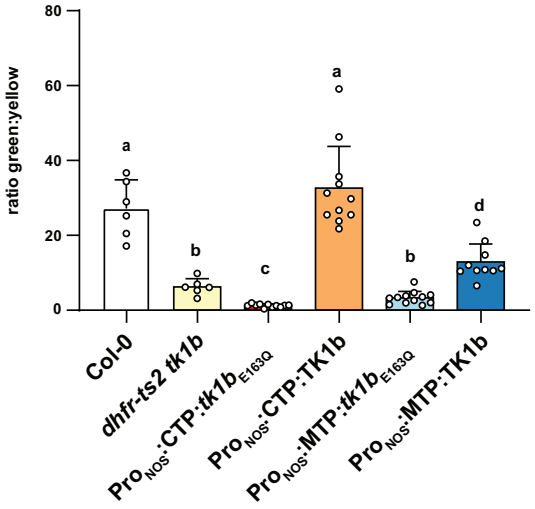

Figure 11 Phenotypic analysis of the chloroplast- or mitochondria-specific complementation with *TK1b* in the *dhfr-ts2 tk1b* background. TK1b fused to a CTP or an MTP was expressed under the control of a nos promoter (Pro_{NOS}). The wild-type version of TK1b and a catalytically inactive mutant version ($TK1b_{E163Q}$) were expressed in transgenic plants with *dhfr-ts2 tk1b* mutant background. Images of cotyledons were taken 5 days after transfer to long-day growth conditions. The ratio of green to yellow pixels was quantified for each individual plant. For all transgenic plants, two independent lines were selected and analyzed. Six to twelve biological replicates (individual plants) were analyzed. Two-sided Tukey's pairwise comparisons using the sandwich variance estimator were used for statistical analysis. Error bars are SD. Different letters indicate significant differences ($P < 0.05$) between genotypes. Adjusted *P*-values for multiple comparisons can be found in Supplemental Data Set 2.

With the onset of cpDNA replication (6 h after transfer to long-day growth conditions; Paszkiewicz et al., 2017), the concentrations of dATP and dTTP decrease transiently, which is probably due to their consumption by the chloroplast replication machinery. Only the cpDNA genome is replicated during germination (Paszkiewicz et al., 2017) and the cpDNA amount increases 5 times during maturation of the proplastid (Fujie et al., 1994), creating a high demand for dNTPs (see "Material and Methods" for an estimation of the required amounts). The cpDNA content is thus particularly affected by a genetic block of thymidylate formation, whereas the mtDNA is not (Figures 6 and 8; Supplemental Figure S9, A and B). Together these data suggest that cpDNA is the main sink for dNTPs during germination.

Deoxy-UMP for DHRF-TS2 is not mainly supplied by $DUT1_{org}$ in mitochondria of germinating seeds

In this study, we identified a variant of DUT1 that is located in mitochondria and chloroplasts ($DUT1_{org}$; Figure 2) and we were able to create a $dut1_{org}$ mutant. We speculated that the main role of $DUT1_{org}$ might be to supply dUMP as substrate for the mitochondrial dTMP-synthesizing enzyme DHFR-TS2. For cytosolic DUT1 such a role has been demonstrated in other organisms (Vértessy and Tóth, 2009; Martínez-Arribas et al., 2020). If $DUT1_{org}$ has this role, effects on the thymidylate pools should be similar in the $dut1_{org}$ mutant and the *dhfr-ts2* mutant. However, while the *dhfr-ts2* mutant has less dTMP compared to the wild-type during early seedling establishment, the dTMP pool in the $dut1_{org}$ mutant is unaltered compared to the wild-type (Figure 7B). Additionally, the strong *dhfr-ts2 tk1b* phenotype is not be observed for the $dut1_{org}$ *tk1b* double mutant (Figure 3), although this would be expected if $DUT1_{org}$ supplies substantial amounts of dUMP for DHFR-TS2. Yet, DUT_{org} may nonetheless be involved in de novo T synthesis because its absence appears to stimulate salvage, maybe to compensate for reduced biosynthesis. The induction of salvage is indicated by less dT in the $dut1_{org}$ mutant compared to the wild-type during germination (Figure 5A).

In summary, we discovered that DUT1 is also located in the mitochondria and the chloroplasts where its main function is probably to sanitize the dNTP pools and not to generate dUMP as DHFR-TS2 substrate in mitochondria. However, we cannot exclude that $DUT1_{org}$, DCD or so far unknown enzymes contribute to the dUMP pool in a redundant manner so that a lack of $DUT1_{org}$ or DCD alone is insufficient to affect dUMP and consequently thymidylate pools similarly to what was observed for DHFR-TS2.

A loss of DCD function increases the concentration of dCTP and has limited influence on the formation of thymidylates

In rice, it was suggested that the formation of thymidylates depends greatly on DCD catalyzing the deamination of dCMP to dUMP, the DHFR-TS substrate (Niu et al., 2017). Here we were able to determine the absolute concentrations of nucleotides and observed clearly increased levels of dCTP in the *dcd* mutant compared to the wild-type but only a slight decrease in dTTP in the early and dTMP in the late seedling establishment phase. This is consistent with our observation that the *dcd tk1b* double mutant is phenotypically similar to the *tk1b* mutant and not to the *dhfr-ts2 tk1b* double mutant that is impaired in salvage and de novo T biosynthesis in mitochondria (Figure 3). In contrast to rice, it appears that DCD plays only a limited role in thymidylate biosynthesis in Arabidopsis. Instead DCD might have an important role in balancing the dNTP pools by limiting the dCTP pool size. Nonetheless, in a genetic background over accumulating deoxycytidilates (in a mutant of *CYTIDINE DEAMINASE*) we previously observed more dTMP and dTTP (Straube et al., 2021a) indicating that under these conditions DCD contributes to thymidylate synthesis in Arabidopsis.

Limited transport capacity for thymidylates during germination may cause the dependency on dT salvage in chloroplasts

During early seedling establishment (48 h), the salvage of dT in the chloroplast by TK1b is predominantly responsible for providing dTMP as precursor for cpDNA replication. This was demonstrated by (1) severely reduced cpDNA, (2) reduced dTMP concentration, and (3) an accumulation of

Downloaded from https://academic.oup.com/plcell/article/34/10/3790/6647853 by Technische Informationsbibliothek (TIB) user on 28 September 2022

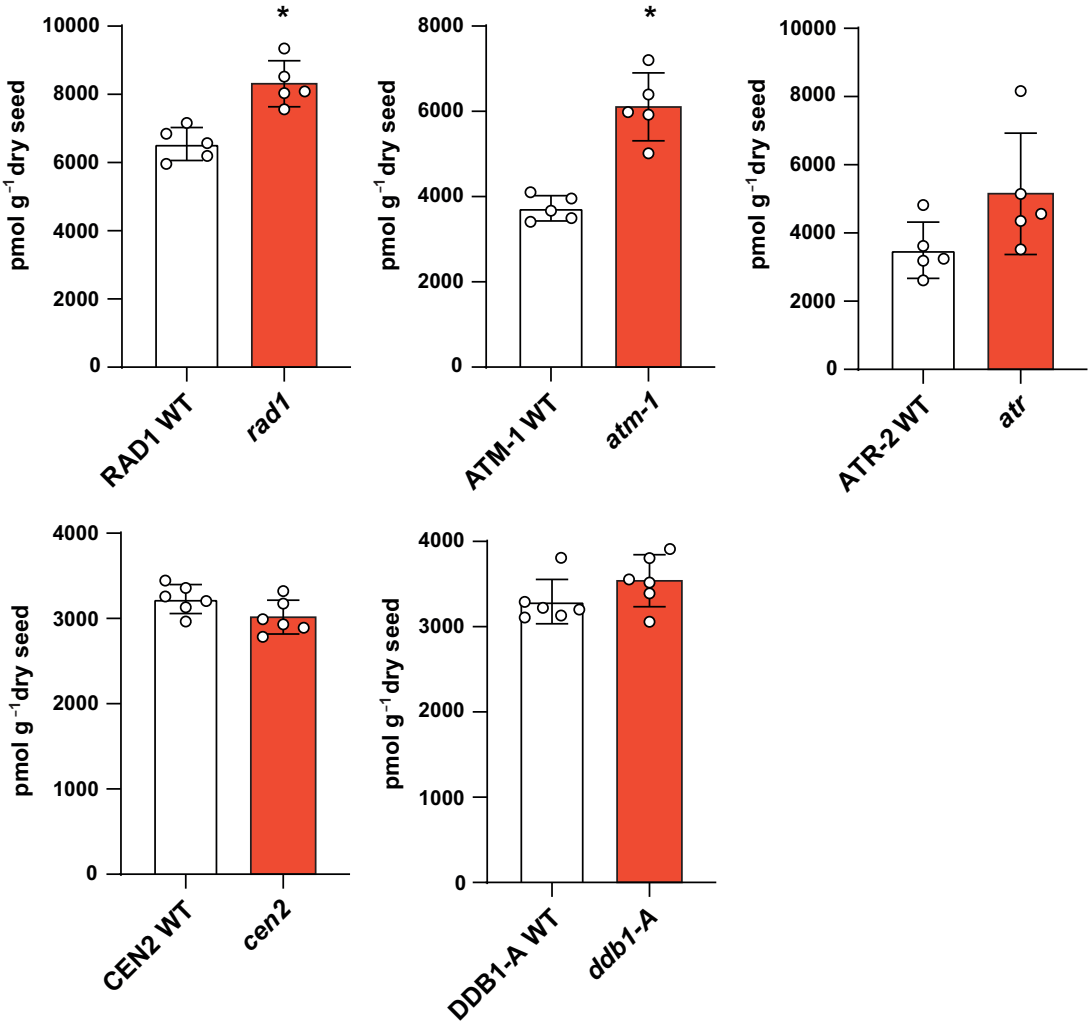

Figure 12 Concentrations of dT in wild-type and mutants affected in global genome repair during early seedling establishment. Seeds were imbibed in water for 48 h at 4°C in the dark, transferred for 48 h to long-day growth conditions, and harvested. Concentrations of dT in plants lacking RAD1, ATM-1, ATR-2, CEN2, and DDB1-A and their corresponding wild-types segregated from the respective mutant populations are shown. Two-sided Tukey's pairwise comparisons using the sandwich variance estimator were used for statistical analysis. Asterisks indicate significant differences ($P < 0.05$) to the wild-type. Six biological replicates (pooled seedlings) were analyzed. Error bars are SD. Adjusted *P*-values for statistical comparisons can be found in Supplemental Data Set 2.

other dNTPs and rNTPs in the *tk1b* mutant compared to the wild-type. A reduction of cpDNA replication in the *tk1b* mutant was observed previously in Arabidopsis (Le Ret et al., 2018). However, here we show that the impact of defective organellar dT salvage is by far more severe than previously reported. This can be explained by different sampling time points (48 h here and 6 days in Le Ret et al., 2018). The strong impact on cpDNA, which we observed early for the *tk1b* mutant alone (48 h), was previously only observed later for the *tk1a tk1b* double mutant (6 days) (Le Ret et al., 2018), which is in line with our interpretation that at later time points a loss-of-function in *TK1b* can be compensated by *TK1a*. Here we identified a time point during early seedling establishment (48 h) when such a compensation is very limited or not at all possible. Is this simply because TK1a is not active at this time point? This seems unlikely because the transcript for TK1a is clearly present during germination and early seedling establishment (Law et al., 2014; Supplemental Figure S1) and more importantly dT is accumulating at this time point in the *tk1a* mutant suggesting that in the wild-type TK1a is phosphorylating dT to dTMP in the cytosol (Figure 7A). If TK1a is active at this time point, why can it not compensate a *tk1b* mutation? A possible explanation is that the import capacity for thymidylates into plastids is limited during germination and early seedling establishment (up to 48 h) and only becomes sufficient to support cpDNA synthesis in the established seedling (144 h). In contrast, import of the TK substrate dT appears to be sufficient at all times. Possible candidates for organellar thymidylate transporters are NDT1 and NDT2, which transport NAD^+ but with lower efficiency also thymidylates (Palmieri et al., 2009) and whose genes are induced during early seedling establishment (Narsai et al., 2011). The onset of thymidylate transport post 48 h allows the cytosolic

Downloaded from https://academic.oup.com/plcell/article/34/10/3790/6647853 by Technische Informationsbibliothek (TIB) user on 28 September 2022

formation of thymidylates by DHFR-TS1 and TK1a to compensate for a lack of dT salvage in chloroplasts, which explains the reversion of the pigmentation and cpDNA phenotypes in established seedlings of the *tk1b* single and *tk1b dhfr-ts2* double mutants (Supplemental Figure S6, A and B). Interestingly, only in the *tk1b dhfr-ts2* double mutant variegated adult plants were obtained (although quite rarely) in which whole sections of the plant were albinotic (Supplemental Figure S6C). The lesions observed in the cotyledons might in rare cases also occur in the adult plant for unknown reasons.

In summary, there is no redundancy between TK1a and TK1b at early time points of germination, whereas later they do seem partially redundant probably because thymidylates are then sufficiently exchanged between compartments. This shows that apparently functionally redundant genes can have a unique role depending on the particular developmental stage of the plant. At least in eudicots, an organellar and a cytosolic TK are conserved (Le Ret et al., 2018), also suggesting that both isoenzymes have nonredundant roles.

Although at early time points, TK1a-mediated thymidylate production cannot compensate the lack of thymidylates in the plastids in *tk1b* mutants, mitochondrial thymidylate production by DHFR-TS2 can partially support dTMP formation during early seedling establishment (Figure 7). Additionally, the *dhfr-ts2 tk1b* mutant has a more severe phenotype compared to the *tk1b* single mutant. It is puzzling that cytosolic thymidylates cannot support the chloroplast at all in germination, whereas mitochondrial thymidylates can.

The prominent role of dT is highlighted by its strong accumulation and the absolute requirement for its salvage

We observed a strong accumulation of dT that is continuously rising throughout germination (Figure 4B). Interestingly, the absolute amount of dT is similar to the combined amounts of dTMP and dTTP and it remains unclear why so much dT is generated and what is its source. Maybe because the plastids rely on dT import but apparently cannot import thymidylates during germination, the cellular dT concentration must be high. The dT may be generated by dephosphorylation of dTMP originating from de novo T synthesis. In this model dT salvage, that is, the re-phosphorylation to dTMP, would be placed downstream of the de novo T synthesis (Figure 1). Apart from serving to provide dT for the plastids, this energy consuming process may also improve the purity of the thymidylate pool. The substrate specificity of TK1 may represent a molecular filter excluding noncanonical or damaged nucleotides from the dTMP pool.

Although de novo T synthesis would be an obvious source for the dT accumulating during germination, it is unclear how RNR activity could lead to excess thymidylates over the other deoxynucleotides, because the allosterically regulated enzyme is known to produce dNDPs in stochiometric amounts (Nordlund and Reichard, 2006). If de novo T synthesis is the main source of thymidylates during germination, it is also curious that first dTMP is made, then it is dephosphorylated and then it is salvaged to dTMP again, which appears to be a futile cycle.

Because of these unsolved issues, we also followed up an alternative hypothesis regarding the origin of dT. We tested whether DNA strand degradation caused by global genome repair may be a source of dT. Global genome repair must produce dG and dC as well as dA and dT in stoichiometric amounts as a result of the fixed ratio of nucleotides in the DNA. However, dA was not detected, whereas dT was readily detectable in our analysis and its concentration was always at least one order of magnitude higher than that of dC (Figure 4B). Additionally, several mutants with a defect in global genome repair did not have reduced amounts of dT. It is thus unlikely that genome repair is a quantitatively significant source of dT during germination, although we cannot exclude the possibility that other mutants with an impact on DNA repair such as *sog1* (Yoshiyama et al., 2009), potentially combined with the application of genotoxic stress, can cause altered dT concentrations during germination. The quantification of dT in seeds and during germination (Figure 4B) also disfavors the hypothesis that dT itself is a metabolite stored in seeds that is used for dTTP synthesis. The dT concentration is low in the beginning of germination and then rises continuously, whereas a storage component should be consumed over time. Thus, the question of the origin of dT remains open.

In the literature, salvage is usually discussed as a process that reintegrates nucleosides or nucleobases, which are substrates for a degradation pathway. Energy conservation is often described as the purpose of salvage (Zrenner et al., 2006; Ashihara et al., 2020; Witte and Herde, 2020). The importance of pyrimidine salvage is underlined by the fact that not only the double mutant of *tk1a* and *tk1b* is not viable (Clausen et al., 2012) but also the double mutant of *ukl1 ukl2*, in which the salvage of the ribonucleoside uridine is abolished, is not viable (Chen and Thelen, 2011). A role for dT salvage in the defense against genotoxic stress in chloroplasts and the cytosol was demonstrated previously (Pedroza-García et al., 2015, 2019; Xu et al., 2015). Here we show that dT salvage has a severe impact on thymidylate pools also in the absence of any genotoxic stress and plays a vital role during germination. The general importance of dT salvage disfavors the idea that this pathway merely serves as an energy-conserving mechanism that reintegrates "accidentally" dephosphorylated dTMP. Thymidine salvage rather represents a major pathway for providing thymidylates. TKs in other organisms are usually discussed in tumorgenesis, DNA repair, and viral infection (Bitter et al., 2020) but in plants dT salvage seems to have a more fundamental role adapted to the plant lifestyle, which involves germination of dormant seeds and chloroplast metabolism.

Material and methods

Plant materials

T-DNA insertion mutant lines of Arabidopsis (*A. thaliana*) for *DHFR-TS1* (AT2G16370; GK-010G06) and *DHFR-TS2*

Downloaded from https://academic.oup.com/plcell/article/34/10/3790/6647853 by Technische Informationsbibliothek (TIB) user on 28 September 2022

(AT4G34570; GK-893C02), both previously described in Gorelova et al. (2017); *TK1a* (AT3G07800; SALK_097767C) and *TK1b* (AT5G23070; SALK_074256C), both previously described in Clausen et al. (2012); *ATM-1* (AT3G48190; SALK_006953), described in Garcia et al. (2003); *ATR-2* (AT5G40820; SALK_032841) and *DDB1-A* (AT4G05420; SALK_038757), both previously described in Molinier et al. (2008), and *CEN2* (AT4G37010; SALK_127583) described in Molinier et al. (2004); and *RAD1* (AT5G41150; SALK_096156), previously described in Yoshiyama et al. (2009); and *DCD* (AT3G48540; SALK_057582; Niu et al., 2017) were obtained from the Nottingham Arabidopsis Stock Centre and homozygous T-DNA insertion mutants were screened by PCR. The primers used are shown in Supplemental Data Set 1. The mutant line for $DUT1_{org}$ (AT3G46940) was newly obtained by applying the CRISPR/Cas9 technique (see below). The mutation was introduced in the region encoding the transit peptide. The loss of the $DUT1_{org}$ protein was confirmed by transient expression and subcellular localization of the enzyme fused to a fluorescent tag using confocal microscopy. Double mutants were obtained by crossing the respective single mutants. All single and double mutant lines were grown together in parallel in a randomized fashion with Col-0 serving as the wild-type control, or their corresponding wild-type segregated from the respective mutant population to obtain a uniform seed batch. The seed material used for preparing the time course experiment consisted of about 1-year-old Col-0 seeds originating from multiple Col-0 plants. For all experiments involving the mutant collection the uniform seed batch was used. The age of the seeds at the time of analysis was 4 months. The seeds of the mutants involved in global genome repair were 2 months old.

Growth conditions

For phenotypic analysis, seeds were sown on soil (Steckmedium, Klasmann-Deilmann, Geeste, Germany), pretreated at 4°C in the dark for 48 h, and then transferred to a growth chamber set to 16-h day/8-h night (long-day), 22°C day/20°C night, 100 µmol s^{-1} m^{-2} light (Osram Fluora 36W/77, Osram, Munich, Germany), and 70% humidity. For metabolite and qPCR analysis, seeds were surface sterilized with 70% (v/v) EtOH for 20 min, dried until all EtOH evaporated and weighed in 10 ± 0.5 mg aliquots. The seeds were transferred onto two layers of 6 × 6 cm autoclaved filter paper soaked with 2-mL cold and sterile modified liquid half strength MS media as described by Niehaus et al. (2020) (3-mM $CaCl_2$, 1.5-mM $MgSO_4$, 1.25-mM KH_2PO_4, 18.7-mM KNO_3, 0.1-mM $FeSO_4$, 0.1-mM Na_2EDTA, 0.13-mM $MnSO_4$, 0.1-mM H_3BO_3, 0.03-mM $ZnSO_4$, 1-µM Na_2MoO_4, 0.1-µM $CuSO_4$, 0.1-µM $NiCl_2$, 0.5-g L^{-1} MES, pH adjusted to 5.7 with KOH) in a closed unsealed petri dish (94 × 16 mm). Seeds were evenly spread across the filter paper to minimize the number of seeds touching each other. The plates with the seeds were pretreated at 4°C in the dark for 48 h, and then transferred to a growth chamber set to 16-h day/8-h night (long-day), 22°C day/20°C night, 100 µmol s^{-1} m^{-2} (Osram Fluora 36W/77) light, and 70% humidity. For time points beyond 48 h after transfer to long-day growth conditions, plates were carefully watered with 2-mL sterile bi-distilled water each, and 48 h later 2-mL sterile modified half-strength liquid MS media were added.

Phenotypic analysis and quantification of chlorotic leaf areas

The images used for phenotypic analysis were taken using a Nikon SMZ25 stereo microscope equipped with a Nikon DS-Ri2 microscope camera (Nikon, Minato, Japan) set to a resolution of 4,908 × 3,264 pixels. Images were taken 3–6 days after transfer to long-day growth conditions with identical instrument and light settings to ensure comparability. The chlorotic leaf area and green leaf areas were quantified using Fiji (Schindelin et al., 2012) with ImageJ 1.53c. First, the image was loaded into Fiji, and subsequently the Color Threshold was determined using the Hue, Saturation, Brightness Color Space (Image → Adjust → Color Threshold). For the chlorotic leaf area, the Hue was set to 35–45, saturation was kept at 0–255, and the Brightness was set automatically. The Thresholding method was set to default. For the green leaf area, the Hue was set to 46–100, and all other settings were kept the same. For each individual image, the green leaf area/chlorotic leaf area ratio was calculated.

Cloning

The constructs used for generating the $dut1_{org}$ knockout mediated by CRISPR/Cas9 and the chloroplast- or mitochondria-specific complementation of tk1b were cloned using the MoClo system (Weber et al., 2011; Engler et al., 2014). For this, a variety of different intermediate vectors had to be created that were used in combination with already published ones. The vector collection used for introducing the CRISPR-mediated lesion in DUT1 was previously used in Rinne et al. (2021). The MoClo Toolkit and the Plant Parts Kit were a gift from Nicola Patron and Sylvestre Marillonnet (Addgene kit #1000000044, Addgene kit #1000000047), the pHEE-2E-TRI was a gift from Qi-Jun Chen (Addgene plasmid #71288). The guideRNA used for the $dut1_{org}$ loss-of-function was chosen by applying the criteria proposed by Doench et al. (2014). The final level_2 vector used for generating the mutant was assembled from four independent level_1 vectors. The level_1 vector mediating the phosphinothricin resistance for later plant selection was cloned by combining pICH87633, pICH43844, and pICH41421 with the recipient vector pICH47732 in a BsaI cut/ligation, resulting in pICH47732_Basta_pos1_fwd (V183). For the level_1 vector containing the Cas9WT + Intron under the control of an egg-cell specific promoter, first the Cas9 + Intron was amplified from the vector pB330p6i2xoR-UcasW-U6Os4 (DNA Cloning Service) using the primers P773 and P774. The resulting PCR product was subsequently cloned into pICH41308 in a BbsI cut/ligation resulting in pICH41308_CDS1_Cas9 + Intron (V150). The egg-cell specific promoter was amplified from the vector pHEE2E-TRI (Wang et al., 2015) using the primers P769 and P770, and the resulting PCR product was cloned into

Downloaded from https://academic.oup.com/plcell/article/34/10/3790/6647853 by Technische Informationsbibliothek (TIB) user on 28 September 2022

pICH41295 in a BbsI cut/ligation resulting in pICH412 95_Pro + 5U_egg-cell-specific (V140). Next, V140, V150, and pICH41276 were cloned into the recipient vector pICH47742 in a *Bsa*I cut/ligation leading to pICH47742_Cas9 + Intron_ pos2_fwd (V182). For the level_1 vector containing the tGFP under the control of the napinA promoter, first the napinA promoter had to be amplified from gDNA originating from *Brassica napus* using the primers P767 and P768. The resulting PCR product was then cloned into pICH41295 in a BbsI cut/ligation resulting in pICH41295_Pro + 5U_napinA (V139). The tGFP first had to be amplified from pICSL50016 using the primers P626 and P627 and was then cloned into pICH41308 leading to pICH41308_tGFP (V134). Thereafter, V139, V134, and pICH41432 were cloned into pICH47761 in a BsaI cut/ligation resulting in pICH47761_napinA_tGFP_pos4_fwd (V181). The level_1 vector containing the guideArray under the control of the AtU6-26 promoter was generated by first amplifying the two parts of the guideArray using specific primers P293/P606 and P605/P272 with the plasmid pGTR (Xie et al., 2015; V113) as template, and subsequently fused together in a BsaI cut/ligation. This fused guideArray was again amplified using P294/P274 (as described in Xie et al., 2015). Subsequently, the guideArray was cloned into the MoClo compatible gRNA shuttle vector (J. Streubel, unpublished material) downstream of the ATU6-26 promoter in a BbsI-mediated cut/ligation reaction. This vector was cloned into pICH47751 in a BsaI cut/ligation resulting in pICH4 7751_org.dut1_guide_pos3_fwd. In a last step V183, V182, V181, pICH47751_org.dut1_guide_pos3_fwd and pICH41780 were cloned into the final recipient vector pAGM4723 in a BbsI cut/ligation resulting in pAGM4723_CRISPR_org.dut1 (H410).

In total ten transgenic T1 lines were obtained of which one (line 10) showed a heterozygous editing event in the gene encoding DUT1. The progeny of this line was tested for the absence of the CRISPR construct, but still had to have the editing event.

For the chloroplast- or mitochondria-specific complementation experiment of *tk1b*, an inactive and active version of TK1b, lacking the subcellular localization sequence, were needed. Additionally, both versions had to be made compatible with the MoClo system by removing a *Bbs*I recognition site inside the CDS. By introducing a missense mutation using primer-directed mutagenesis, an E codon was changed to a Q codon at position 163 (corresponding to E98 in human TK1; Welin et al., 2004), resulting in a CDS for the inactive version of TK1b ($TK1b_{E163Q}$). The BbsI site was removed using a similar approach, but in this case, a sense mutation was introduced. To exclusively localize both versions to the chloroplast or mitochondria, the optimized CTP described by Shen et al. (2017) and the MTP of *Sc*CoxIV (Maarse et al., 1984) were added to the 5′-ends of the truncated sequences, respectively.

To generate the level_0 vector containing the inactive and truncated version of TK1b directed to the chloroplast, the following primers were used in a PCR on gDNA: P2137 and P2138, P2139 and P2140, and P2141 and P2143. All three PCR products and the synthetic fragment of CTP were then cloned into pICH41308 in a BbsI cut/ligation resulting in pICH41308_CDS1_CTP_truncated_inactive_TK1b (H959). The level_0 vector containing the active and truncated version directed to the chloroplast was created using the following primers in a PCR on gDNA: P2143 and P2144, P2145, and P2146. The two resulting PCR products and the synthetic fragment of CTP (B9; Integrated DNA Technologies) were cloned into pICH41308 in a BbsI cut/ligation resulting in pICH41308_CDS1_CTP_truncated_active_TK1b (H960).

The level_0 vectors needed for the mitochondrial complementation were generated by first amplifying the ScCoxIV transit peptide with the primers P2316 and P2317 with pAGM1482 as template. The inactive and active truncated versions of TK1b were amplified using P2318 and P2319 on H959 or H960, respectively. The level_0 vector containing the inactive and truncated version directed to the mitochondrion was created by combining both PCR products in a BbsI cut/ligation with pICH41308, resulting in pICH41308_CDS1_ScCoxIV_truncated_inactive_TK1b (H1007). In case of the level_0 vector containing the active and truncated version of TK1b directed to the mitochondrion, both PCR products were combined with pICH41308 in a BbsI cut/ligation, resulting in pICH41308_CDS1_Sc CoxIV_truncated_active_TK1b (H1008).

For creating the level_1 vectors, the vectors H959, H960, H1007 and H1008 were individually combined with pICH42211, pICH44179, and pICH44300 and cloned into pICH47732 in a BsaI cut/ligation, leading to the vectors pICH47732_CTP_inactive_TK1b_pos1_fwd (H962), pICH477 32_CTP_active_TK1b_pos1_fwd (H963), pICH47732_ScC oxIV_inactive_TK1b_pos1_fwd (H1015) and pICH47732_Sc CoxIV_active_TK1b_pos1_fwd (H1016).

In a last step, the level_1 vectors were individually combined with a level_1 vector mediating a phosphinothricin resistance for later plant selection (V166, Niehaus et al., 2020) and pICH41744 and cloned into pAGM4723 in a BbsI cut/ligation, resulting in the level_2 vectors pAGM47 23_CTP_inactive_TK1b_Basta (H965), pAGM4723_CTP_ active_TK1b_Basta (H966), pAGM4723_ScCoxIV_inactive_ TK1b_Basta (H1018), and pAGM4723_ScCoxIV_active_T K1b_Basta (H1019).

For each final construct, 12–15 T1 lines were selected for Basta resistance and subsequently checked for homozygosity in the T2 generation. For each construct two independent homozygous T2 lines were selected (H965: line 1.1 and 2.4; H966: line 1.4 and 2.1; H1018: line 1.6 and 2.1; H1019: line 1.2 and 2.1).

The vectors needed for the subcellular localization of the C-terminal eYFP tagged DHFR-TS2 (AT4G34570), TK1b (AT5G23070), DCD (AT3G48540), TMPK (AT5G59440), and DUT1 (AT3G46940) were generated by amplifying the sequences with cDNA or gDNA (only *TMPK*) as template with P149/P150 (*DHFR-TS2*), P218/P219 (*TK1b*), N398/N399 (*DCD*), P1698/P1699 (*TMPK*), and P607/P608 (*DUT1*),

Downloaded from https://academic.oup.com/plcell/article/34/10/3790/6647853 by Technische Informationsbibliothek (TIB) user on 28 September 2022

respectively. The resulting PCR products and the recipient vector pXCS-eYFP (V36; Dahncke and Witte, 2013) were digested with EcoRI and XmaI and ligated, resulting in pXCS_eYFP-Thy2 (H26), pXCS_eYFP_TK1b (H76), pXCS_eYFP_dCMP-deam (X165), pXCS_eYFP_DUT1 (H239), and pXCS_eYFP_org.dut1 (H1210). In the case of TMPK, the PCR product and V36 were digested with HindIII and XmaI and ligated, resulting in pXCS_eYFP_TMPK (H875). For each construct five T1 lines were selected for Basta resistance. For confocal microscopy analysis, plants of the T2 generation were pretested for the presence of the eYFP signal and subsequently used for confocal microscopy.

Estimation of the amount of dTTP needed for cpDNA replication during germination

It is assumed that a seed has roughly as many cells as an Arabidopsis embryo 9 days after pollination ($\sim 15 \times 10^3$ cells per embryo; Kiyosue et al., 1999) and contains on average of seven chloroplasts per cell as described previously for an embryo of the same age (Mansfield and Briarty, 1992). The cpDNA copy number per plastid in a mesophyll cell is 20–35 (Zoschke et al., 2007); however, this number is highly variable especially in plant development (Oldenburg and Bendich, 2015; Dobrogojski et al., 2020). Here we assumed that there is only one cpDNA copy per plastid, which is likely an underestimation. Following these assumptions, in one seed 105×10^3 cpDNA copies are present. Furthermore, we assumed that the cpDNA copy number increases 5 times during germination as reported for proplastid maturation in meristems (Fujie et al., 1994). Considering the size (154,478 bp) and the GC content (36%) of cpDNA, 9.84×10^4 molecules of dTTP are needed to replicate one plastidic genome. Thus, for one seed $\frac{(105\times10^3)\times(9.84\times10^4)\times5}{6.022\times10^{23}\ \text{(Avogadro constant)}}$ 0.086 pMol dTTP are required for a five-fold increase of cpDNA amount. Assuming that 1 g of seeds (the reference unit used for nucleotide quantification) contains 5×10^4 seeds (Jako et al., 2001), 0.086 pMol $\times 5 \times 10^4$ = 4,300 pmol g^{-1} dTTP and an equivalent amount of dATP are required for cpDNA synthesis. Similarly, for dGTP and dCTP $\frac{(105\times10^3)\times(5.61\times10^4)\times5}{6.022\times10^{23}\ \text{(Avogadro constant)}} = 0.049$ pMol per seed and 2,450 pmol g^{-1} dGTP and dCTP are required for replicating the cpDNA.

Nucleic acid isolation and cDNA preparation

For the isolation of gDNA and total RNA, ~50 mg plant material was harvested at the respective time points and transferred to a 2-mL safe-lock tube containing five 2-mm steel beads and one 11-mm steel bead. Frozen samples were ground in a bead mill at 16 Hz for 4 min. For gDNA extraction, a CTAB-based method including an RNA-digestion step was used. Total RNA was extracted using the NucleoSpin RNA Plant (Machery-Nagel, Dueren, Germany) according to the manufacturer's protocol, but instead of the suggested RA1 buffer, the RAP buffer was used for the cell lysis. Synthesis of cDNA was done with the RevertAid First Strand cDNA Synthesis Kit (Thermo Fisher, Waltham, MA, USA) according to the manufacturer's protocol. Total RNA (2 µg) per sample was transcribed using an oligo dT primer.

qPCR analysis

All qPCR experiments were performed using QuantStudio3 (Thermo Fisher, Waltham, MA, USA) in combination with qPCRBIO SyGreen Mix (PCR Biosystems, London, UK), both used according to the manufacturer's protocol. Each reaction had a total volume of 10 µL. The following program was used: 3 min at 95°C, 40 cycles of 5 s at 95°C followed by 30 s at 60°C. After the PCR Stage the Melt Curve Stage was done by heating the sample to 95°C for 15 s, holding it at 60°C for 1 min and slowly heating it again to 95°C at a rate of 0.1°C s^{-1}. Melting curves showed a single peak for all amplified PCR products. For each experiment three technical replicates per sample and three biological replicates were analyzed. To determine the relative genome abundance of the mtDNA and cpDNA, four different primer pairs binding specifically to the plastid or mitochondrial genomes were used. The amplifications were compared using Ct values to that obtained from primer pair binding to the nuclear genome. The signals shown in Figures 6, 8, and 9 and Supplemental Figure S9 were obtained by amplifying *RBCL* (AtCG00490) in the case of the plastid genome, *COX1* (AtMG01360) for the mitochondrial genome, and *UBC21* (At5G25760) as a reference for the nuclear genome. The primers used for qPCR were already published and are listed in Supplemental Data Set 1 with their corresponding citations. Results were analyzed according to Livak and Schmittgen (2001), and for determination of the relative genome abundance the $2^{-\Delta Ct}$ method was used.

Confocal microscopy and image analysis

For subcellular localization, all constructs except pXCS_eYFP_TMPK (H875), were stably transformed into *A. thaliana*. Samples were analyzed by confocal microscopy as previously described by Dahncke and Witte (2013). Mitochondria of seedling roots were labeled in vivo with tetramethylrhodamine methyl ester (TMRM) as described in Niehaus et al. (2020). Both TMRM and the *Sc*COXIV:mCherry show unspecific labeling, TMRM also stains the cell wall, whereas *Sc*COXIV:mCherry is also localized to the nucleus, most likely due to high overexpression. Microscopy was performed using a Leica SP8 confocal laser microscope with an HC PL APO 40x/1.10 water immersion objective (Leica Microsystems, Wetzlar, Germany). The settings for the respective fluorescent proteins/chemicals were as following. eYFP: excitation 514 nm, collection bandwidth 519–539 nm, laser intensity 1%–2%, gain 30%. mCherry: excitation 552 nm, collection bandwidth 600–620 nm, laser intensity 0.5%–1%, and gain 50%. TMRM: excitation 552 nm, collection bandwidth 570–620 nm, laser intensity 1%, and gain 30%.

The confocal microscopy images of the co-localized candidates DCD and DHFR-TS2 were analyzed using the "Just Another Colocalisation Plugin" in ImageJ (Bolte and Cordelieres, 2006). Here the Pearson's coefficient and Van

Downloaded from https://academic.oup.com/plcell/article/34/10/3790/6647853 by Technische Informationsbibliothek (TIB) user on 28 September 2022

Steensel's crosscorrelation function (Van Steensel et al., 1996) were calculated for several images using a dx range from −150 to 150 pixels. For images taken in leaves, the signal of the eYFP fusion proteins was compared to the chloroplastic autofluoresence. In case of images taken in root tissue, incubated with TMRM, the signal of the eYFP fusion protein was compared to the mitochondrial TMRM signal. For the analysis of the dual-localized proteins TK1b, $DUT1_{org}$, and TMPK, the "Plot Profile" function of ImageJ was used (Sharma et al., 2018). The analyzed region of the respective candidates was indicated by a dotted white line in Supplemental Figure S3.

Metabolome analysis

Seedlings of the respective time points were completely transferred from the soaked filter paper using a flat spatula and forceps and transferred to a 2-mL safe-lock tube containing five 2-mm steel beads and one 11-mm steel bead and rapidly cooled down in liquid nitrogen. Subsequently, samples could be stored at −80°C for several weeks or were further processed by grinding them in a frozen state in a bead mill for 4 min at 16 Hz twice with cooling in liquid nitrogen between grinding steps. Further steps were performed according to Straube et al. (2021a) with the exception that the bead mill step after addition of the extraction buffer was replaced with two rounds of vortexing at maximum speed for 12 s. For the quantification of nucleotides, a modified gradient for the Hypercarb chromatography was used: 0 min, 100% A; 3 min, 100% A; 18 min, 70% A; 19 min, 0% A; 22 min, 0% A; 22.5 min, 100% A until 30 min. The mobile phase A consisted of 5-mM ammonium acetate, pH 9.5, in deionized water and the mobile phase B consisted of 100% acetonitrile. The chromatography was performed employing a flowrate of 0.6 mL min^{-1} and a column temperature of 35°C. The injection volume was increased to 20 µL.

Nucleosides were analyzed using an Agilent 1290 Infinity II LC System coupled with an Agilent 6470 triple quadrupole mass spectrometer. Chromatographic separation was achieved using a 4.6 × 50 mm Polaris C18-A column with 3-µm particle size (Agilent, Palo Alto, CA, USA). The flowrate was 0.6 mL min^{-1}, the column temperature was set to 30°C and the injection volume was 10 µL. Mobile phase A was 0.1% (v/v) formic acid in water and mobile phase B was 0.1% (v/v) formic acid in methanol. The following gradient was used: 0 min, 96% A; 8.00 min, 35% A; 8.20 min, 100% A; 10.00 min, 100% A; 10.10 min, 96% A until 12.50 min. In-source parameters used are: Gas temperature 250°C, gas flow 12 L min^{-1}, nebulizer pressure 35 psi, sheath gas temperature 395°C, sheath gas flow 12 L min^{-1}, capillary voltage 4,000 V, and nozzle voltage 500 V. All nucleosides were measured in positive mode using the multiple-reaction-monitoring mode. Transitions (precursor ions and product ions) and fragmentor energies for nucleoside analysis are the same as described in Straube et al. (2021a).

The isotope standard for dC was generated by complete dephosphorylation of a dCTP isotope standard (Eurisotope, Saint-Aubin, France) using Shrimp Alkaline Phosphatase (New England BioLabs, Ipswich, MA, USA). Full conversion was confirmed by LC–MS analysis.

The metabolite quantification refers to the weight of the starting material (dry seeds). For each sample a similar amount (10 ± 0.5 mg) of dry seeds was weighed and the weight was noted and used for calculation. For each time point all material was harvested and used for metabolite extraction. Thus, the values in the time course reflect the total amount of the indicated metabolite present in seedlings or germinated seeds that originate from one gram of dry seeds. This procedure eliminates a bias due to the different uptake of water in the individual phases of germination and seedling establishment.

Only for the comparison of genotypes at the late seedling establishment time point (144 h; Figure 10 and Supplemental Figure S12) ca. 100 mg of seedlings (fresh weight) were used for metabolite extraction. Here, the metabolite concentration refers to the fresh weight of the respective seedlings.

Statistical analysis

Statistical analysis was performed as described by Heinemann et al. (2021). Here, R Software version 4.1.1 was used together with RStudio version 1.4.1717 and CRAN packages multcomp and sandwich to perform two-sided Tukey's pairwise comparisons. Heteroscedasticity of the dataset was considered with the sandwich variance estimator (Herberich et al., 2010; Pallmann and Hothorn, 2016). The adjusted *P*-values of the individual datasets are listed in Supplemental Data Set 2.

Accession numbers

Information regarding used mutants can be found in the GenBank/EMBL data libraries under the following accession numbers: *DHFR-TS1* (AT2G16370), *DHFR-TS2* (AT4G34570), *TK1a* (AT3G07800), *TK1b* (AT5G23070), *DCD* (AT3G48540), *DUT1* (AT3G46940), *TMPK* (AT5G59440), *ATM-1* (AT3G48190), *ATR-2* (AT5G40820), *CEN2* (AT4G37010), *DDB1-A* (AT4G05420), and *RAD1* (AT5G41150)

Supplemental data

The following materials are available in the online version of this article.

Supplemental Figure S1. Gene expression profiles of genes putatively involved in thymidylate formation.

Supplemental Figure S2. Generation of the $dut1_{org}$ mutant line.

Supplemental Figure S3. Subcellular localization of DHFR-TS2, TK1b, DCD, and TMPK.

Supplemental Figure S4. Quantitative image analysis for colocalization studies.

Supplemental Figure S5. Determination of the relative cotyledon growth in wild-type and mutants lacking enzymes putatively involved in thymidylate homeostasis in established seedlings.

Supplemental Figure S6. Recovery of *dhfr-ts2*, *tk1b*, and *dhfr-ts2 tk1b* mutants in comparison to wild-type.

Downloaded from https://academic.oup.com/plcell/article/34/10/3790/6647853 by Technische Informationsbibliothek (TIB) user on 28 September 2022

Supplemental Figure S7. Concentrations of ribonucleotides and ribonucleosides at different time points during seed germination and in the establishing seedling.

Supplemental Figure S8. Relative amounts of xanthosine in wild-type and mutants lacking enzymes putatively involved in thymidylate homeostasis during germination.

Supplemental Figure S9. Abundance of the mtDNA relative to the ncDNA in wild-type and mutants lacking enzymes putatively involved in thymidylate homeostasis during germination and early and late seedling establishment.

Supplemental Figure S10. Concentrations of ribonucleotide triphosphates in the wild-type and mutant seeds lacking enzymes putatively involved in thymidylate homeostasis during early seedling establishment.

Supplemental Figure S11. Relative abundances of cpDNA and mtDNA during early seedling establishment determined by the amplification of four genes, respectively.

Supplemental Figure S12. Concentrations of ribonucleotide triphosphates in the wild-type and mutants lacking enzymes putatively involved in thymidylate homeostasis during late seedling establishment.

Supplemental Table S1. Abbreviations.

Supplemental Data Set 1. List of all oligonucleotides used in this study

Supplemental Data Set 2. Adjusted *P*-values for all multiple comparisons

Acknowledgments

The authors are grateful to Hildegard Thölke and Anastasia Krivenko for technical assistance, Nabila Firdoos for the cloning of the CRISPR level_1 vectors and Jana Streubel for providing the pDIE vector series.

Funding

This work was supported by the Deutsche Forschungsgemeinschaft (grant no. HE 5949/3-1 to M.H.), (grant no. WI3411/8-1 to C-P.W.), and (grant no. INST 187/741-1 FUGG).

Conflict of interest statement. None declared.

References

Anderson DD, Quintero CM, Stover PJ (2011) Identification of a de novo thymidylate biosynthesis pathway in mammalian mitochondria. Proc Natl Acad Sci USA **108**: 15163–15168

Ashihara H, Crozier A, Ludwig IAA (2020) Plant Nucleotide Metabolism: Biosynthesis, Degradation, and Alkaloid Formation. Wiley Blackwell, Chichester

Barroco RM, van Poucke K, Bergervoet JH, Veylder L, de Groot SP, Inze D, Engler G (2005) The role of the cell cycle machinery in resumption of postembryonic development. Plant Physiol **137**: 127–140

Baumann H, Hofmann R, Lammers M, Schimpff-Weiland G, Follmann H (1984) Aurintricarboxylic acid and polynucleotides as novel inhibitors of ribonucleotide reductases. Zeitschrif Naturforsch C Biosci **39**: 276–281

Bitter EE, Townsend MH, Erickson R, Allen C, O'Neill KL (2020) Thymidine kinase 1 through the ages: a comprehensive review. Cell Biosci **10**: 1–16

Bolte S, Cordelieres FP (2006) A guided tour into subcellular colocalization analysis in light microscopy. J Microsc **224**: 213–232

Bray CM, West CE (2005) DNA repair mechanisms in plants: crucial sensors and effectors for the maintenance of genome integrity. New Phytologist **168**: 511–528

Bryant JA (1980) Biochemical aspects of DNA replication with particular reference to plants. Biol Rev Cambridge Philos Soc **55**: 237–284

Buckland RJ, Watt DL, Chittoor B, Nilsson AK, Kunkel TA, Chabes A (2014) Increased and imbalanced dNTP pools symmetrically promote both leading and lagging strand replication infidelity. PLoS Genet **10**: e1004846

Castroviejo M, Tharaud D, Mocquot B, Litvak S (1979) Factors affecting the onset of deoxyribonucleic acid synthesis during wheat embryo germination. Study of the changes in DNA polymerases A, B and C and the pool of DNA precursors. Biochem J **181**: 193–199

Chen M, Thelen JJ (2011) Plastid uridine salvage activity is required for photoassimilate allocation and partitioning in Arabidopsis. Plant Cell **23**: 2991–3006

Clausen AR, Girandon L, Ali A, Knecht W, Rozpedowska E, Sandrini MPB, Andreasson E, Munch-Petersen B, Piškur J (2012) Two thymidine kinases and one multisubstrate deoxyribonucleoside kinase salvage DNA precursors in *Arabidopsis thaliana*. FEBS J **279**: 3889–3897

Corral MG, Haywood J, Stehl LH, Stubbs KA, Murcha MW, Mylne JS (2018) Targeting plant DIHYDROFOLATE REDUCTASE with antifolates and mechanisms for genetic resistance. Plant J **95**: 727–742

Dahncke K, Witte CP (2013) Plant purine nucleoside catabolism employs a guanosine deaminase required for the generation of xanthosine in Arabidopsis. Plant Cell **25**: 4101–4109

Dellaquila A, Lioi L, Scarascia I (1980) Deoxyribonucleic-acid synthesis and deoxyribonucleic-acid polymerase-activity during early germination of wheat embryos at high and low viability. Biol Plant **22**: 287–293

Dobrogojski J, Adamiec M, Lucinski R (2020) The chloroplast genome: a review. Acta Physiol Plant **42**: 98

Doench JG, Hartenian E, Graham DB, Tothova Z, Hegde M, Smith I, Sullender M, Ebert BL, Xavier RJ, Root DE (2014) Rational design of highly active sgRNAs for CRISPR-Cas9-mediated gene inactivation. Nat Biotechnol **32**: 1262-U130

Dubois E, Cordoba-Canero D, Massot S, Siaud N, Gakiere B, Domenichini S, Guerard F, Roldan-Arjona T, Doutriaux MP (2011) Homologous recombination is stimulated by a decrease in dUTPase in Arabidopsis. PLoS One **6**: e18658

Engler C, Youles M, Gruetzner R, Ehnert TM, Werner S, Jones JDG, Patron NJ, Marillonnet S (2014) A golden gate modular cloning toolbox for plants. ACS Synth Biol **3**: 839–843

Franzolin E, Pontarin G, Rampazzo C, Miazzi C, Ferraro P, Palumbo E, Reichard P, Bianchi V (2013) The deoxynucleotide triphosphohydrolase SAMHD1 is a major regulator of DNA precursor pools in mammalian cells. Proc Natl Acad Sci USA **110**: 14272–14277

Fujie M, Kuroiwa H, Kawano S, Mutoh S, Kuroiwa T (1994) Behavior of organelles and their nucleoids in the shoot apical meristem during leaf development in Arabidopsis-thaliana l. Planta **194**: 395–405

Garcia V, Bruchet H, Camescasse D, Granier F, Bouchez D, Tissier A (2003) AtATM is essential for meiosis and the somatic response to DNA damage in plants. Plant Cell **15**: 119–132

Gorelova V, Lepeleire J, de van Daele J, Pluim D, Mei C, Cuypers A, Leroux O, Rebeille F, Schellens JHM, Blancquaert D, et al. (2017) Dihydrofolate reductase/thymidylate synthase fine-tunes the folate status and controls redox homeostasis in plants. Plant Cell **29**: 2831–2853

Downloaded from https://academic.oup.com/plcell/article/34/10/3790/6647853 by Technische Informationsbibliothek (TIB) user on 28 September 2022

Guillet M, van der Kemp PA, Boiteux S (2006) dUTPase activity is critical to maintain genetic stability in Saccharomyces cerevisiae. Nucleic Acids Res **34**: 2056–2066

Heinemann KJ, Yang SY, Straube H, Medina-Escobar N, Varbanova-Herde M, Herde M, Rhee S, Witte CP (2021) Initiation of cytosolic plant purine nucleotide catabolism involves a monospecific xanthosine monophosphate phosphatase. Nat Commun **12**: 6846

Herberich E, Sikorski J, Hothorn T (2010) A robust procedure for comparing multiple means under heteroscedasticity in unbalanced designs. PLoS One **5**: e9788

Jako C, Kumar A, Wei YD, Zou JT, Barton DL, Giblin EM, Covello PS, Taylor DC (2001) Seed-specific over-expression of an Arabidopsis cDNA encoding a diacylglycerol acyltransferase enhances seed oil content and seed weight. Plant Physiol **126**: 861–874

Kiyosue T, Ohad N, Yadegari R, Hannon M, Dinneny J, Wells D, Katz A, Margossian L, Harada JJ, Goldberg RB, et al. (1999) Control of fertilization-independent endosperm development by the MEDEA polycomb gene in Arabidopsis. Proc Natl Acad Sci **96**: 4186–4191

Kohalmi SE, Glattke M, Mcintosh EM, Kunz BA (1991) Mutational specificity of dna precursor pool imbalances in yeast arising from deoxycytidylate deaminase deficiency or treatment with thymidylate. J Mol Biol **220**: 933–946

Kohler RH, Zipfel WR, Webb WW, Hanson (1997) The green fluorescent protein as a marker to visualize plant mitochondria in vivo. Plant J **11**: 613–621

Law SR, Narsai R, Whelan J (2014) Mitochondrial biogenesis in plants during seed germination. Mitochondrion **19 Pt B**: 214–221

Le Ret M, Belcher S, Graindorge S, Wallet C, Koechler S, Erhardt M, Williams-Carrier R, Barkan A, Gualberto JM (2018) Efficient replication of the plastid genome requires an organellar thymidine kinase. Plant Physiol **178**: 1643–1656

Lincker F, Philipps G, Chabouté ME (2004) UV-C response of the ribonucleotide reductase large subunit involves both E2F-mediated gene transcriptional regulation and protein subcellular relocalization in tobacco cells. Nucleic Acids Res **32**: 1430–1438

Livak KJ, Schmittgen TD (2001) Analysis of relative gene expression data using real-time quantitative PCR and the 2(-Delta Delta C(T)) Method. Methods (San Diego, CA) **25**: 402–408

Maarse AC, Adolphus Vanloon PG, Riezman H, Gregor I, Schatz G, La Grivell (1984) Subunit-iv of yeast cytochrome-c oxidase - cloning and nucleotide sequencing of the gene and partial amino-acid sequencing of the mature protein. EMBO J **3**: 2831–2837

Mansfield SG, Briarty LG (1992) Cotyledon cell development in *Arabidopsis thaliana* during reserve deposition. Can J Bot **70**: 151–164

Marciniak B, Bucholc M, Buchowicz J (1987) Early DNA-synthesis during the germination of wheat embryos. Phytochemistry **26**: 331–334

Martínez-Arribas B, Requena CE, Pérez-Moreno G, Ruíz-Pérez LM, Vidal AE, González-Pacanowska D (2020) DCTPP1 prevents a mutator phenotype through the modulation of dCTP, dTTP and dUTP pools. Cell Mol Life Sci **77**: 1645–1660

Masubelele NH, Dewitte W, Menges M, Maughan S, Collins C, Huntley R, Nieuwland J, Scofield S, Murray JA (2005) D-type cyclins activate division in the root apex to promote seed germination in Arabidopsis. Proc Natl Acad Sci USA **102**: 15694–15699

Molinier J, Lechner E, Dumbliauskas E, Genschik P (2008) Regulation and role of Arabidopsis CUL4-DDB1A-DDB2 in maintaining genome integrity upon UV stress. PLoS Genet **4**: e1000093

Molinier J, Ramos C, Fritsch O, Hohn B (2004) CENTRIN2 modulates homologous recombination and nucleotide excision repair in Arabidopsis. Plant Cell **16**: 1633–1643

Mori Y, Kimura S, Saotome A, Kasai N, Sakaguchi N, Uchiyama Y, Ishibashi T, Yamamoto T, Chiku H, Sakaguchi K (2005) Plastid DNA polymerases from higher plants, *Arabidopsis thaliana*. Biochem Biophys Res Commun **334**: 43–50

Nagy GN, Leveles I, Vertessy BG (2014) Preventive DNA repair by sanitizing the cellular (deoxy) nucleoside triphosphate pool. FEBS J **281**: 4207–4223

Narsai R, Law SR, Carrie C, Xu L, Whelan J (2011) In-depth temporal transcriptome profiling reveals a crucial developmental switch with roles for RNA processing and organelle metabolism that are essential for germination in Arabidopsis. Plant Physiol **157**: 1342–1362

Nelson BK, Cai X, Nebenfuhr A (2007) A multicolored set of in vivo organelle markers for co-localization studies in Arabidopsis and other plants. Plant J Cell Mol Biol **51**: 1126–1136

Niehaus M, Straube H, Kuenzler P, Rugen N, Hegermann J, Giavalisco P, Eubel H, Witte CP, Herde M (2020) Rapid affinity purification of tagged plant mitochondria (Mito-AP) for metabolome and proteome analyses. Plant Physiol **182**: 1194–1210

Niu M, Wang Y, Wang C, Lyu J, Wang Y, Dong H, Long W, Di Wang, Kong W, Wang L, et al. (2017) ALR encoding dCMP deaminase is critical for DNA damage repair, cell cycle progression and plant development in rice. J Exp Bot **68**: 5773–5786

Nordlund P, Reichard P (2006) Ribonucleotide reductases. Ann Rev Biochem **75**: 681–706

Oldenburg DJ, Bendich AJ (2015) DNA maintenance in plastids and mitochondria of plants. Front Plant Sci **6**: 883

Osaki Y, Kodama Y (2017) Particle bombardment and subcellular protein localization analysis in the aquatic plant Egeria densa. PeerJ **5**: e3779

Pallmann P, Hothorn LA (2016) Analysis of means: a generalized approach using R. J Appl Stat **43**: 1541–1560

Palmieri F, Rieder B, Ventrella A, Blanco E, Do PT, Nunes-Nesi A, Trauth AU, Fiermonte G, Tjaden J, Agrimi G, et al. (2009) Molecular identification and functional characterization of *Arabidopsis thaliana* mitochondrial and chloroplastic NAD(+) carrier proteins. J Biol Chem **284**: 31249–31259

Parent JS, Lepage E, Brisson N (2011) Divergent roles for the two polI-like organelle DNA polymerases of Arabidopsis. Plant Physiol **156**: 254–262

Paszkiewicz G, Gualberto JM, Benamar A, Macherel D, Logan DC (2017) Arabidopsis seed mitochondria are bioenergetically active immediately upon imbibition and specialize via biogenesis in preparation for autotrophic growth. Plant Cell **29**: 109–128

Pedroza-García JA, Nájera-Martínez M, de la Paz Sanchez M, Plasencia J (2015) *Arabidopsis thaliana* thymidine kinase 1a is ubiquitously expressed during development and contributes to confer tolerance to genotoxic stress. Plant Mol Biol **87**: 303–315

Pedroza-García JA, Nájera-Martínez M, Mazubert C, Aguilera-Alvarado P, Drouin-Wahbi J, Sánchez-Nieto S, Gualberto JM, Raynaud C, Plasencia J (2019) Role of pyrimidine salvage pathway in the maintenance of organellar and nuclear genome integrity. Plant J Cell Mol Biol **97**: 430–446

Rajjou L, Duval M, Gallardo K, Catusse J, Bally J, Job C, Job D (2012) Seed germination and vigor. Ann Rev Plant Biol **63**: 507–533

Rinne J, Witte CP, Herde M (2021) Loss of MAR1 function is a marker for co-selection of CRISPR-induced mutations in plants. Front Genome Ed **3**: 723384

Ronceret A, Gadea-Vacas J, Guilleminot J, Lincker F, Delorme V, Lahmy S, Pelletier G, Chabouté ME, Devic M (2008) The first zygotic division in Arabidopsis requires de novo transcription of thymidylate kinase. Plant J Cell Mole Biol **53**: 776–789

Schimpff G, Müller H, Follmann H (1978) Age-dependent DNA labeling and deoxyribonucleotide synthesis in wheat seeds. Biochim Biophys Acta **520**: 70–81

Schindelin J, Arganda-Carreras I, Frise E, Kaynig V, Longair M, Pietzsch T, Preibisch S, Rueden C, Saalfeld S, Schmid B, et al. (2012) Fiji: an open-source platform for biological-image analysis. Nat Methods **9**: 676–682

Downloaded from https://academic.oup.com/plcell/article/34/10/3790/6647853 by Technische Informationsbibliothek (TIB) user on 28 September 2022

Schmidt TT, Sharma S, Reyes GX, Kolodziejczak A, Wagner T, Luke B, Hofer A, Chabes A, Hombauer H (2019) Inactivation of folylpolyglutamate synthetase Met7 results in genome instability driven by an increased dUTP/dTTP ratio. Nucleic Acids Res **48**: 264–277

Sharma M, Bennewitz B, Kloesgen RB (2018) Dual or not dual? Comparative analysis of fluorescence microscopy-based approaches to study organelle targeting specificity of nuclear-encoded plant proteins. Front Plant Sci **9**: 1350

Shen BR, Zhu CH, Yao Z, Cui LL, Zhang JJ, Yang CW, He ZH, Peng XX (2017) An optimized transit peptide for effective targeting of diverse foreign proteins into chloroplasts in rice. Sci Rep **7**: 46231

Sliwinska E, Bassel GW, Bewley JD (2009) Germination of *Arabidopsis thaliana* seeds is not completed as a result of elongation of the radicle but of the adjacent transition zone and lower hypocotyl. J Exp Bot **60**: 3587–3594

Stasolla C, Loukanina N, Ashihara H, Yeung EC, Thorpe TA (2002) Pyrimidine nucleotide and nucleic acid synthesis in embryos and megagametophytes of white spruce (Picea glauca) during germination. Physiol Plant **115**: 155–165

Stillman B (2013) Deoxynucleoside triphosphate (dNTP) synthesis and destruction regulate the replication of both cell and virus genomes. Proc Natl Acad Sci USA **110**: 14120–14121

Straube H, Niehaus M, Zwittian S, Witte CP, Herde M (2021a) Enhanced nucleotide analysis enables the quantification of deoxynucleotides in plants and algae revealing connections between nucleoside and deoxynucleoside metabolism. Plant Cell **33**: 270–289

Straube H, Witte CP, Herde M (2021b) Analysis of nucleosides and nucleotides in plants: an update on sample preparation and LC-MS techniques. Cells **10**: 689

Strugala K, Buchowicz J (1984) The use of [deoxyadenosine-h-3] to measure the rate of dna-synthesis in germinating wheat embryos. Plant Sci Lett **34**: 17–23

Thornton JM, Collins ARS, Powell AA (1993) The effect of aerated hydration on DNA synthesis in embryos, of Brassica oleracea L. Seed Sci Res **3**: 195–199

Van Steensel B, van Binnendijk EP, Hornsby CD, van der Voort HT, Krozowski ZS, de Kloet ER, van Driel R (1996) Partial colocalization of glucocorticoid and mineralocorticoid receptors in discrete compartments in nuclei of rat hippocampus neurons. J Cell Sci **109**: 787–792

Vértessy BG, Tóth J (2009) Keeping uracil out of DNA: physiological role, structure and catalytic mechanism of dUTPases. Account Chem Res **42**: 97–106

Wang C, Liu Z (2006) Arabidopsis ribonucleotide reductases are critical for cell cycle progression, DNA damage repair, and plant development. Plant Cell **18**: 350–365

Wang ZP, Xing HL, Dong L, Zhang HY, Han CY, Wang XC, Chen QJ (2015) Egg cell-specific promoter-controlled CRISPR/Cas9 efficiently generates homozygous mutants for multiple target genes in Arabidopsis in a single generation. Genome Biol **16**: 144

Waterworth WM, Bray CM, West CE (2015) The importance of safeguarding genome integrity in germination and seed longevity. J Exp Bot **66**: 3549–3558

Weber E, Engler C, Gruetzner R, Werner S, Marillonnet S (2011) A modular cloning system for standardized assembly of multigene constructs. PLoS One **6**: e16765

Weitbrecht K, Mueller K, Leubner-Metzger G (2011) First off the mark: early seed germination. J Exp Bot **62**: 3289–3309

Welin M, Kosinska U, Mikkelsen NE, Carnrot C, Zhu C, Wang L, Eriksson S, Munch-Petersen B, Eklund H (2004) Structures of thymidine kinase 1 of human and mycoplasmic origin. Proc Natl Acad Sci USA **101**: 17970–17975

Witte CP, Herde M (2020) Nucleotide metabolism in plants. Plant Physiol **182**: 63–78

Xie K, Minkenberg B, Yang Y (2015) Boosting CRISPR/Cas9 multiplex editing capability with the endogenous tRNA-processing system. Proc Natl Acad Sci USA **112**: 3570–3575

Xu J, Deng Y, Li Q, Zhu X, He Z (2014) STRIPE2 encodes a putative dCMP deaminase that plays an important role in chloroplast development in rice. J Genet Genom **41**: 539–548

Xu J, Zhang L, Yang DL, Li Q, He Z (2015) Thymidine kinases share a conserved function for nucleotide salvage and play an essential role in *Arabidopsis thaliana* growth and development. New Phytologist **208**: 1089–1103

Yoshiyama K, Conklin PA, Huefner ND, Britt AB (2009) Suppressor of gamma response 1 (SOG1) encodes a putative transcription factor governing multiple responses to DNA damage. Proc Natl Acad Sci USA **106**: 12843–12848

Zoschke R, Liere K, Boerner T (2007) From seedling to mature plant: Arabidopsis plastidial genome copy number, RNA accumulation and transcription are differentially regulated during leaf development. Plant J **50**: 710–722

Zrenner R, Stitt M, Sonnewald U, Boldt R (2006) Pyrimidine and purine biosynthesis and degradation in plants. Ann Rev Plant Biol **63–57**: 805–836

Downloaded from https://academic.oup.com/plcell/article/34/10/3790/6647853 by Technische Informationsbibliothek (TIB) user on 28 September 2022

Supplemental Table S1. Abbreviations

Abbreviation	Meaning
(d)N	deoxyribonucleoside and ribonucleoside
(d)NT	deoxyribonucleotides and ribonucleotides
ATP	adenosine triphosphate
CCF	cross correlation function
CDA	CYTIDINE DEAMINASE
cds	coding sequence
cpDNA	plastidic DNA
CTP	chloroplast transit peptide
dA	deoxyadenosine
dATP	deoxyadenosine triphosphate
dC	deoxycytidine
DCD	DEOXYCYTIDINE MONOPHOSPHATE DEAMINASE
dCMP	deoxycytidine monophosphate
dCTP	deoxycytidine triphosphate
dG	deoxyguanosine
dGTP	deoxyguanosine triphosphate
DHFR-TS	DIHYDROFOLATE REDUCTASE-THYMIDYLATE SYNTHASE
dN	deoxyribonucleoside
dNDP	deoxyribonucleotide diphosphate
dNK	DEOXYNUCLEOSIDE KINASE
dNMP	deoxyribonucleotide monophosphate
dNT	deoxyribonucleotide
dNTP	deoxyribonucleotide triphosphate
dT	thymidine
dTDP	deoxythymidine diphosphate
dTMP	deoxythymidine monophosphate
dTTP	deoxythymidine triphosphate
dU	deoxyuridine
dUDP	deoxyuridine diphosphate
dUMP	deoxyuridine monophosphate
DUT1	dUTP PYROPHOSPHATASE 1
dUTP	deoxyuridine triphosphate
eYFP	enhanced yellow fluorescent protein
mtDNA	mitochondrial DNA
MTP	mitochondrial transit peptide
ncDNA	nuclear DNA
NDK	NUCLEOTIDE DIPHOSPHATE KINASES
NDT	NAD+ TRANSPORTER
nosP	nopaline synthase promoter
NSH1	NUCLEOSIDE HYDROLASE 1
NTP	ribonucleotide triphosphates
ORF	open reading frame

PCC	pearson correlation coefficient
q-PCR	quantitative polymerase chain reaction
RNR	RIBONUCLEOTIDE REDUCTASE
rNTP	ribonucleotide triphosphate
TAIR	The Arabidopsis Information Resource
TK1	THYMIDINE KINASE
TMPK	dTMP KINASE
TMRM	tetramethylrhodamine methyl ester
UMP	uridine monophosphate
UTP	uridine triphosphate
UTR	untranslated region

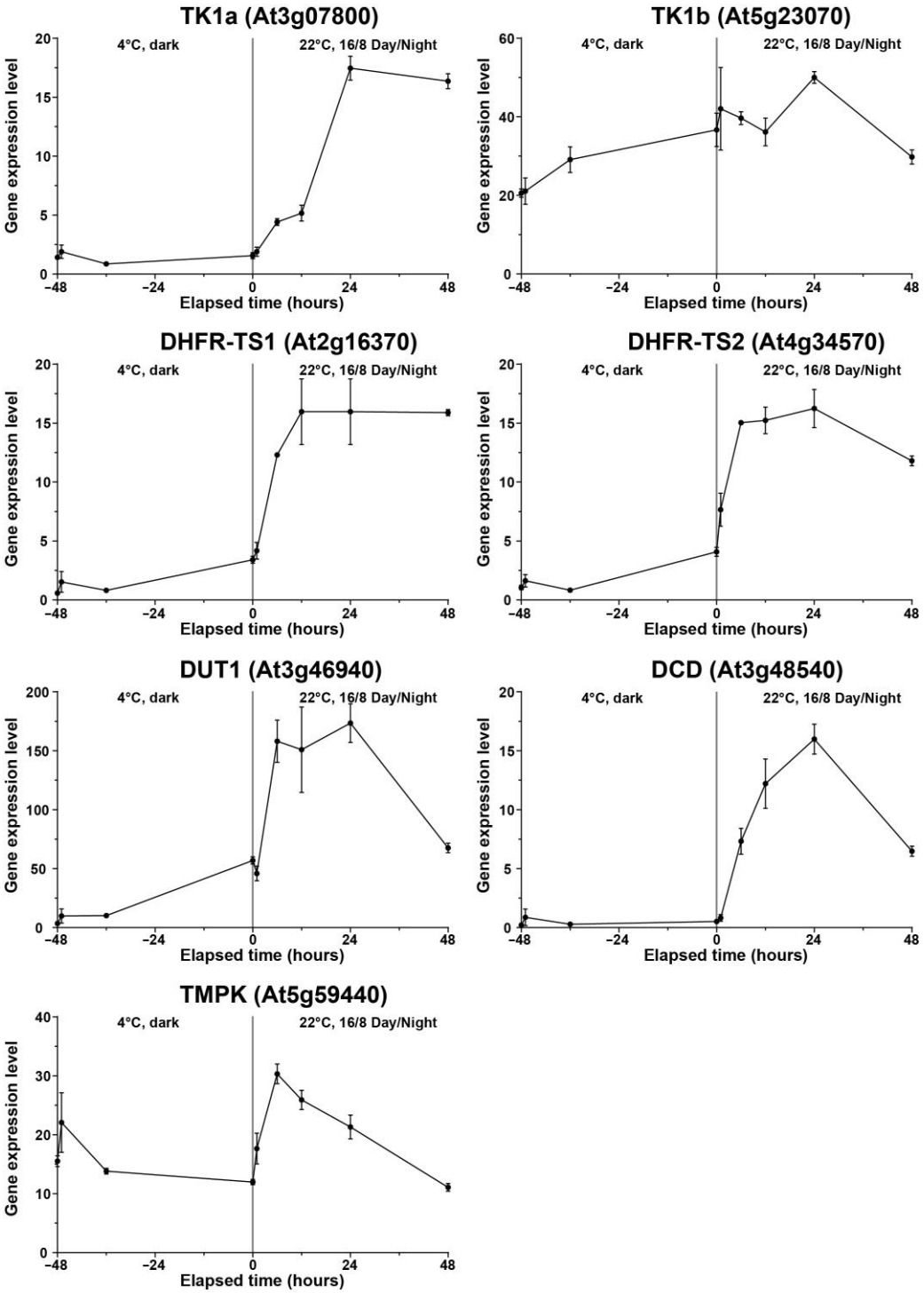

Supplemental Figure S1. Gene expression profiles of genes putatively involved in thymidylate formation. Gene expression data are obtained from a germination study using the same protocol and time points as in the experiments reported here (Narsai et al., 2011; three biological replicates, error bars are SD) and were replotted (BAR eFP browser) to allow a direct comparison with Figure 4 and Supplemental Figure S7. (Supports Figure 1)

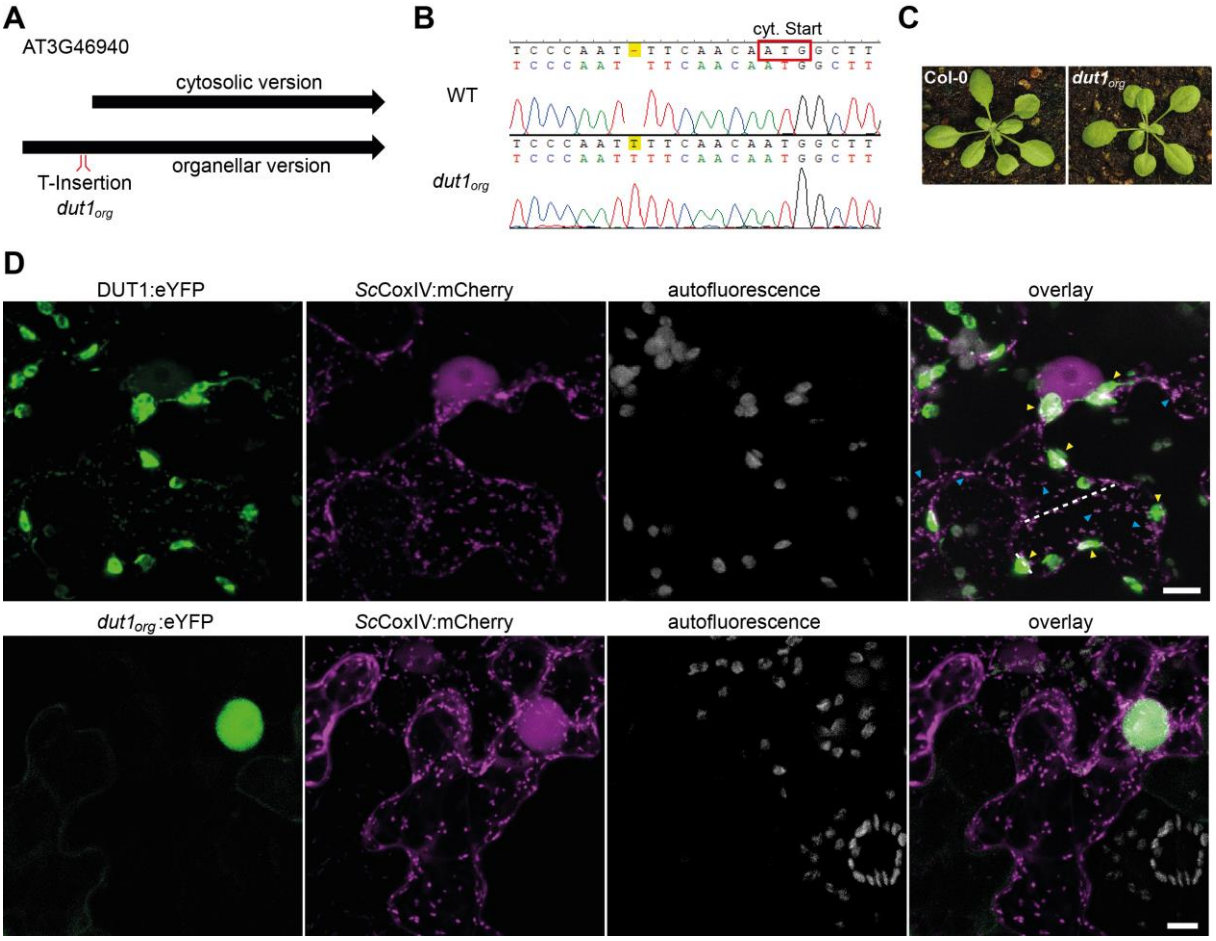

Supplemental Figure S2. Generation of the *dut1*$_{org}$ mutant line. A mutant line lacking the organellar version of DUT1 was created with CRISPR/Cas. (**A**) The short and long ORFs coding for the cytosolic and the organellar DUT1 variant are schematically shown including the guideRNA targeting site and the editing event. (**B**) Confirmation of the editing event by cDNA amplification and subsequent sequencing of the PCR product. The cytosolic start codon is shown in a red box and the editing event is highlighted in yellow. (**C**) Phenotypic comparison of a *dut1*$_{org}$ and a wild-type plant 20 days after transfer to long-day growth conditions. (**D**) Confocal microscopy images showing the subcellular localization of DUT1 produced from the long intact ORF (upper panels) and the respective edited ORF (lower panels). Images were taken three days after agrobacteria infiltration of *N. benthamiana*. From left to right are shown: DUT1:eYFP, mitochondrial *Sc*COXIV:mCherry, chloroplast autofluorescence and an overlay of all three channels. The white dotted lines represent the sectors used for the plot profile analysis (Supplemental Figure S4D). Exemplary, selected mitochondria and chloroplasts showing dual localization are marked with blue and yellow arrowheads, respectively. Scale bars = 10 µm. (Supports Figure 2)

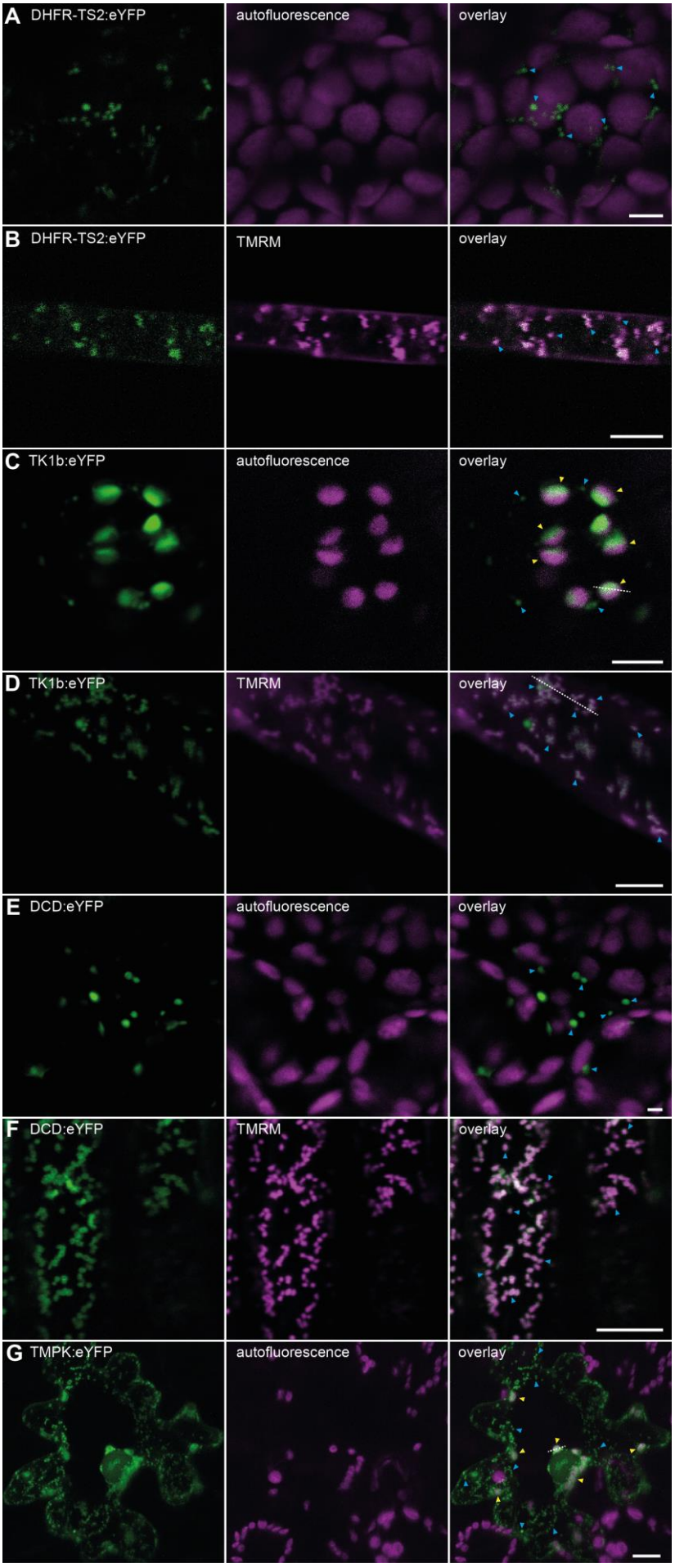
A DHFR-TS2:eYFP
autofluorescence
overlay
B DHFR-TS2:eYFP
TMRM
overlay
C TK1b:eYFP
autofluorescence
overlay
D TK1b:eYFP
TMRM
overlay
E DCD:eYFP
autofluorescence
overlay
F DCD:eYFP
TMRM
overlay
G TMPK:eYFP
autofluorescence
overlay

Supplemental Figure S3. Subcellular localization of DHFR-TS2, TK1b, DCD and TMPK. Stable transformed Arabidopsis seeds expressing C-terminal eYFP fusions with DHFR-TS2, TK1b and DCD, respectively, were imbibed in water for 48 h at 4°C in the dark and transferred for 48 h to long-day growth conditions. Confocal microscopy images of cotyledon tissues were taken for (**A**) DHFR-TS2 (**C)** TK1b and (**E**) DCD. Images show (from left to right): the eYFP signal, chloroplast autofluorescence and an overlay of both channels. Confocal microscopy images of root tissue were taken for (**B**) DHFR-TS2 (**D)** TK1b and (**F**) DCD. Images show (from left to right): eYFP signal, signal from TMRM staining indicating the presence of mitochondria and an overlay of both channels. (**G)** Confocal microcopy images of a *N. benthamiana* leaf transiently expressing the TMPK:eYFP construct. Images were taken three days after agrobacteria infiltration. Images represent (from left to right): eYFP signal, chloroplast autofluorescence and the overlay of both channels. The white dotted lines in (**C**) and (**D**) represent the sectors used for the plot profile analysis (see Supplemental Figure S4C). Exemplary, selected mitochondria and chloroplasts showing an eYFP signal are marked with blue and yellow arrowheads, respectively. Scale bars = (**A**) 6 µm, (**B**) 8 µm, (**C**) 6 µm, (**D**) 5 µm, (**E**) 3 µm, (**F**) 10 µm and (**G**) 10 µm. (Supports Figure 1)

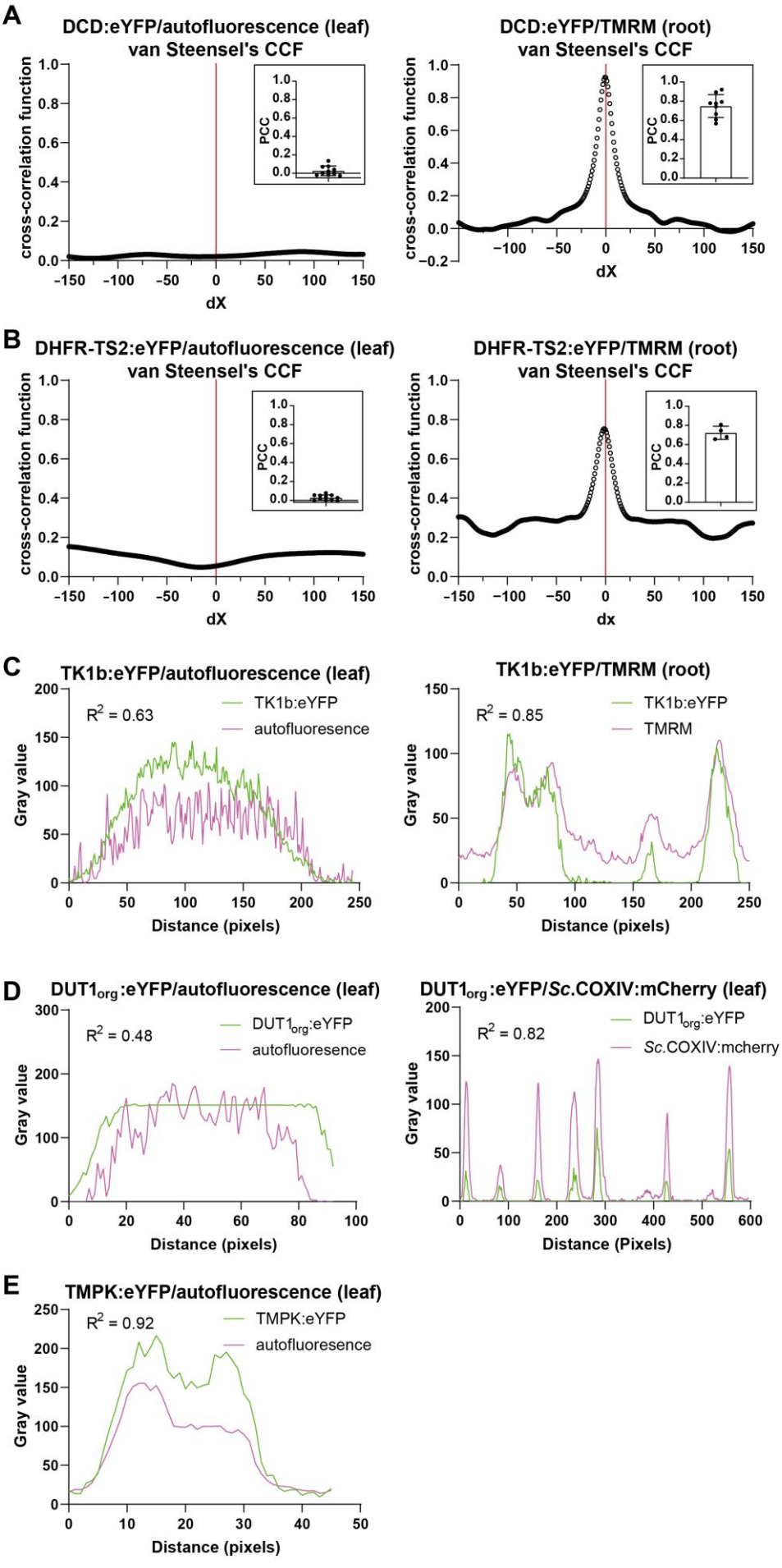
A
DCD:eYFP/autofluorescence (leaf)
van Steensel's CCF
cross-correlation function
dX
PCC
DCD:eYFP/TMRM (root)
van Steensel's CCF
cross-correlation function
dX
PCC
B
DHFR-TS2:eYFP/autofluorescence (leaf)
van Steensel's CCF
cross-correlation function
dX
PCC
DHFR-TS2:eYFP/TMRM (root)
van Steensel's CCF
cross-correlation function
dx
PCC
C
TK1b:eYFP/autofluorescence (leaf)
R2 = 0.63
TK1b:eYFP
autofluoresence
Gray value
Distance (pixels)
TK1b:eYFP/TMRM (root)
R2 = 0.85
TK1b:eYFP
TMRM
Gray value
Distance (pixels)
D
DUT1org:eYFP/autofluorescence (leaf)
R2 = 0.48
DUT1org:eYFP
autofluoresence
Gray value
Distance (pixels)
DUT1org:eYFP/Sc.COXIV:mCherry (leaf)
R2 = 0.82
DUT1org:eYFP
Sc.COXIV:mcherry
Gray value
Distance (Pixels)
E
TMPK:eYFP/autofluorescence (leaf)
R2 = 0.92
TMPK:eYFP
autofluoresence
Gray value
Distance (pixels)

Supplemental Figure S4. Quantitative image analysis for colocalization studies. Fusion proteins only localized in mitochondria ((**A**) DCD:eYFP and (**B**) DHFR-TS2:eYFP) were analyzed with Van Steensel's Cross Correlation Function (CCF) using the plastidic autofluorescense of leaves (left) and the TMRM signal indicating the presence of mitochondria (right, staining is more efficient in roots) as markers. The inset shows the Pearson correlation coefficient (PCC) for n = 4–10 micrographs (each data point representing one micrograph). Error bars are SD. For eYFP fusion proteins that are dual localized (mitochondria and chloroplast) the signal of a profile line (drawn in the respective micrograph in Supplemental Figures S2 and S3) was plotted (green line) and a correlation with the respective marker (purple line) was calculated as R^2 value. The marker for colocalization with plastids was the autofluorescense (on the left (**C**) TK1b:eYFP, (**D**) $DUT1_{org}$:eYFP, (**E**) TMPK:eYFP) and with mitochondria (on the right TMRM staining for (**C**) TK1b:eYFP and *Sc*COXIV:mCherry coexpression for (**D**) $DUT1_{org}$:eYFP). (Supports Figure 1)

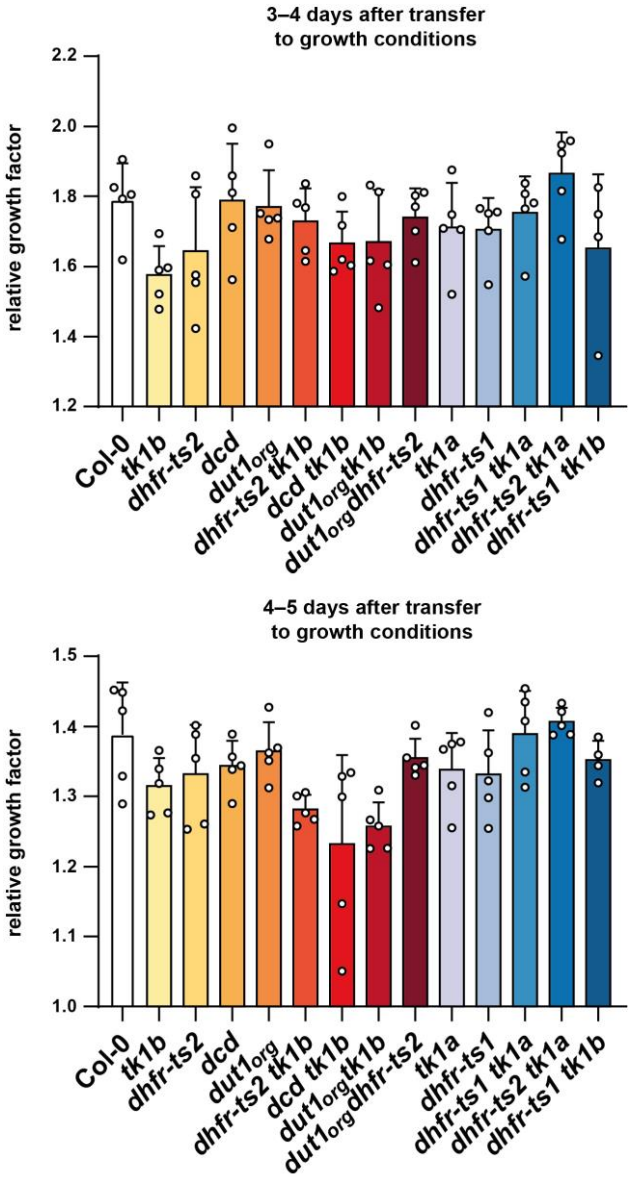

Supplemental Figure S5. Determination of the relative cotyledon growth in wild-type and mutants lacking enzymes putatively involved in thymidylate homeostasis in established seedlings. Seeds were imbibed in water for 48 h at 4°C in the dark and transferred to long-day growth conditions. Images were taken at three, four and five days and the sum of yellow and green pixels was determined and used for the calculation of the relative growth rate of the cotyledons from individual plants for the time period of three to four days and four to five days. Four to five biological replicates (pooled seedlings) were analyzed. Error bars are SD. Two-sided Tukey's pairwise comparisons using the sandwich variance estimator were used for statistical analysis. No significant differences ($p < 0.05$) to Col-0 were observed. Adjusted *p*-values for multiple comparisons can be found in Supplemental Data Set S3. (Supports Figure 3)

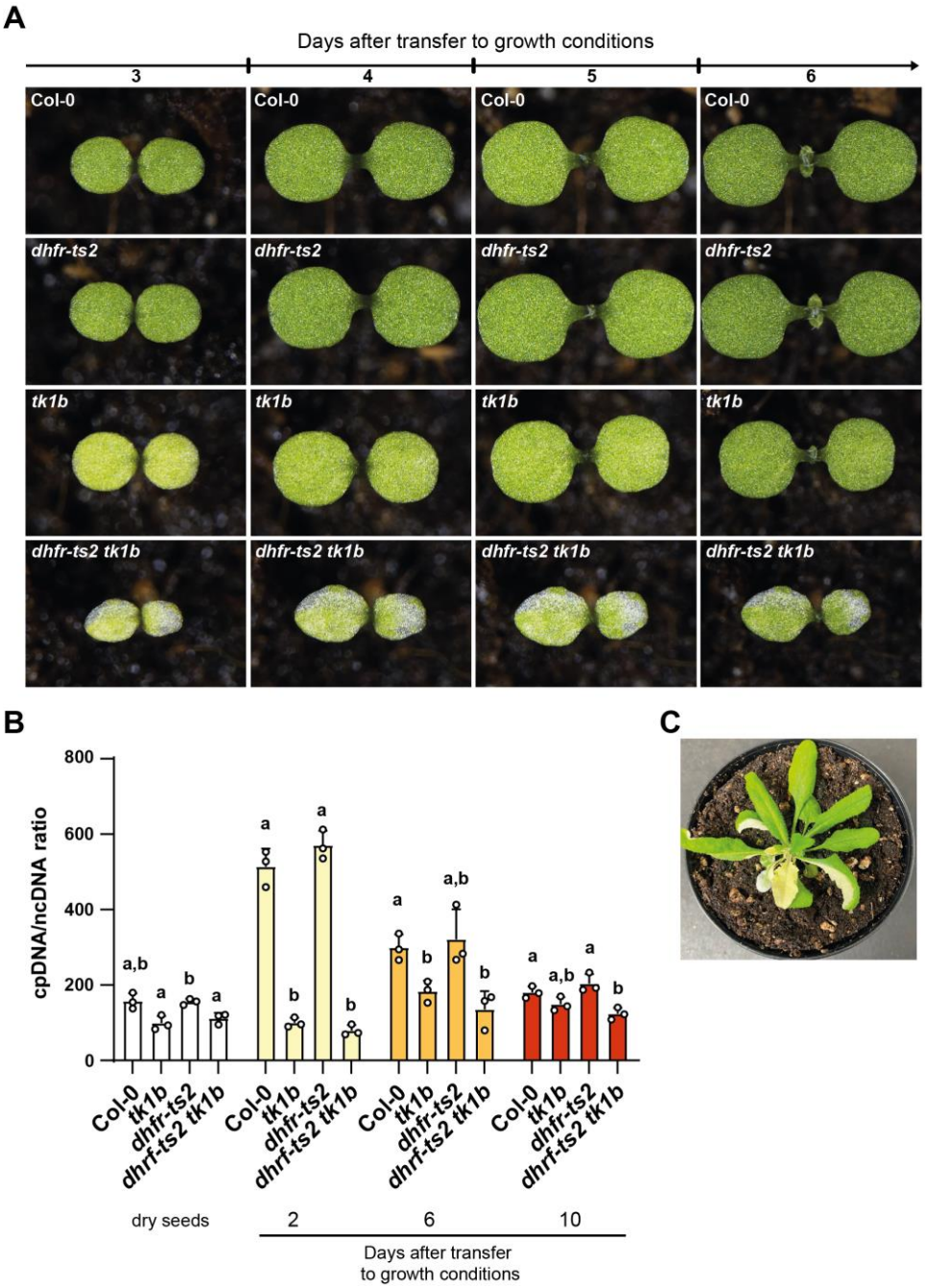

Supplemental Figure S6. Recovery of *dhfr-ts2*, *tk1b*, *dhfr-ts2 tk1b* mutants in comparison to wild-type. Seeds were imbibed in water for 48 h at 4°C in the dark and transferred to long-day growth conditions. (**A**) Images were taken of one specific plant at day three to six and are representative for 4 to 5 documented individuals. (**B**) One gene from cpDNA (*RBCL*) and ncDNA (*UBC21*) was amplified by qPCR, respectively, and cpDNA/ncDNA ratios were calculated. **(C)** Image of the rarely occurring albinotic section phenotype of *dhfr-ts tk1b*. Different letters indicate significant differences ($p < 0.05$) between genotypes. Three biological replicates (pooled seedlings) were analyzed. Error bars are SD. Adjusted *p*-values for multiple comparisons can be found in Supplemental Data Set S3. (Supports Figure 3)

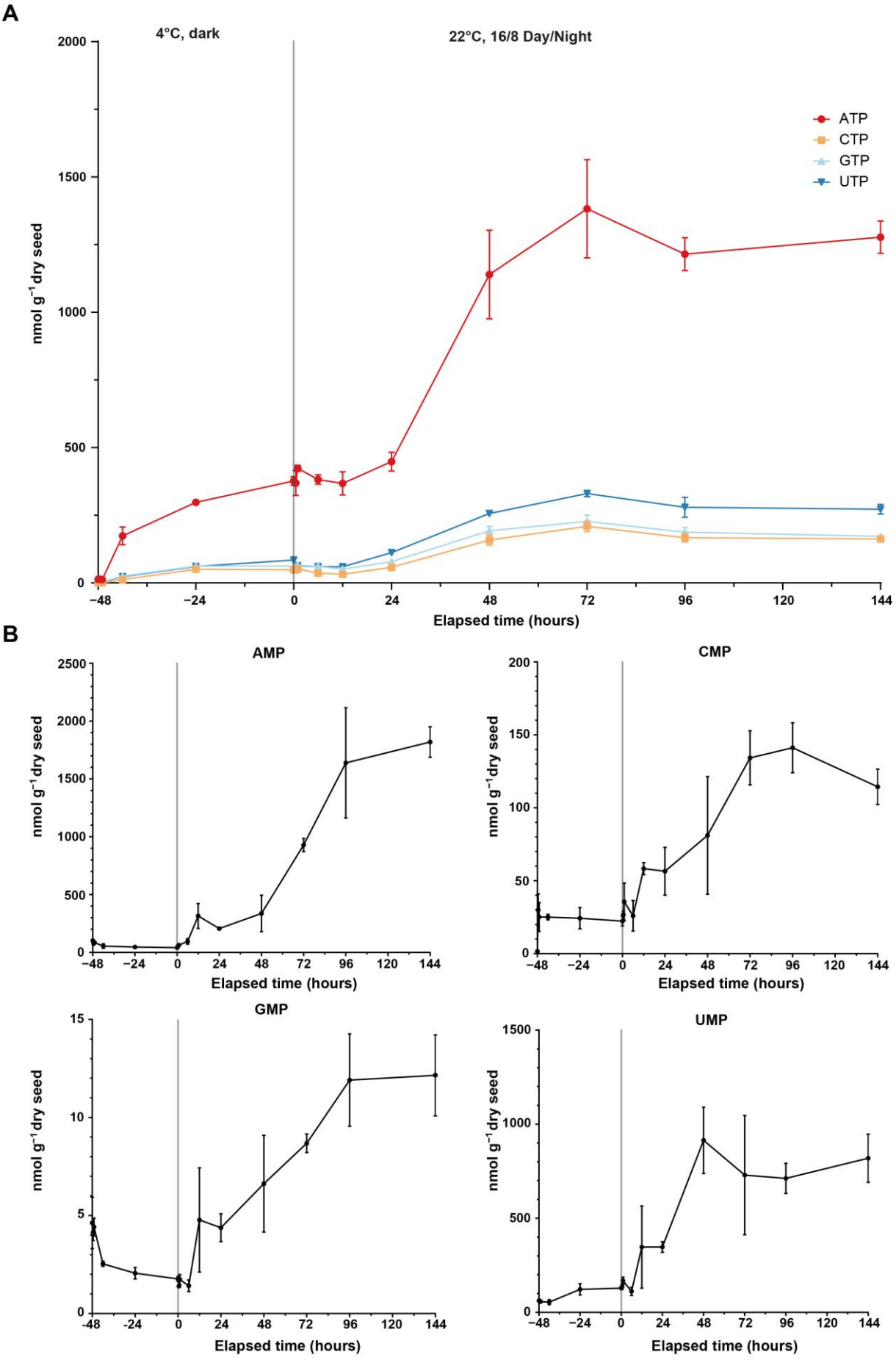
A
4°C, dark
22°C, 16/8 Day/Night
ATP
CTP
GTP
UTP
nmol g⁻¹ dry seed
Elapsed time (hours)
B
AMP
CMP
GMP
UMP
nmol g⁻¹ dry seed
Elapsed time (hours)

Supplemental Figure S7. Concentrations of ribonucleotides and ribonucleosides at different time points during seed germination and in the establishing seedling. Concentrations of (**A**) ATP, CTP, GTP, UTP, (**B**) AMP, CMP, GMP and UMP were quantified with LC-MS before transfer to long-day growth conditions (−48 h, −47.5 h, −42 h, −24 h; dark and 4°C), at transfer to long-day growth conditions (0 h) and after transfer to long-day growth conditions (0.5 h, 1 h, 6h, 12 h, 24 h, 48 h, 72 h, 96 h, 144 h). While seeds at the −48 h time point were dry, all other samples were imbibed in water. Four biological replicates (pooled seeds/seedlings) were analyzed. Error bars are SD. (Supports Figure 4)

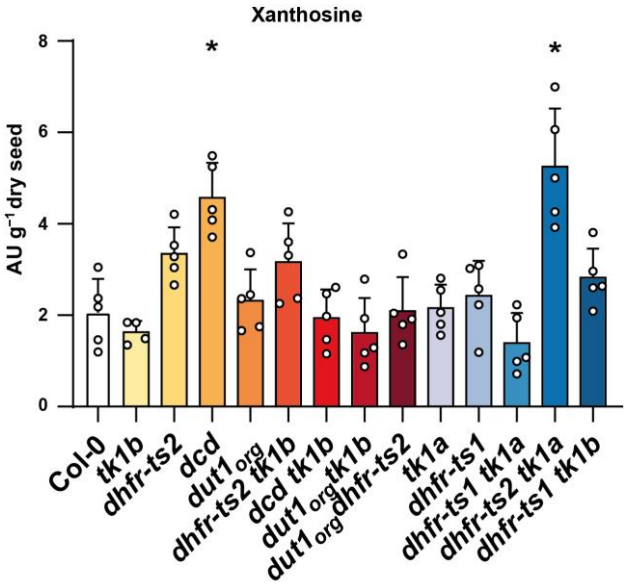

Supplemental Figure S8. Relative amounts of xanthosine in wild-type and mutants lacking enzymes putatively involved in thymidylate homeostasis during germination. Seeds were imbibed in water for 48 h at 4°C in the dark, transferred for 3 h to long-day growth conditions and harvested for LC-MS analysis. Due to the unavailability of a xanthosine isotope standard, the response on column for xanthosine was normalized to the response on column of the dT isotope standard, resulting in an arbitrary unit (AU). Two-sided Tukey's pairwise comparisons using the sandwich variance estimator were used for statistical analysis. Asterisks indicate significant differences ($p < 0.05$) to Col-0. Error bars are the standard deviation for $n = 5$ biological replicates (pooled seedlings). Adjusted p-values for multiple comparisons can be found in Supplemental Data Set S3. (Supports Figure 5)

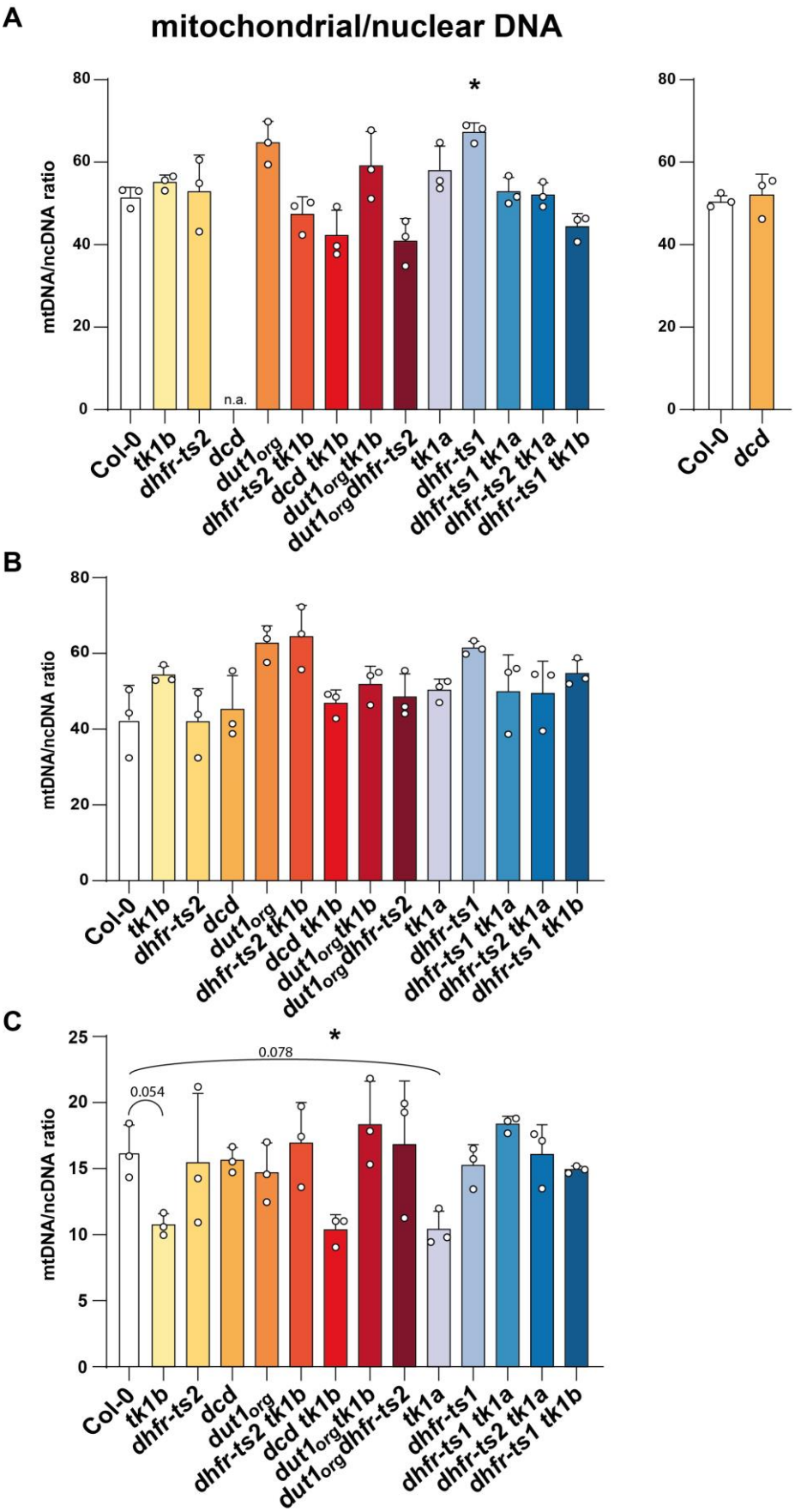
A
mitochondrial/nuclear DNA
mtDNA/ncDNA ratio
n.a.
*
Col-0
tk1b
dhfr-ts2
dcd
dut1org
dhfr-ts2 tk1b
dcd tk1b
dut1org tk1b
dut1org dhfr-ts2
tk1a
dhfr-ts1
dhfr-ts1 tk1a
dhfr-ts2 tk1a
dhfr-ts1 tk1b
B
C
0.078
0.054

Supplemental Figure S9. Abundance of the mtDNA relative to the ncDNA in wild-type and mutants lacking enzymes putatively involved in thymidylate homeostasis during germination and early and late seedling establishment. Seeds were imbibed in water for 48 h at 4°C in the dark, transferred for (**A**) 3 h, (**B**) 48 h and (**C**) 144 h to long-day growth conditions and harvested. QPCR was performed with primers amplifying one gene from mtDNA (*COX1*) and ncDNA (*UBC21*), respectively. The mtDNA/ncDNA ratios were calculated from Ct values for the respective genes. Two-sided Tukey's pairwise comparisons using the sandwich variance estimator were used for statistical analysis. Asterisks indicate significant differences ($p < 0.05$) to Col-0; $p > 0.05$ are indicated if value comparisons are made in the text. Three biological replicates (pooled seedlings) were analyzed. Error bars are SD. Adjusted *p*-values for multiple comparisons can be found in Supplemental Data Set S3. (Supports Figure 6, 8 and 9)

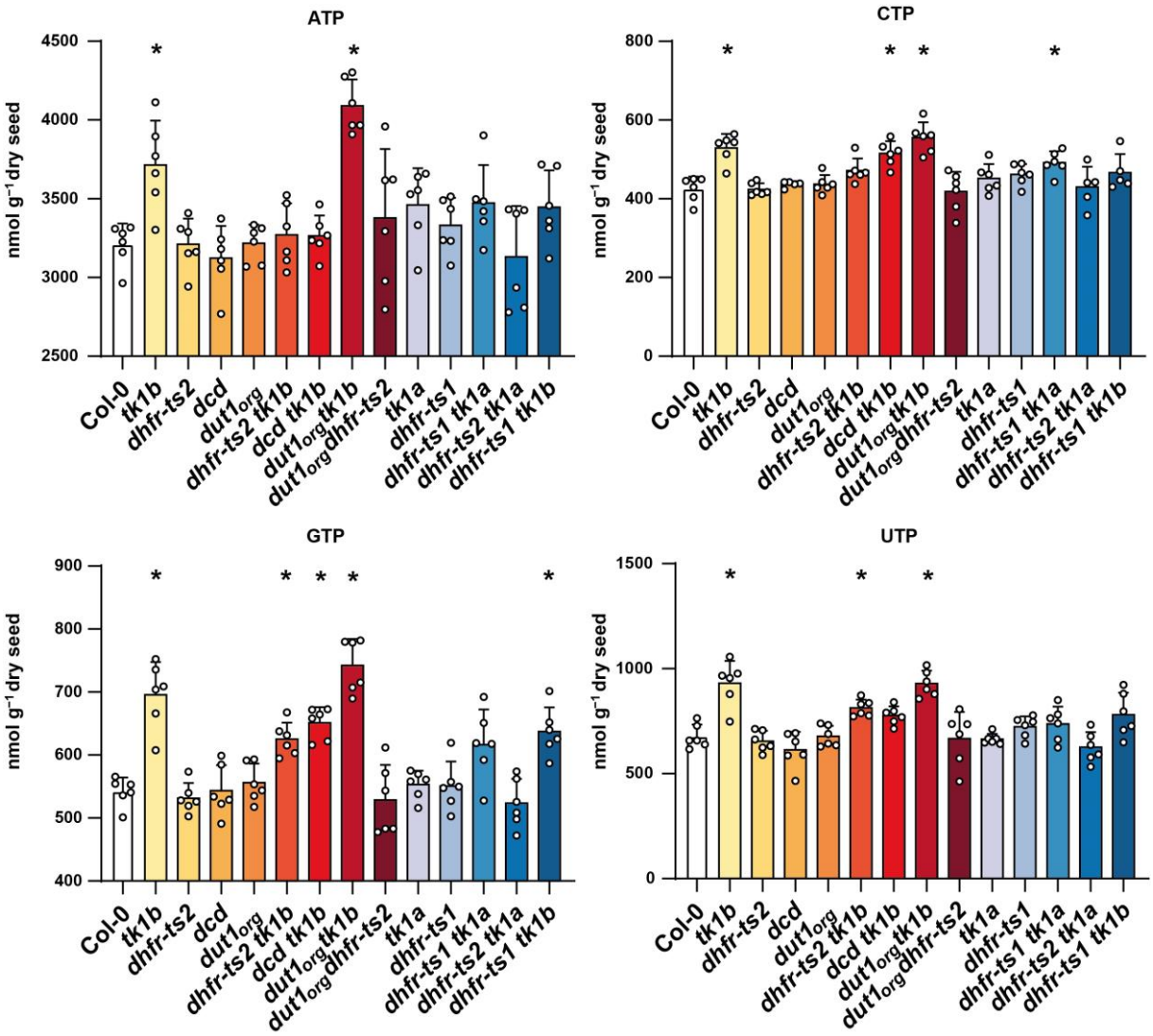

Supplemental Figure S10. Concentrations of ribonucleotide triphosphates in the wild-type and mutant seeds lacking enzymes putatively involved in thymidylate homeostasis during early seedling establishment. Seeds were imbibed in water for 48 h at 4°C in the dark, transferred for 48 h to long-day growth conditions and harvested for LC-MS analysis. Concentrations of ATP, CTP, GTP and UTP in seeds are shown. Two-sided Tukey's pairwise comparisons using the sandwich variance estimator were used for statistical analysis. Asterisks indicate significant differences ($p < 0.05$) to Col-0. Five to six biological replicates (pooled seedlings) were analyzed. Error bars are SD. Adjusted *p*-values for multiple comparisons can be found in Supplemental Data Set S3. (Supports Figure 7)

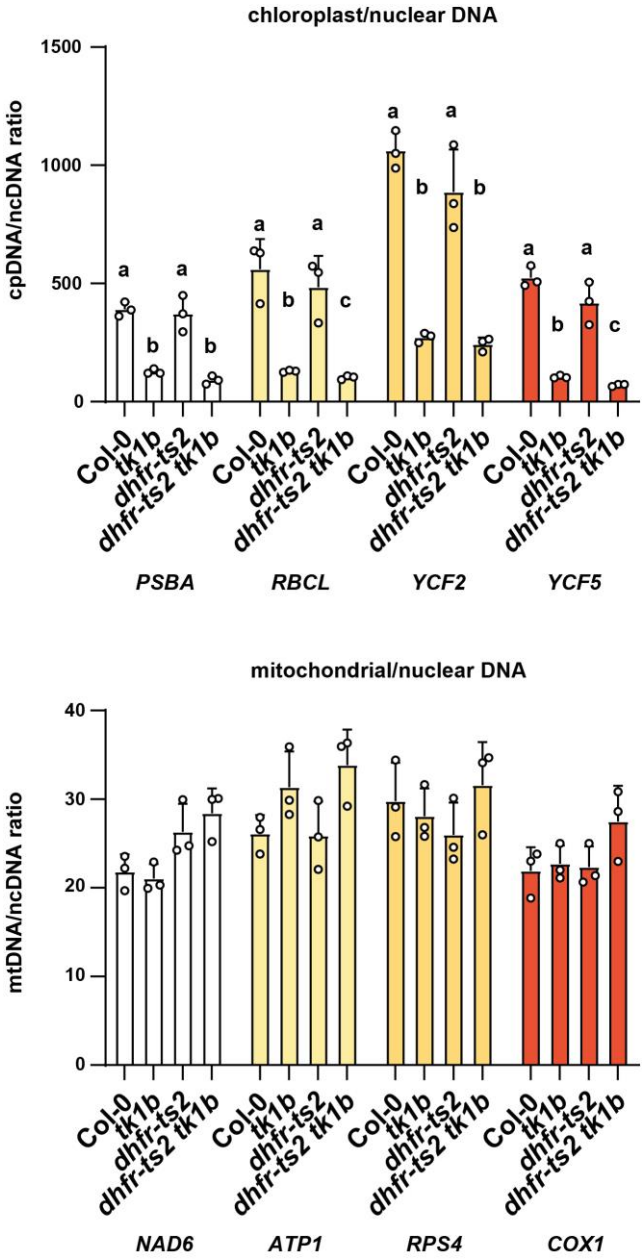

Supplemental Figure S11. Relative abundances of cpDNA and mtDNA during early seedling establishment determined by the amplification of four genes, respectively. Seeds were imbibed in water for 48 h at 4°C in the dark, transferred for 48 h to long-day growth conditions and harvested. QPCR was performed with primers amplifying four genes from cpDNA (*PSBA*, *RBCL*, *YCF2* AND *YCF5*), mtDNA (*NAD6*, *ATP1*, *RPS4* and *COX1*) located at distant positions on the plastid and mitochondrial genomes and one gene from ncDNA (*UBC21*). The cpDNA/ncDNA and mtDNA/ncDNA ratios were calculated from Ct values for the respective genes. Different letters represent significant differences ($p < 0.05$) between genotypes. Three biological replicates (pooled seedlings) were analyzed. Error bars are SD. Two-sided Tukey's pairwise comparisons using the sandwich variance estimator were used for statistical analysis. Adjusted *p*-values for multiple comparisons can be found in Supplemental Data Set S3. (Supports Figure 8)

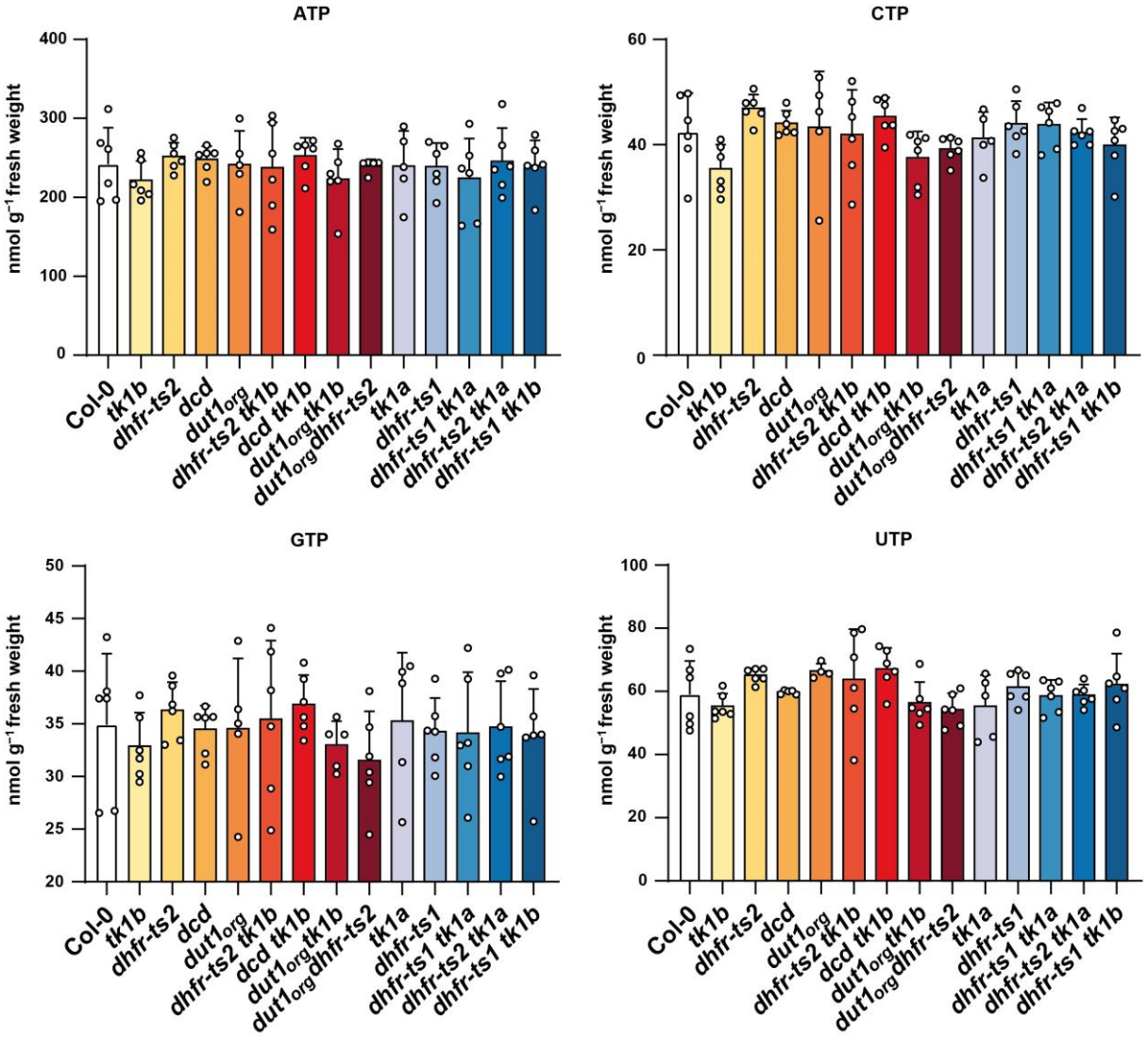

Supplemental Figure S12. Concentrations of ribonucleotide triphosphates in the wild-type and mutants lacking enzymes putatively involved in thymidylate homeostasis during late seedling establishment. Seeds were imbibed in water for 48 h at 4°C in the dark, transferred for 144 h to long-day growth conditions and harvested for LC-MS analysis. Concentrations of ATP, CTP, GTP and UTP in seeds are shown. No significant differences ($p < 0.05$) between wild-type and mutants were observed. Five to six biological replicates (pooled seedlings) were analyzed. Error bars are SD. Two-sided Tukey's pairwise comparisons using the sandwich variance estimator were used for statistical analysis. Adjusted *p*-values for multiple comparisons can be found in Supplemental Data Set S3. (Supports Figure 10)

3 Appendix

3.1 Curriculum Vitae

Name: Markus Niehaus

Date of Birth: 07.05.1991

Place of Birth: Lohne (Oldenburg)

Education:

since 2022 Post-Doc at Institute of Plant Nutrition
Leibniz Universität Hannover, Germany

2016 – 2022 Doctoral candidate at Institute of Plant Nutrition
Leibniz Universität Hannover, Germany
Thesis:
The deoxypyrimidine nucleotide metabolism in plant mitochondria.
Grade: magna cum laude

2014 – 2016 Master of Science Plant Biotechnology
Leibniz Universität Hannover, Germany
Thesis:
Functional Analysis of Candidate Genes for P Deficiency Induced Root Hair Growth in *Brassica carinata* by Knock-down and Overexpression.
Grade: 1,2

2011 – 2014 Bachelor of Science Plant Biotechnology
Leibniz Universität Hannover, Germany
Thesis:
Influence of the Nitrogen Supply on Pods and Grain Development in *Brassica napus*. In Vitro Cultivation of Single Pods.
Grade: 1,7

2010 General university entrance qualification (Abitur)
Gymnasium Antonianum Vechta

3.2 List of publications

- The nucleotide metabolome of germinating Arabidopsis thaliana seeds reveals a central role for thymidine phosphorylation in chloroplast development

  Niehaus, M., Straube, H., Specht, A., Baccolini, C., Witte, C-P., Herde, M. (2022)
  The Plant Cell
  DOI: 10.1093/plcell/koac207

- Rapid Affinity Purification of Tagged Plant Mitochondria

  Niehaus, M., Herde, M. (2022):
  Methods in Molecular Biology, Affinity Chromatography, Pages 121 – 133
  DOI: 10.1007/978-1-0716-2176-9_9

- Enhanced nucleotide analysis enables the quantification of deoxynucleotides in plants and algae revealing connections between nucleoside and deoxynucleoside metabolism

  Straube, H., **Niehaus, M**., Zwittian, S., Witte, C-P., Herde, M. (2020)
  The Plant Cell, Vol. 33, Issue 2, Pages 270 - 289
  DOI: 10.1093/plcell/koaa028

- Rapid affinity purification of tagged plant mitochondria (Mito-AP) for metabolome and proteome analyses

  Niehaus, M., Straube, H., Künzler, P., Rugen, N., Hegermann, J., Giavalisco, P., Eubel, H., Witte, C-P., Herde, M. (2020)
  Plant Physiology, Vol. 182, Issue 3, Pages 1194 - 1210
  DOI: 10.1104/pp.19.00736

- Molecular background of Pi deficiency-induced root hair growth in Brassica carinata–A fasciclin-like arabinogalactan protein is involved

  Kirchner, T.W., **Niehaus, M**., Rössig, K.L., Lauterbach, T., Herde, M., Küster, H., Schenk, M.K. (2018)
  Frontiers in Plant Science
  DOI: 10.3389/fpls.2018.01372

- Efficient generation of mutations mediated by CRISPR/Cas9 in the hairy root transformation system of Brassica carinata

  Kirchner, T.W., **Niehaus, M**., Debener, T., Schenk, M.K., Herde, M. (2017)
  PloS ONE, Vol. 12, Issue 9
  DOI: 10.1371/journal.pone.0185429

Acknowledgements

First of all, I would like to thank Dr. Marco Herde for the trust he placed in me to work with me on this project, but also for the numerous discussions, both scientific and not so scientific, during my time and his tireless will and dedication to make me a better scientist.

Special thanks to Prof. Dr. Claus-Peter Witte for giving me the opportunity to join his group, the helpful scientific discussions and his great efforts in trying to make my science look perfect.

I would also like to thank Prof. Dr. Hans-Peter Braun and Prof. Dr. Thomas Pfannschmidt for taking over the functions in the examination committee.

I also wish to thank the whole group, Andre Specht for helping me with some experiments and him always being able to fix everything, Hildegard Thölke for helping me in the lab and always being positive and helpful, Iris Wienkemeier for keeping everything organized and reminding me to take some days of vacation, my former office wife Katharina Heinemann for the endless and mostly unscientific discussions and clementine breaks, Henryk Straube for being very helpful when it came to metabolite analysis and discussion of weird results, Dr. Nieves Medina-Escobar for reminding me to keep the lab clean and the numerous discussions about Confocal Microscopy, Jannis Rinne for showing me how to do stuff more easy in the lab and his helpfulness towards students, Luisa Voß for taking over the role of Kathi and the continuation of the clementine breaks, Adiel Lopez for being my new office wife and her trying to fill the gap Kathi left and my stomach with nice Mexican food, Nabila Firdoos for discussions about plants and always being happy, Xiaoguang Chen for showing me nice Chinese food and many interesting discussions, and also to all the bachelor and master students I had along the way who helped me in various ways to finish my work: Nergis Özmen, Zachary Mullin-Bernstein, Louisa Behnsen, Rene Grove, Lukas Wiechmann, Sören Ahrens and Annika Wallbott.

Finally, I would like to thank my family and friends for their endless support and always being there when something went wrong, their patience and understanding when I had to cancel appointments due to work, and them always reminding me that I am a plant doctor and as such should know every single disease and symptom a plant can get and how to cure it.